Technische Universität Darmstadt

Material- und Geowissenschaften

Recycling of Nd-Fe-B permanent magnets by hydrogen processes

Eng. Alexandru Lixandru

- A thesis presented for the academic degree of doctor (Dr.-Eng.) -

Referee: Prof. Dr. Oliver Gutfleisch

Co-referee: Prof. Dr. Yongxiang Yang

-Darmstadt 2018-

Alexandru Lixandru: *Recycling of Nd-Fe-B permanent magnets by hydrogen processes*

Darmstadt, Technische Universität Darmstadt,

Publication year of the thesis On TUprints: 2018

URN: urn:nbn:de:tuda-tuprints-73922

Date of the oral examination: 17 January 2018

Date of submission: November 2017

Date of the oral examination: 17 January 2018

1. Referee: Prof. Dr. Oliver Gutfleisch

2. Co-referee: Prof. Dr. Yongxiang Yang

Statement of the dissertation

I hereby declare, that I have prepared the present dissertation without the help of third parties and only with the indicated sources and tools. All sites taken from sources are identified as such. This work has not yet been submitted to an examining authority in the same or similar form.

Darmstadt, 30 October 2017

Alexandru Lixandru

Abstract

This thesis is based on the work carried out since January 2014 as a Marie Curie Fellow at Fraunhofer ISC, Project Group IWKS and as a Ph.D. student in the Functional Materials department at Technische Universität Darmstadt. In the first part of my thesis, different waste streams of electrical and electronic equipment from an industrial recycling plant were analyzed in order to localize, identify and collect rare-earth permanent magnets of Nd-Fe-B type. This particular type of magnets were mainly found in hard disk drives from laptops and desktop computers, as well as in loudspeakers from compact products such as flat screen TVs, PC screens, and laptops. The study includes a systematic survey of the chemical composition of the Nd-Fe-B magnets found in the selected waste streams, which illustrates the evolution of the Nd-Fe-B alloys over the years. The study also provides an overview over the types of magnets that are integrated in different waste electric and electronic equipment. After localizing, identifying and recovering the rare-earth permanent magnets from waste electrical and electronic equipment, these magnets were processed together with other Nd-Fe-B scrap magnets from electric motors with a hydrogen based recycling process (hydrogen decrepitation (HD) and hydrogenation disproportionation desorption and recombination (HDDR) processes). The effects of the main HDDR processing parameters: hydrogen pressure, hydrogen desorption rate and temperatures on the magnetic properties of the recycled materials have been investigated systematically and are presented in the second section of the chapter 4. The optimum hydrogen pressures required for the complete disproportionation of the various magnet compositions were determined. It was found that a hydrogen heat treatment composed of two steps (780 °C and 840 °C) and a moderate desorption rate can be used for the magnets having a higher Dy and Co content to obtain high quality anisotropic HDDR powders. In addition to this section, it was performed a study where it was investigated the effects of increasing the Dy content on the processing parameters of the HDDR process. The variation of the magnetic properties for the magnets with different Dy contents processed at different hydrogen pressure, temperature and hydrogen desorption rate are presented in this study. The obtained recycled powders by HD and by HDDR were consolidated by either sintering, spark plasma sintering or bonding with epoxy resin. For the scrap magnets with a low content of Dy and Co, a better recovery of the magnetic properties (above 90%) was achieved compared with the magnets from electric motors (high Dy and Co) where the recovery rate is ~60%. For these magnets a “refreshing” of the recycled powders with 10% $Nd_{90}Al_{10}$ and $Pr_{75}Cu_{6.25}Co_{18.75}$ was applied. Different post sintering treatments were applied for these recycled magnets in order to equally distribute the fresh added powder. All these treatments are presented in this study.

Contents

List of figures

List of tables

Nomenclature

M	magnetization
M_r	remanent magnetization
M_s	saturation magnetization
J_S	saturation polarization
H	magnetic field
H_c	coercivity or coercive force
H_{ci}	intrinsic coercivity
H_d	demagnetizing field
H_N	nucleation field
H_A	anisotropy field
$H_{\parallel}c$	easy direction of magnetization
$H_{\perp}c$	hard direction of magnetization
N_d	demagnetization factor
B	flux density
$(BH)_{max}$	energy product
P	operating point
μ_0	permeability of the vacuum
m	magnetic moment
V	atomic volume
α_K	Kronmüller parameter
K_1, K_2 and K_3	anisotropy constants
E_A	anisotropy-energy
T_C	Curie temperature
CGS	centimeter–gram–second system of units

SI	international system of units
HD	hydrogen decrepitation
d-HDDR	dynamic hydrogenation disproportionation desorption recombination
DTA	differential thermal analysis
ICP-OES	inductively coupled plasma optical emission spectrometry
XRD	X-ray diffraction
XRF	X-ray fluorescence
SEM	scanning electron microscope
FEG	field emission gun
PPMS	physical property measurement system
VSM	vibrating sample magnetometer
SPS	spark plasma sintering
REEs	rare earth elements
RE	rare earth
WEEE	waste electrical and electronic equipment
EEE	electrical and electronic equipment
HDDs	hard disk drives
VCMs	voice coil motors
CRT	cathode ray tubes
PC	personal computer
LCD screens	liquid crystal display screens
PMR	precious metal recycling
PCB	polychlorinated biphenyl
PRC	plastics recycling center

1. Introduction

The research for new magnetic materials with an energy density higher than the energy density produced by the Alnico permanent magnets, leaded to the discovery of the magnets based on Sm-Co. But the worldwide development of this type of magnets based on Sm-Co, was halted by the production costs of the magnets. The materials were expensive and the supply with cobalt was irregular and uncertain. Initially it was tried to substitute Co with Fe in $SmCo_5$ and in Sm_2Co_{17} with the aim to combine the iron with the rare earths in a crystalline structure with uniaxial anisotropy, but the desire structure was not achieved **[1].**

The most favorable combination of rare earth-transition metal is iron and neodymium, unfortunately there are not suitable compounds of Nd-Fe in the binary phase diagram. So, the challenge was to find a ternary compound stable with Fe. **[2]**. This challenge was solved by two independent groups in 1982. Croat and his team used the melt spinning technique to alloy the metals and to produce nano-crystalline Nd-Fe-B, while Sagawa and his team realized a magnetic compound by traditional sintering route **[3, 4]**.

Later E. F. Kneller and R. Hawig designed the model of the permanent magnet called exchange-spring magnet **[5]**. For the Nd-Fe-B system, the hard magnetic nano-composites were first time obtained in 1991. If the hard-magnetic grains ($Nd_2Fe_{14}B$) has approximately 10 nm and the soft magnetic grains (α-Fe) has about 5 nm, then the created composite behaves as a permanent magnet. Due to their nano-dimensions, the soft magnetic phase is strengthened by the exchange interaction, leading to a parallel alignment of the magnetic moments, improving the remanence of the magnet. If for an isotropic magnet with uniaxial anisotropy the ratio $M_r/M_s = 0.5$, for the exchange interaction magnets the ration $M_r/M_s > 0.5$**[5].**

Skomski and Coey, underlined the possibility of achieving an energy density larger than 1 MJ/m^3 **[6]**, which is 2.5 times higher than the value achieved by the most performant Nd-Fe-B based magnet (444 kJ/m^3) **[7].** These theoretical findings have significantly increased the research interest in the field of rare earth permanent magnets.

Today, the research in the field of sintered permanent magnets based on Nd-Fe-B, is focused on achieving values of the energy product higher than 451 kJ/m^3 **[8]** (value obtained in laboratory conditions by the German company Vacuumschmelze GmbH in 2002). The current highest energy product for a commercially available permanent magnet material is 414 kJ/m^3 for a Shin-Etsu Nd-Fe-B alloy. The evolution of the energy product is shown in figure 1.1.

At the same time, researcher aim to increase the thermal stability of the magnets, so as to exhibit working temperatures up to 225° C, and also to improve the corrosion resistance without changing the microstructure of the magnets.

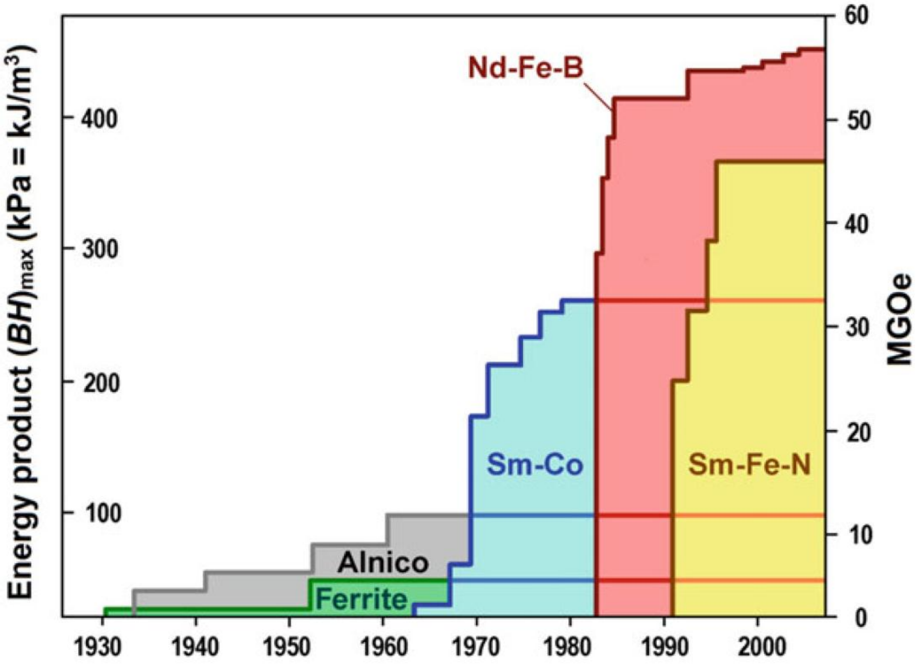

Figure 1.1: Energy product development for different permanent magnets **[22].**

The rare earth permanent magnets are used widely in a growing number of different applications and fields. Rare earth permanent magnets are used mainly in applications which are restricted by size, weight and performance. The high performance of the rare earth permanent magnets makes this type of magnets essential for miniaturizing a variety of instruments and equipment. Because of their unique physical properties, the rare earth permanent magnets are widely used in applications like: wind turbines, electric vehicles and defense applications.

The e-bike motors are an important application for the Nd-Fe-B magnets **[9]**. A part of the hybrid and electric vehicles (e.g. Mitsubishi, Toyota, Nissan, Chevrolet, BMW, VW or Mercedes) are using rare earth permanent magnets motors **[9]**. Another important application for the rare earth permanent magnets is the hard disk drive voice coil motor (VCMs) **[11].** A different application, where the Nd-Fe-B magnets are used, is the audio system market. These magnets are widely used in small speakers for mobile phones, notebooks, laptops, tablets and headphones. Other applications that use Nd-Fe-B magnets are: automotive alternators, motors for electric power steering, automated/manual transmission motors, starter motors, fuel pumps and ABS motors **[9, 12]**. Another important market where the Nd-Fe-B magnets are used is in the compressors of the air conditioners **[10]**.

From 2007 on, China is the largest manufacturer of permanent magnets. In 2007, 64% of the total production of permanent was supplied by China. Table 1 shows the worldwide production of permanent magnets **[13]**.

Table 1: Worldwide permanent magnets production in 2007 (ton/year) **[13].**

	Alnico	Sintered		Bonded			Total	
		Ferrite	NdFeB	NdFeB	Flex. Ferrite	Rigid Ferrite		
China	2 000	370 000	16 900	3 200	64 000	4 950	461 050	63.80 %
Japan	300	32 700	10 100	600	3 970	9 800	57 470	8.00 %
S.E Asia	800	21 600	-	1 000	10 700	6 800	40 900	5.70 %
USA	300	20 000	-	160	26 500	3 800	50 760	7.00 %
Europe	600	18 000	800	150	41 000	1 300	61 850	8.60 %
Others	-	40 000	-	170	9 000	900	50 070	6.90 %
Total	4 000 0.60 %	502 300 69.60 %	27 800 3.80 %	5 280 0.70 %	155 170 21.50 %	27 550 3.80 %	722 100 100 %	100 %

Also, China is the biggest miner of rare earths, mining nearly 90 % of world total production **[14]**. In 2010 the entire world reserves of rare earth were approximately 110 million tons, from which China holds 55 million tons, Commonwealth of Independence States – former Soviet Union: 19 million tons, the United States: 13 million tons, India: 3.1 million tons, Australia: 1.6 million tons, Brazil: 0.48 million tons, Malaysia: 0.3 million tons and other countries: 18 million tons **[14]**. The main rare earth consumers are USA, Europe, Japan, Korea and China **[14]**.

40 % of the mined rare earths are used for the production of the permanent magnets, 19 % in chemical catalysts, 13 % in polishing powders and 8 % in glasses, 8 % for phosphors and 12 % other applications **[15]**. Due to the Chinese monopoly on the production and processing of rare earths, the world-wide supply for the downstream goods production depends on China. All this became a problem when China decided to change its export policy, becoming less and less interested in exporting its rare earths by decreasing its exports with increasing the export taxes on rare earths **[16].** The Chinese rare earths exports drop from 57,400 tons in 2007 to just 15,660 tons in 2011 **[15]**. This policy created an artificial rise of the price of rare earths (see figure 1.2) and triggered concerns among its customers: the European Union, Japan and the USA. In 2011 the price of praseodymium increases with 200 %, neodymium with 300 %, dysprosium with 700 % and terbium with 650 % (source for the metal prices: www.metal-pages.com, last seen 25 October 2017).

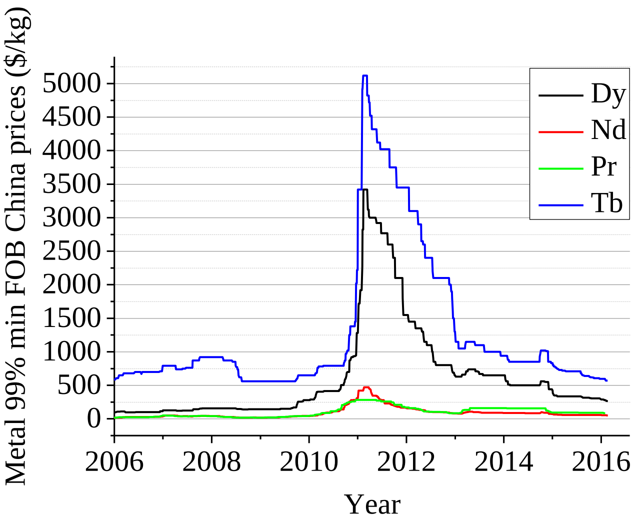

Figure 1.2: The evolution over the years of FOB China metal 99 % prices for Dy, Nd, Pr, Tb (source for the metal prices: www.metal-pages.com, last seen 25 October 2017).

In mid-2010, European Commission published a list of raw materials that are critical for many emergent technologies, highlighting the vulnerability due to the political tensions or shortages. According to the European Commission: *a raw material is considered "critical" if the impact on the economy, due to possible supply contraction, is higher than other raw materials*. The evaluation criteria include: evaluating the economic and political situation of the producing countries, the potential of substitution and the level of recycling rates. European Commission considers the rare earths as the elements with the highest supply risk **[17]**. A summarized graph of the European Commission report on critical raw materials for the EU is presented in figure 1.3.

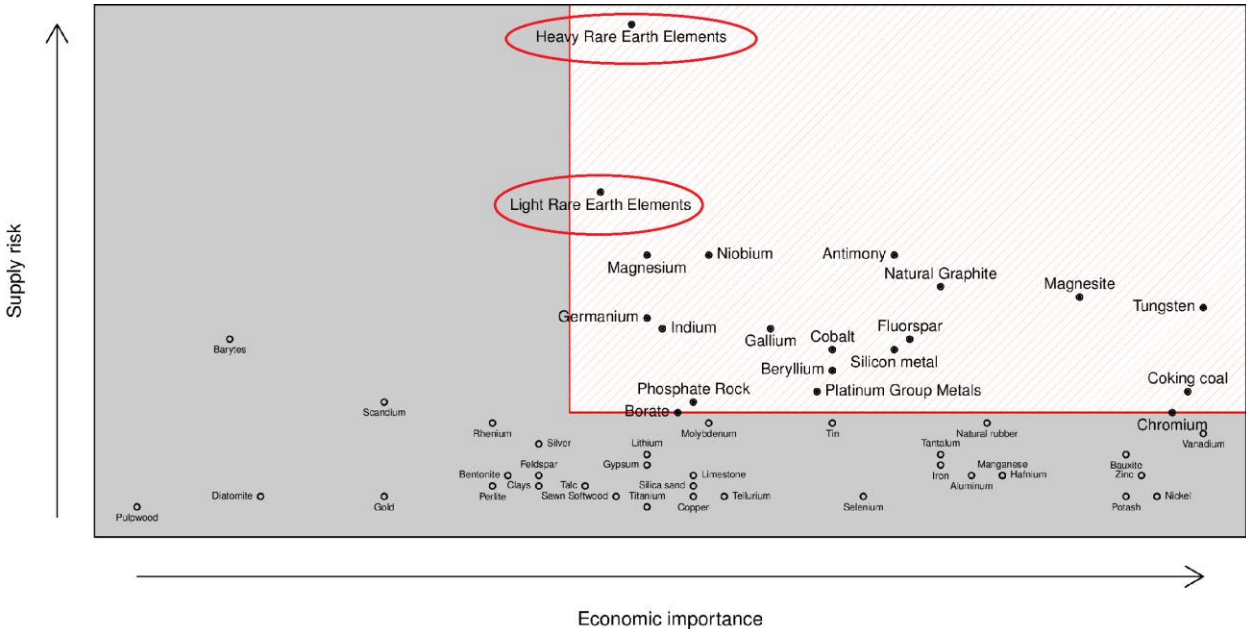

Figure 1.3: Illustration of the critical raw materials for the EU, image from 2014 EU reports **[17].**

European countries, which do not have the rare earth resources to satisfy the demand for these critical materials, are intensifying their efforts to increase the recovery and the recycling of the rare earths from hi-tech wastes. The reason for the recycling includes environmental factors but also economic reasons. Recycling of the critical elements can offer the security of the supply for a country. An important environmental issue that can be solved by recycling of the critical elements like the rare earths, is the pollution impact. It is well known that beside the low concentration of resources, the biggest problem is that the rare earths are associated with radioactive elements like uranium and thorium. During the production cycles, huge quantities of water need to be consumed; also the acidic substances and the electricity used for their extraction plays an important role. All this environmental issue can be improved by the recycling of the rare earths from electronic waste.

Another problem is represented by the fact that some abundant elements, like lanthanum or cerium, are usually underpriced and sell on the market below the average production costs. Elements with a higher price compensate this difference in order to keep a positive overall return for the rare earth producers (although most of the rare earth elements have similar processing costs) **[18]**. Mining for specific rare earth elements less abundant (heavy rare earth elements) can cause over-production for the more abundant elements (light rare earth elements), which are also less demanded. This imbalance between the demand of individual rare earths elements and their natural abundance in ores is called the “balance problem” **[19]**. The “balance problem” can be partially solved by recycling and recovering the heavy rare earth elements from the electronic waste. In this way the mining need for certain rare earth elements will decrease **[20]**.

Recycling of these “metals” is not yet commercially conducted. In fact, less than 1 % of the rare earths are currently being recycled **[17]** mainly due to low collection rates, lack of information about the quantity of rare earth materials available for recycling, recycling-unfriendly product designs and lack of mature and economically feasible recycling technologies. The first part of this work, chapter 4.1, consists of a study on different permanent magnet waste streams from electrical and electronic waste and aims to improve the identification and recovery of the products with high volumes of rare earths. Data regarding the identification, collection, disassembling and the chemical composition of the magnets are presented. Apart from the importance of the localization-identification-collection of the rare earth magnets, essential issues like recovering of 90 % of the magnetic properties of the scrap magnets, production of sintering of Nd-Fe-B magnets from recycled materials of different qualities, production of bonded magnets and spark plasma sintering magnets with high degree of texture, and comparative multi-scale characterization of bonded/spark plasma sintering/conventional sintering magnets made from recycled materials were carried out. For this, chapter 4.3 of the thesis combines low and high temperature hydrogen treatments - hydrogen decrepitation (HD) process and dynamic hydrogenation disproportionation desorption recombination (d-HDDR) process - employed to produce new anisotropic powder from scrap sintered Nd-Fe-B magnets. The behavior of different types of scrap permanent magnets when exposed to carefully controlled hydrogen pressure, temperature and hydrogen desorption rate is analyzed in chapter 4.4. Different types of scrap permanent magnets that come from electrical motors and mixtures of scrap permanent magnets are covered in the study. The main composition of these scrap permanent magnets is (Nd,Dy,Pr)-FeCo -B with small additions of Cu and Ga. The obtained powder after the HD and d-HDDR processes was consolidated by conventional sintering, spark plasma sintering and by embedding the powders, and the result are presented in chapter 4.6. The recycled powder quality was ameliorated by mixing it with fresh powder in order to overcome the detrimental effects. During the recycle process the oxygen and carbon content was monitored. The obtained samples at different steps of the recycle process were complex characterized and presented in the following sub-sections of chapter 4.6. The results presented in my thesis could be consider as initial steps in a future recycling process based on low and high temperature hydrogen treatments, and with small adjustments of the processing parameters, this process can be easily upscale in order to obtain recycled magnets with high degree of texture and with a recovery of the magnetic properties of up to 90 %.

2. Fundamental concepts of hard-magnetic materials.

2.1. Intrinsic magnetic properties

The intrinsic magnetic properties of the magnetic materials, refer to the atomic origin of magnetism, and are the properties that are characteristic of the crystal structure and chemical composition and they are not affected by the microstructure (e.g. grain size or grain orientation). The intrinsic magnetic properties include: the Curie temperature T_C, the saturation magnetization M_s and the magneto-crystalline anisotropy H_a. The Curie temperature T_C and the spontaneous magnetization or saturation magnetization M_s of the permanent magnets are characteristics of iron-series (3d) transition-metal sub-lattice. Some heavy atoms - like 4d, 5d, 4f, 5f - have also a magnetic moment, their magnetization been diluted by the atomic volume, according to the formula:

$$M_s = m/V \tag{2.1}$$

where M_s is the magnetization, m is the magnetic moment and V is the atomic volume.

Curie temperature

The Curie temperature of the main phase of the hard-magnetic material should be as high as possible to ensure a large field of applications. The Curie temperature of the rare earth-transition metal depends on the properties of the rare-earths, on the ratio of the rare elements used and on the used transition metal. Typical values of the Curie temperature in $R_2Fe_{14}B$ compounds can be seen in figure 2.1.

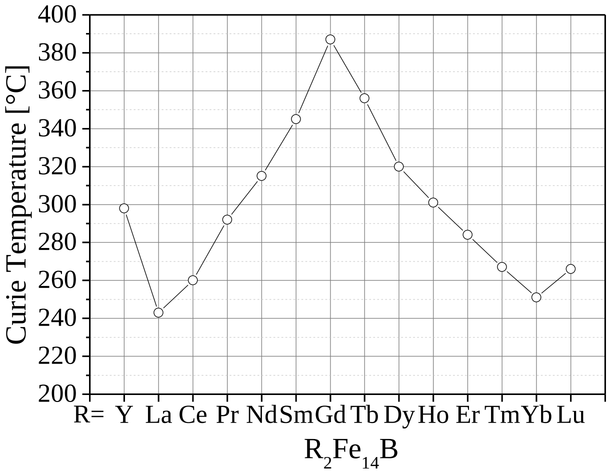

Figure 2.1: Curie temperature of different $R_2Fe_{14}B$ compounds **[21].**

Saturation magnetization

The saturation magnetization Ms determines the maximum value of the magnetic field that can be generated by the material. The saturation magnetization should have high values in the range of the interest working temperature. This allows high saturation inductions which determines high residual magnetic flux density and high energy product $(BH)_{max}$ respectively. The saturation magnetization is influenced by the strength of the magnetic moments, by the crystal structure and by the presence of non-magnetic elements in the structure.

In the case of a ferromagnetic material, the technical saturation magnetization is influenced also by the degree of alignment of the magnetic moments, as thermal vibration of the atoms will determine misalignment of the magnetic moments. The spontaneous magnetization usually represents the magnetization of single magnetic domain, but is also referred to the saturation magnetization. Table 2.1 gives useful properties of $R_2Fe_{14}B$ compounds and of materials commonly used in magnetic applications.

Table 2.1: Curie temperature (T_C) and the saturation polarization (J_S) at room temperature for different magnetic materials **[21].**

$R_2Fe_{14}B$ (R=)	T_C (°C)	J_S (T)	Material	T_C (°C)	J_S (T)
Y	298	1.38	Fe	770	2.15
La	243	1.38	Co	1131	1.76
Ce	260	1.17	Ni	358	0.60
Pr	292	1.56	$Nd_2Fe_{14}B$	312	1.60
Nd	312	1.60	$SmCo_5$	720	1.14
Sm	345	1.50	Sm_2Co_{17}	820	1.25
Gd	387	0.84	$BaFe_{12}O_{19}$	450	0.48
Tb	356	0.70	$SrFe_{12}O_{19}$	450	0.48
Dy	320	0.71	Fe 3wt% Si	740	2.00
Ho	301	0.81	Fe 4wt% Si	690	1.97
Er	284	0.90	Fe 35wt% Co	970	2.45
Tm	267	1.15	Fe 78wt% Ni	580	0.70
Yb	251	-	Fe 50wt% Ni	500	1.55
Lu	266	1.17	$MnO.Fe_2O_3$	300	0.51

Magnetic anisotropy

The magnetic anisotropy is measured as a potential energy of a unit volume of the magnetic materials, which depends on the orientation of the magnetization relative to the crystal axes. To maintain the magnetization in a desired direction, the permanent magnets need a high magnetic anisotropy. The anisotropy depends on the temperature and tends to zero at T_C, if there is no applied field. Most permanent magnet alloys have uniaxial crystal structures, and an easy magnetization axis (c-axis) perpendicular to the basal plane (a–b plane) **[22]**. In the case of rare-earth transition-metal alloys the magnetic anisotropy is ensured by the rare-earth sub-lattice. The unit anisotropy energy can be expressed as:

$$E_A(\theta, \varphi) = K_1 \sin^2\theta + K_2 \sin^4\theta + K_3 \sin^4\theta \cos^4\varphi + \ldots, \tag{2.2}$$

where K_1, K_2 and K_3 are the anisotropy constants and where the direction of the magnetization relative to the c-axis and the a-axis is given by the polar angles θ and φ respectively.

The simplest anisotropy-energy expression for a magnet of volume V is:

$$E_A = K_1 V \sin^2 \theta. \tag{2.3}$$

This anisotropy is called second-order (or lowest-order) uniaxial anisotropy, and K_1 is the first uniaxial anisotropy constant **[23]**. The preferred magnetization direction is along the c-axis (so call easy-axis anisotropy) in hexagonal or tetragonal structures, if K_1 predominates and $K_1 > 0$, but if $K_1 < 0$, the preferred magnetization direction is perpendicular to the c-axis (called easy-plane anisotropy). If K_1 is not predominant, the preferred magnetization can be in other directions. If is taken in consideration only K_1 and K_2:

$$\theta = 0 \quad \text{if } K_1 + K_2 > 0 \text{ and } K_1 > 0,$$

where θ is given by the relation:

$$\sin^2\theta = -K_1/2K_2 \qquad \text{if } 0 < -K_1 < 2K_2.$$

When K_1 predominates, the anisotropy constants K_1 and K_2 are related to the anisotropy field H_A and the magnetic polarization J_S by:

$$H_A = (2K_1 + 4K_2 + 6K_3) / J_S, \tag{2.4}$$

The units for H_A is in MA/m when K_1, K_2 and K_3 are expressed in MJ/m^3 and J_S in T. To determine the experimental values of the anisotropy constants, magnetization curves measured in various directions on single crystals, needs to be performed.

The anisotropy field H_A can be determining by measuring magnetization curves with the field perpendicular and parallel to the direction of the easy magnetization, with the anisotropy field being defined as the intersection of the two obtained magnetization curves.

Magnetocrystalline anisotropy

Magnetocrystalline anisotropy can be explained in terms of the magnetization process which is different when the field is applied along different crystallographic directions (the magnetic moments are higher in one crystallographic direction than another), and it is a result of crystal-field interaction and spin-orbit coupling. A consequence of the magnetocrystalline anisotropy is the easy and hard directions of magnetization. When the magnetic moments are placed in a magnetic field, they will orient preferentially along a certain axis (easy axis). It is possible to align the magnetic moments also in a non-preferred orientation, by applying a larger field (this is so called hard axis). The magnetization curves of a single crystal show different evolutions, when it is magnetize in different directions (see figure 2.2).

Rare earth permanent magnets have one preferred direction of magnetization, which makes them easy to align in this axis and difficult to magnetize in other hard axis. This property makes them very difficult to be demagnetized, as it requires high demagnetizing fields to change the direction of orientation of the magnetization of the domains.

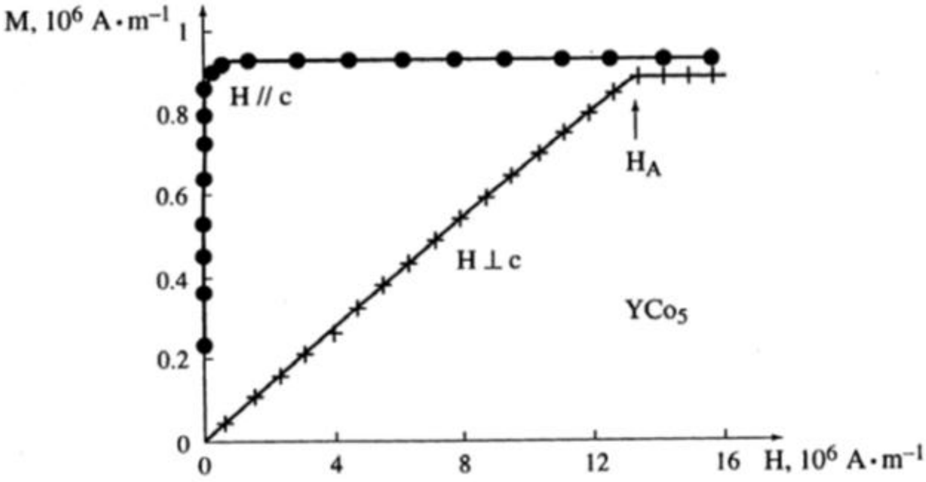

Figure 2.2: Magnetization of a crystal of the intermetallic compound YCo_5. (H∥c represent the easy direction and H⊥c represent the hard direction) **[24].**

2.2 Extrinsic magnetic properties

The extrinsic properties are the magnetic properties which describe the real properties of the magnet (determined by the microstructure) and which derive from the hysteresis loop. M-H hysteresis loops are obtained as a response of the volume-averaged magnetization M, to an external magnetic field $H_{external}$. Figure 2.3 show a typical M-H hysteresis loop.

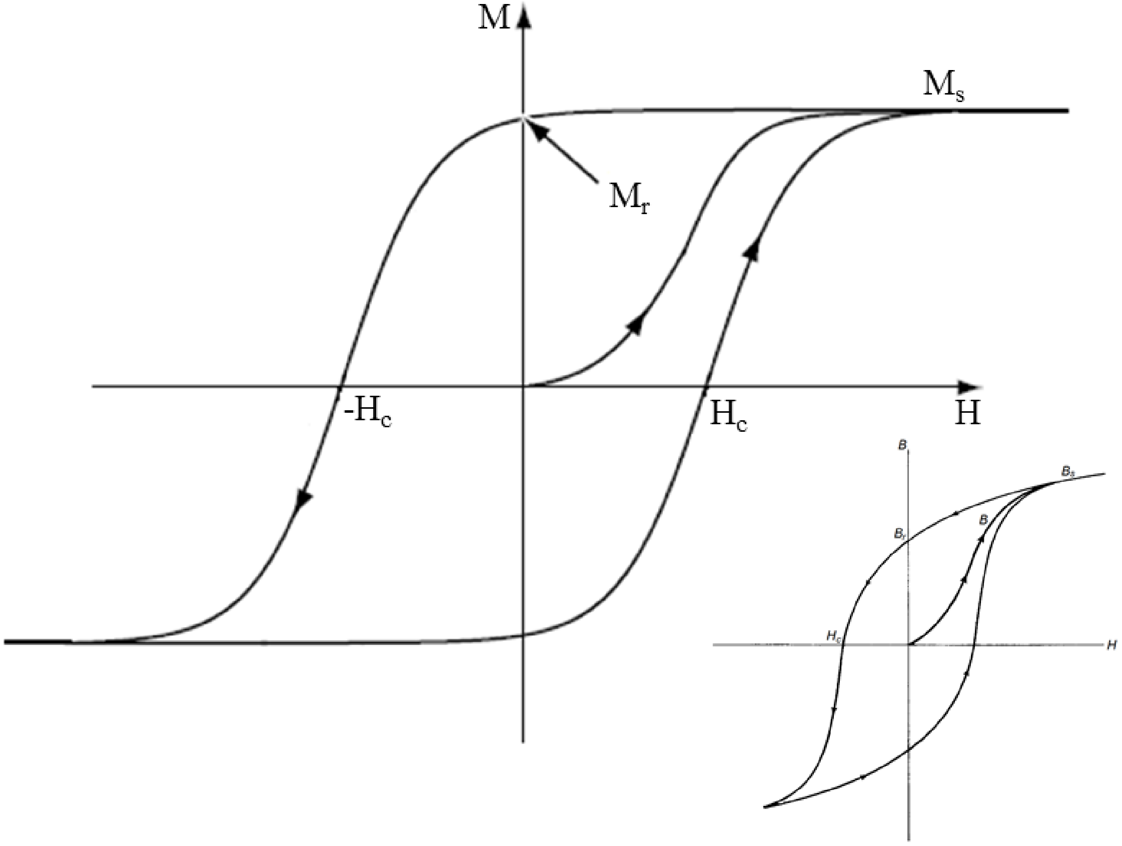

Figure 2.3: M-H and B-H hysteresis loops of a ferromagnetic material starting from the demagnetized state.

Since $B = \mu_0 H + \mu_0 M$, B-H loops show the flux density B as a function of $H_{external}$.

Two very important extrinsic properties, the coercivity H_c (or coercive force) and the remanence M_r (or remanent magnetization), derives from the M-H loops. The energy product $(BH)_{max}$ is determined from the B-H loops. Some extrinsic properties values of different magnets are shown in table 2.2.

Table 2.2: Extrinsic properties of commercial permanent magnets **[22].**

Material	Composition (appr.)	μ_0M_r	M_r	μ_0H_c	H_c	$(BH)_{max}$	$(BH)_{max}$
		T	kA/m	T	kA/m	kJ/m^3	MGOe
Magnetite	Fe_3O_4	0.15	120	0.025	20	0.75	0.1
Carbon steel	$Fe_{95}MnC_4$	1.00	800	0.005	4	1.6	0.2
Vicalloy	$Co_{50}Fe_{39}V_{11}$	0.75	600	0.025	20	7	0.9
Cunico	$Cu_{48}Ni_{22}Co_{30}$	0.34	270	0.066	53	7.2	0.9
Honda steel	$Fe_{58}Co_{34}Cr_3W_1C_4$	0.90	720	0.025	20	8	1.0
Co ferrite	$CoFe_2O_3$	0.25	200	0.065	52	9.6	1.2
Cunife	$Cu_{57}Ni_{21}Fe_{22}$	0.54	430	0.055	44	12	1.5
Lodex	$Fe_{65}Co_{35}$ in Pb	0.74	590	0.094	75	28	3.5
Mn-Bi	MnBi	0.42	330	0.330	260	33	4.1
Ba ferrite	$BaFe_{12}O_{19}$	0.43	340	0.210	170	36	4.5
Alnico 5	$Fe_{50}Co_{24}Ni_{14}Al_8Cu_2$	1.25	1000	0.064	50	44	5.5
Sr ferrite	$SrFe_{12}O_{19}$	0.42	330	0.350	275	43	5.4
Fe-Cr-Co	$Fe_{56}Cr_{25}Co_{14}V_3Ti_2$	1.35	107	0.055	44	44	5.5
Mn-Al	$Mn_{53}Al_{45}C_2$	0.56	450	0.230	180	44	5.5
Co-Pt	CoPt	0.65	520	0.450	360	73	8.8
Alnico 9	$Fe_{36}Co_{35}Ni_{13}Al_7Cu_3Ti_5$	1.12	890	0.140	110	84	10.6
Sm-Co (1:5)	$SmCo_5$	0.88	700	2.100	1700	150	19
Sm-Co (2:17)	Sm_2Co_{17}	1.08	860	1.400	1100	220	28
Nd-Fe-B	$Nd_2Fe_{14}B$	1.28	1020	1.300	1000	405	51

The hysteresis loops should be corrected by a factor called demagnetizing factor. By reducing the demagnetizing field, the hysteresis loops becomes more rectangular. After saturation has been reached, if H is reduced to zero the induction will decrease from B_s to B_r and is called residual induction. If the applied field is reversed the induction will decrease to zero when the applied field is equal to the coercivity, H_c. At this point the magnetization, M, is still positive and is given by the relation $B = \mu_0H + \mu_0M$, resulting that $M = H_c/4\pi$ for CGS units and H_c for SI units. The reverse field required to reduce the magnetization to zero, is called intrinsic coercivity, H_{ci}. If the field is further increase, the reverse saturation will be reached, $- B_s$. By reducing to zero the applied field and applying again the initial field, the induction will follow the curve and it will result $-B_r$, $+H_c$, and $+B_s$. By cycling a magnet on a loop, the magnet will be always magnetized in one direction when the field is removed. To demagnetize a magnet, it needs to be subjected to a series of alternating fields with a decreasing amplitude, resulting in smaller and smaller induction loops until it reaches the origin point. This process is known as field demagnetization. Another alternative is to heat the magnet above the Curie temperature at which the magnet becomes paramagnetic. This is known as thermal demagnetization.

Coercivity

The field at which the magnetization is reduced from remanence to zero is called coercive field, H_c. The coercive field covers a wide interval, from 1 A/m for very soft magnets (pure iron) or amorphous alloys, up to 10 MA/m for the strong hard magnets. The coercivity gives the classification of the magnets as hard magnetic material (permanent magnets), semi-hard magnetic materials (storage media) and soft magnetic materials.

According to the Stoner-Wohlfarth model the coercivity is equal to the anisotropy field. In reality the coercivity of an optimized permanent magnet is between 20% and 40% of the anisotropy field. Figure 2.4 shows the difference between the Stoner-Wohlfarth model and a typical loop. This difference is cause by the imperfections such as surface irregularities, grain boundaries and metallurgical inhomogeneities **[23]**.

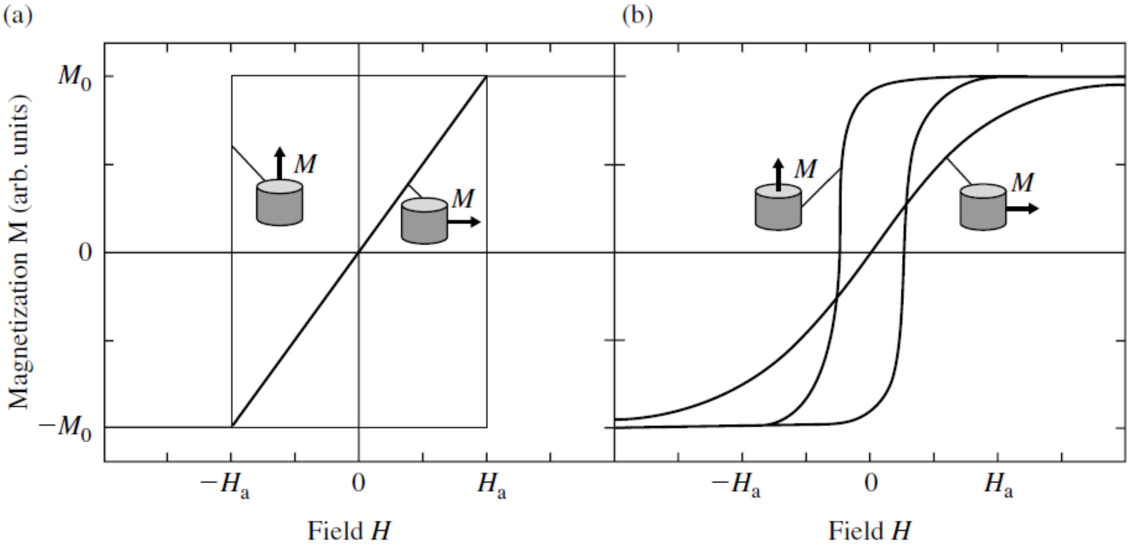

Figure 2.4: Hysteresis loops: (a) Stoner-Wohlfarth predictions and (b) typical loops encountered in practice. Both the coercivity and the loop shape are poorly reproduced by the Stoner-Wohlfarth model **[26].**

The coercivity can be defined as:

$$H_c = \alpha_K \frac{2K_1}{\mu_0 M_s} - D_{eff} M_s - \Delta H\,(T,\eta) \tag{2.5}$$

where α_K is the Kronmüller parameter, D_{eff} is a magnetostatic interaction parameter (the so-called demagnetization factor) and ΔH is the fluctuation-field contribution caused by thermal activation. The comparatively small ΔH term, means that the coercivity depends on the sweep rate $\eta = dH/dt$ **[23]**.

Two main types of mechanisms influence the coercivity, the nucleation and the pinning mechanisms. The nucleation-controlled magnets are the magnets which contain almost no defects, and the nucleation field determines the coercivity. Opposite to the nucleation type of magnets, the pinning type of magnets has many defects, and here the coercivity is determined by a lack of the domain walls motion. In the permanent-magnet materials, $Nd_2Fe_{14}B$ and $SmCo_5$, the coercivity is nucleation controlled. Permanent magnetic materials of Sm_2Co_{17} type are pinning controlled.

The coercivity of a magnetic material is affected also by the particle size. For example, the coercivity increases with decreasing of the particle size, reaching a maximum where the coherent rotation of a single domain particle is realized. Further decrease in the particle size will result also in the decreasing of the coercivity. A variation of the coercivity as function of size is presented in figure 2.5. **[25]**.

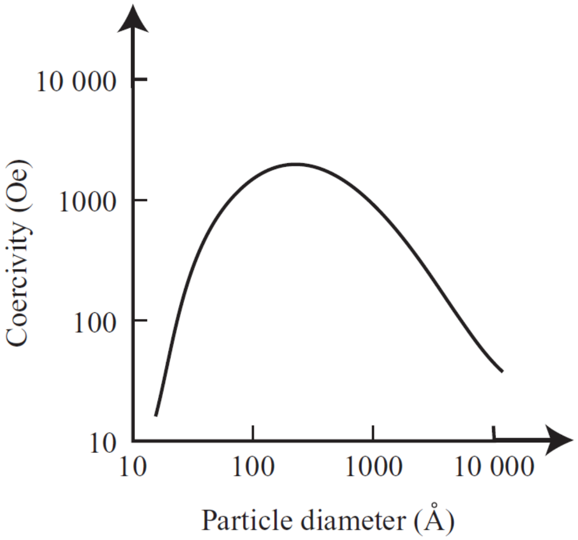

Figure 2.5: Coercivity as a function of particle size **[25].**

Remanence

The remanence can be defined as the magnetization obtained after removing of the external magnetic field that was applied to saturate a magnetic material. Different notations of the remanence, like Br, Jr or Mr are used. For particles with a relative good anisotropy, after applying and removing of a large field, the magnetization of each grain will orient the easy axis on the direction of the field. A perfect c-axis alignment is difficult to realize in practice. The remanence enhancement is related also with the degree of texture of a nano-crystalline magnet. In hard magnets is known that exchange coupling between randomly oriented grains results in remanence enhancement.

Maximum energy product

The performance of a magnet is given by its energy product. The maximum energy product, $(BH)_{max}$ is a parameter which estimates the strength of a hard magnet, and which quantify the energy density made by the magnet for external work. The maximum energy product is defined as the product between the flux density, B and the corresponding opposing field H.

The energy product is related to the B-H loops and is determined from the hysteresis loops by creating the largest square possible, as it is illustrated in the figure 2.6 and is represented by the rectangular grey shape.

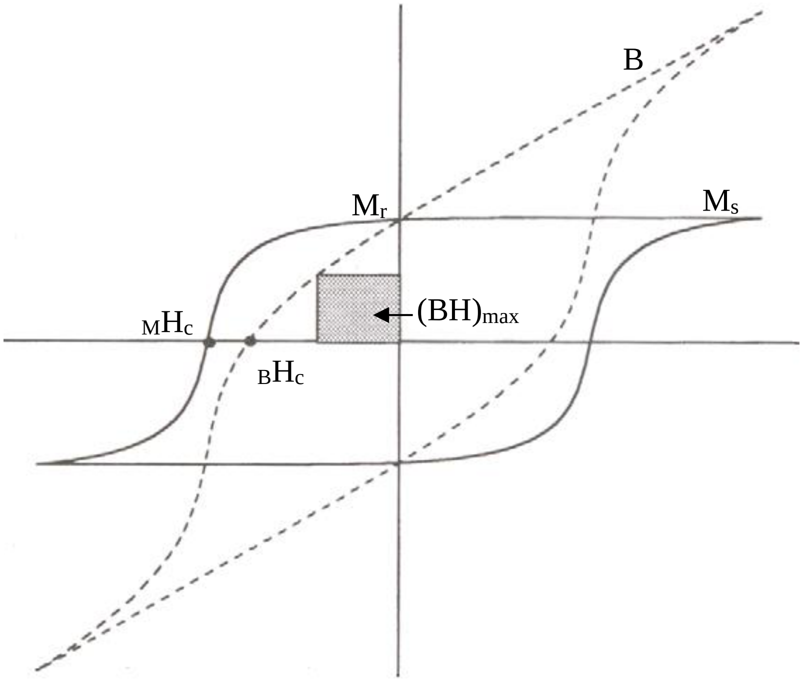

Figure 2.6: B-H and M-H hysteresis loops for hard magnets and the maximum energy product illustrated by the grey rectangle.

Typical values of the maximum energy product range between 30 - 50 kJ/m^3 (3.8 - 6.3 MGOe) for ferrites, up to 451 kJ/m^3 (56 MGOe) for sintered $Nd_2Fe_{14}B$.

2.3 Static working point

The Nd-Fe-B permanent magnets are characterized by a large resistance to demagnetizing factors. The operating point of a permanent magnet, which is part of an assembly, is changing during the time when the device is operating. The operating point of a magnet is given by the intersection of the load line with the demagnetization curve of the magnet, like in the figure 2.7.

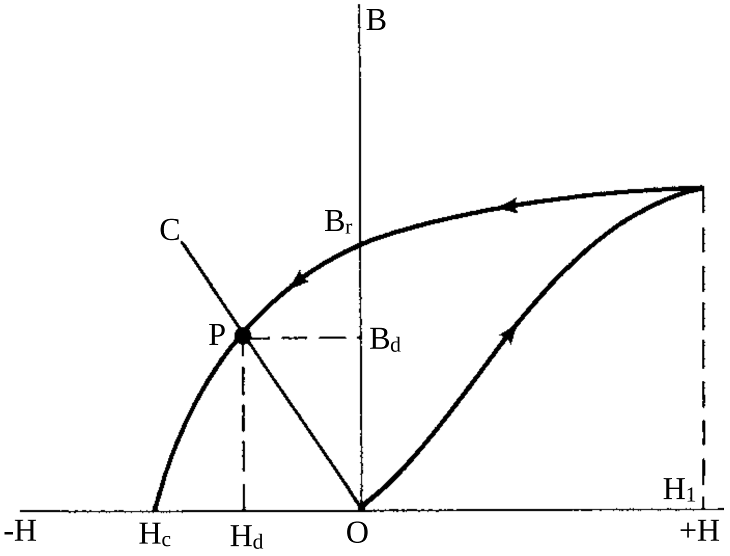

Figure 2.7: Initial magnetization and demagnetization curve of a permanent magnet. Where H_1 is the magnetization field, B_r is the residual induction (remanence), H_c is the coercivity, H_d represent the demagnetizing field, P is the working point, B_d is the induction in the magnet and OC represent the load line **[27].**

The shape of the curve along with the remanence and coercivity determine the usefulness of the permanent magnet. The slope of the load line is affected by the demagnetization factor, N_d, which depends on the geometry of the magnet. Since the operating point of the magnets depends on the slope generated by the load line, results that the operating point is affected by the demagnetization factor.

For some applications like electric motors, the magnet can be subjected to large demagnetizing fields from the currents in the windings or from magnetized soft magnetic materials. If these fields are large enough they could demagnetize the permanent magnets. In dynamic application, the operating point of a magnet is cycling along the demagnetization curve. If the intrinsic coercivity is low, the induction demagnetization curve can be nonlinear. In this condition the operating point of magnet can fall under the knee of the induction demagnetization curve and the induction is reduced irreversible (in figure 2.9 this behavior is represented by case **2**, **3**, or **4**). In the case of a high intrinsic coercivity, the induction demagnetization curve can be linear. In this situation, the induction is reversible around the operating point (case **1**). This behavior is presented in figure 2.8.

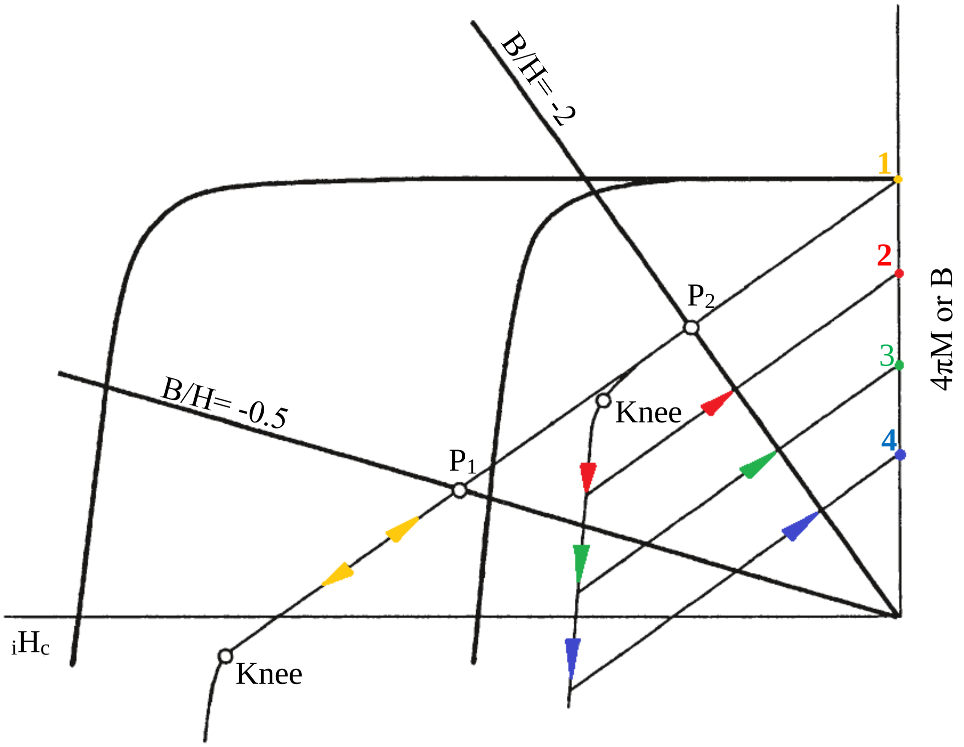

Figure 2.8: Representation of the linearity of the induction demagnetization curves **[28].**

The maximum operating temperature represents the maximum temperature limit where the induction demagnetization curve of the magnet is maintaining his linearity. So in order to increase the operating temperature, the intrinsic coercivity needs to be increased, which will result in maintaining the linearity of the inductive demagnetization curve at the required operating temperature.

2.4 Demagnetizing field

If a field is applied to a sample which has the form of a bar, like in figure 2.9, and after its removing, 2 poles will form at the end of the sample bar. In figure 2.9 a it can be seen the H lines radiating from the north pole to south pole. Both the inside and outside field liens, act from north pole to south pole and tend to demagnetize the magnetic bar. This kind of demagnetizing action of a magnetized sample affects the magnetic measurements and has a strong influence on the behavior of different magnetic materials used in many devices.

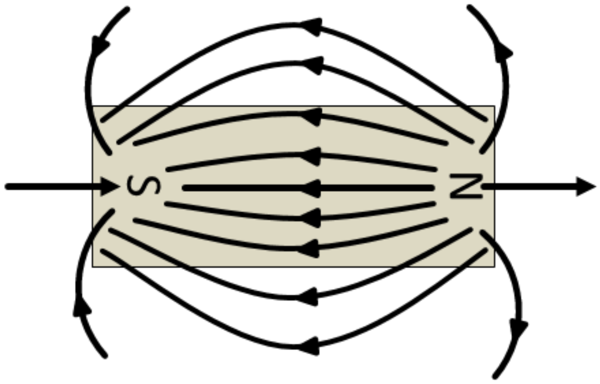

a) H field line of a magnetic sample in zero applied field

Inside the magnet

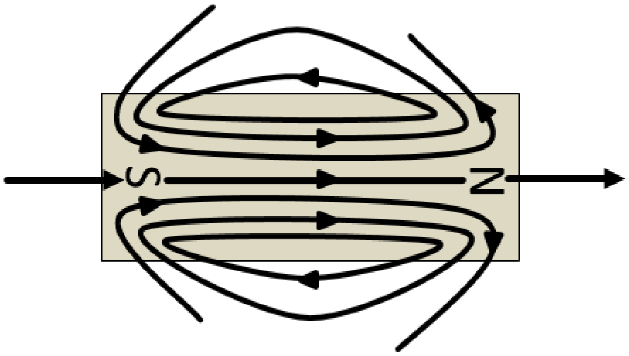

b) B field line of a magnetic sample in zero applied field

Figure 2.9: Field lines of a magnet in zero applied field.

The demagnetizing field H_d acts in the opposite direction of the magnetization, M. In the case of figure 2.9a the demagnetizing field H_d, is the only field acting and can be expressed like:

$$B = -\mu_0 H_d + \mu_0 M \tag{2.6}$$

Inside the magnet, the flux density B, is pointing to the same direction like $\mu_0 M$, but is all the time smaller than $\mu_0 M$, because the $\mu_0 H_d$ cannot exceed the values of $\mu_0 M$.

In the figure 2.9b the lines of the B field produce by the magnetic sample are continuous. Inside the magnet, the flux density lines point the direction from south to north. Outside the magnet, the flux density can be express as:

$$B = \mu_0 H \tag{2.7}$$

Since the demagnetizing field, H_d is stronger near to the poles, the flux density, B is not uniform in the entire sample and the lines diverge to the end, resulting in a weak flux density at the ends of the magnet, in comparison to the value of the flux density measured in the center of the magnet.

The non-uniformity of the induction inside of the magnet can be attributed to the shape of the sample, in this case a bar magnet. So, in order to have a uniform distribution of the magnetization, M or of the flux density B, ellipsoid can be considered. An unmagnetized ellipsoid is magnetized uniformly when is placed in a uniform magnetic field. In this situation, the uniformity of the magnetization M, or of the flux density B, can be achieved due to the uniformity through the entire volume of the demagnetizing field H_d **[27]**.

The demagnetizing field is proportional with the magnetization which creates it:

$$H_d = -N_d M \tag{2.8}$$

where N_d is the demagnetizing factor. This factor depends on the shape of the body. The sum of the demagnetizing factors along the three orthogonal axes is 1 **[29]**:

$$N_a + N_b + N_c = 1 \tag{2.9}$$

For a sphere the value of the demagnetizing factor along any diameter is 1/3 **[29]**.

The flux density drop is low in the case of the rare earth permanent magnets and most of the time these magnets are not magnetized lengthwise **[27]**.

2.5. HD and HDDR processes

2.5.1 Hydrogen Decrepitation (HD) process

$Nd_2Fe_{14}B$ alloys have the capability to reversibly absorb large quantities of hydrogen gas. The hydrogen treatments, of the Nd-Fe-B materials at room temperature and under low pressures, lead to the embrittlement and to the crumbling of the materials. This process is known as hydrogen decrepitation (HD). The absorption of the hydrogen gas is accompanied by a volume increase which leads to pulverization of the material, which if it is combined with milling results in producing of fine Nd-Fe-B particles. This was investigated and reported by Dalmas de Réotier et al. **[37]** and by Harris et al. **[38]**. By exposing Nd-Fe-B to hydrogen, at approximately 1 bar hydrogen pressure, at room temperature, absorption of the hydrogen take place, first by the neodymium rich phase from the grain boundary, which leads to the hydrogenation of the $Nd_2Fe_{14}B$ matrix phase, resulting in a particle size reduction of the cast material **[32, 39]**. A schematic view of the process is presented in figure 2.10.

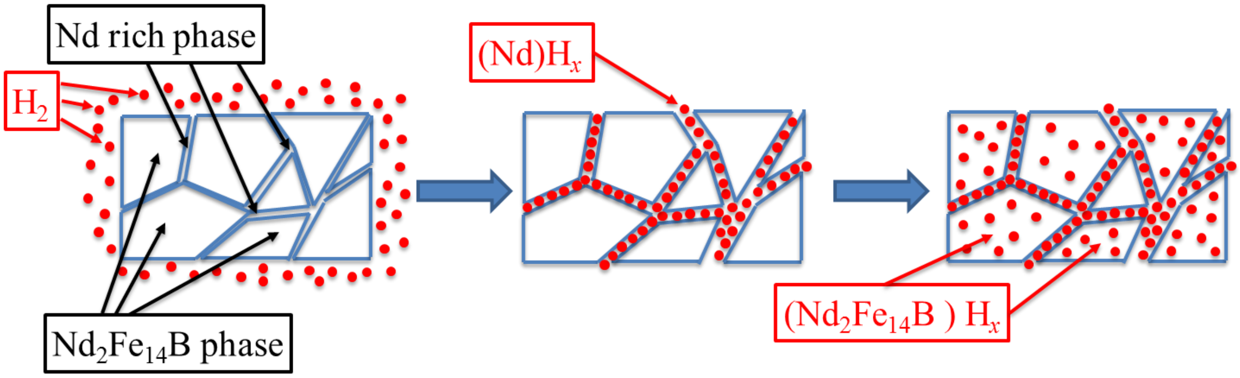

Figure 2.10: Schematic drawing of the hydrogen decrepitation process.

The hydrogen decrepitation process results in a 4.8% volume expansion for the $Nd_2Fe_{14}B$ phase and 16.4% for the NdH_3 **[40, 46, 50]**. The volume growth of the neodymium rich hydrogenated phase causes the appearance of the cracks between matrix grains. The hydrogen passes through the cracks inside the alloy and after hydrogenating the $Nd_2Fe_{14}B$ phase, transgranular cracks appears **[41]**. The expansion take place in the entire magnet forcing it to decrepitate, resulting a hydrogenated powder partially demagnetized.

Verdier et al. **[42]** studied the interaction of the hydrogen with different Nd-Fe-B based alloy containing different additives like Ga, Nb, and V. He suggested that the hydrogen absorption process is closely linked to the composition of the alloy and to the microstructure. Also the stability of the Nd-Fe-B powder depends on the proportion of the Nd rich phase. The powders completely formed from hydrides are extremely instable to air exposure, due to their preferability formation of the $Nd(OH)_3$. The addition of V reduces the stability of the hydrogenated powders, because its rises the proportion of Nd rich phase present at the grain boundary. The Ga or Co additions improve the corrosion resistance, by combining with a part of the free Nd from the grain boundary. A partially degassing of the powder at about 560 °C results in the formation of Nd and NdH_2, which are more stable, improving the time processability of the powders **[42]**.

Harris et al. **[43]** and Williams et al. **[44]** showed that the hydrogen desorption presents three stages. The first stage is at 200 °C, where the hydrogen is released by the $Nd_2Fe_{14}B$ matrix phase, follow closed by the transformation of the Nd trihydride to Nd dihydride and hydrogen at 250 °C. The Nd dihydride decomposes into Nd metal and H_2 gas at about 600 °C. Yartys et al. **[45]** further studied different rare earth hydrides and reported that the Nd trihydride starts its transformation to Nd dihydride and hydrogen at 220 °C, with the peak of the degasing reaction at 380 °C. The reaction is completed at the temperature of 450 °C. The transformation reaction of the Nd dihydride to Nd metal and H_2 gas start at the temperature of 550 °C, has his peak at the temperature of 720 °C and the reaction is completed at the temperature of 800 °C.

After the hydrogen decrepitation processing, the absorbed H_2 reduced drastically the anisotropy field of the $Nd_2Fe_{14}B$ phase from 76 kOe to 20 kOe at room temperature, and as a consequence the coercivity is reduced substantially **[46]**. To note that the hydride formation of the $Nd_2Fe_{14}B$ increases the saturation magnetization, M_s due to the increased volume of the unit cell **[46]**, the $(BH)_{max}$ is significantly reduced **[47]**, so a heat treatment is required to remove the hydrogen and to regain the magnetic properties. A totally desorption of the hydrogen can be realized during the sintering process. In order to obtain good magnetic properties, the main phase $Nd_2Fe_{14}BH_x$, should have sufficient time to allow the hydrogen desorption before reaching temperature higher than 600 °C. If the desorption of the hydrogen is not completed, the ternary hydride, $Nd_2Fe_{14}BH_x$, will disproportionated at temperature above 600 °C, into binary Nd hydride, α – Fe, and Fe_2B. During the desorption process a temperature above 600 °C from the Nd hydride will be desorbed the H_2 gas; resulting the Nd metal which will not affect the coercivity, but precipitation of the Fe and Fe_2B in the main phase, can generate nucleation centers for the domain wall which will prevent the development of a large coercivity **[32]**.

2.5.2 Hydrogenation Disproportionation Desorption Recombination (HDDR) process

An effective way to obtain anisotropic powders used for the production of the bonded magnets is by hydrogenation disproportionation desorption recombination (HDDR) process. The HDDR process represents an extension of the hydrogen decrepitation (HD) process, and starts with the hydrogenation of the $Nd_2Fe_{14}B$ phase at low temperatures, followed by the disproportionation/decomposition of the $Nd_2Fe_{14}B$ into $NdH_{2+\delta}$ + α-Fe + Fe_2B at temperature above 600 °C, then desorption of the H_2 gas from the $NdH_{2+\delta}$ and, finally the recombination of the Nd + α-Fe + Fe_2B into $Nd_2Fe_{14}B$ **[48, 49]**. Since the recombination into $Nd_2Fe_{14}B$ is a solid-state reaction, the final $Nd_2Fe_{14}B$ presents fine grains.

The HDDR process is consisted of two reactions:

$$Nd_2Fe_{14}B + \frac{1}{2}xH_2 \rightleftarrows Nd_2Fe_{14}BH_x \tag{2.17}$$

$$Nd_2Fe_{14}B + 2.7H_2 \rightleftarrows 2NdH_{2.7} + 12Fe + Fe_2B \tag{2.18}$$

The reaction (2.18) has an enthalpy, expressed per mole H_2, more negative than the reaction (2.17), but in order to take place, higher activation energy is required, because the reaction exhibits the phase separation of the $Nd_2Fe_{14}BH_x$, into grains consisting of $NdH_{2.7}$, Fe_2B and α-Fe. An essential requirement of the HDDR process is to have a process working temperature above 600 °C. Temperatures higher than 600 °C are required, for the phase transformation, because for the reaction (2.18) a long-range diffusion of the metal atoms is required **[32]**. According to Book and Harris **[39]** the disproportionation starts from the Nd-rich grain boundary, suggesting that the Nd-rich phase acts as a hydrogen diffusion path during the disproportionation reaction. These microstructural changes are summarized schematically in figure 2.11.

Further vacuum heat treatment of the disproportionated powder leads to the hydrogen desorption from the $NdH_{2.7}$ phase, resulting in the formation of the Nd metal, which recombines with the α-Fe and Fe_2B, into $Nd_2Fe_{14}B$ **[32]**. First step in the recombination process is the diffusion of Fe atoms from the α-Fe phase intro the Nd-rich phase **[50]**. In the end, the resulting powder consists of $Nd_2Fe_{14}B$ phase with much finer grains (<1 μm). The grains of the $Nd_2Fe_{14}B$ as cast alloy are quite large due to their formation by nucleation and growth from the liquid phase at high temperatures. In the case of the HDDR, the recombination reaction is a solid-state reaction which implies nucleation and growth rates much lower, leading to much finer grains. For an established composition, the dimensions of the grains can be controlled by adjusting the process parameters (temperature, time, hydrogen pressure).

A schematic illustration of the HDDR process is presented in figure 2.12. On the left-hand side of the schematic representation, the hydrogenation and disproportionation reactions take place. The right-hand side of the figure 2.12 (from 2.5 hours till the end) represents the hydrogen desorption and recombination reactions.

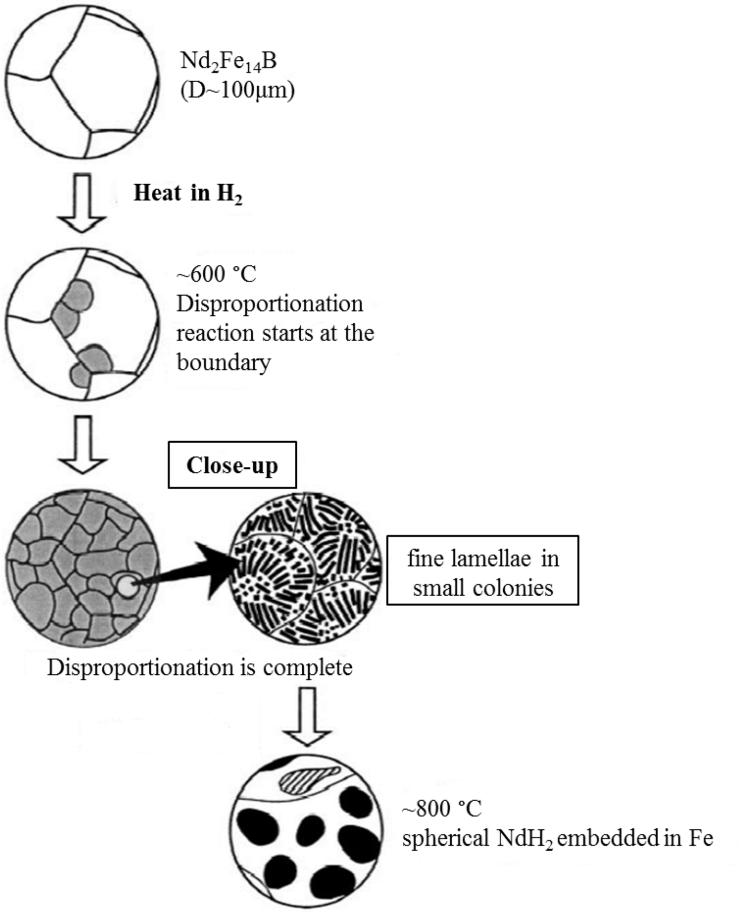

Figure 2.11: Schematic illustration of the microstructural evolution during the disproportionation reaction **[52]**.

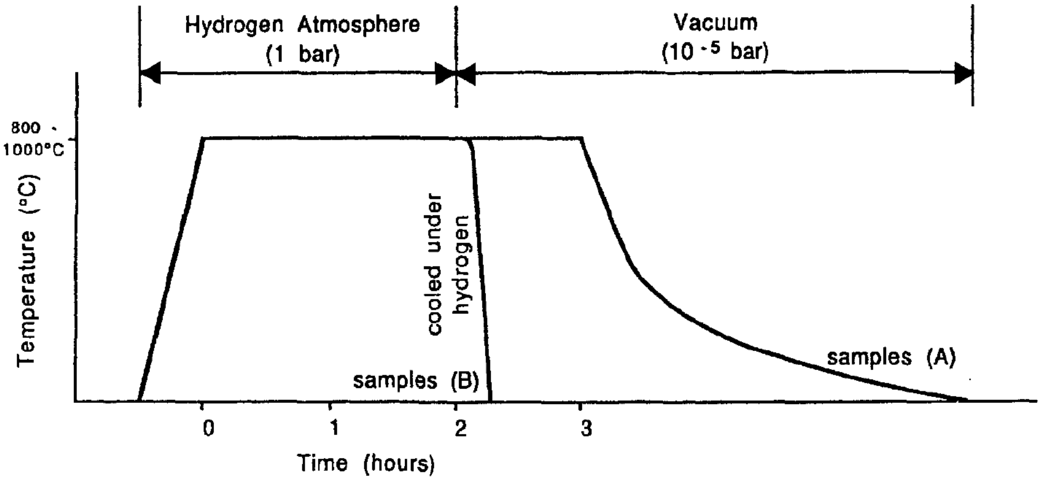

Figure 2.12: Schematic illustration of the hydrogenation disproportionation desorption recombination (HDDR) process **[51]**.

Highly anisotropic powder will result after the HDDR process, if the orientation of the original grains is transmitted to the newly created submicronic grains. This effect is known as texture memory effect. Additives like Zr, Hf, and Ga were found to introduce anisotropy to the HDDR powder **[53, 54]**. Many studies **[55, 56, 57, 58]**, showed that additions like zirconium and gallium substitutes into the Nd respective Fe sites in $Nd_2Fe_{14}B$. Therefore, no hydrogen absorption will take place during the HDDR process in those regions of $Nd_{2-x}Zr_xFe_{14}B$ grains where Zr concentration is relatively high, respectively in those regions of $Nd_2Fe_{14-x}Ga_xB$ grains where Ga concentration is relatively rich. These regions therefore do not participate in the HDDR process, and they keep their original lattice orientation, becoming nucleation centers in the recombination process **[59]**. This model been contradicted later by the model proposed by Gutfleisch et al. Additives like Co and Ga have an impact on the recombination temperature and on the time of the recombination, reducing them **[60]**. By increasing the Co content a decrease in the amount of hydrogen absorbed during the disproportionation was observed by Fujita and Harris **[61]**. Different studies made by Nakamura et al. **[62, 63, 64]**, and Sugimoto et al. **[52]** showed that a right combination of heat treatments and hydrogen pressures could eliminate the additives, and that they are not necessary to induce anisotropy to the HDDR powder. Also, Nakamura et al. **[63, 64]** had showed that additions of Co and/or Ga increase the recombination pressure. Gutfleisch et al. **[65, 66]** proposed that the orientation of the grain is given by the Fe_2B phase which will memorize the particle orientation during the disproportionation and will transfer it to the grains during the recombination stage.

Mishima et al. implemented a method where the HDDR process is composed of four different steps, while the conventional HDDR has only two steps, and they named this method *dynamic*-HDDR **[126]**. In their study the hydrogen pressure during the disproportionation step was carefully controlled and varied between 0.01 MPa and 0.1 MPa. The results suggested that by controlling the disproportionation and recombination reactions to a low rate (e.g. keeping a constant pressure of hydrogen - 0.2 MPa - during disproportionation and recombination) and at the same time completing the phase transformations, can constantly induce the magnetic anisotropy of NdFeB alloys and produce anisotropic magnet powder with excellent magnetic properties **[126]**.

2.6 Recycling by HD and HDDR

2.6.1 Recycling by hydrogen decrepitation (HD) process

Zakotnik et al. **[67] s**tudied the usage of hydrogen decrepitation process in order to recycled scrap sintered magnets. In his work Zakotnik used Nd-Fe-B sintered magnets recovered form voice coil motors of hard disk drives. The collected magnets were broken and subjected to the HD process under 1 bar hydrogen pressure. The resulted powder was sintered at various temperatures and times. The author also mentions that full density could not be obtained and that the maximum energy product of the recycled magnets was 15% smaller than that of the starting magnets.

The hydrogen decrepitation process can be used to separate and remove the magnets from hard disk drives, without disassembling or shredding of the devices. In his work, Walton et al. **[68]** used the hydrogen for the extraction of the Nd-Fe-B magnets from hard disk drives. Prior the process, the voice coil motors were separated by the rest of the hard disk drive, by cutting the corner of the hard disk drives (where the voice coil motor is localized) with an industrial cropper. The cut corners were subjected to a uniaxial pressing for the damaging of the Nd-Fe-B magnets, in order to create fresh surfaces from where the hydrogen decrepitation process will start. The hydrogen decrepitation process transforms the magnets into powder and in the same time the magnets loses their magnetization.

The demagnetized powder, resulted after the hydrogen decrepitation process can be processed in different ways:

- The decrepitated powder can be milled, aligned, pressed and sintered into new magnets.
- The powder can be subjected to further process by HDDR and after used in the production of the bonded magnets.
- The powder can be chemically processed by hydrometallurgical and pyrometallurgical routes and obtain rare earths oxides, which can be further processed to obtain rare earth elements.

Figure 2.13 gives an overview of the manufacturing route in the production of sintered rare earth permanent magnets. It is well known that Dy is less prominent in ores, so for the production of heavy rare earths, is assume to mine huge quantities of ores in order to obtain Dy **[14]**. This heavy rare earth element -Dy-, is used in the production of the permanent magnets that are integrated in applications requiring a higher operating temperature e.g. electric motors. This implies a heavy pollution of the environment and the separation of the rare earth elements is costly. Most of the time, the rare earth extraction is associated with the radioactive thorium which is part of the ore **[20]**. The recycling of the Nd-Fe-B magnets by hydrogen treatments represents a cheap route to produce new magnets, because the mining and separation of the rare earths can be skipped in this situation. The disadvantage of the recycling process is that the recycled magnets will have a composition highly dependent on the input scrap material. The magnetic properties of the recycled magnets will be influenced by the degree of oxidation of the scrap magnets and by the grade of the impurities that will be found in the composition of the recycled magnets.

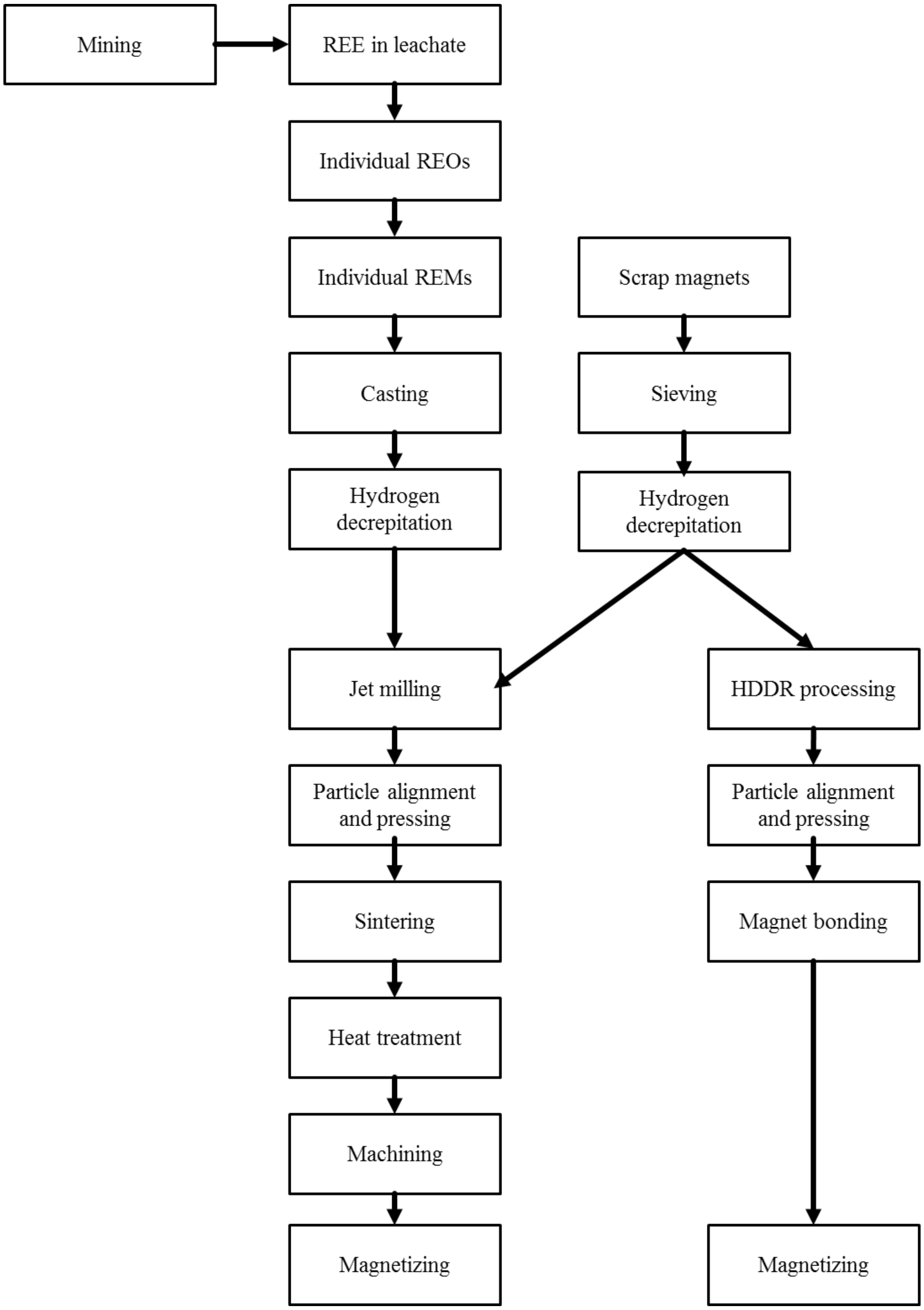

Figure 2.13: Overview of the manufacturing route in the production of sintered rare earth permanent magnets, from ore to magnet (left) and an overview of the possible re-processing/recycling routes (right). Adaptation from Buschow fig. 3.3 page 509 **[32]**

2.6.2 Recycling by Hydrogenation Disproportionation Desorption Recombination (HDDR) process

In his early work Zakotnik et al. suggested as possible route of recycling Nd-Fe-B sintered magnets: the HD and the HDDR process. In his work, Zakotnik et al. used for the HDDR process a hydrogen pressure of 0.4 bar and a temperature of 800°C, and the result was isotropic powder **[69]**.

Perigo et al. **[70]** investigate the recycling of sintered Nd-Fe-B magnets via the HDDR process. In his work the HDDR processing parameters were change in order to optimize the magnetic properties. The temperature of the recombination stage was varied between 800 and 920°C and the hydrogen pressure between 60 kPa and 150 kPa. His work resulted in obtaining isotropic powders with: J_r=0.58 T and μ_0H_c=1.15 T, obtained at a recombination temperature of 860 °C and a hydrogen pressure of 135 kPa.

In his work da Silva et al. **[71]** mixed recycled powders prepared by HDDR with commercial MQEP powders. For the hybrid magnets resulted by mixing the two powders, was reported that small addition of the HDDR recycled powder, up to 5 wt%, has no effect but further increase will deteriorate the magnetic properties of the hybrid magnet.

Gutfleisch et al. **[72]** in his work used two types of sintered magnets, one with a low concentration of additives and one with high Dy content. In his work the hydrogen pressure of the HDDR was adapted for the two types of magnet, and it is shown that for the magnet with a low concentration of additives a low hydrogen pressure (25 kPa) is required to obtain good magnetic properties. For the other magnets was shown that the Dy and Co slows the disproportionation reaction. For these magnets was shown that 70 kPa hydrogen pressure is corresponds to the completion of the recombination and at this hydrogen pressure was obtained the highest coercivity 1.9 T and a remanence of 0.63 T. As a final result, anisotropic resin bonded magnets were produced and was stated that the HDDR process can be adapted to specific composition for optimum magnetic properties.

In another work done by Sheridan et al. **[73]**, the author used HD and HDDR for scrap magnets to investigate the effect of varying the HDDR processing temperature over the temperature range of 835-930 °C. In his work the author showed that the best magnetic properties for an alloy with low Dy content (0.8 atomic %) was obtained at the temperature of 930 °C and at a hydrogen pressure of 1.5 bar, for which the remanence of the recycled magnet was 1.1 T (1.35 T was the remanence of the scrap magnet) and the coercivity of 0.8 T (1.1 T was the coercivity of the scrap magnet). To mention is that the recycled magnet was anisotropic. As an upgraded of his previous work, Sheridan et al. **[74]**, on the same magnets with low Dy content and a new composition with a higher Dy content (1.8 atomic %), studied the same behavior on the recycled magnetic properties with the increasing temperature of the HDDR process. The study shows that for the magnet with a higher Dy content, the disproportionation reaction starts and finishes at a much higher hydrogen pressure than that for the magnet with a lower Dy content. For the magnet with high Dy content the results for the remanence (0.94 T) and coercivity (740 kAm^{-1}) are lower than those of the initial scrap sintered magnet with a J_r= 1.1 T and a coercivity bigger than 1450 kAm^{-1}.

3 Experimental methods

3.1 Material selection

The thesis is devoted to the investigation of six different types of scrap magnets from devices with different usage. The scrap magnets were produced by different manufacturers. The chemical compositions of these scrap magnets are given in table 3.1.

Table 3.1: Elemental compositions of the scrap magnets/mixture of magnets (composition is given in wt%).

magnet	Fe	Nd	Pr	Dy	Gd	Ho	Co	Ga	Nb	Cu	Al	B
type 1	bal.	17.50	5.06	5.71	0.56	0.64	2.04	0.25	0.28	0.31	0.79	0.96
type 2	bal.	21.00	4.40	2.90	1.90	-	1.53	0.07	0.21	0.28	0.95	0.96
type 3	bal.	24.20	0.19	6.31	-	-	3.13	0.27	-	0.22	0.39	0.89
type 4	bal.	24.30	0.15	5.95	-	-	3.10	0.27	-	0.24	0.37	0.92
mix IT	bal.	23.60	5.32	1.08	1.03	-	0.41	0.06	0.11	0.11	0.75	1.03
mix motor	bal.	23.80	2.38	5.80	0.33	0.14	2.21	0.23	-	0.23	0.56	0.92

The chemical analysis of the scrap magnets was performed using Inductively Coupled Plasma Optical Emission Spectrometry (ICP-OES) on a PerkinElmer - Optima 8300 system.

The *type 1* and *type 2* scrap magnets are used in electric motors, produced by different manufacturers. *Type 3* and *type 4* are scrap blocks from which are cut/processed magnets used for electric motors. The magnet called *mix IT* represents a mixture of scrap magnets from loudspeakers and voice coil motors from hard disk drives. This mix called *mix IT* is composed of 38 scrap magnets from different laptop loudspeakers and 12 scrap magnets from different laptop hard disk drives. The magnet called *mix motor* corresponds to a mixture of the previous four different types of scrap magnets from electric motors. Images of the scrap magnets in their initial stage are depicted in figure 3.1.

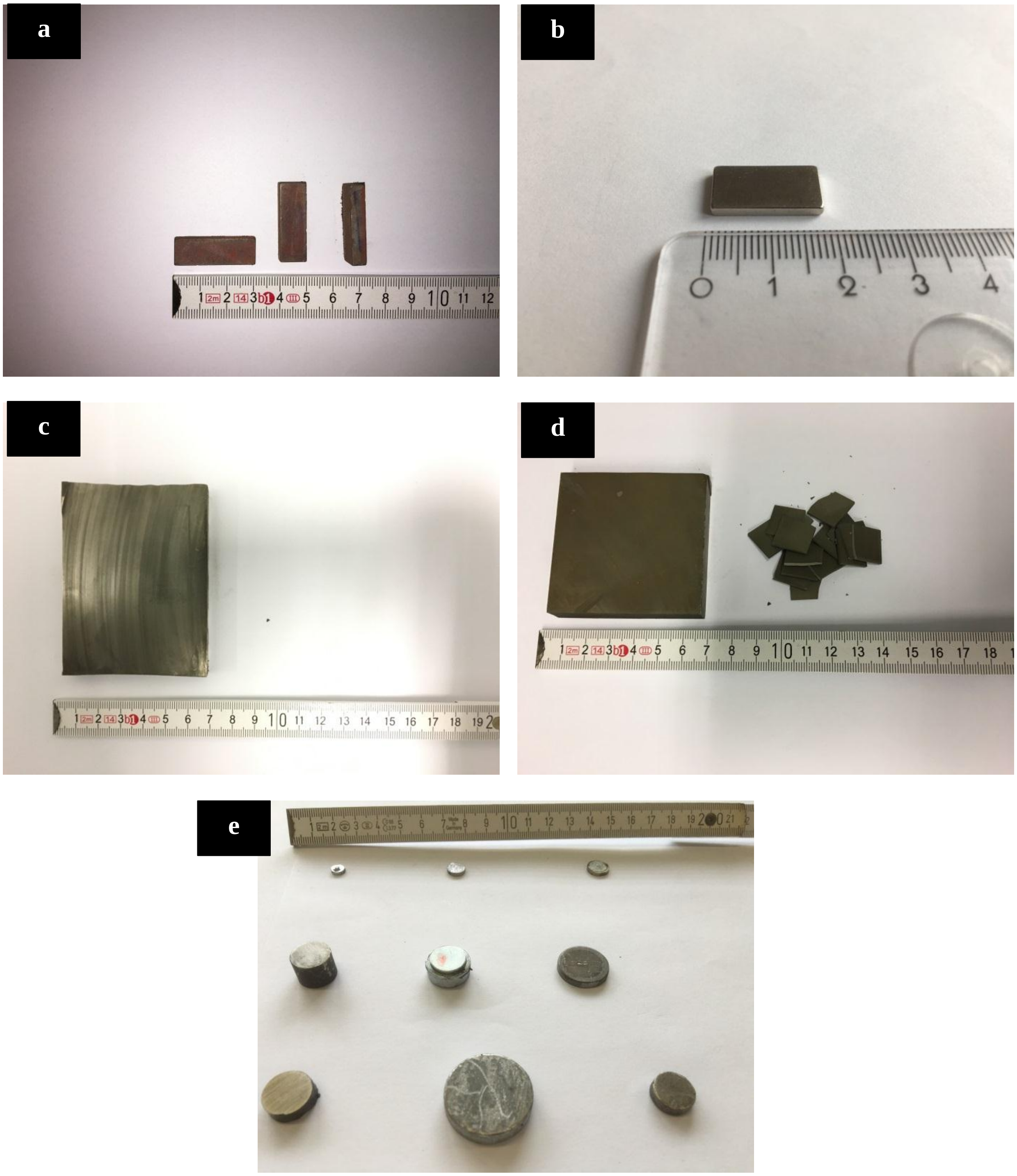

Figure 3.1: Scrap magnets in their initial form as they were received, magnets from electric motors: a) *type 1*, b) *type 2*, c) *type 3*, d) *type 4* and magnets from laptops: e) *mix IT*.

3.2 Sample preparation

Type 1 and *type 2* scrap magnets; were manually grinded with sandpaper in order to remove the coating and the oxidation layer from the surface. This creates fresh surfaces to react with the hydrogen during the hydrogen decrepitation process. The uncoated scrap blocks (*type 3* and *type 4*) were broken into small pieces using a hammer. Prior, the scrap blocks were grinded with sandpaper for removal of the surface oxidation.

All the scrap magnets used for the *mix IT* type were broken in half in order to create a fresh surface from where the hydrogen reaction will start. After the hydrogen decrepitation reaction, the powder was gently ground with a mortar and pestle, and subsequently sieved in order to remove the broken coating of the scrap magnets. Images of the prepared magnets for the hydrogen decrepitaion process are presented in the figure 3.2

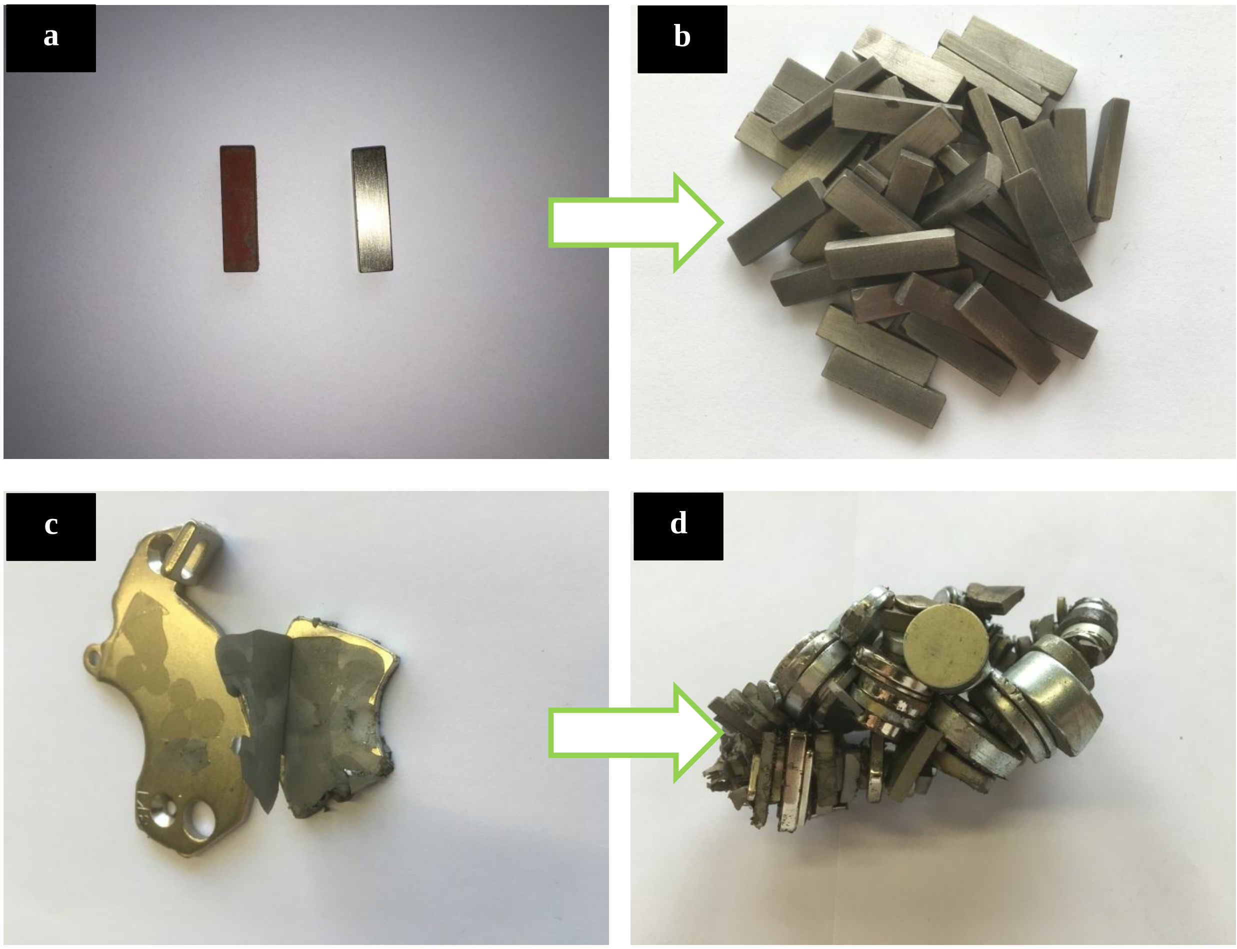

Figure 3.2: Scrap magnets prepared for the hydrogen decrepitation, with the removed coating for the magnets from the electric motors before HD process (a, b) and the coated magnets from loudspeaker and HDD in c and d images.

Due to the small size of the magnets from laptops loudspeakers and hard disk drives, the coating of these magnets was removed after the HD process.

3.3 Hydrogen Decrepitation (HD) of the scrap magnets

The hydrogen decrepitation of the scrap magnets was performed on batches of 100 g to 150 g. Such amount of sample is necessary in order to avoid an overheating of the hydrogen reactor which does not possess a cooling system. With this amount, the exothermic reaction generated by the decrepitation process, produces a relatively low overheating of the reactor, which is not threatening the seals of the reactor.

The prepared batches of scrap magnets were placed into the hydrogen reactor, which was connected to the system with a quick-fit connector as shown in figure 3.3. The system was evacuated to 10^{-1} mbar and then flushed with argon. To prevent a future oxidation of the recycled powder, this protocol was repeated three times, before filling the reactor with hydrogen up to a pressure of 1 bar. The hydrogen pressure was maintained constant for one hour, whereupon the hydrogen valve was closed. Since there is no change of the hydrogen pressure reading of the reactor manometer, this is corresponding to the end of the decrepitation reaction. To ensure that the decrepitation reaction is complete, the powder is kept under 1 bar hydrogen atmosphere, and the reactor is transferred in a safety cabinet where it is stored.

After 24 hours, the reactor is evacuated and transferred to an argon box where the decrepitated powder is handled and stored under argon atmosphere. The resulting powder was crushed in an Ar box with a mortar and pestle. Then the powder was sieved using a 40 µm mesh, in order to remove the residual protection layer.

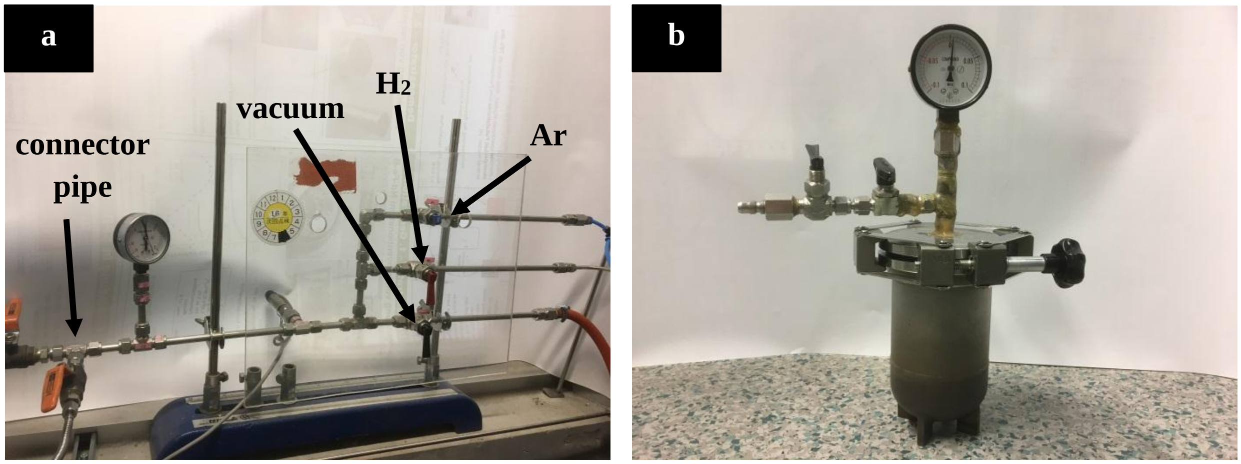

Figure 3.3: Hydrogen decrepitation system: a) reactor connections to the vacuum/hydrogen/argon b) hydrogen reactor.

3.4 Hydrogenation Disproportionation Desorption Recombination (HDDR) system and its operation

After the hydrogen decrepitation (HD) process of the scrap magnets, the powder is subjected to a hydrogen treatment at temperature above 650 °C known as hydrogenation disproportionation desorption recombination (HDDR). The entire HDDR system and the process parameters such as hydrogen pressure, temperature and desorption rate of hydrogen, are controlled via a PC. Hence the system is called dynamic-hydrogenation disproportionation desorption recombination (d-HDDR). A simplified schematic drawing of the d-HDDR system is illustrated in the figure 3.4.

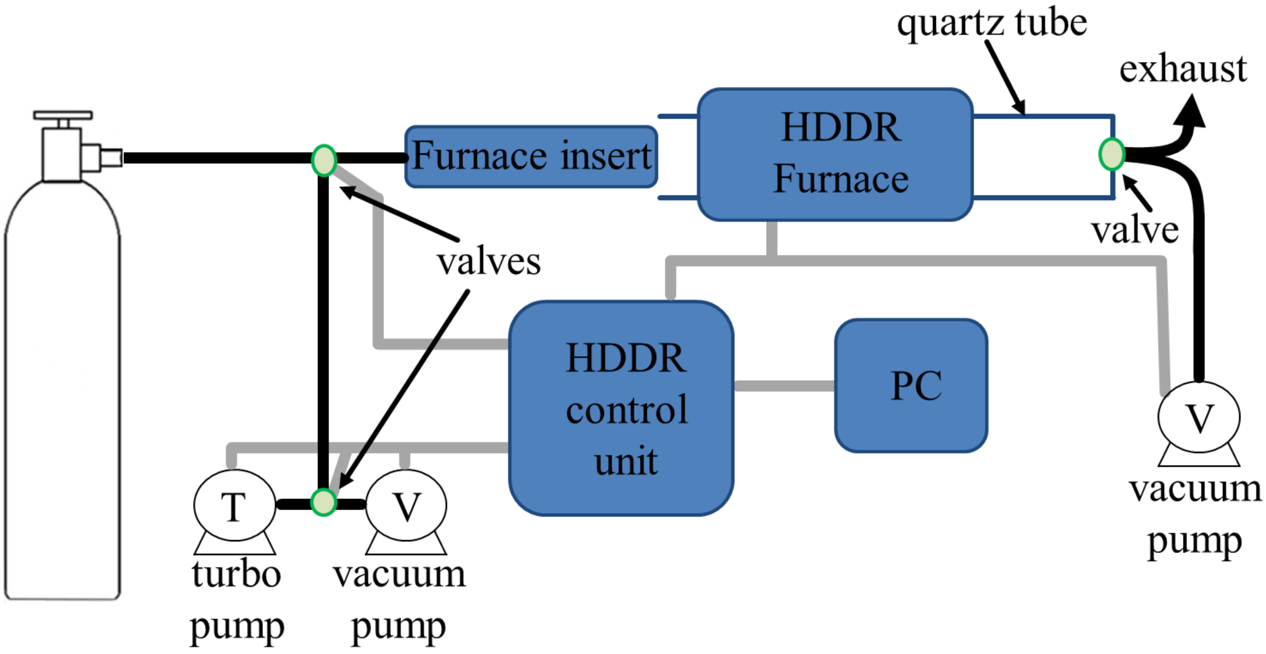

Figure 3.4: Schematic drawing of the d-HDDR system.

Batches of 6 g from the decrepitated powders are employed in the d-HDDR process. The decrepitated powder was filled in sample holder in Ar box. After filling, the sample holder is inserted in to the Inconel tube, which is connected to the HDDR furnace insert with a clamp.

After filling the HDDR insert in Ar box, the insert is transferred and connected to the HDDR furnace. The HDDR insert is introduced into a quartz tube and evacuated during the HDDR process for safety reasons.

During cooling step of the HDDR process, a nitrogen flow passes through the quartz tube and speed up the cooling of the HDDR insert and of the sample. The hydrogen pressure value is monitored by a pressure sensor, which will maintain the desire pressure value by actuating the electronic valves. The hydrogen desorption rate is maintained to the desired value via a bypass system installed before the electronic evacuation valve.

Once the sample holder is loaded and the HDDR insert is connected to the HDDR system, a pre-evacuation of the sample chamber is done. When the vacuum level reaches the value of 0.9×10^{-3} mbar, the HDDR process starts by inserting the hydrogen with the desired pressure and by starting the heating system. A schematic representation on the entire HDDR process is displayed in figure 3.5.

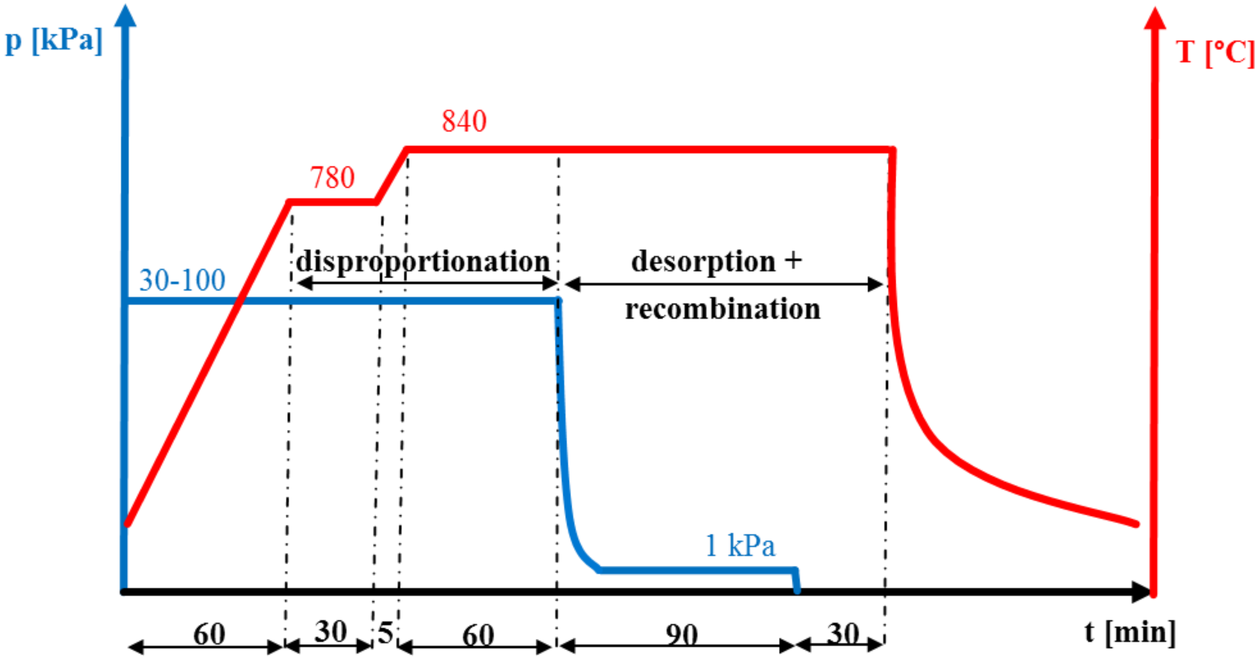

Figure 3.5: Schematic drawing of the hydrogen pressure and temperature evolution during the HDDR process.

To reach the desired temperature (780°C), a heating rate of 13 °C /min was adopted. The disproportionation reaction consists in two steps. For the first, when the processing temperature was reached, the temperature was maintained for 30 minutes. Then the temperature was raised to 840°C in five minutes, and maintained for another 60 minutes till the disproportionation reaction is complete.

The disproportionation process is followed by a recombination reaction. The recombination reaction is initiated by reducing the hydrogen pressure to 1 kPa with different hydrogen desorption rates. The hydrogen pressure is maintained at the pressure of 1 kPa for 90 minutes, whereupon the turbo pump is connected and is pumping for 30 minutes. After, the HDDR furnace is moved away to the left side, as explained in the previous sections, and a flow of nitrogen is cooling the Inconel tube till it reaches room temperature. During this time the turbo pump is connected and pumping the sample chamber.

The HDDR process parameters namely the temperature, hydrogen pressure and hydrogen desorption rate were optimized for each specific scrap magnet.

3.5 Crystallographic characterization

The HDDR powders were characterized by x-ray diffraction (XRD). XRD experiments were carried out on a Philips PANalytical powder diffractometer in reflection mode, using Co-Kα radiation with a scan step of 0.013° and an angular 2θ range from 15° to 90°. For the XRD measurements, in Ar-box the disproportionated powder was dispersed and the samples were prepared for the XRD measurements by covering the powder with Kapton foil, in order to prevent the exposure of the powder to the environment.

3.6 Microstructural analysis

For the microstructural analysis the bulk samples were bonded in a conductive epoxy resin and then ground and polished with grinding papers with different grain size (starting from 320, 400, 600, 1200, 2000 up to 4000). Afterwards for the flat, polished surface a diamond suspension with a grain size of 3 µm and 1 µm was used. As a final step it was used a neutral oxide polishing agent OP-AN.

The prepared samples were investigated using scanning electron microscope (SEM). The system used was Zeiss Merlin high resolution field emission gun (FEG) equipped with a Gemini II column. Secondary electrons was used in order to reveal the morphology of the samples and back scattering electrons coupled with element mapping for chemical elemental analyses.

3.7 Magnetic characterization

The magnetic measurements were performed on different systems. HDDR powders were measured with a PPMS-VSM (physical property measurement system) from Quantum Design. For the characterization of the bulk scrap magnets or the recycled sintered magnets, the magnetic properties were measured with a pulsed field magnetometer from Metis Instruments & Equipment and with a permagraph C – 300 (hysteresis graph) from MAGNET-PHYSICS.

For the PPMS measurements the HDDR processed powder (~50 mg) was mixed with paraffin wax and encapsulated in aluminum capsules. Then the capsules were heated to a temperature that melts the paraffin wax and a 2 T magnetic field is applied in order to align the powder particles. Afterwards the samples were fixed on the PPMS sample holder and were measured along the directions parallel and perpendicular to the orienting field. Using the assumed theoretical density of 7.5 g/cm^3 of the Nd-Fe-B materials, the specific magnetization values measured were converted to polarization. A demagnetization factor of 1/3 was considered for the measured samples.

To be able to measure the bulk samples using a closed loop system the sample needs to meet the requirements of the permagraph/hysteresis graph. In this case the samples should have parallel flat faces with at least 2 mm in depth and a maximum diameter of 26 mm in order to fit on the compensated surrounding coil of the system. The maximum field that can be reached with this system is 2.1 T. For the magnets with coercivity larger than 2.1 T, the measurement technique used was the pulsed field magnetometer, which can reach a field of 7 T. In this case like in the PPMS measurements, the magnetic measurements are in open circuit. In the case of the measurements in open circuit, the problem is to correct the values of the applied field H_a, to values of the real field H_{real}, by subtracting the values of the demagnetizing field H_d, as described by the relation:

$$H_{real} = H_a - H_d \quad (3.1)$$

where $H_d = N_d M$ and N_d is the demagnetizing factor of the sample.

For the measurements done with the pulsed field magnetometer this correction is made directly by the software of the device.

3.8 Magnet preparation from recycled powder

The obtained powders after the HDDR processing route were subjected to different sintering processes. After the HDDR process, the powder was ground using a pestle and mortar and prior the sintering step, the powder was sieved to a granulation up to 40 µm.

Using a system composed of an electromagnet and a hydraulic press, the resulting powder was placed in a press form made of hardened steel. The powder was aligned in a magnetic field of 1.6 T and then using the hydraulic press, the powder was pressed up to a pressure of 260 MPa. The obtained green compact was subjected to conventional vacuum sintering for one hour in a Carbolite split tube furnace.

For the fast sintering process, a spark plasma sintering (SPS) system was used. The system used was Spark Plasma Sintering Furnace type HP D 25 produce by FCT Systeme GmbH. With this system it was possible to reach high and precise heating and cooling rates. The same powder obtained after the HDDR process and sieved to a granulation up to 40 µm was employed. For this fast sintering the powder was placed in a graphite die and the die was placed in a magnetic field of approximately 1.6 T to orient the powder. After the alignment of the powder the die was carefully transferred and placed in the SPS furnace. For the sintering process the goal was to keep the powders at high temperature as less as possible in order to avoid an excessive grain growth. For this reason, the powder was heated to the desired temperature in 10 minutes. After reaching the desired temperature, the sintering temperature was kept for 10 minutes and then the samples were cooled to room temperature in 10 minutes. The entire sintering process was done under a pressure of 39×10^6 Nm^{-2} (39 MPa) in vacuum.

For both sintering processes (traditional sintering and SPS), the preparation, the filling of the press form/die, the orientation of the powder, and the pressing of the powder was done under inert gas, in this case argon.

3.9 DTA

The differential thermal analyses were performed on a homemade device. The analyses were performed under 1 bar hydrogen pressure or continuous pumping, under continuous heating from room temperature up to 900 °C, with a heating rate of 10 K/min. For each experiment was used the same amount of powder (1 gram). First the powder was heated under continuous pumping up to 350 °C. When the temperature was achieved, the heating source was switched off and the powder was let to cool down to room temperature. As a second proceeding, when the powder reached the room temperature, hydrogen was inserted into the sample chamber and the powder was heated up to 900 °C. This will show the interstitial absorption of the hydrogen and the disproportionation reaction. When the temperature was achieved, the powder was let to cool down with the oven to room temperature. As a final proceeding, the powder was heated up to 900 °C under continuous pumping, and when the temperature is achieved, the oven supply was cut. This will show the hydrogen desorption and recombination reactions.

3.10 ICP-OES and light elements

The chemical composition of the scrap magnets was determined using inductively coupled plasma optical emission spectrometry (ICP-OES) system (PerkinElmer - Optima 8300). For the individual electric motors scrap magnets, samples of 100 mg were cut from the bulk scrap material while the two mixtures, were samples in powder form (100 mg) after the HD process. ICP-OES measurements were performed after a complete dissolution in an acid mixture of HCl and HNO_3. Prior the ICP-OES measurements, the magnets coating was removed.

Light elements, like oxygen and carbon, were quantified using two LECO devices (LECO 836 Series for the determination of the oxygen/nitrogen/hydrogen and LECO 844 Series for the determination of carbon/sulfur). Bulk or powders samples of 100mg each were analyzed.

4. Results and discussions

This thesis treats different aspects of the recycling process of different scrap sintered Nd-Fe-B magnets using different low and high temperature hydrogen treatments. The entire content of the results is schematically illustrated in figure 4.1. The main challenges of the magnet recycling from waste electric and electronic equipment, are that the magnets are present in small quantities in electronic equipment components. They are often embedded and glued in place within the products, have a protective coating layer of nickel, copper or zinc, and they are magnetized making their extraction and recycling difficult. However, when extracted, Nd-Fe-B magnets can be directly re-used or recycled to regain the magnet alloys for the production of new magnets. Although the rare-earth content of different end-of-life electronic products such as HDDs have been estimated previously **[77]**, a real-life survey of rare earth identification in various streams of waste electric and electronic equipment plants has not been carried out. The first part of the chapter presents a study made on different streams of waste electrical and electronic equipment in order to localize, identify and collect rare earth permanent magnets, that are, Nd-Fe-B, study realized at a big recycling plant.

The focus of the work was: i) to adapt the hydrogenation disproportionation desorption recombination (HDDR) process to recycle Nd-Fe-B sintered magnets of different composition, containing various kinds of additives, ii) to sinter the Nd-Fe-B magnets from recycled materials of different qualities and iii) to have a comparative multi-scale characterization of recycled magnets. For this, collected scrap permanent magnets were prepared for the hydrogen decrepitation process and for the HDDR process. My work consisted in the development and optimization of the recycling process, for the $Nd_2Fe_{14}B$-based sintered magnets scrap from electric motors and electronic devices. In this section a detailed description of the adjustment of the HDDR processing parameters (hydrogen pressure, processing temperature and hydrogen desorption rate) is described. Afterwards, in order to clarify different aspect of the HDDR process, a different study made on as cast Nd-Fe-B alloys with different Dy content was undertaken. Here the results on the investigation of the impact of the Dy content on the HDDR processing parameters were presented. The two-step hydrogen treatment route was employed to process the scrap magnets allowing to obtain submicron crystalline textured powders (see figure 4.37 and figure 4.59) that were further used for the fabrication of recycled magnets. Next the recycled HDDR powder was bonded and sintered by different methods – traditional sintering and spark plasma sintering – in order to obtain bulk recycled magnets. Beside the adjustment of sintering process for the obtained recycled magnets a comparative multi-scale characterization by different means was performed. Following, in the last section, the obtained HDDR powder is mixed with different new powders (row materials) in order to improve the magnetic properties of the recycled magnets. The oxygen content of the recycled magnets was carefully investigated after each step of the recycling process. This magnet-to-magnet recycling process is highly attractive in terms of materials costs and ecological impact.

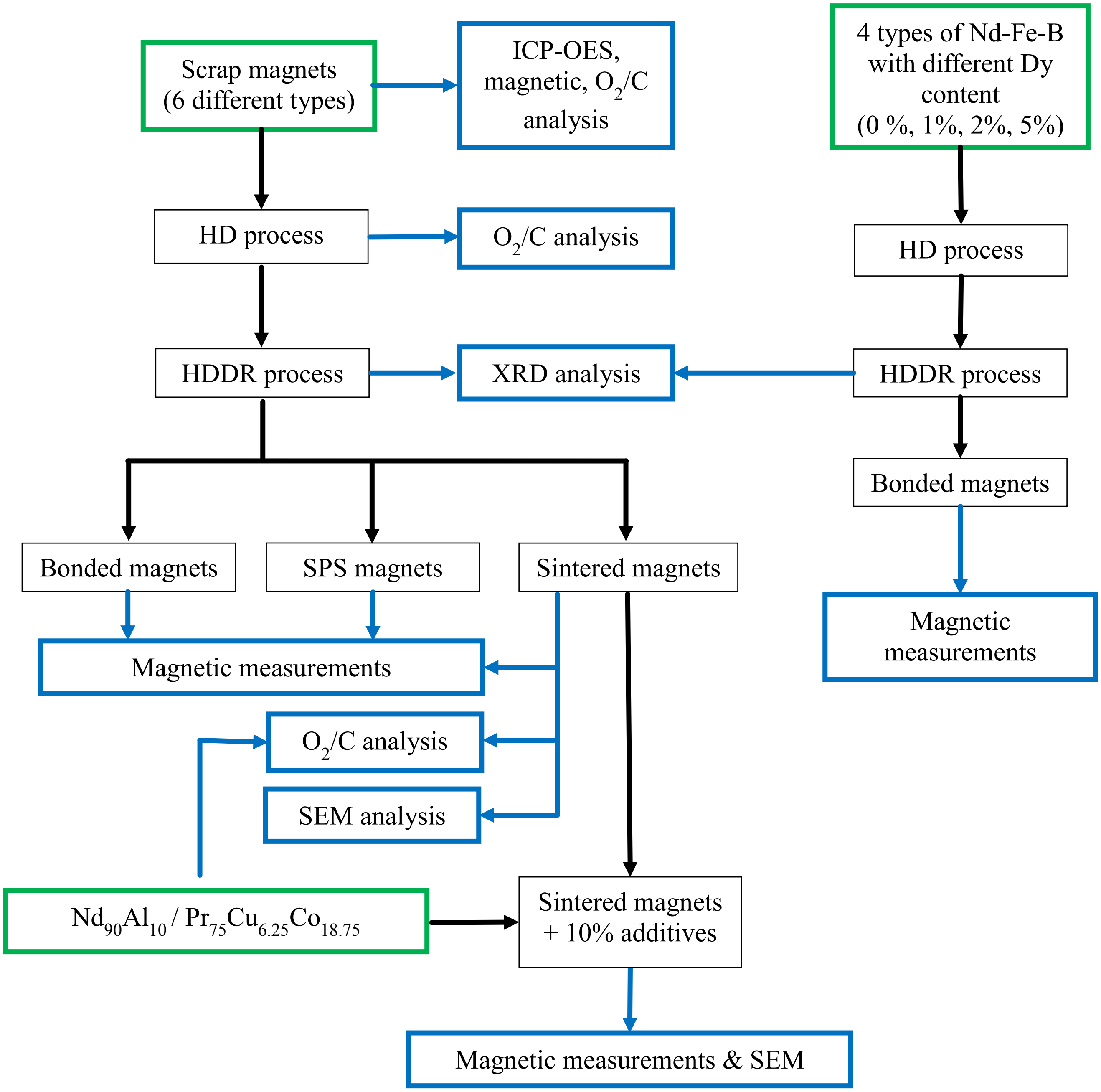

Figure 4.1: Schematically illustration of the content of the results and discussion chapter.

4.1 Localization, identification, and recovery of rare earth permanent magnets from waste of electrical and electronic equipment

The works for this part were performed at the recycling company Stena Technoworld, Halmstad, Sweden as a case study representing a large recycling company in Western Europe (see further details in figure 4.2). At Stena Technoworld, over a period of five weeks, Mai - June 2015, different waste of electrical and electronic equipment (WEEE) streams were analyzed and products were dismantled to localize and identify Nd-Fe-B magnets. Since the study was performed in the spring of 2015, the following presented results e.g. chemical composition of the magnets or the localization of the rare earth permanent magnets may be different at the time when the thesis is read, or in the next years.

The total inflow of WEEE is approximately 1000 tons per month, of which 750 tons comes from Sweden and 250 tons (only CRT and flat screen TVs) from Denmark. The first treatment at the WEEE recycling plant is the sorting and depolluting, where the objects containing hazardous waste are removed manually. Batteries, mercury, PCB-containing capacitors, lead and asbestos are examples of hazardous waste that are removed. LCD screens are dismantled due to their lead-containing lamps, and CRT screens because of their lead glass.

During the dismantling other constituents such as circuit boards, aluminum parts and copper coils are also plucked out and sorted. Non-hazardous products are sorted depending on their main constituent, such as loudspeakers being sorted into a wood fraction, vacuum cleaners and microwave ovens into a plastics fraction. Small electronics such as mobile phones and electric toothbrushes are sorted into a separate stream. Most of the material is shredded and then separated using various techniques in what is called the PMR (Precious Metal Recycling) process, and PRC (Plastics Recycling Center). The process ends up with the following fractions, the products at the WEEE recycling plant, which are sold to their costumers: ferrous, copper, aluminum, circuit boards, precious metals and copper, recyclable plastics, brominated plastics, and other.

This study is focused on the first treatment, in order to identify the streams that has the potential to become valuable secondary resources for recycling of Nd-Fe-B magnets. Various WEEE appliances were disassembled using screwdrivers, cutting pliers and a hammer. Each extracted magnet was demagnetized by heating to 350 °C in a muffle furnace, and the surface was then ground in order to remove the protective coating layer. A portable XRF device (Thermo Scientific Niton XL3t) was used to determine the chemical composition of the collected scrap magnets. Americium-241 isotope was used as the X-Ray generating source, since it permits distinguishing between REEs such as neodymium, dysprosium and praseodymium. The rare earth content, total and individual, was of particular interest.

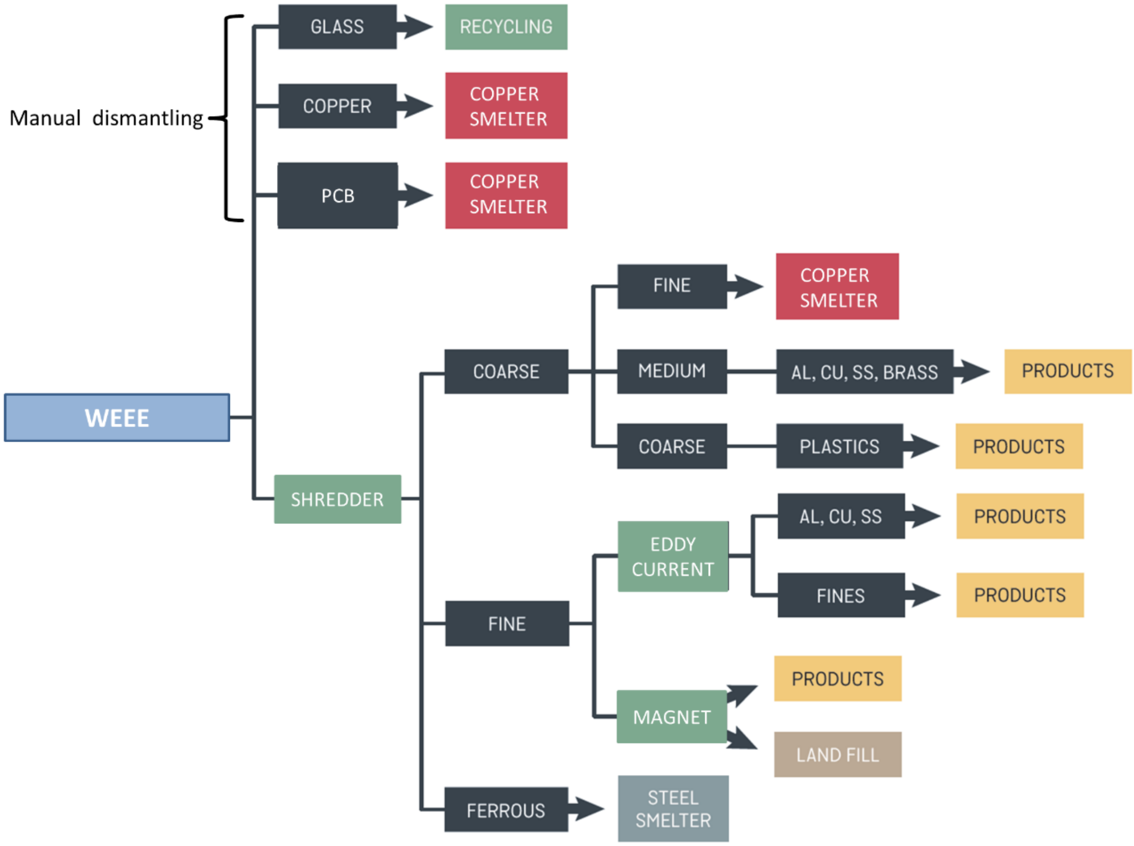

Figure 4.2: Schematic illustrations of the selection and recycling process developed at Stena Technoworld's recycling plant.

According to the European directives the electrical and electronic equipment can be divided in the following types: large household appliances; small household appliances; IT and telecommunication equipment; consumer equipment and photovoltaic panels; lighting equipment; electrical and electronic tools (with the exception of large-scale stationary industrial tools); toys, leisure and sports equipment; medical devices (with the exception of all implanted and infected products); monitoring and control instruments; automatic dispensers **[75]**.

The aim of this work was to cover in my study the devices, which may contain Nd-Fe-B magnets. For this purpose, the following devices were chosen from the different categories for disassembling and analysis:

1. Large household category: *microwaves, electric fans and air conditioner appliances;*

2. Small household appliance: *vacuum cleaners (including handhold and smaller dimensions vacuum cleaners);*

3. IT and telecommunication equipment: *printers and copying equipment, pocket calculators, mobile telephones, desktop computers, minicomputers, laptops, notebook computers, notepad computers;*

4. Consumer equipment and photovoltaic panels: *radio sets, television sets and video cameras;*

5. Electrical and electronic tools: *power tools including drills, saws, and screwdrivers;*

6. Toys, leisure and sports equipment: *small electric toys with electric motors, electric scooters;*

7. Monitoring and control instruments: *alarms*.

The selection principle of the previous presented and analyzed devices was based on the held knowledge and of the probability that the device will integrate permanent magnets in his construction.

4.1.1 WEEE fraction containing Nd-Fe-B magnets: Laptops, loudspeakers

From the IT and telecommunication equipment category, appliances such as computers, printers and copying equipment and cellular telephones were analyzed. Laptops, notebooks, minicomputers and notepads are some of the most valuable secondary resources as they contain many critical metals such as gallium, indium, platinum-group metals (PGM's), cobalt and rare earth elements.

An obvious stream that contains Nd-Fe-B magnets is hard disk drives (HDDs), which have been studied thoroughly and identified as an important secondary resource for the rare earth permanent magnets by many authors **[76, 77, 78, 79]**. HDDs contain between 1 g and 30 g of Nd-Fe-B sintered magnet depending on the size of the drive **[80].** Habib et al. **[79]** tracked the REEs during shredding and further separation of hard disks in a WEEE recycling plant in Denmark and found that 90 % of the Nd-Fe-B magnets got stuck to various ferrous parts of shredder and other equipment. Instead it was suggested to remove the magnets before shredding. However, the magnets are often present in small quantities in electronic equipment components, they are often embedded and glued in place within the products, often provided with a protective coating layer, and of course they are magnetized. These are all things that make their extraction and recycling difficult.

At Stena's recycling plant, an amount of circa 2,500 kg of HDDs is separated and collected every month. An estimation based on an average HDD weight of 544 g and an average 2.6±1.5 wt.% Nd-Fe-B per HDD **[80]**, this adds up to between 27.5 and 102.5 kg Nd-Fe-B per month that could be recycled. Since HDDs have been investigated thoroughly by many authors, this study focusses on other potential Nd-Fe-B resources in electronic waste.

Laptops are manually disassembled at Stena Technoworld. Lithium ion batteries are collected separately for recycling and safety reasons, circuit boards and the screens are also taken out and sorted. Apart from the hard disk drives, Nd-Fe-B magnets were found in the loudspeakers in all laptops that were disassembled in this study. The laptop loudspeakers can be easily dismantled/collected as they are present mostly beneath the laptop screens (which are removed from the laptop body at Stena Technoworld) or just under the keyboard, and can easily be plucked out. Figure 4.3 exemplify location/position of the loudspeaker in laptops. Normally only a few screws needed to be unscrewed before the speakers or speaker assembly could be plucked out. The speakers were usually found inside a plastic casing that had to be broken to reach the speaker. The speaker itself most of the time contained one magnet and sometimes two magnets together with one or two discs made of iron and zinc, inside a yoke. The Nd-Fe-B magnets are coated with a Zn layer.

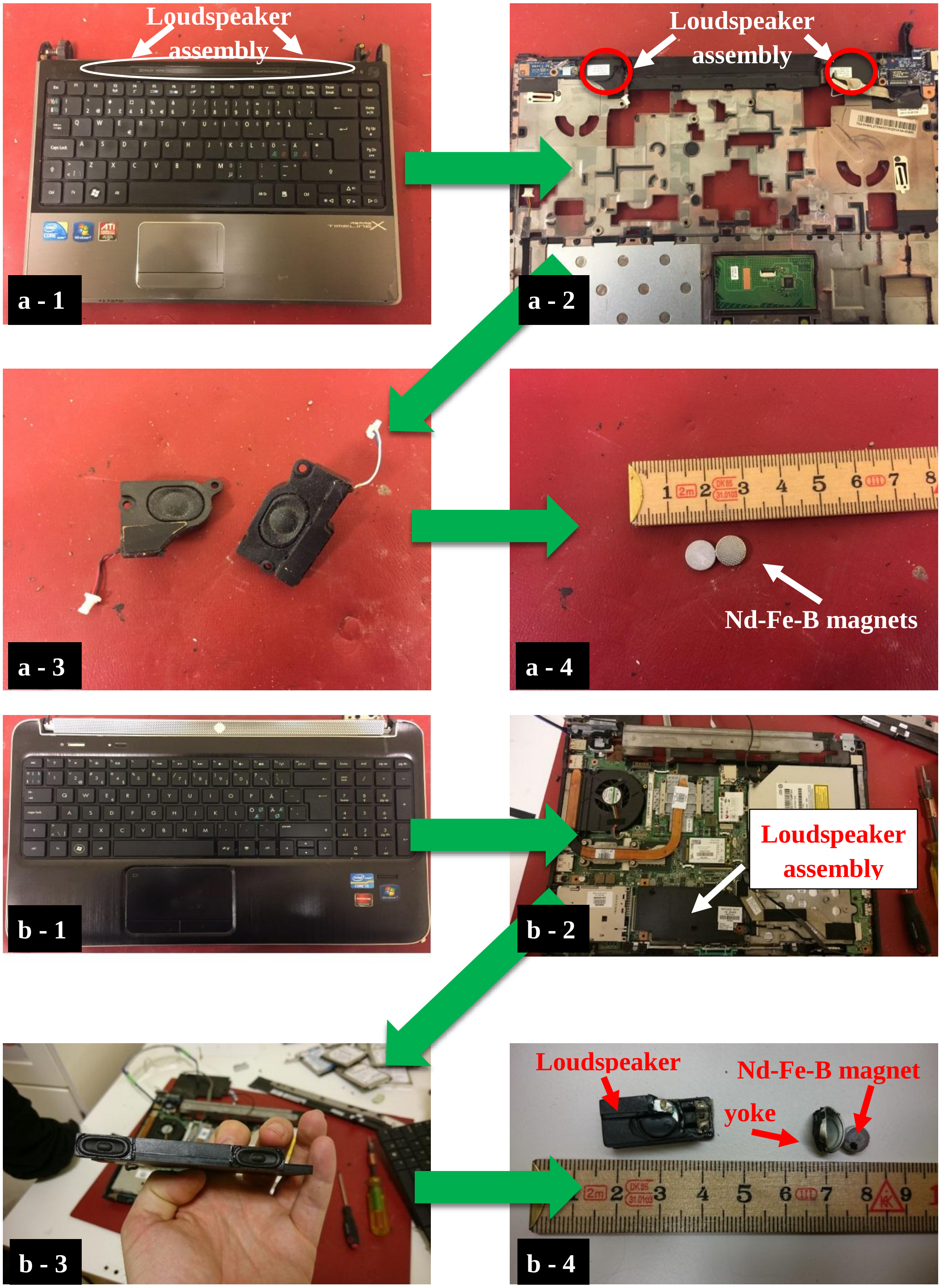

Figure 4.3: Possible location of the loudspeakers in laptops: (a: 1-4) beneath the laptop screens or (b: 1-4) under the keyboard.

The market for the laptops is very broad, from larger high-performance gaming laptops to small ultra-mobile laptops. Table 4.1 provides a summary of the evolution of the laptop loudspeaker magnets. The weight of the magnets represents a mean of the studied laptops that were produced in the same year.

Table 4.1: Magnets mass of the laptop loudspeaker.

Year	No of studied laptops	loudspeaker magnets mass [g]
1997	1	1.0
1998	4	2.4
2002	5	1.5
2003	5	1.4
2004	1	1.9
2005	1	0.9
2007	5	2.4
2008	5	2.3
2009	4	2.0
2010	5	1.3
2011	5	1.2
2012	5	1.4
2013	3	1.1

For a more precise content of the elements, which are present in the collected magnets from laptops loudspeakers, 4 magnets were selected randomly and for these magnets, ICP-OES measurements were performed after a complete dissolution in an acid mixture of HCl and HNO_3. Prior the ICP-OES measurements, the magnets coating was removed. The typical chemical composition of the magnets is presented in the Table 4.2.

Table 4.2: Elemental analysis by ICP-OES of randomly selected magnets from laptops loudspeakers.

	Fe wt%	Nd wt%	Pr wt%	Dy wt%	Co wt%	Nb wt%	Gd wt%	Cu wt%	Al wt%	Ga wt%	Zn wt%	B wt%
Sample 1	64.91	22.92	7.47	0.19	0.37	0.09	0.06	0.19	0.54	0.20	0.58	0.84
Sample 2	66.43	24.18	4.42	2.75	0.03	0.03	-	0.05	0.54	-	0.86	0.94
Sample 3	62.96	24.75	8.02	0.26	0.03	0.05	0.16	0.05	0.96	-	0.55	1.03
Sample 4	65.06	21.69	6.75	3.44	1.34	0.02	-	0.19	0.59	-	0.02	1.01

The present study reflects two main trends: the Dy content of the magnets systematically decreased over the years, that is, from 1997 onwards. Dy was completely removed starting with 2012, that is, in the very aftermath of and in reaction to the rare earth crisis. In fact, during the 2010/2011 crisis, particularly the price of neodymium and dysprosium increased drastically. In this time, the price of neodymium and dysprosium were approximatively two times and ten times, respectively, higher than that of praseodymium. Over the time period, also the neodymium content decreased. It can be also observed that the Pr content is increasing over the years. This can be explained by the fact that small amount of Nd is substituted with Pr, in order to allow the use of didymium (a mixture of Nd and Pr) in the magnet manufacturing process, reducing slightly the production cost. The evolution of the Dy, Pr, and Nd over the years is presented in the figure 4.4. The year represents the laptop released year, corresponding to the magnets from which were extracted. The content of the rare earths in wt% represents a mean of the studied magnets from laptops loudspeakers that were produced in the same year. Sample size: 5 laptops for each year, except the years 1997, 2004 and 2005 with 1 laptop; 1998, 2009 with 4, and 2013 with 3 laptops, were studied, for the missing years no laptops were studied. The price of the Dy, Pr, Nd represents the FOB China metal 99 % prices. The source for the metal prices is www.metal-pages.com and was last seen in 5 October 2017.

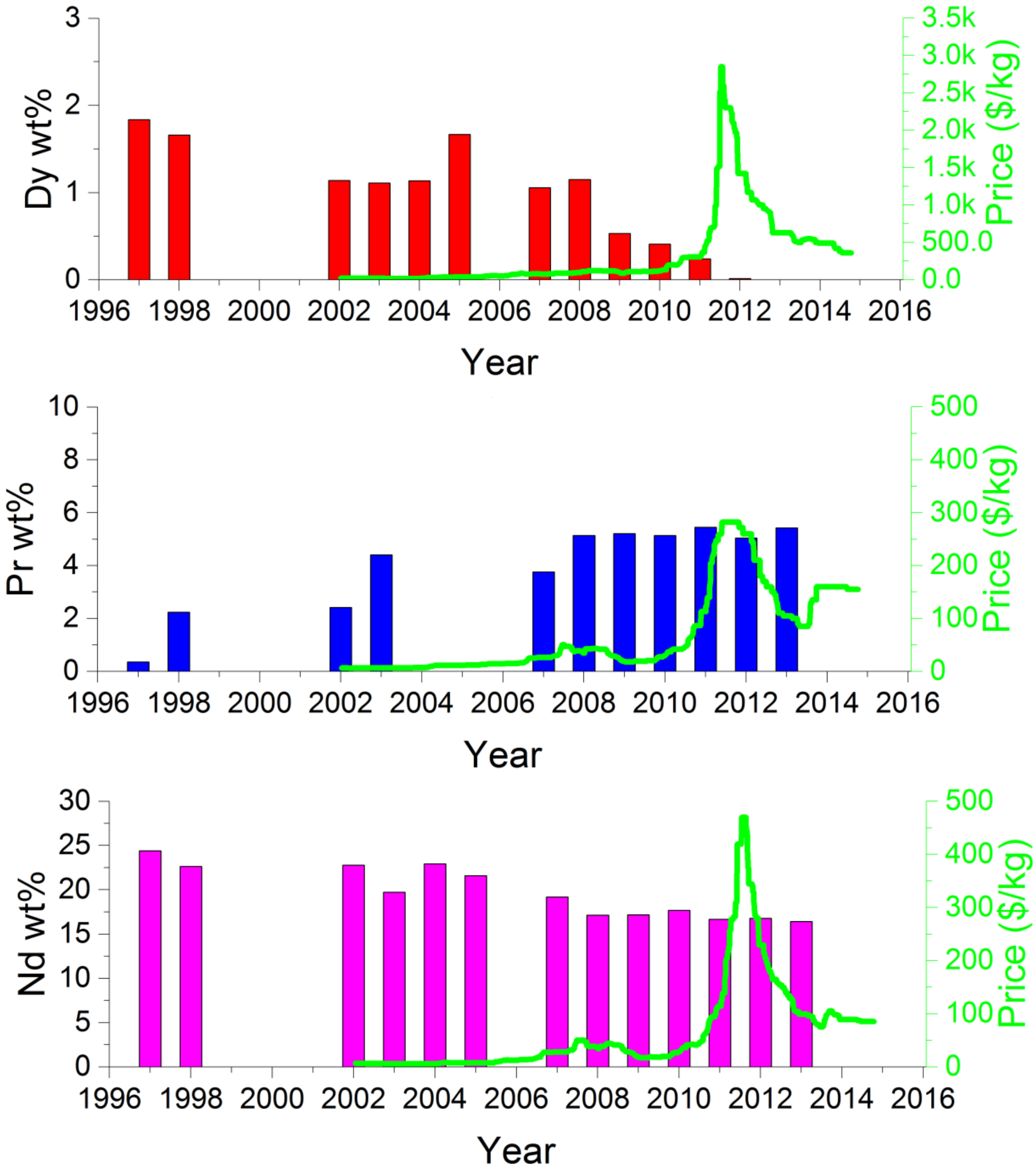

Figure 4.4: Content evolution of the Dy, Pr and Nd from loudspeakers magnets collected from laptops and FOB China metal 99 % prices of the Dy, Pr and Nd evolution.

4.1.2 WEEE fraction containing Nd-Fe-B magnets: TV/PC screens, loudspeakers case

Devices of the consumer equipment category, such as audio systems, television sets, PC screens and video cameras, were also explored. In the older generation television sets based on cathode ray tubes (CRT), all the identified magnets used in their loudspeakers were ferrites. In order to remove the lead-contain glass from the TV, Stena Technoworld manually dismantles the TV frames from the body and so the loudspeakers were easily identified and plucked out of the TV frames.

For the younger generation of TVs based on flat screens and flat panels, the loudspeakers contain Nd-Fe-B magnets. The technological choice for Nd-Fe-B makes sense considering the fact that those higher energy densities is required when it comes to integrating high quality speakers in a reduced device volume of a flat screen compared to a CRT TV set. A range of different configurations were found. Some flat TVs contained only ferrites or Nd-Fe-B magnet speakers, while a majority of the units studied contained a combination of both. Since the lead-containing LCDs are manually dismantled, it was easy to identify and collect the speakers from these. LEDs and Plasma screens are however not disassembled, because they go directly to the shredder, so more labor is required to extract the speakers from these. A typical configuration and the location of the loudspeakers in the flat TVs/PC screens are illustrated in the figure 4.5.

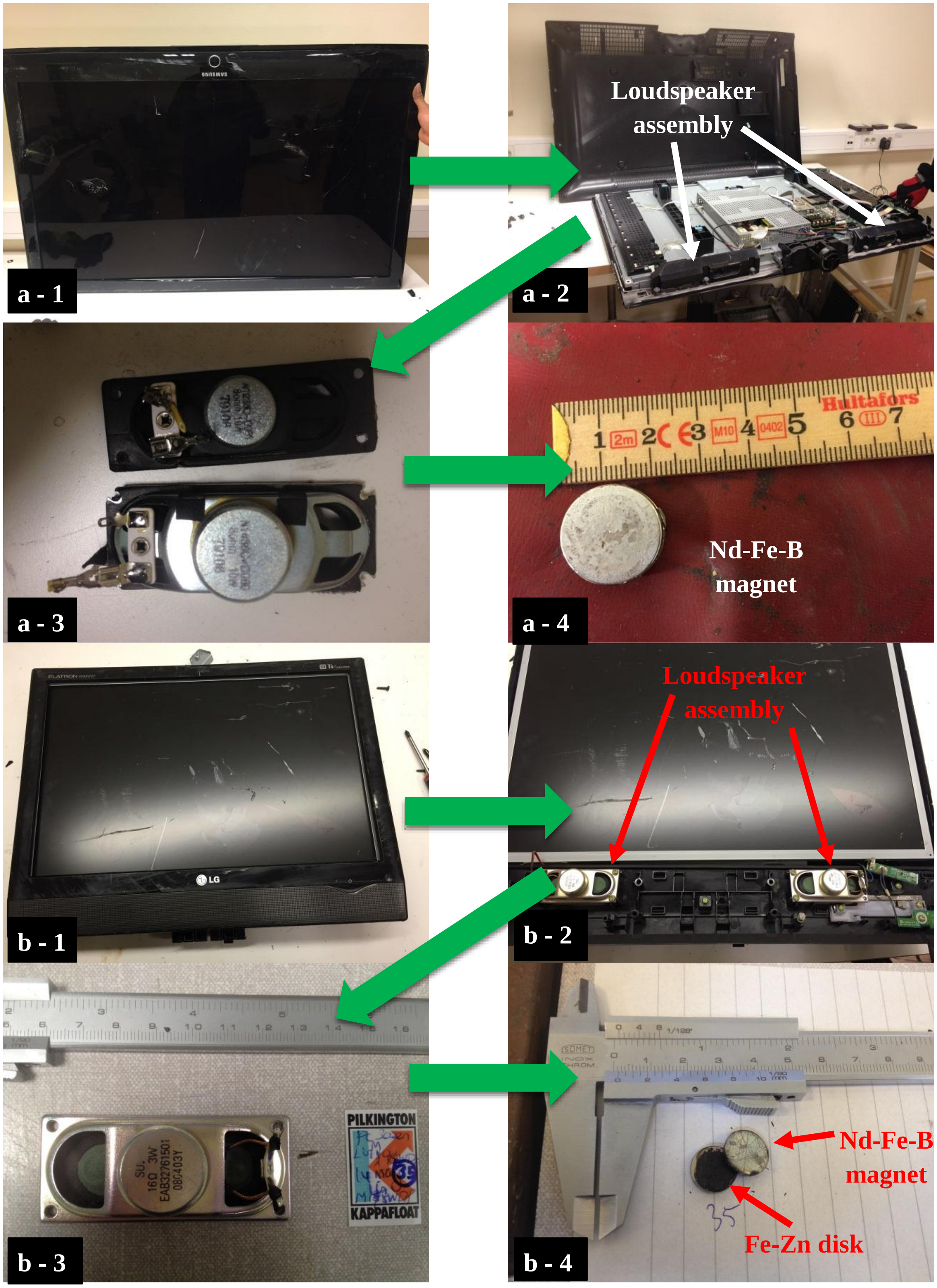

Figure 4.5: Exemplification of the disassembling process and the localization of the loudspeakers/ Nd-Fe-B magnets for flat TV (a: 1-4) and PC screen (b: 1-4).

In figure 4.6 a picture of one of the loudspeaker assemblies of the previous shown TV is presented. In this case, the TV has two loudspeaker assemblies and each assembly has two loudspeakers. Both loudspeakers contain Nd-Fe-B magnets.

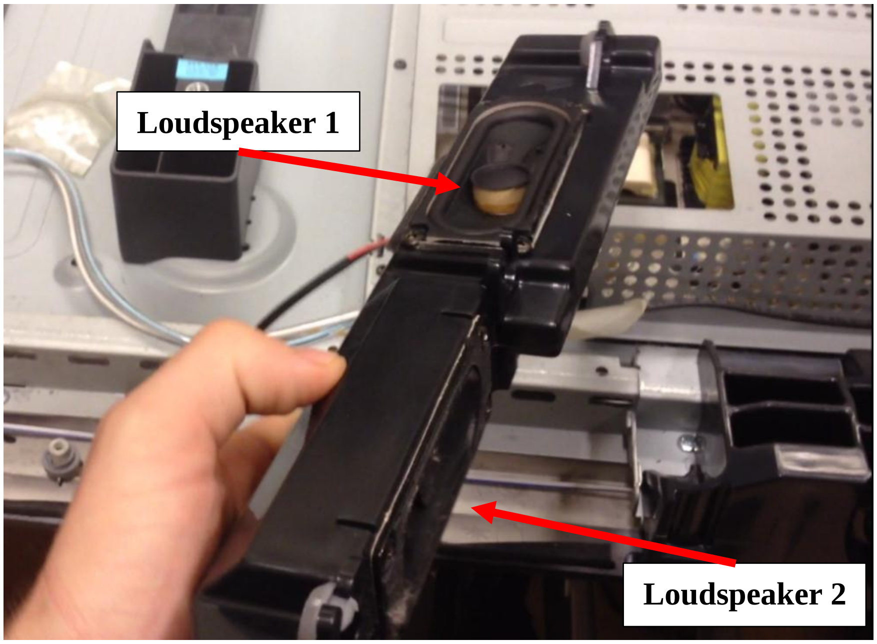

Figure 4.6: Closer look of the TV loudspeaker assembly, and the location of the two loudspeakers.

The mass of the flat TV/PC screens loudspeakers magnets is shown in the following table 4.3. This mass represents an average of all the magnets found in loudspeakers from flat TV/PC screens. Like in the case of the laptops, the magnets used in the TV/PC screen loudspeakers have similar composition with Nd, Pr, and Dy as the key rare earth metal constituents. For the values of the Dy/Nd/Pr content the values represent the average of the Dy/Nd/Pr from the magnets produced in the specified year.

Table 4.3: Magnets mass and rare earths content of flat TV/PC screens loudspeakers.

Year	PC screens					TV				
	No of studied units	loudspeaker magnets mass [g]	Dy wt%	Nd wt%	Pr wt%	No of studied units	loudspeaker magnets mass [g]	Dy wt%	Nd wt%	Pr wt%
2002	1	2.4	0.43	19.10	1.85	-	-	-	-	-
2003	5	3.0	1.34	20.70	4.44	-	-	-	-	-
2004	5	5.2	0.82	21.75	4.81	-	-	-	-	-
2005	3	2.9	0.67	20.36	4.04	2	2.83	0.72	23.13	1.28
2006	2	5.5	0.40	19.58	4.56	1	3.60	0.54	20.57	4.72
2007	-	-	-	-	-	1	29.88	0.95	17.31	4.48
2008	1	3.7	0.70	16.48	4.69	-	-	-	-	-
2009	-	-	-	-	-	-	-	-	-	-
2012	-	-	-	-	-	1	12.34	0	17.95	5.36

At Stena Technoworld, about 4.5 % of the WEEE feed (total 1,000 t per month) are flat screen TVs, of which two thirds are liquid crystal display (LCD) TVs and one third are plasma or light emission diode (LED) TVs (the amount of the latter type is constantly increasing). Between 3 and 30 g of Nd-Fe-B was found per unit (average 12 g), and the size of the loudspeakers and that of the magnets was found to vary with the size of the screen.

Every month also around 220 t of PC monitors are recycled, 70 t of which are flat screens and 150 t represent CRT monitors. Some flat PC screens contain loudspeakers and are found to be the ones exclusively with Nd-Fe-B magnets. The speakers are present at the bottom of the PC screen. Once the plastic casing is unscrewed, the speakers beneath the casing could be easily removed.

External loudspeakers were mainly found sorted into a stream of wood containing electronics. They required a large amount of force to break the structures and extract the speakers from the wooden boxes. More than 50 loudspeakers of various sizes were studied, and although the focus was to find speakers with Nd-Fe-B magnet, only 3 were found with the rare earth magnets, with the rest being based on ferrites. Only two docking stations/(portable) loudspeakers were found, which is a quite a new type of product where compactness is of importance, and the loudspeakers in both of these were based on Nd-Fe-B magnets. The case was the same for the two high-end over-ear headphones that were studied.

4.1.3 WEEE fraction containing non-rare earth permanent magnets

In the following, all the equipment analyzed that did not contain Nd-Fe-B magnets are presented. It was discovered that the majority of the permanent magnets from the WEEE are ferrite permanent magnets.

All studied motors that engage the fans used by microwaves (sample size: 8 devices), electric fans (sample size: 5 devices) and air conditioners (sample size: 5 devices) were based on ferrite magnets.

A total number of 25 vacuum cleaners (appliance included in the small household category) produced by different manufactures and with different dimensions were analyzed. All these were driven by a permanent magnet motor based on ferrites. In the study, also one vacuum cleaner from the 80's was found and this was equipped with an induction motor.

Another part of the studied appliances that did not contain rare earth permanent magnets came from the IT and telecommunication category, that is, printers and copying equipment, which contains small motors with ferrite magnets. Here a total number of approximatively 15 printers were dismantled and all the small motors from the printers had ferrite magnets.

From the electrical and electronic tools category, the following appliances were studied: 12 hand drills, 5 electric saws, 16 electric screwdrivers, 3 hand sanders, 2 grass trimmers and 2 electric chain saws. All of the appliances here were equipped with electric motors based on ferrite magnets.

From the monitoring and control instruments category and from the toys, leisure and sports equipment all the small electric motors found where equipped with ferrite magnets and also all the loudspeakers found in these categories used ferrite magnets. Practically speaking, in these two categories it is impossible to find rare earth permanent magnets. Most likely, this is due to the fact that the overall prices of the entire appliances are generally very low.

Other EEE categories such as lighting equipment, medical devices, and automatic dispensers were not covered in the study, as they were not part of the waste streams recycled at Stena.

4.1.4 Estimation of Nd-Fe-B magnet recovery from loudspeakers in various devices

Table 4.4 summarizes the possible amount of Nd-Fe-B magnets that could be obtained from loud speaker and HDD resources at Stena Technoworld. The assumptions made were based on the data collected for the different streams and in each case, a higher and lower estimate of possible Nd-Fe-B magnet recovery is given. In the case of laptops, approximately 5 t are disassembled per month. A rough estimation assuming a laptop weight of 2.5-3.5 kg and of 1.5-2.0 g (average 1.8g) of Nd-Fe-B magnet from loudspeakers per laptop, results that between 1.3 and 4 kg Nd-Fe-B magnet per month could be recycled. The estimation of magnets from TV is complicated as the devices were found to contain either ferrites, mixture of ferrites and Nd-Fe-B or purely Nd-Fe-B magnets in their loudspeakers. About two-thirds of flat screen TVs are considered to contain Nd-Fe-B magnets. Furthermore, with an average TV weight of 10-15 kg and an average of 10-15 g Nd-Fe-B per TV assumed, between 20 and 45 kg of Nd-Fe-B magnet can be recycled per month. Though all the PC screen magnets were found to be made of Nd-Fe-B not all PC screens had loudspeakers. Hence, a modest assumption of 20 % of PCs screens with loudspeakers is taken. The total weight of the magnets in them varies between 2 and 15 g. With an average screen weight of 4-6 kg and 4-7 g Nd-Fe-B per screen (average 5.4 g), around 7.0 and 21.0 kg of Nd-Fe-B magnet can be recovered in a month. Overall, it can be noticed that the total Nd-Fe-B magnet recovered from these various loudspeakers can be substantial and is in fact comparable to the possible magnet recovery from HDDs.

Table 4.4: Possible quantities of Nd-Fe-B magnet that can be collected from different electronic waste streams.

Product type	Product flows [kg/month]	Nd-Fe-B per product			Nd-Fe-B flows estimation	
		grams			kg/month	
		min	average	max	low	high
HDDs (3.5")	2,500	6.0	14.1	22.0	27.5	102.5
Laptops	5,000					
- *speakers*		0.6	1.8	5.3	1.3	4.0
- *HDDs*		2.0	2.5	5.0	3.1	5.0
PC Screens	70,000	1.7	5.4	15.0	7.0	21.0
TVs	45,000	3.0	12.0	33.0	20.0	45.0

4.2 Characterization of the extracted materials

Four different types of magnets were provided by different motor manufacturers. The 4 types of magnets were shipped as: 2 types of scrap magnets (*type 1* and *type 2*) as they were used in the motors, having different shapes and coated with a nickel protection layer. The last two types of scrap materials (*type 3* and *type 4*) were un-machined block pieces of magnets. The fifth type of magnet materials is a mixture of six different types of scrap magnets from electric motors (type *mix motor*). This mixture is composed of the previous four types of scrap magnets plus two types that are not included in this work. The last type is a mixture of different scrap magnets from different loudspeakers and hard disk drives from laptops (38 scrap magnets from different laptop loudspeakers and 12 scrap magnets from different laptop hard disk drives – type *mix IT*). These magnets, were collected from the recycled plant of Stena Technoworld from Sweden, the identification and collecting proceedings were presented previous in chapter 4.1. It could be considered that this type of mixture reflexes a real situation that could be found in recycling plant for Nd-Fe-B permanent magnets.

The composition of *type 1*, given in wt%, is presented in table 4.5. The oxygen and carbon content of this type of magnets was measured with 0.08 wt% and with 0.07 wt% respectively.

Table 4.5: Chemical composition of the *type 1* magnets (in wt%).

magnet	**Fe**	**Nd**	**Pr**	**Dy**	**Gd**	**Ho**	**Co**	**Ga**	**Nb**	**Cu**	**Al**	**B**
type 1	bal.	17.50	5.06	5.71	0.56	0.64	2.04	0.25	0.28	0.31	0.79	0.96

In sintered magnets Dy is used to increase the anisotropy energy which implies the coercivity enhancement. Dy is mostly located in the matrix phase by substituting Nd **[81].** Ho has the same effect like Dy, but Dy is commonly used due to his better efficiency / cost ratio. Pr is used to substitute 20 % - 25 % of Nd, in order to allow in the manufacturing process, the use of didymium, a combination of Nd and Pr, which will decrease a little the price. Co used to substitute Fe in the matrix phase. By substituting the Fe, Co improves the Curie temperature by increasing the transition-metal-transition-metal exchange interactions **[81]**. Ga substitution for Fe in $Nd_2Fe_{14}B$ phase leads to the increases in Curie temperature, but part of the Ga content is included also in the rare earth rich phase **[84, 85]**. Ga enrich grain boundary phase has a decrease content of Fe and Co which causes an enhanced pinning force which will result in enhancing the coercivity **[85]**. Cu, Al and Nb are located on the grain boundary phase **[81, 82, 83].** Most of the time, Al and Cu are used as densifying agents, by decreasing the sintering temperature and ensuring a good densification **[81]**. The reparation of the elements from *type 1* magnets is shown in figure 4.9. This type of magnets presents a rectangular shape measuring 30 mm x 10 mm x 5.5 mm as shown in figure 4.7a. The magnet shows a remanence of 1.10 T and a coercivity of 2.86 T. The demagnetization curve is presented in figure 4.7b.

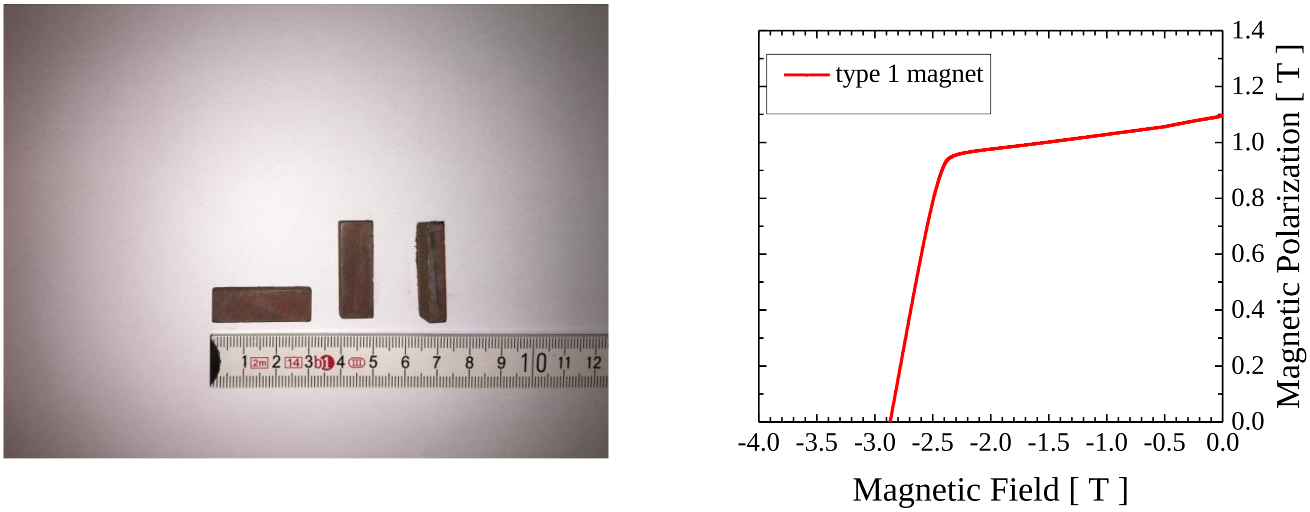

a) **b)**

Figure 4.7: a) Scrap magnets *type 1*, b) Demagnetization curve of *type 1* magnets.

The magnet microstructure of *type 1* of is presented in figure 4.8. The image shows the typical microstructure of sintered magnets with particle size between 5 µm and 20 µm.

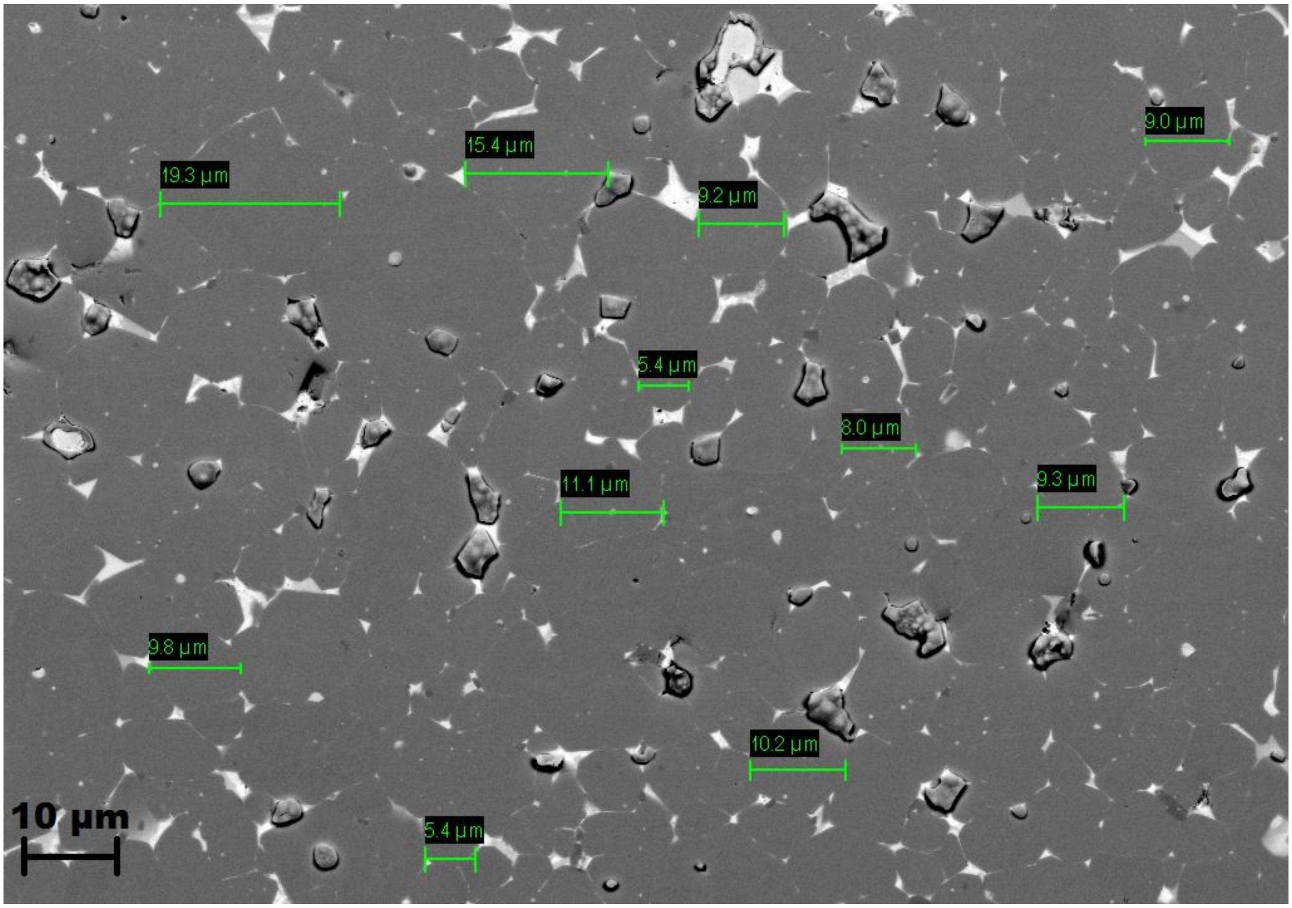

Figure 4.8: Backscattered electron SEM image of a *type 1* magnet.

The microstructure of the *type 1* sintered scrap magnets consist of $(Nd,Dy,Pr)_2(FeCo)_{14}B$ particles surrounded by Nd-Pr-Gd-Cu rich grain boundary phase with small additions of Ga. The map distribution of the elements is shown in figure 4.9.

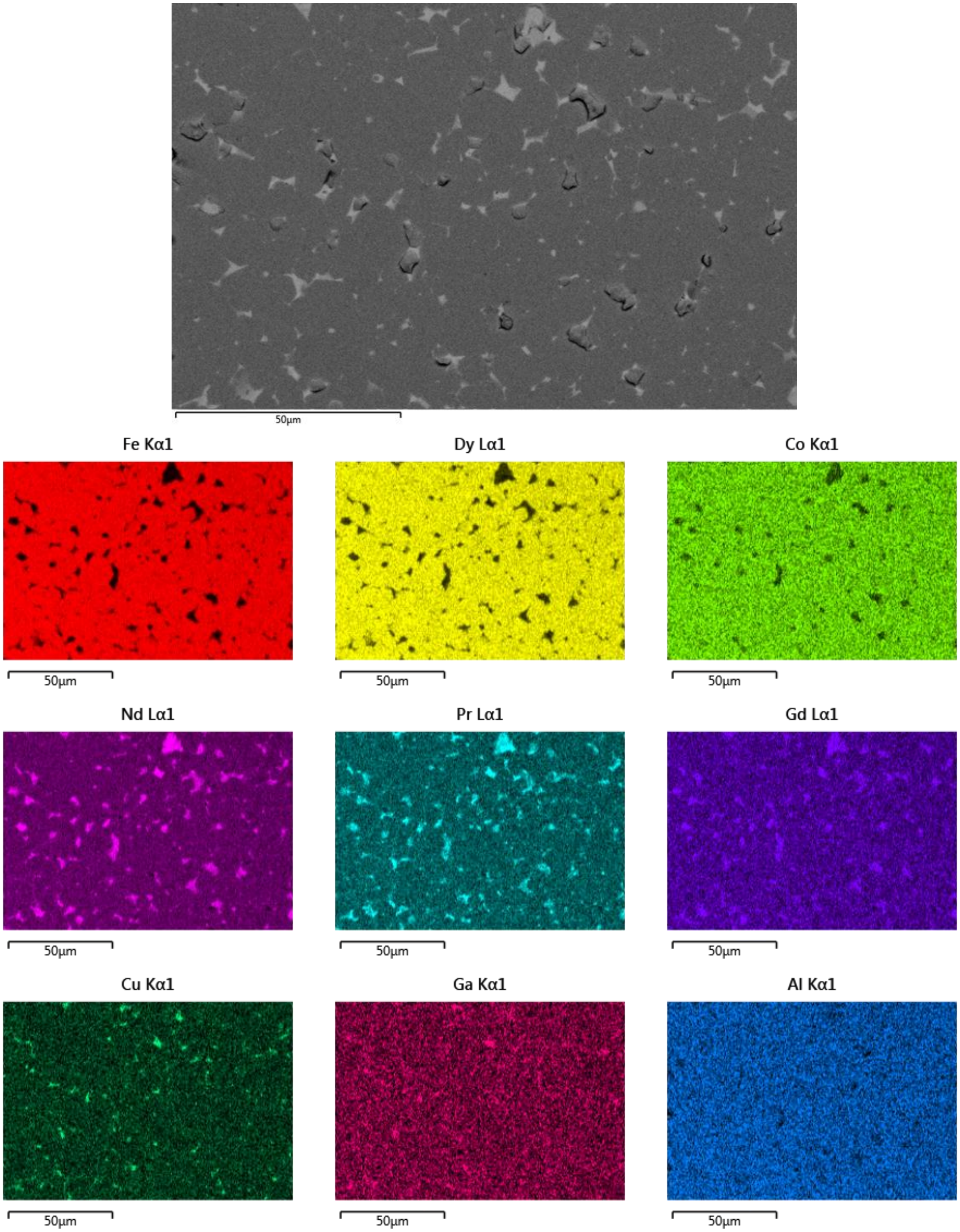

Figure 4.9: Backscattered electron SEM image of the *type 1* scrap magnets and the individual element maps (scale bar: 50 µm).

Type 2 magnets have a rectangular shape measuring 18 mm x 11.7 mm x 2 mm and are shown in figure 4.10a. ICP-OES analyses of these magnets shown a composition similar with the *type 1* magnets, but with a much lower content of Dy and Co. The chemical composition is show in table 4.6.

Table 4.6: Chemical composition of *type 2* scrap magnet (in wt%).

magnet	**Fe**	**Nd**	**Pr**	**Dy**	**Gd**	**Ho**	**Co**	**Ga**	**Nb**	**Cu**	**Al**	**B**
type 2	bal.	21.00	4.40	2.90	1.90	-	1.53	0.07	0.21	0.28	0.95	0.96

The magnetic measurement of this type of magnets shows a remanence of 1.15 T and a coercivity of 2.28 T. The demagnetization curve is presented in figure 4.10b.

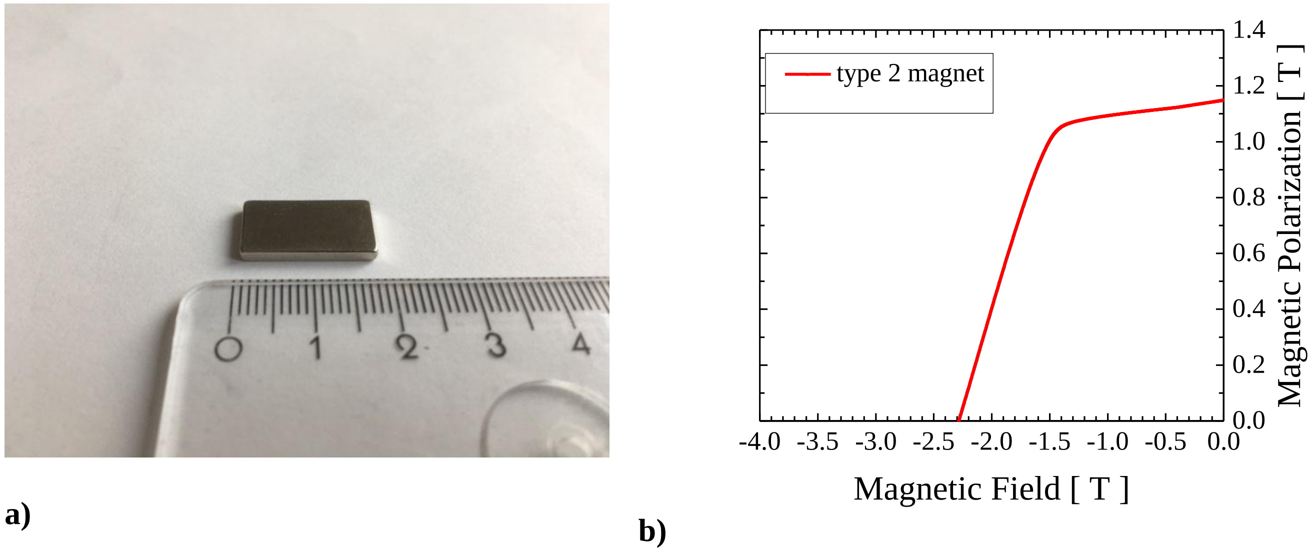

a)

b)

Figure 4.10: a) image of the scrap magnet *type 2* and b) demagnetization curve.

In the case of *type 2* magnets the microstructural analyses highlight a similar microstructure like in the case of *type 1* magnets, with particle sizes between 5 µm and 20 µm. An image of the microstructure is presented in figure 4.11.

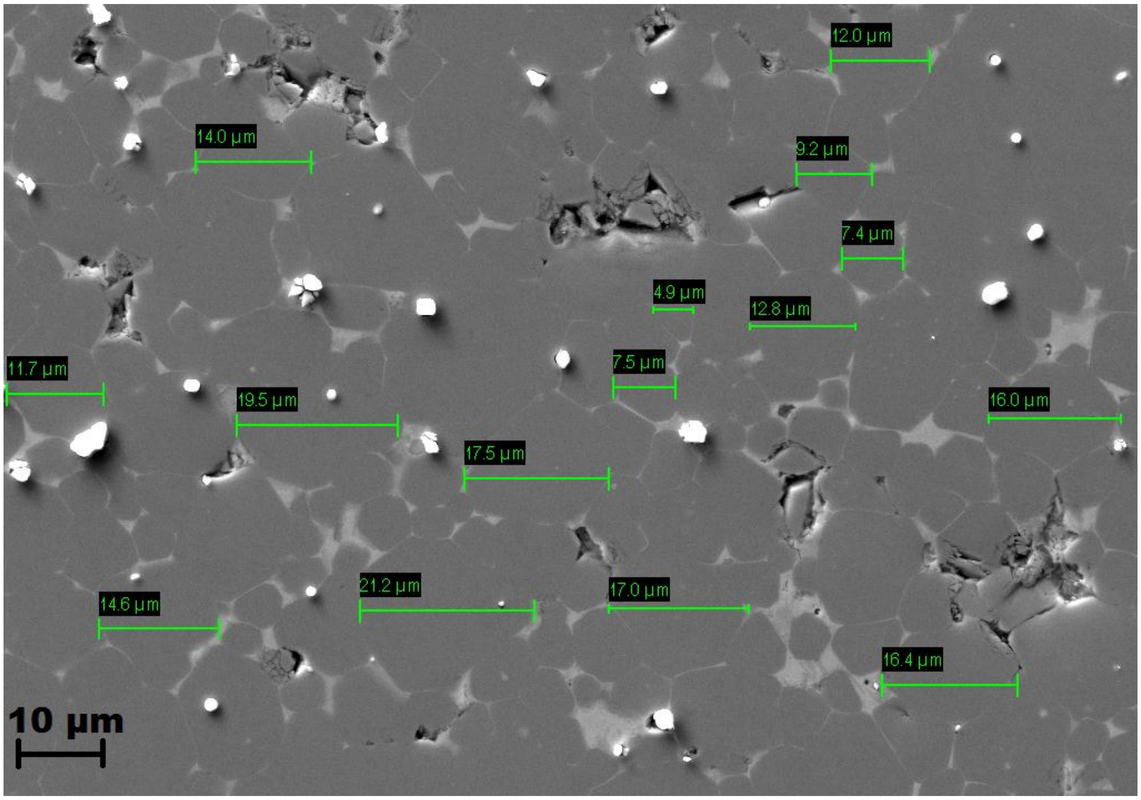

Figure 4.11: Secondary electron SEM microstructural analysis of the scrap sintered magnets *type 2.*

Like in the previous case the $(Nd,Pr,Dy)_2(Fe,Co)_{14}B$ grains (in gray contrast in the picture) are surrounded by RE rich boundary (white contrast in the picture). In this case the RE rich phase is composed of Nd-Pr-Gd-Cu-Ga. Since the rare earths are very reactive with oxygen, along the grain boundary where the rare earths are predominant could be found also spots that contain oxygen. The white dotes from the surface of the sample are oxides, that appeared after the polishing process, this is also confirmed by the elemental mapping presented in the figure 4.12. A distribution map of the elements contained by the *type 2* magnets is shown in figure 4.12. The similarity of Fe and Dy distribution in all the EDX maps is due to the fact that it was chosen Fe Kα and Dy Lα, for which the x ray absorption edges largely overlap and thus cannot be distinguished.

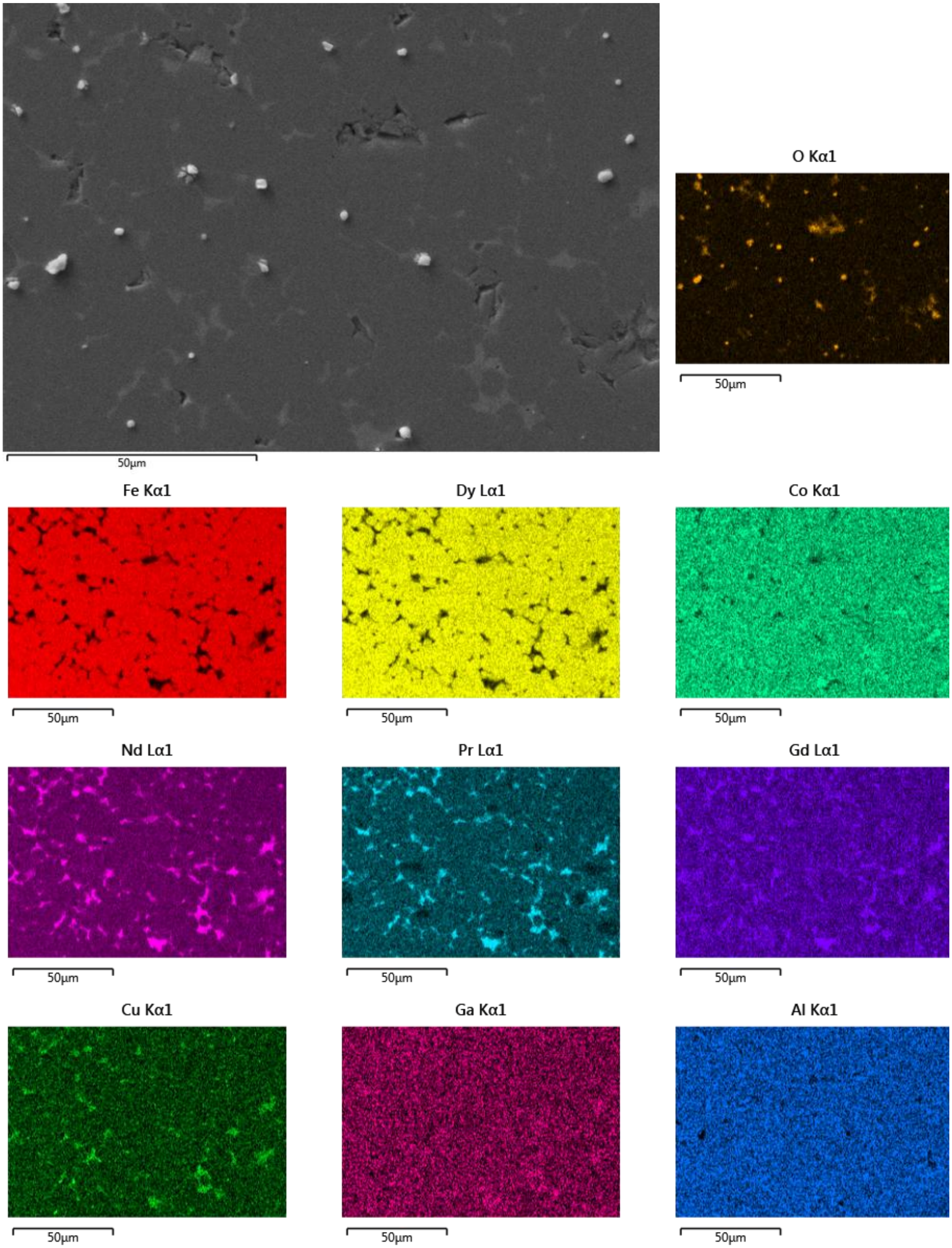

Figure 4.12: Backscattered electron SEM image of the *type 2* magnet and the individual element maps (scale bar: 50 µm).

The main composition of the *type 3* magnet is presented in table 4.7. By comparing *type 3* magnet composition with *type 1* and *type 2*, this type of magnets has the highest Dy and Co content, with 6.31 wt% and 3.13 wt% respectively. In this case the Pr content is reduced and the Nd content is higher comparing to the previous two cases. The oxygen content of block material is 0.26 wt% and the carbon content is 0.06 wt%.

Table 4.7: Type 3 magnets chemical composition (in wt%).

magnet	**Fe**	**Nd**	**Pr**	**Dy**	**Gd**	**Ho**	**Co**	**Ga**	**Nb**	**Cu**	**Al**	**B**
type 3	bal.	24.20	0.19	6.31	-	-	3.13	0.27	-	0.22	0.39	0.89

Figure 4.13a presents the initial as received block of sintered magnetic material, which was further used. On the left side, figure 4.13b shows the demagnetization curve of the *type 3* magnetic material. This type of material has a remanence of 1.13 T and coercivity of 2.27 T.

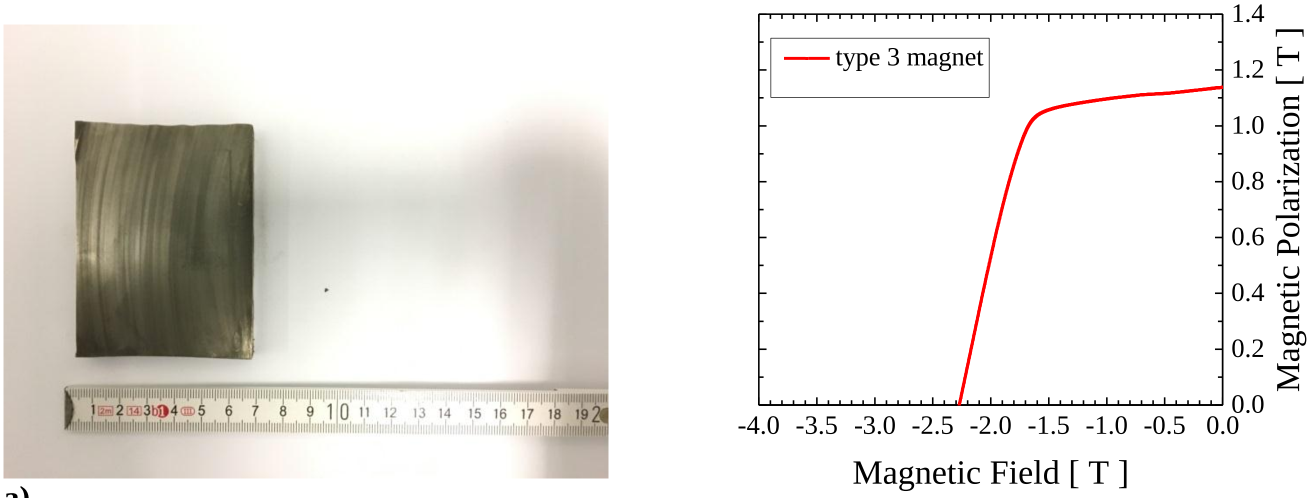

a)

b)

Figure 4.13: a) block sintered scrap magnet representing *type 3* b) demagnetization curve of *type 3* magnet.

Again the microscopy reveals a microstructure compose of $(Nd,Pr,Dy)_2(Fe,Co)_{14}B$ particles surrounded by a phase rich in rare earths. The particles size is between 5 µm and 20 µm. The rare earth phase is constituted by Nd-Gd-Cu-Ga. Figure 4.14 shows the microstructure of the *type 3* magnet and the elemental mapping distribution. In this case the Pr mapping, the element is less highlight due to the low content of Pr, as it can be observed also from the chemical compositions analysis.

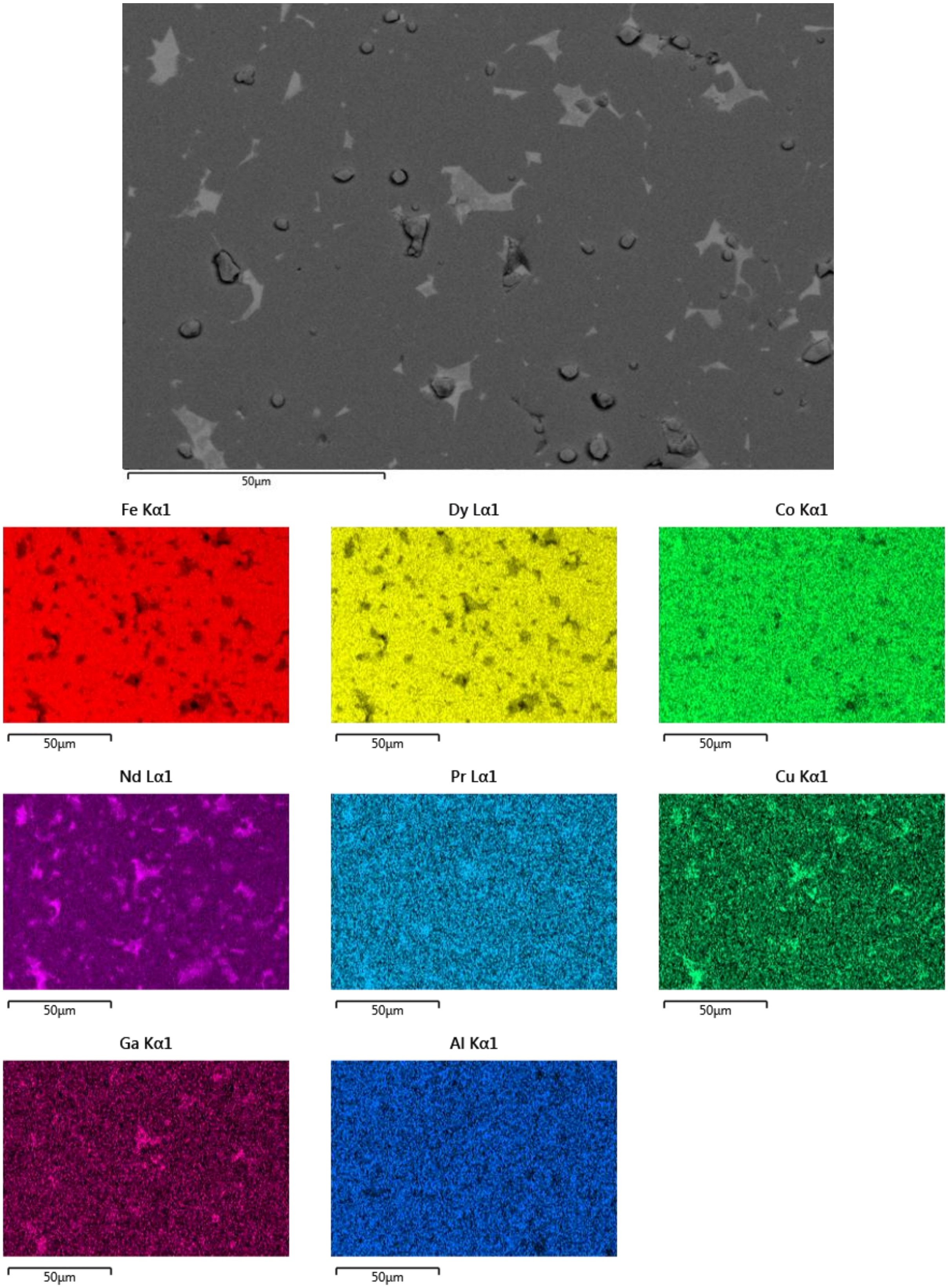

Figure 4.14: Backscattered electron SEM image of the *type 3* magnet and the individual element maps (scale bar: 50 µm).

Type 4 magnet has a similar composition as *type 3* magnet; the material received was also a block of uncoated sintered Nd-Fe-B which is shown in figure 4.15a. The composition of *type 4* magnet is shown in table 4.8. The oxygen content of *type 4* magnets is 0.22 wt% and the carbon content is 0.057 wt%.

Table 4.8: Chemical analyses of type *4* magnet (in wt%).

magnet	**Fe**	**Nd**	**Pr**	**Dy**	**Gd**	**Ho**	**Co**	**Ga**	**Nb**	**Cu**	**Al**	**B**
type 4	bal.	24.30	0.15	5.95	-	-	3.10	0.27	-	0.24	0.37	0.92

A small brick (10 mm x 0.5 mm x 0.5 mm) was cut from the block material and measured on the easy direction of magnetization. The demagnetization curve is shown in figure 4.15b. The measured romance was 0.94 T and the coercivity was 2.33 T.

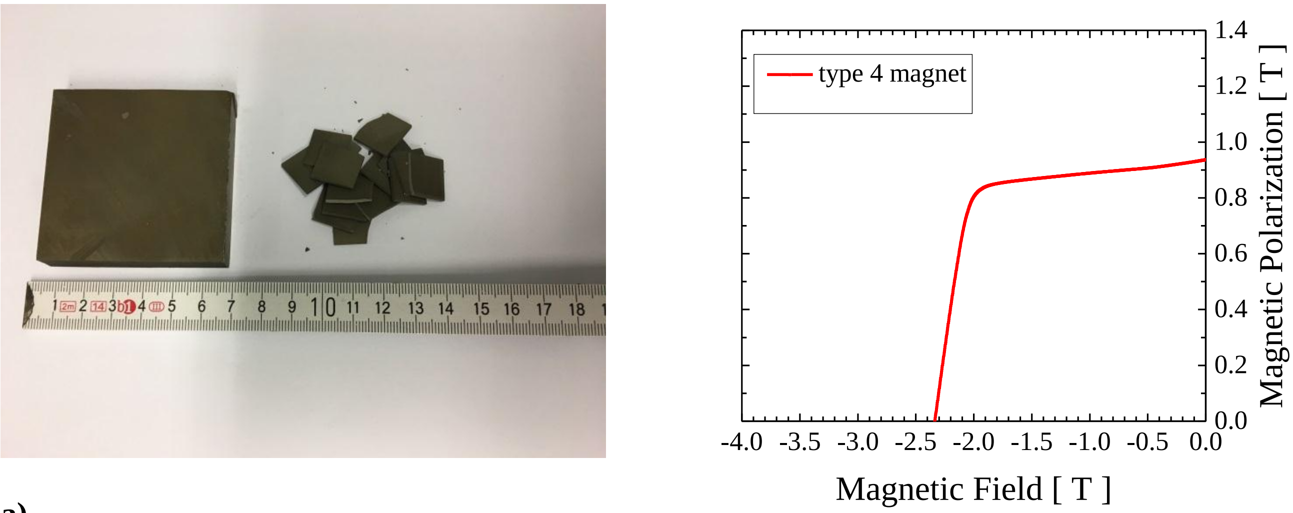

a)

b)

Figure 4.15: a) block piece of the *type 4* magnet and b) demagnetization curve of the *type 4* magnet.

The microstructural observation for type 4 magnet highlights a similar microstructure like for the previous three types of magnets but with a slightly bigger particle size. In this case the grain size is between 8 µm and 23 µm. The SEM observation of the microstructure of type 4 magnet is shown in figure 4.16

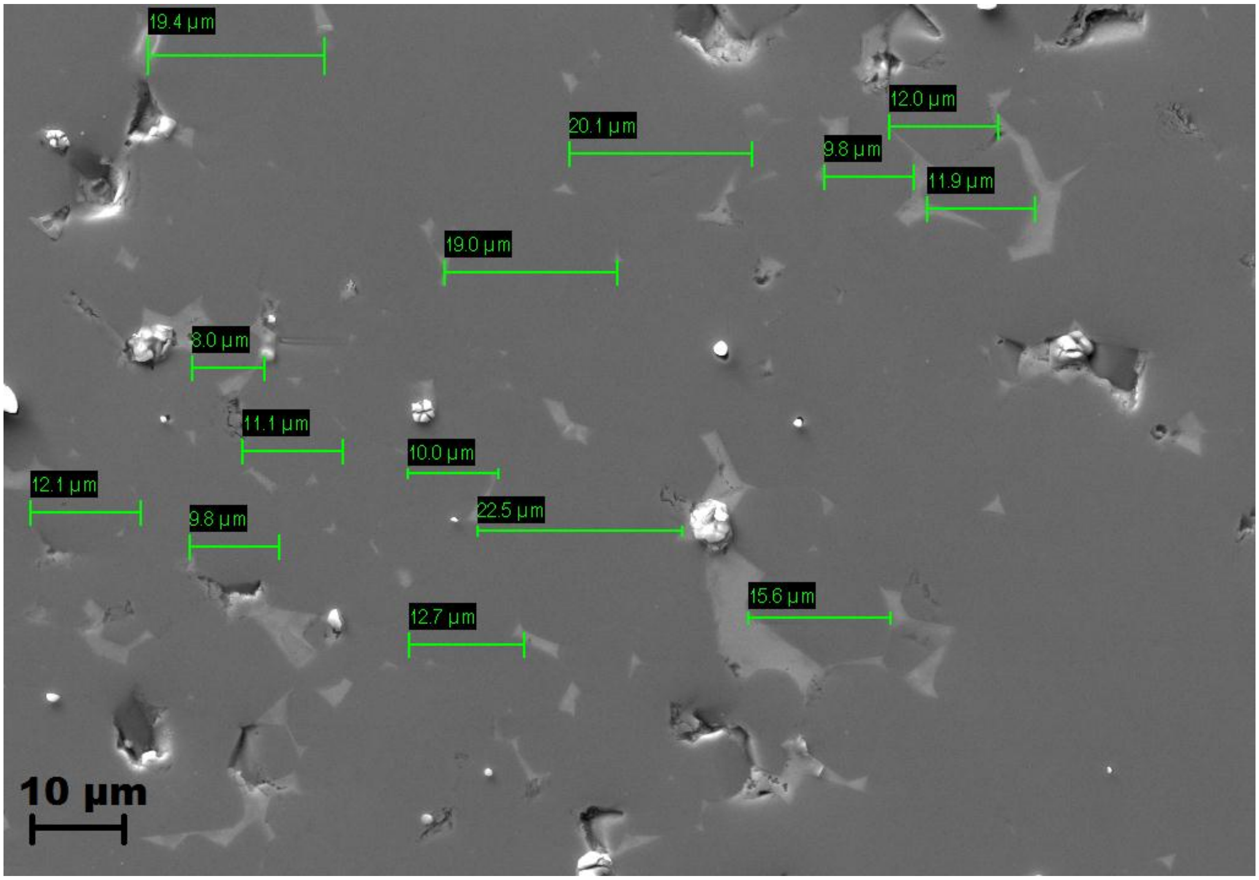

Figure 4.16: Secondary electron SEM image of the sintered material *type 4*.

The microstructure of type 4 magnet consist of $(Nd,Pr,Dy)_2(Fe,Co)_{14}B$ particles surrounded by a rare earths rich phase. This rare earth rich phase is composed of Nd-Gd-Cu-Ga. This is confirmed by the elemental mapping shown in figure 4.17. Since Pr content is low his is well distributed din the entire magnet and his present along the grain boundary is not well seen. Like for the previous cases Cu and Al plays the role of densifying agents and the oxygen is concentrated along the grain boundary.

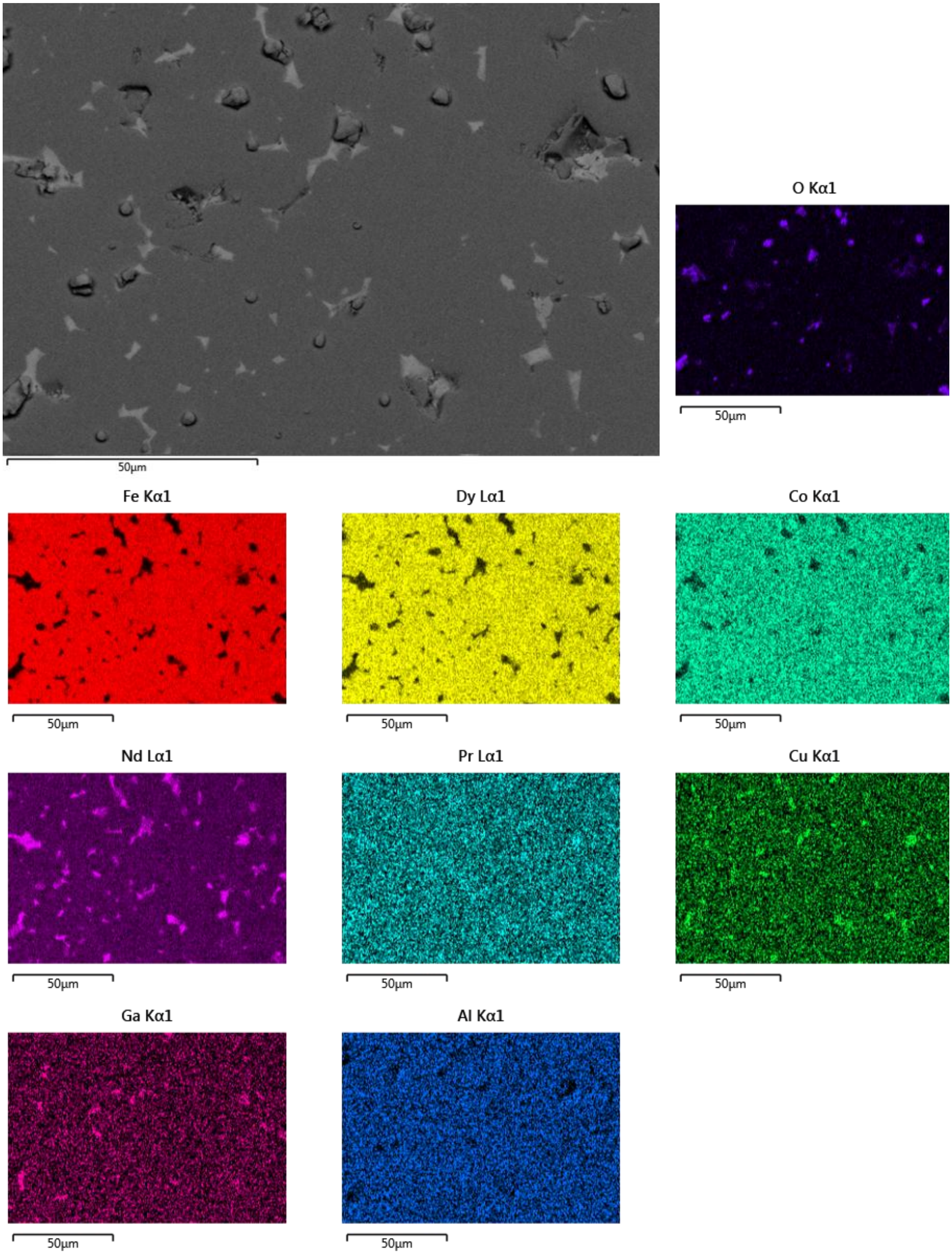

Figure 4.17: Backscattered electron SEM image of the *type 4* magnet and the individual element maps (scale bar: 50 µm).

Since *mix motor* type is a mixture most of them from the previous 4 types, the composition of this mixture is closed to the composition of the previous types. This composition is shown in table 4.9. Due to his composition it is expected that the mixture to have approximately the same magnetic properties, with a remanence between 1.0 T and 1.15 T and a coercivity around 2.0 T.

Table 4.9: Chemical composition of *mix motor* type (in wt%).

magnet	**Fe**	**Nd**	**Pr**	**Dy**	**Gd**	**Ho**	**Co**	**Ga**	**Nb**	**Cu**	**Al**	**B**
mix motor	bal.	23.80	2.38	5.80	0.33	0.14	2.21	0.23	-	0.23	0.56	0.92

To insure a good homogeneity of the powder, the hydrogenated powder was well mixed for a couple of minutes, and afterward 5 different samples were collected from different parts of the entire mixture. The samples were analyzed by ICP-OES and the results are shown in table 4.10.

Table 4.10: ICP-OES measurement for comparison of the homogeneity of the mix motor powder (values are given in wt%).

	Fe	**Nd**	**Pr**	**Dy**	**Gd**	**Ho**	**Co**	**Ga**	**Nb**	**Cu**	**Al**	**B**
meas. 1	bal.	23.40	2.17	5.79	0.35	0.13	2.25	0.23	-	0.24	0.59	0.95
meas. 2	bal.	23.40	2.21	5.47	0.34	0.13	2.21	0.24	0.10	0.24	0.60	0.96
meas. 3	bal.	22.94	2.25	5.57	0.33	0.13	2.22	0.24	-	0.23	0.58	0.95
meas. 4	bal.	22.80	2.48	5.73	0.33	0.14	2.21	0.23	-	0.23	0.56	0.92
meas. 5	bal.	22.58	2.51	5.88	0.34	0.14	2.23	0.23	-	0.23	0.57	0.96

As it can be observed the variations in the values of the elements are insignificant and it can be concluded that the powder is well homogenized. To note that this composition is specific only for this case and that the composition is dependent on the starting magnets that compose the mixture and to the weight ratio in which they are mixed.

The *mix IT* type is a mixture composed of 38 scrap magnets from different laptops loudspeakers and 12 scrap magnets from different laptops hard disk drives. In the following (figure 4.18) is presented the demagnetization curves of 3 of the magnets that compose this mixture. These magnets were randomly selected and were measured to have an order of magnitude of the magnetic properties.

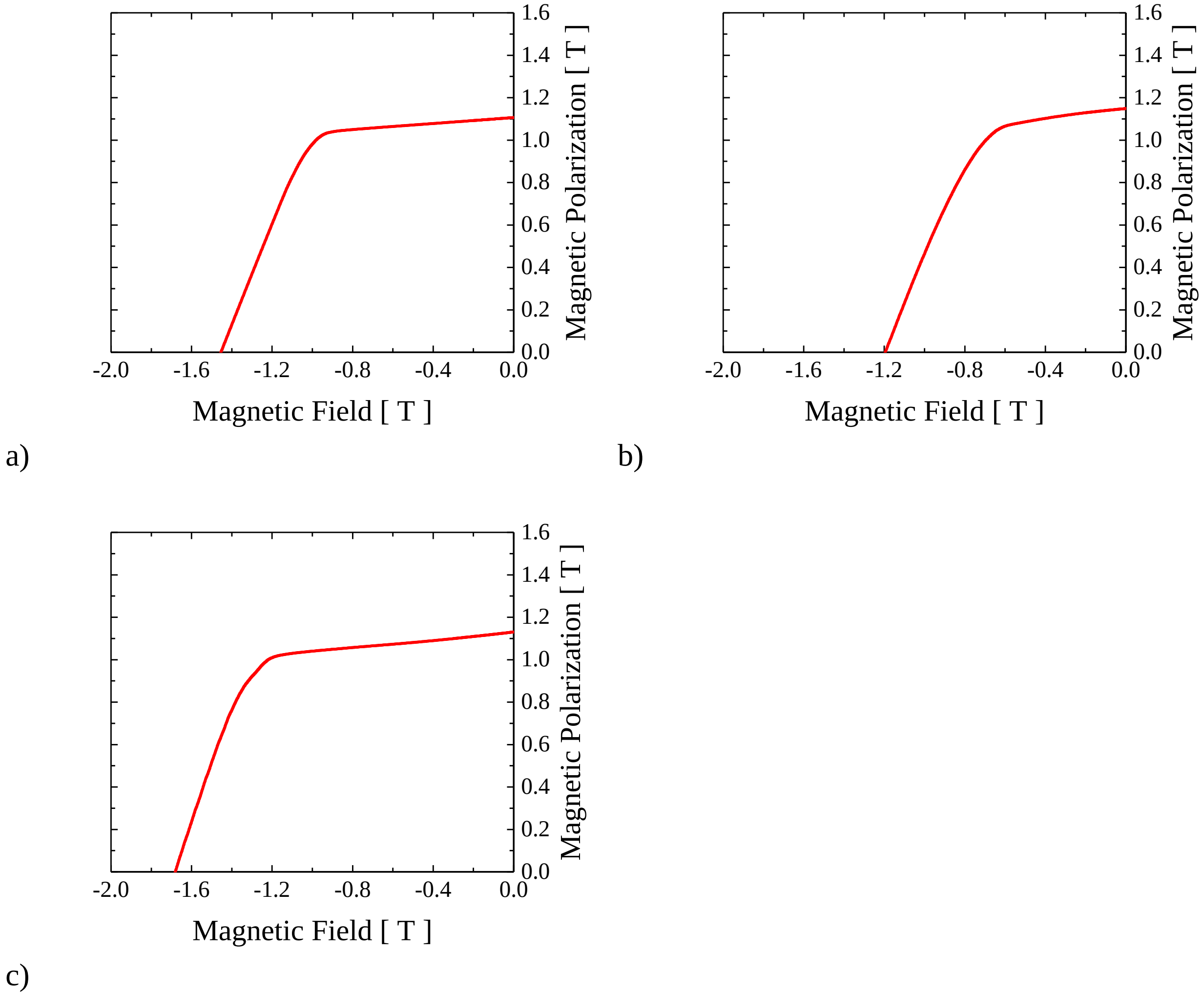

Figure 4.18: Demagnetization curves for the 3 randomly selected magnets from laptops loudspeakers.

For the magnets from laptops loudspeakers it can be conclude that the remanence is situated between 1.0 T and 1.2 T and the coercivity can take values between 1.2 T and 1.7 T.

The chemical analyses of *mix IT* type shows low Dy and Co content, in comparison with the previous 4 types that have a high content of Dy and Co. The composition of the *mix IT* type is presented in table 4.11.

Table 4.11: Chemical composition of *mix IT* (in wt%).

magnet	**Fe**	**Nd**	**Pr**	**Dy**	**Gd**	**Ho**	**Co**	**Ga**	**Nb**	**Cu**	**Al**	**B**
mix IT	bal.	23.60	5.32	1.08	1.03	-	0.41	0.06	0.11	0.11	0.75	1.03

Also for the *mix IT* it was checked the homogeneity of the powder. Like in the previous case, after mixing the hydrogenated powder, 4 samples were collected and measured by ICP-OES.

The results of the analyses are shown in table 4.12. The results show a small variation in the composition of the mixture, it can be concluded that the mixture is rather homogeneous.

Table 4.12: ICP-OES measurement for comparison of the homogeneity of the mix IT powder (values are given in wt%).

	Fe	**Nd**	**Pr**	**Dy**	**Gd**	**Ho**	**Co**	**Ga**	**Nb**	**Cu**	**Al**	**B**
meas. 1	bal.	23.58	5.32	1.08	1.03	-	0.41	0.06	0.11	0.11	0.75	1.03
meas. 2	bal.	23.13	5.39	1.05	0.97	-	0.39	0.08	0.13	0.10	0.71	0.98
meas. 3	bal.	23.55	5.15	1.13	1.02	-	0.40	0.06	-	0.11	0.72	1.01
meas. 4	bal.	23.52	5.50	1.11	0.96	0.03	0.39	0.06	0.10	0.08	0.62	0.95

4.3 Studying the hydrogen absorption/desorption reactions

During the HDDR process, various process parameters can have effect on the kinetics and microstructure of the powders, which has also an influence on the magnetic properties of the obtained powders. The parameters that can affect the HDDR process are the processing temperature, hydrogen pressure, hydrogen desorption rate, cooling rate and holding time. All these parameters are influenced each other and are sensitive to the composition of the processed materials. So an optimization of the HDDR processing parameters is required. In order to understand and determine the behavior and the changes that take place during the HDDR process, for the different types of scrap Nd-Fe-B magnets, a differential thermal analysis (DTA) equipment was used. The uncoated scrap magnets were crushed with a mortar and pestle. The DTA was performed on powder batches of 1 gram. Prior the analysis, in order to reactivate the surface of the powder, the powder batch was heated under vacuum (below 1 x 10^{-4} mbar) up to a temperature of 400 °C. When the temperature was achieved, it was maintained for 5 minutes and then the powder was let to cool down to room temperature under vacuum. Afterwards, the hydrogen absorption study took place under 1 bar hydrogen pressure and up to a temperature of 900 °C. After the hydrogen absorption process, when the powder reaches room temperature, the hydrogen desorption study was performed under vacuum up to the temperature of 900 °C. Figure 4.19 shows the typical absorption reaction of the 4 types of magnets during a heating rate of 10K/min in a hydrogen atmosphere of 1 bar.

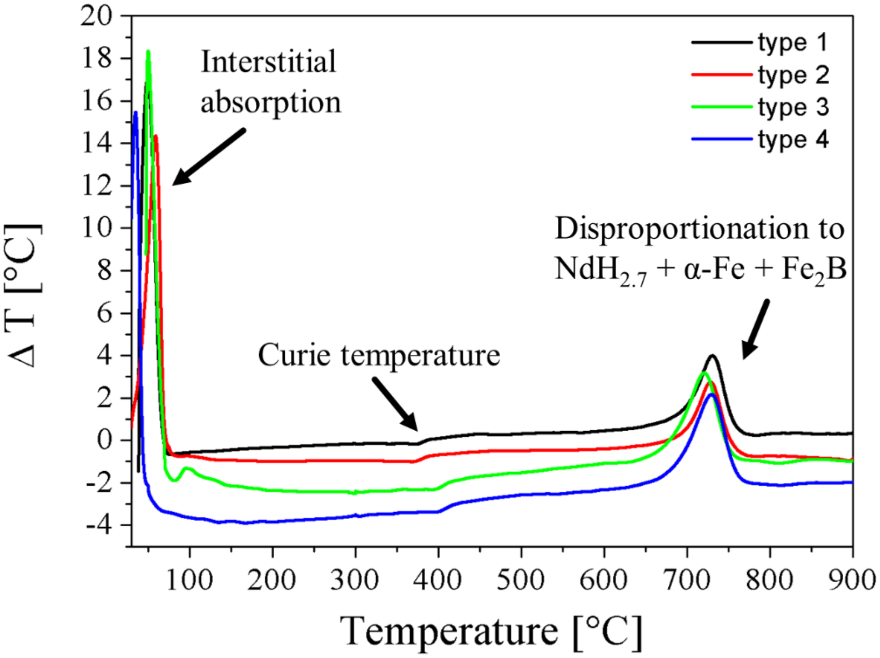

Figure 4.19: Differential thermal analysis curves of 4 types of magnets under 1 bar hydrogen pressure and 10 K/min heating rate.

Both reactions, the hydrogen decrepitation and hydrogen disproportionation are accompanied by an exothermic reaction. The hydrogen decrepitation reaction takes place at lower temperature (up to 100°C) compared with those of the hydrogen disproportionation reaction, which take place at temperatures above 600 °C. As it can be observed from the figure 4.20, which present a zoom image of the interstitial hydrogen absorptions, the curves are distributed over different temperatures.

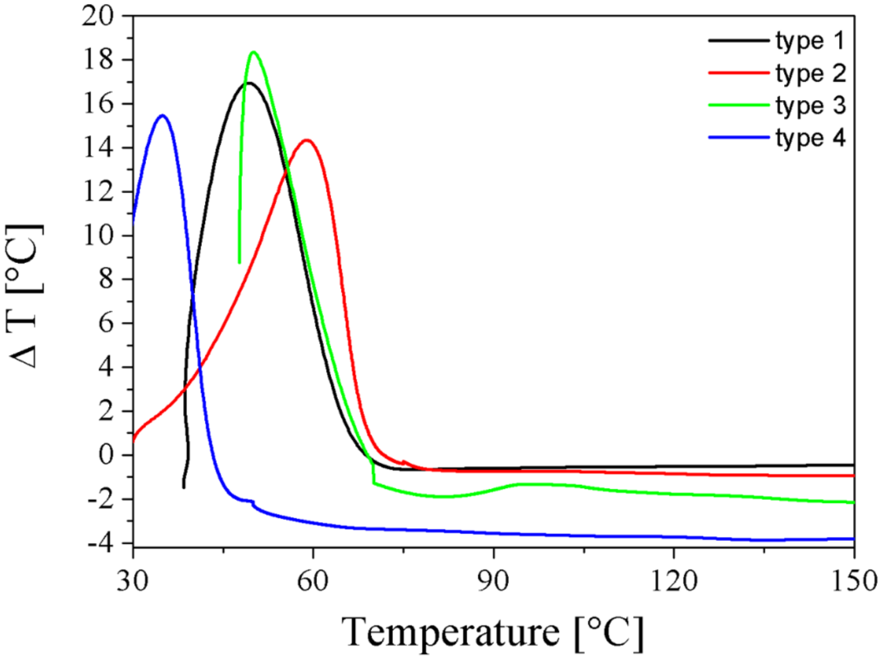

Figure 4.20: Zoom in of the interstitial hydrogen absorption of the 4 types of scrap magnets.

These differences in the starting temperatures and the end temperatures of the interstitial absorption reactions are influenced by the starting temperature of the process (this been 18 °C for the morning processes and 30+ °C for the processes which followed the first process), the composition of the scrap magnets and by the degree of impurities/oxidation of the magnets. The filling of the sample chamber with hydrogen influence also the interstitial absorption behavior. Because the filling was manually, the time required to reach the desired pressure or any pressure overshooting, influence the reaction by increasing or decreasing the time required for the completion of the reaction. In some cases, the pre-pressure rises till 2 bars or even higher prior stabilizing the hydrogen pressure at 1 bar.

Figure 4.21 presents a zoomed image of the Curie temperature of the 4 types of magnets. This temperature represents the Curie temperature corresponding to the hydrogenated scrap magnets, which is shifted to higher temperature in comparison with the Curie temperature of the no- hydrogenated scrap magnets.

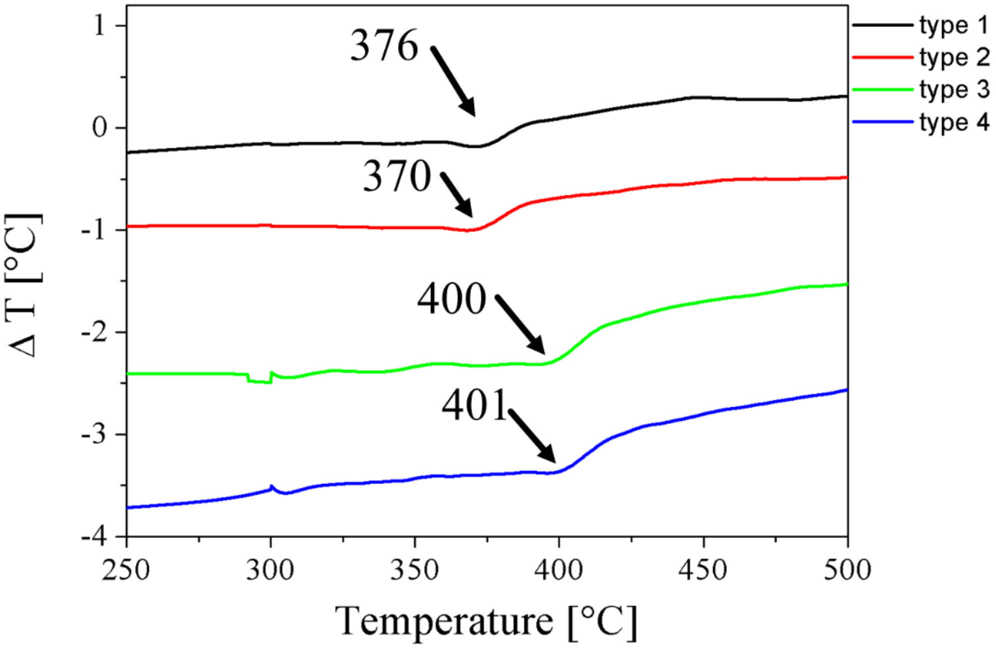

Figure 4.21: Differential thermal analysis showing the Curie temperature of the hydrogenated 4 types of scrap magnets.

The Curie temperature is influenced by the composition of the scrap magnets, manly by the Co content of the magnets. The Curie temperature of hydrogenated 4 types of scrap magnets corresponds also with Co content shown by the ICP-OES measurements. According to the ICP-OES measurements *type 1* magnet has a Co concentration of 2.04 wt% which corresponds on the differential thermal analysis with a Curie temperature of 376 °C. *Type 2* magnet has a smaller content comparing to *type 1* (1.53 wt%), which corresponds also with a smaller Curie temperature of 370 °C shown on the DTA curves. *Type 3* and *type 4* have almost the same Co content of 3.13 wt% and 3.10 wt% respectively, corresponding with a Curie temperature of 400 °C and 401 °C respectively.

I assume that part of the Ga atoms substitutes the Fe atoms in different sites in the $Nd_2Fe_{14}B$ phase (also confirmed by the individual element maps, small quantities of Ga been seen also in the $Nd_2Fe_{14}B$ phase, not only on the grain boundary), which could lead to an increase of the Curie temperature. But since the values of the Ga content for the 4 types of magnets (*type 1* = 0.25 wt%; *type 2* = 0.07 wt%; *type 3* = 0.27 wt%; and *type 4* = 0.27 wt%) are quite similar, it is hard to estimate the impact of the Ga content on the Curie temperature. But if the Ga content is summarized with the Co content, the sum of the two elements will correspond with the trend seen on the differential thermal analysis.

In figure 4.22 it is shown the exothermic peaks generated by the disproportionation reactions corresponding to the 4 types of scrap magnets. The disproportionation reaction is influenced by the magnets additives and is difficult to determine the precise reason of the difference in the temperature of the disproportionation reactions. However, it is known that Co and Ga shifts the disproportionation reaction to higher temperature **[86]**, and this, correlated with the content of rare earths (Nd-Pr-Dy) may explain the different temperature where the disproportionation reaction takes place for the 4 types of scrap magnets. *Type 1* magnet has the smallest amount of Nd-Pr-Dy from all the 4 types of scrap magnets and a Co content of 2.04 wt%, which results in the most accentuated delay of the disproportionation reaction, with the peak of the disproportionation reaction at 730 °C. *Type 2* magnets have almost the same amount of Nd-Pr-Dy but a lower content on cobalt which will result in lowering the disproportionation temperature to the temperature of 728 °C. *Type 3* and *type 4* has the highest Co content, but also a much higher content of Nd-Pr-Dy, approximatively 30 wt%, which compensates the delay in the disproportionation reactions given by the Co content. It is also reported that the alloys that contain cobalt absorb smaller amount of hydrogen **[86]**

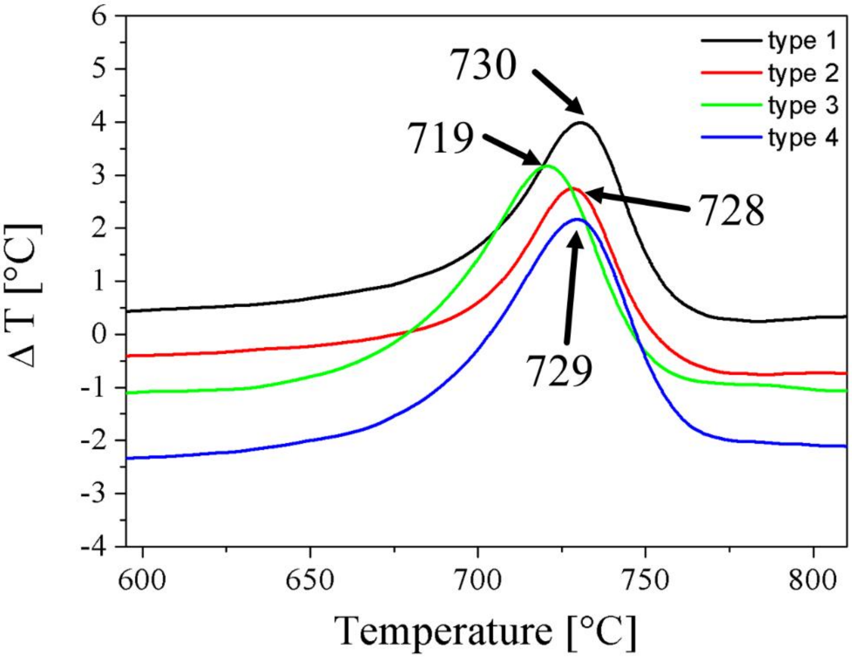

Figure 4.22: Differential thermal analysis curves of the 4 types of magnets processed under 1 bar hydrogen pressure and 10 K/min heating rate corresponding to the disproportionation reaction.

A better view on how the disproportionation reaction is influenced by the magnets additives can be seen on the comparison between the two mixtures shown in figure 4.22-1. Since decrepitated powder was used in the elaboration of the two mixtures, the DTA analysis presents only the disproportionation reactions. In this case it can be easily observed that the disproportionation reaction corresponding to the *mix IT* type, which contains less Co (0.41 wt %), take place at a lower temperature, compared to the *mix motor* type (2.21 wt % Co content).

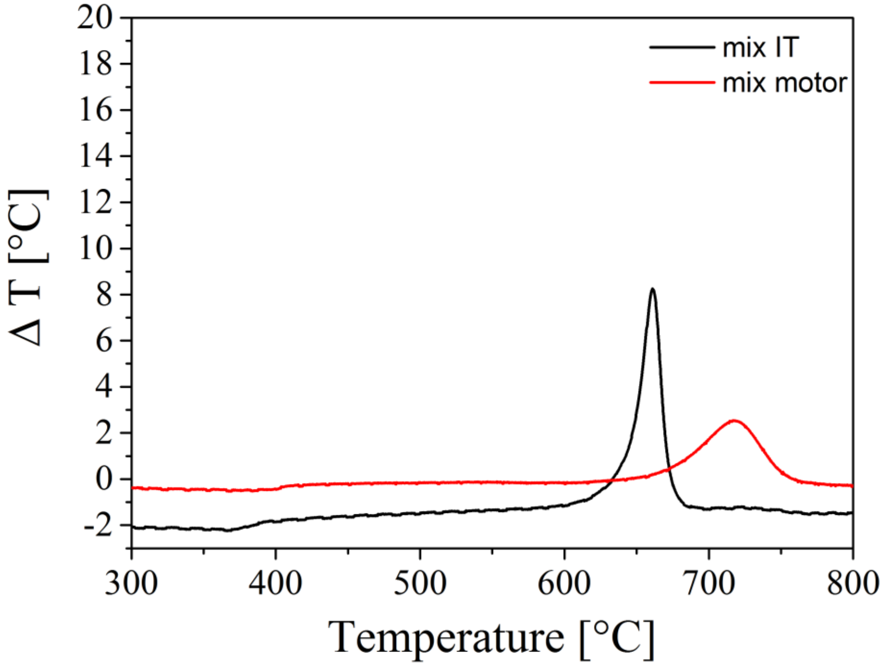

Figure 4.22-1: Differential thermal analysis curves corresponding to the disproportionation reaction of the *mix IT* and *mix motor* type magnets processed under 1 bar hydrogen pressure and 10 K/min heating rate.

To investigate the recombination behavior of the three types of scrap magnets, the samples were disporportionated in the DTA system under 1 bar hydrogen pressure, followed by a cooling to room temperature. Afterwards the hydrogen was evacuated and the powder was heated under vacuum to study the desorption and recombination behavior. This behavior is presented in figure 4.23. The powder was heated up to 900 °C under vacuum at a heating rate of 10 K/min. The desorption and recombination behavior is influenced by the content of additives from the scrap magnets. H. Nakamura reported that Co additions speed up the recombination reaction **[62]**. Further research done by S. Sugimoto confirmed the effect of Co and added also that Ga, or Co and Ga starts earlier the recombination reaction due to the increase of the activation energy **[86]**.

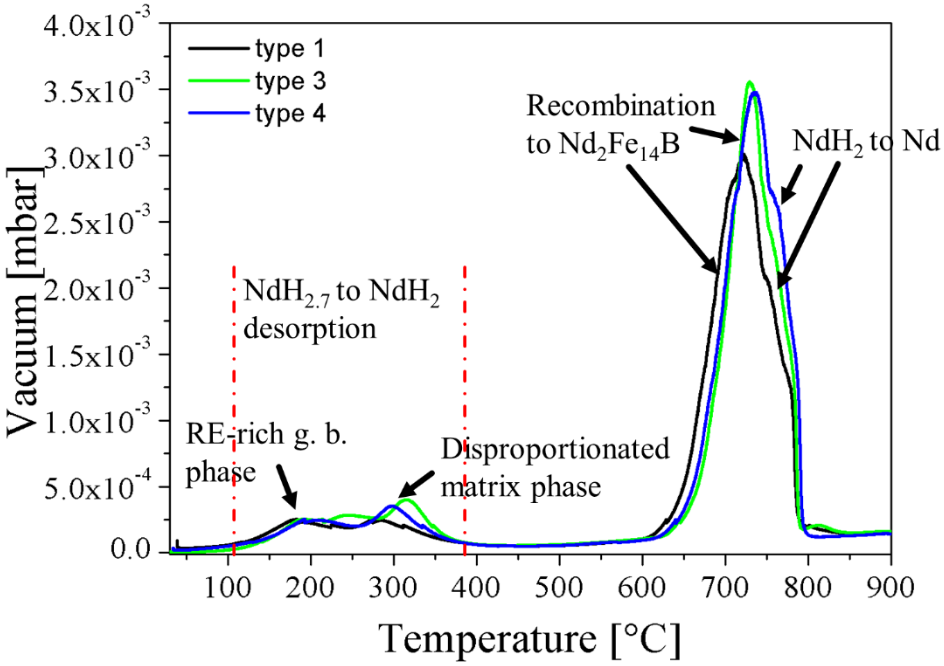

Figure 4.23: Desorption of the disproportionated *type 1*, *type 3* and *type 4*, heated under vacuum at a heating rate of 10 K/min.

The above diagram can be divided in 2 steps: first part of the desorption process that take place at temperature below 400 °C and the recombination process that takes place at temperature above 600 °C. A detailed image of the first stage of the desorption reaction is represented in figure 4.24.

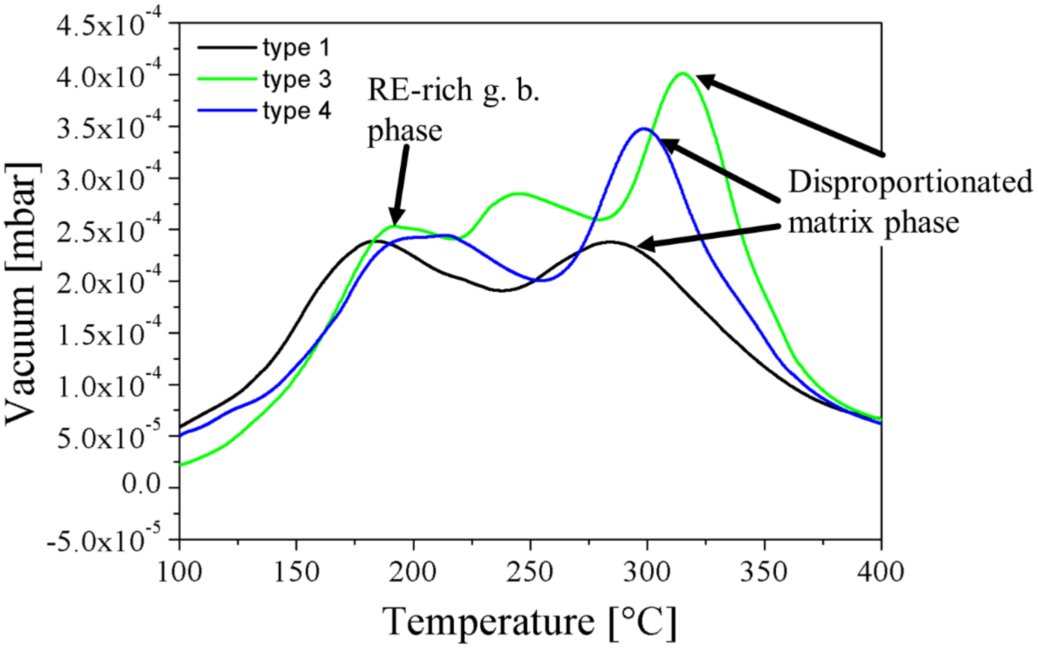

Figure 4.24: DTA desorption plot of the $NdH_{\sim2.7}$ to Nd dihydride from the disproportionated 3 types of scrap magnets, heated under vacuum at 10 K/min.

Between 100 °C and 400 °C take place the desorption of the hydrogen from the $NdH_{\sim2.7}$ and the formation of Nd dihydride **[39, 43, 44, 87, 88]**. In the presented case of the 3 types of scrap magnets these peaks can be explained as following. The initial desorption peak at the temperature of approximatively 200 °C can be attributed to the desorption of the hydrogen from $NdH_{\sim2.7}$ and the formation of Nd dihydride within the RE-rich grain boundary phase, as it corresponds with similar results presented by other researchers **[39, 88, 89]**. The second peaks of the desorption curves at temperatures of ~300 °C ~320 °C, corresponds to the desorption of the hydrogen from the $NdH_{\sim2.7}$ and the formation of Nd dihydride within the disproportionated matrix phase. The 250 °C peak, corresponding only to *type 3* scrap magnets, can be explained by the dissociation of the $Nd(OH)_3$ which gives off H_2O and H_2.

Second stage of the DTA desorption plot (figure 4.23) corresponds to the recombination reaction (as the remaining constituents recombine according to the equation (1)), and to the desorption of the hydrogen from the Nd dihydride and the formation of the Nd.

$$2NdH_{2\pm x} + 12Fe + Fe_2B \rightarrow Nd_2Fe_{14}B + 2xH_2 + \Delta H \qquad (1)$$

ΔH is the endothermic heat of the reaction (with x as a function of hydrogen pressure).

This reaction starts at the temperature of 600 °C and is finished at the temperature of 800°C for all three types of scrap magnets. The main peak corresponds to the combining of the remaining constituents to reform the $Nd_2Fe_{14}B$ phase. Therefore, the right-hand shoulder of the desorption curve from the temperatures above 600 °C can be attributed to Nd dihydride to Nd desorption within the Nd-rich grain boundary phase.

The investigation of the desorption and recombination behavior of the two mixture of scrap magnets is presented in figure 4.25. In this case, it can be better observed the effects of the additives on the recombination reaction. The Co and Ga content of the *mix IT* powder is 0.41 wt% and 0.06 wt% respectively, while *mix motor* powder has a Co content of 2.21 wt% and 0.23 wt% Ga content. This could explain the delay in the recombination reaction of the *mix IT*.

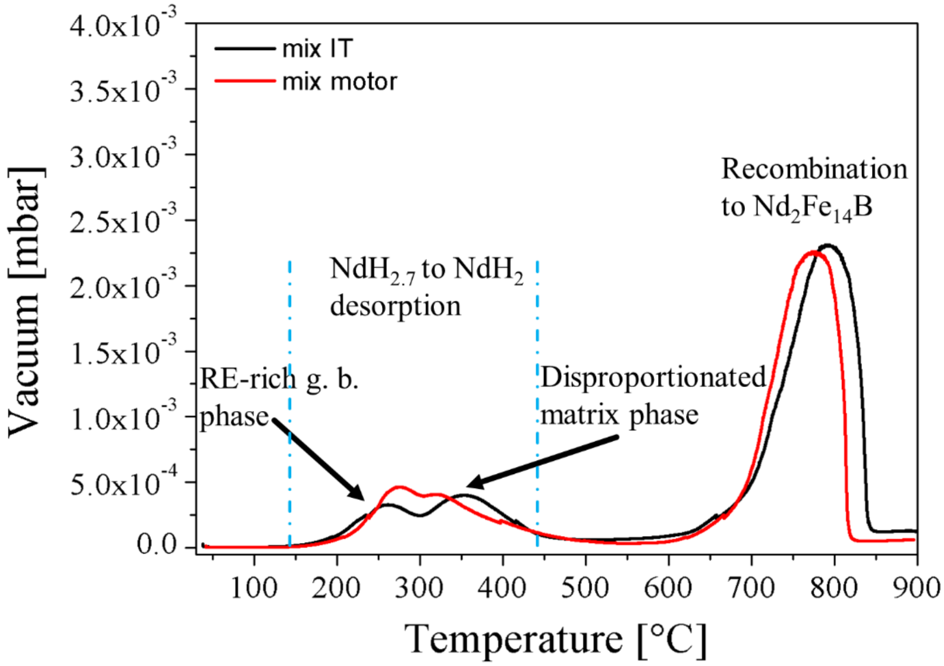

Figure 4.25: Desorption plot of the disproportionated *mix IT* and *mix motor*, heated under vacuum at a heating rate of 10 K/min.

For the first part of the desorption reaction (between ~150 °C and ~450 °C) the same behavior is manifested, with the first peak corresponding to $Nd_{\sim 2.7}$ desorption to Nd dihydride within the Nd-rich grain boundary phase and the right-hand shoulder attributed to $Nd_{\sim 2.7}$ desorption to Nd dihydride within the disproportionated matrix phase. A detailed view of this area is presented in figure 4.26

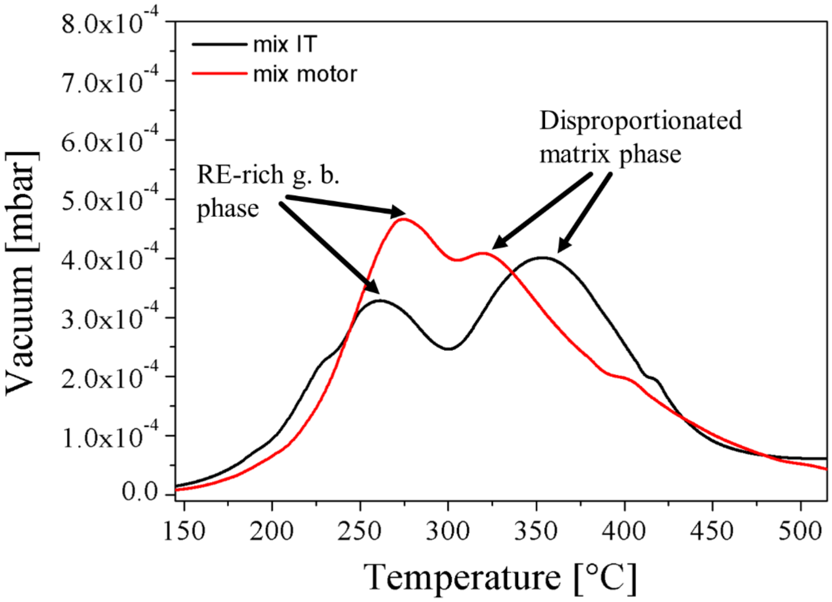

Figure 4.26: Detail of the DTA desorption plot of NdH$_{\sim 2.7}$ to Nd dihydride from the disproportionated *mix IT* and *mix motor* powders, heated under vacuum at 10 K/min.

In a second study the behavior of the disproportionation reaction with the increase of the hydrogen pressure was analyzed. For this study, all the samples were prepared from scrap magnets *type 1*, which was crushed into powder. For all the measurement was used 1 gram of powder *type 1*; the heating rate was 10 K/min. The behavior of the powder at different hydrogen pressures is shown in figure 4.27.

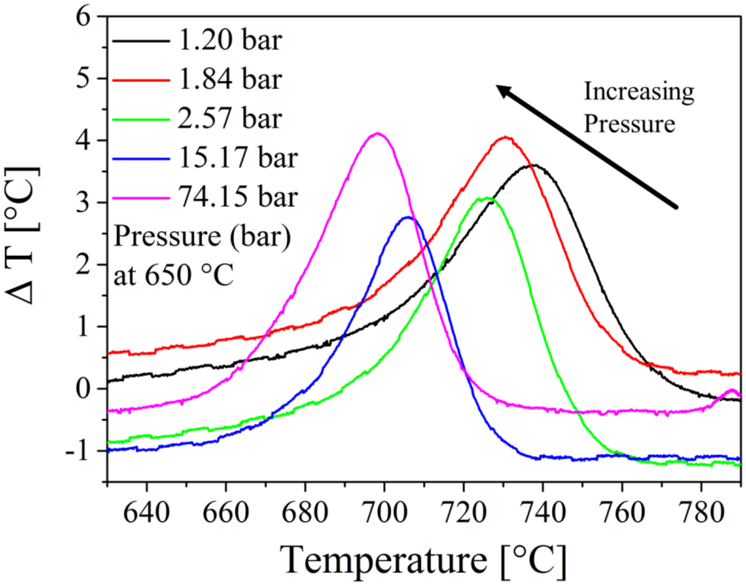

Figure 4.27: DTA of type 1 scrap magnets heated under different hydrogen pressure at 10 K/min heating rate.

It was observed that by increasing the hydrogen pressure, the temperature of the disproportionation reaction decreases. For *type 1* the peaks of the disproportionation reactions are shown in the table 4.13. Also the hydrogen pressure has an influence on the Curie temperature of the hydrogenated powder. The values of the Curie temperature for the different hydrogen pressures are shown in the table 4.13. It was observed that by increasing the hydrogen pressure the Curie temperature of the hydrogenated powder is increasing. This trend is shown in figure 4.28. The increasing Curie temperature of the hydrogenated powder at different hydrogen pressures can be explained by the quantity of the hydrogen absorbed during the hydrogenation of the powder. So by increasing the hydrogen pressure more hydrogen is going into the powder, and this result in the shifting of the Curie temperature to higher values.

Table 4.13: Temperature values for the disproportionation reaction peaks and for the Curie temperature of the hydrogenated powder at different hydrogen pressures.

Hydrogen pressure at 650 °C [bar]	**Disproportionation reaction peak [°C]**	**Curie temperature [°C]**
1.20	737	374
1.84	730	376
2.57	725	376
15.17	705	389
74.15	698	391

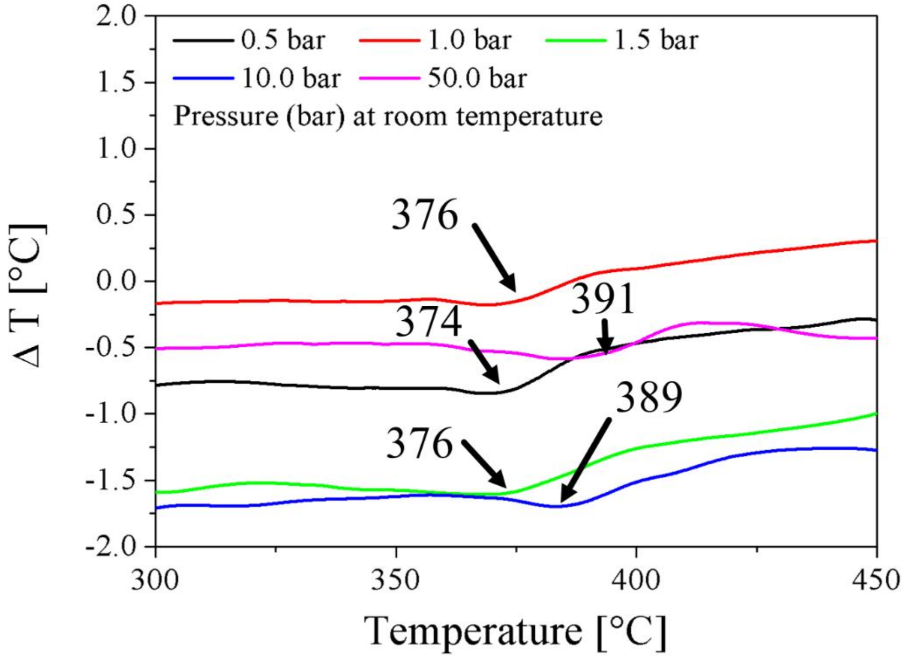

Figure 4.28: Differential thermal analysis showing the Curie temperature of the hydrogenated powder at different hydrogen pressures.

4.4 Adjusting the HDDR processing parameters

For a proper determination of the specific hydrogen pressures needed, disproportionated powders were prepared by stopping the HDDR process just before the hydrogen desorption and recombination stages take place, as is illustrated in figure 4.29. Thus the powder was cooled to room temperature under hydrogen pressure to avoid the recombination of $Nd_2Fe_{14}B$. The disproportionation of the $Nd_2Fe_{14}B$ phase is described by the following solid-state reactions:

$$Nd_2Fe_{14}B + (2 \pm x)H_2 \leftrightharpoons 12\alpha\text{Fe} + 2NdH_{(2\pm x)} + Fe_2B + \Delta H \qquad (2)$$

at temperature above 650 °C, where ΔH is the reaction enthalpy.

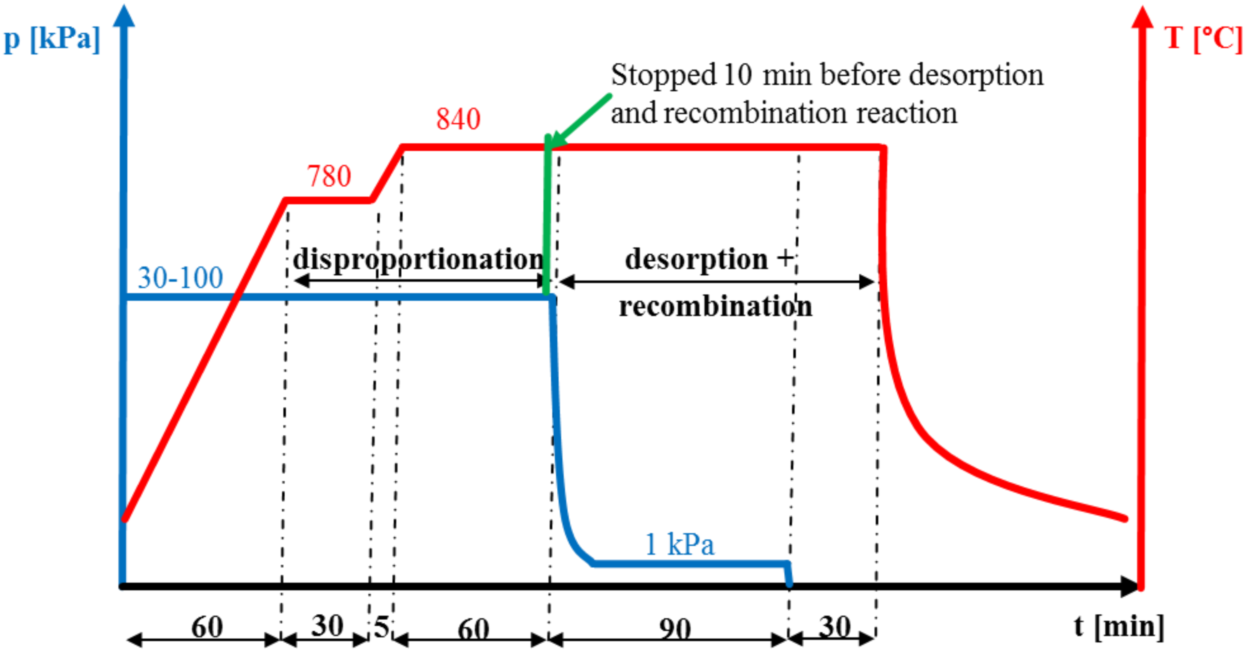

Figure 4.29: Schematic drawing showing the HDDR process and the point where the process was stopped for the study of the disproportionated powders.

The XRD patterns of the disproportionated stage produced at different hydrogen pressures for all studied scrap compositions are introduced in figure 4.30. The patterns of the fully disproportionated powders exhibit the characteristic peaks of the disproportionation reaction products NdH_x, Fe_2B and α-Fe while the partially disproportionated ones feature additional peaks e.g. corresponding to the unreacted $(Nd_2Fe_{14}B_1)H_x$ phase (here the unlabeled peaks).

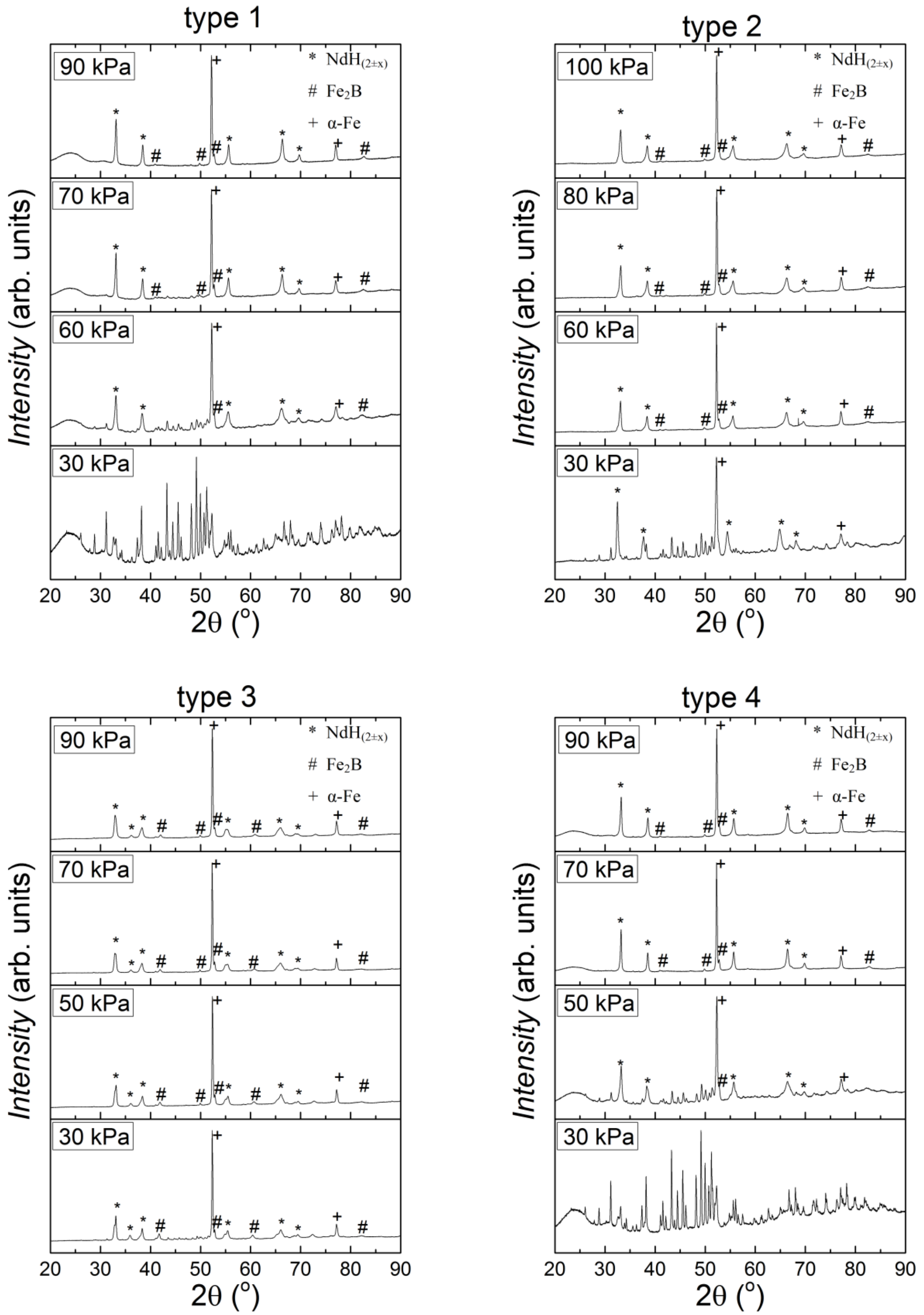
type 1
90 kPa
70 kPa
60 kPa
30 kPa
type 2
100 kPa
80 kPa
60 kPa
30 kPa
type 3
90 kPa
70 kPa
50 kPa
30 kPa
type 4
90 kPa
70 kPa
50 kPa
30 kPa
* $NdH_{(2\pm x)}$
# Fe_2B
+ α-Fe
Intensity (arb. units)
2θ (°)
20
30
40
50
60
70
80
90

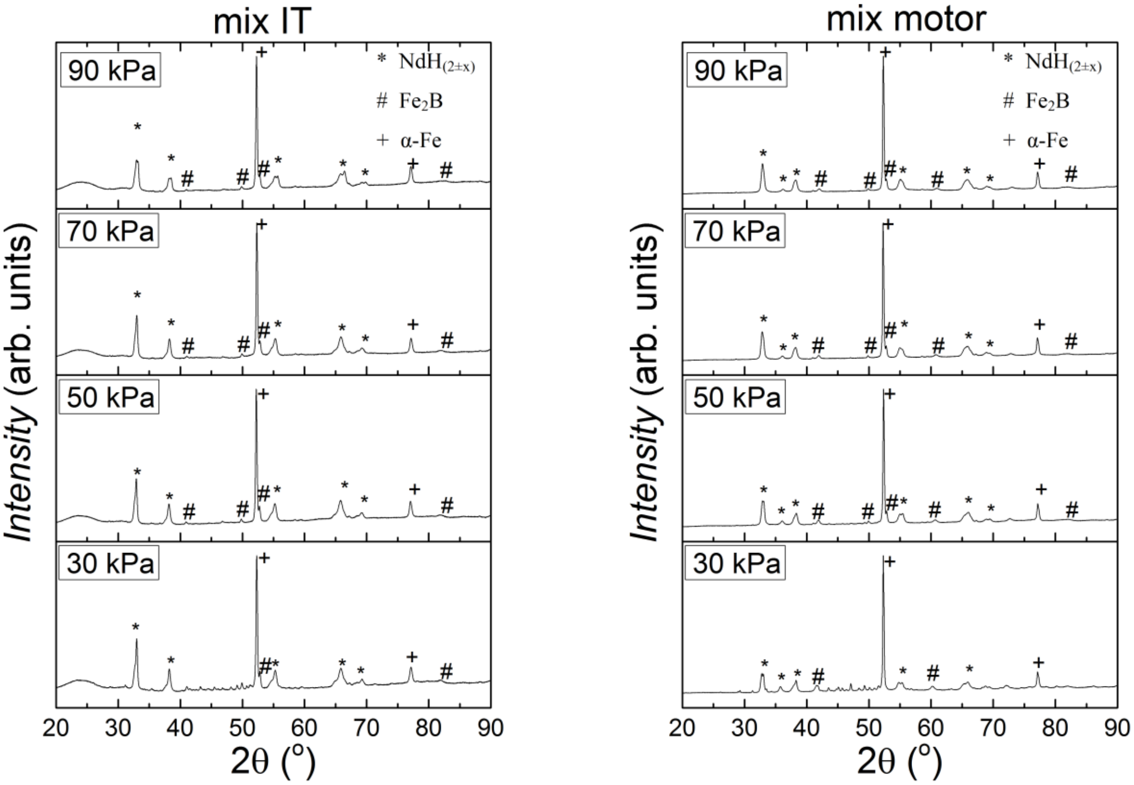

Figure 4.30: XRD patterns of the 6 types of scrap magnets, after the disproportionation step.

It can be seen that the powders processed at hydrogen pressures between 30 kPa and 50 kPa were non-disproportionated or only partially disproportionated. By rising the hydrogen pressure, the $(Nd_2Fe_{14}B)H_x$ phase will further transform in α-Fe, $NdH_{(2\pm x)}$ and Fe_2B, resulting in a decrease of the $(Nd_2Fe_{14}B)H_x$ phase reflections intensity **[90, 91]**. One may conclude here that the pressure at which the reaction starts is not enough to overcome the equilibrium pressure of the reaction, which shows in which direction the reaction will evolve, to the right, forming α-Fe, $NdH_{(2\pm x)}$ and Fe_2B, or to the left to form $Nd_2Fe_{14}B$. The equilibrium point of the reaction is influenced by the Gibbs free energy of the metal hydrides which decreases for NdH_x **[92, 93]**, meaning that it becomes more stable by increasing the hydrogen pressure. The Gibbs free energy of the reaction result is decreasing with the hydrogen pressure increase while on the left side of the reaction; the Gibbs free energy is almost unchanged. It is also known that the disproportionation reaction starts from the rare earth grain boundary, which helps the diffusion of the hydrogen through the center of the grain **[94]**. We have thusly used the XRD patterns to determine the lowest hydrogen pressure where the powder is fully disproportionated, i.e. the hydrogen pressure where the XRD pattern show only reflections of the α-Fe, $NdH_{(2\pm x)}$ and Fe_2B phases.

For a better assessment of the lowest hydrogen pressure the XRD results were further correlated with the hydrogen absorption behavior determined by differential thermal analysis. Since the HDDR processing temperature was the same for all the magnets the completion of the disproportionation reaction was realized by increasing the hydrogen pressure. From the DTA analysis can be observed that for *type 1* magnets the peak of the disproportionation reaction occurs at the temperature of 730 °C. This corresponds to the XRD results which show that *type 1* magnets require the highest hydrogen pressure (90 kPa) in order to complete the disproportionation reaction. The DTA results shows that for *type 2* and *type 4* the disproportionation reactions take place at a lower temperature (the peak of the reaction is at 728 °C for *type 2* and at 729 °C for *type 4*), which confirms the XRD results, which shows that for *type 2* and *type 4* a 70 kPa hydrogen pressure is enough for a fully disproportionation reaction. For the *type 3* scrap magnets the XRD analysis shows that the disproportionation reaction is completed at the same hydrogen pressure of 70 kPa, but from the DTA results the disproportionation reaction occurs at even smaller temperature (the peak of the disproportionation reaction occurs at the temperature of 719 °C).

In order to determine the impact of the HDDR hydrogen pressure parameter on the resulting magnetic properties of the different recycled powders, the complete HDDR process was run while systematically varying the pressure within the ranges of 30 kPa to 150 kPa for *type 1* and 30 kPa to 110 kPa for all compositions. The temperature was set at 780 °C for the first plateau and 840 °C for the second one (from now referred as 780/840 °C) while the hydrogen desorption rate was fixed at 2.2 L/min. The evolution of the coercivity and remanence with hydrogen pressure is presented in figure 4.31.

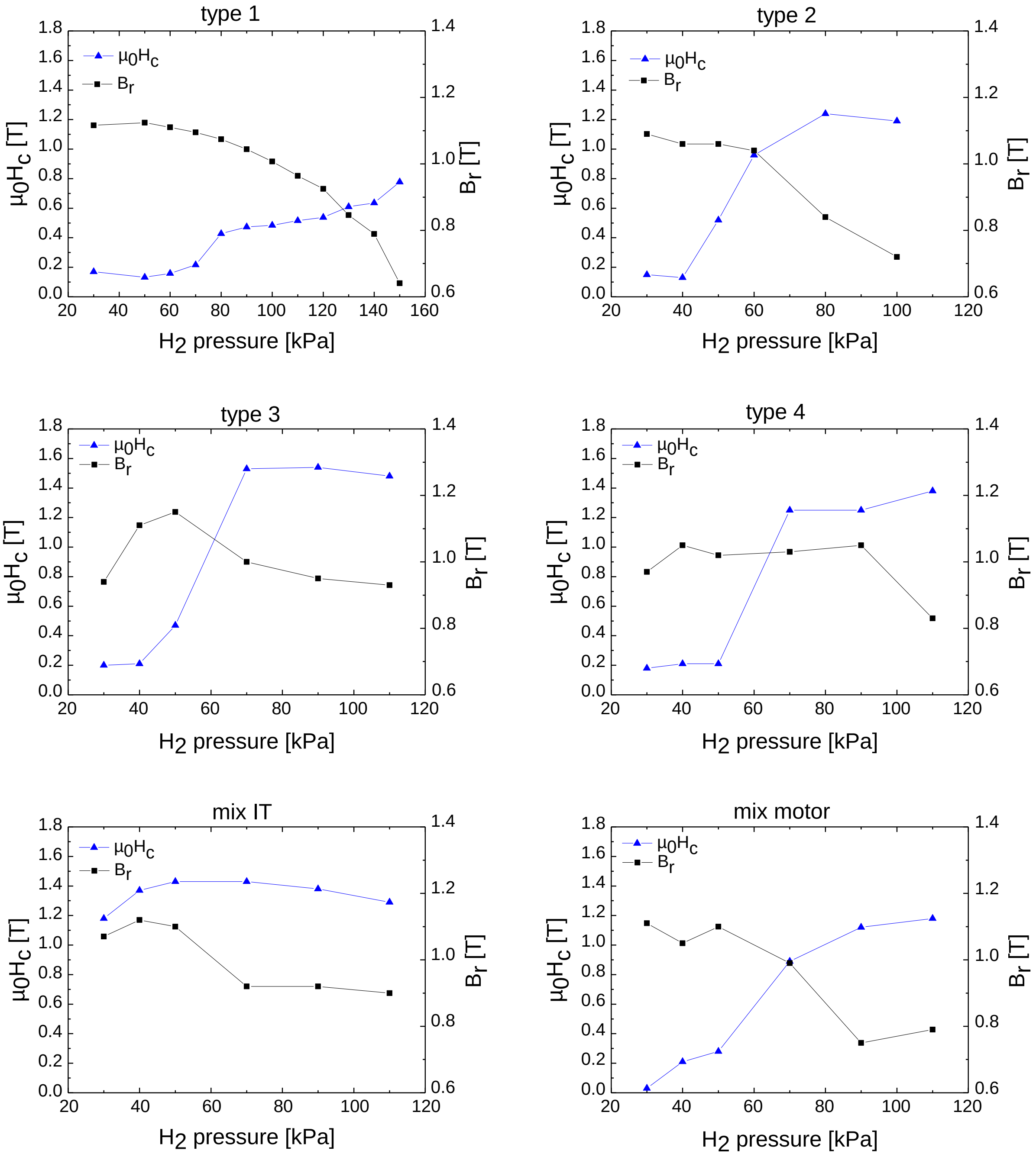

Figure 4.31: The evolution of the coercivity and remanence with hydrogen pressure.

The resulting HDDR powders are anisotropic when the process was conducted at hydrogen pressures of up to 20 kPa, above the critical point where the powder becomes completely disproportionated. Above this limit of +20 kPa, the powder anisotropy starts decreasing. This evolution is shown in figure 4.32.

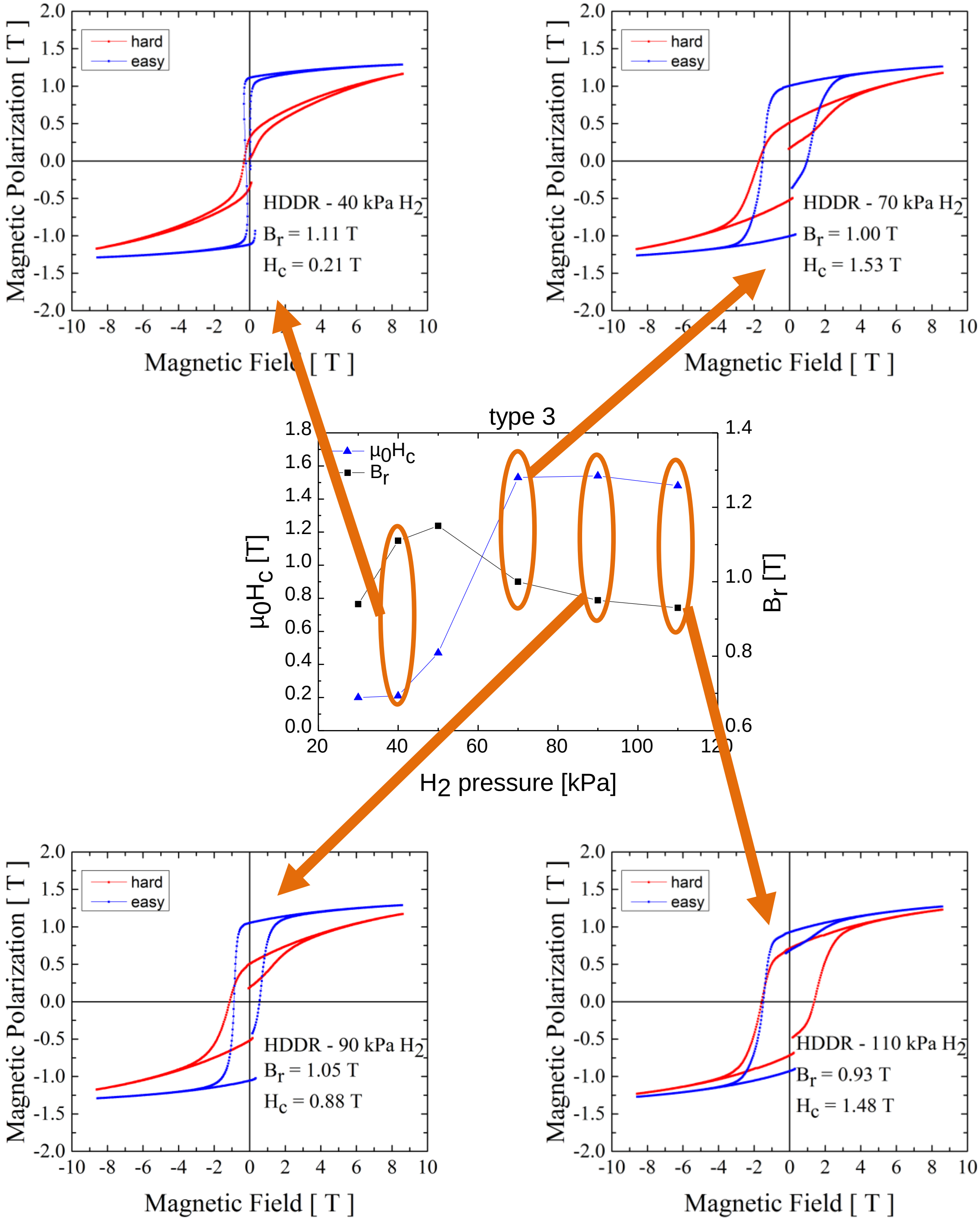

Figure 4.32: Evolution of the hysteresis loops by increasing of the hydrogen pressure for the *type 3* magnets.

The next studied parameter was the desorption rate of the hydrogen. This approach will lead to a systematic understanding of how fast or slow the hydrogen needs to be absorbed from the powder. The desorption rate was varied between 0.3 L/min and 45 L/min. For all the experiments performed where the rate of desorption was studied, the processing temperature was 780/840 °C and the hydrogen pressure was 90 kPa. Desorption rate was performed by pumping with a rotary pump the sample chamber, via a bypass from where desorption rate was controlled. The time allocated for the desorption was 90 minutes. An illustration of the HDDR process, where the desorption was varied, is presented in figure 4.33. The desorption stage is framed by the green bars. In the figure are illustrated four possible hydrogen desorption traces labeled as 1, 2, 3 and 4. For all desorption rates the time allocated for the hydrogen desorption was kept at 90 minutes. For the smallest desorption rate of 0.3 L/min, this time was not enough to allow desorption of the entire hydrogen from the samples and when the turbo pump was connected the hydrogen pressure inside the sample chamber did not reach 1 kPa.

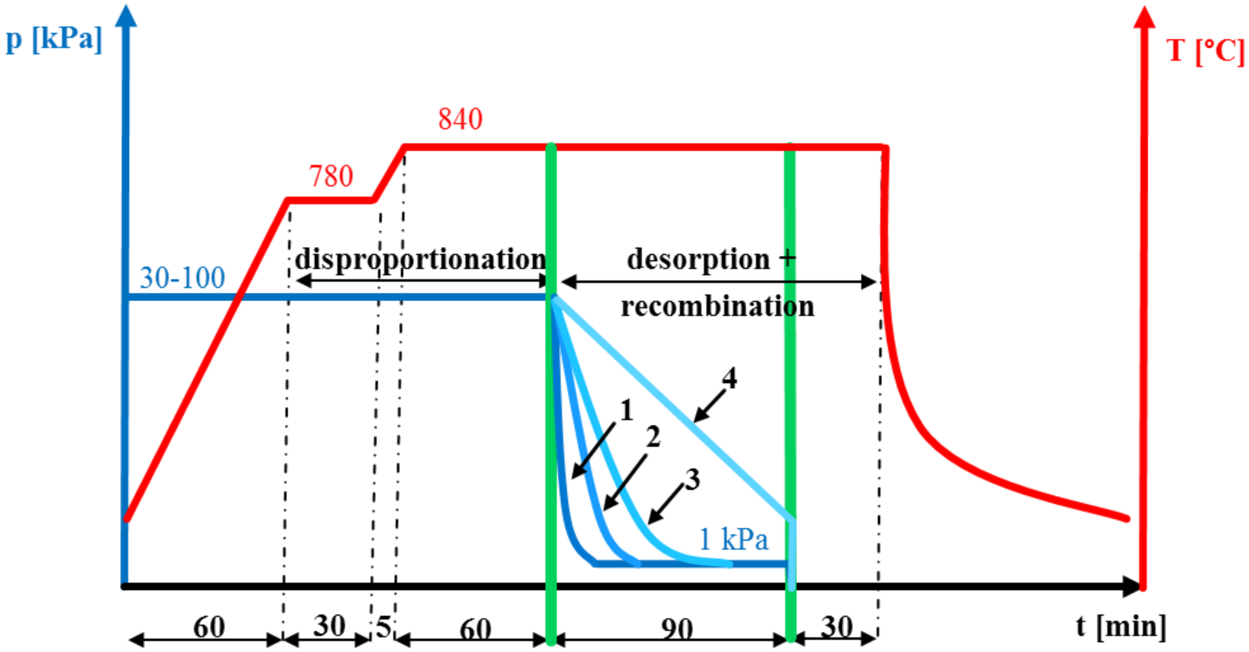

Figure 4.33: Schematic illustration of the HDDR process with a focus on the desorption rate, and possible traces of the hydrogen desorption.

All the samples prepared at different hydrogen desorption rates were embedded and magnetically measured. The dependence of the coercivity and remanence on the rate of desorption is illustrated in figure 4.34.

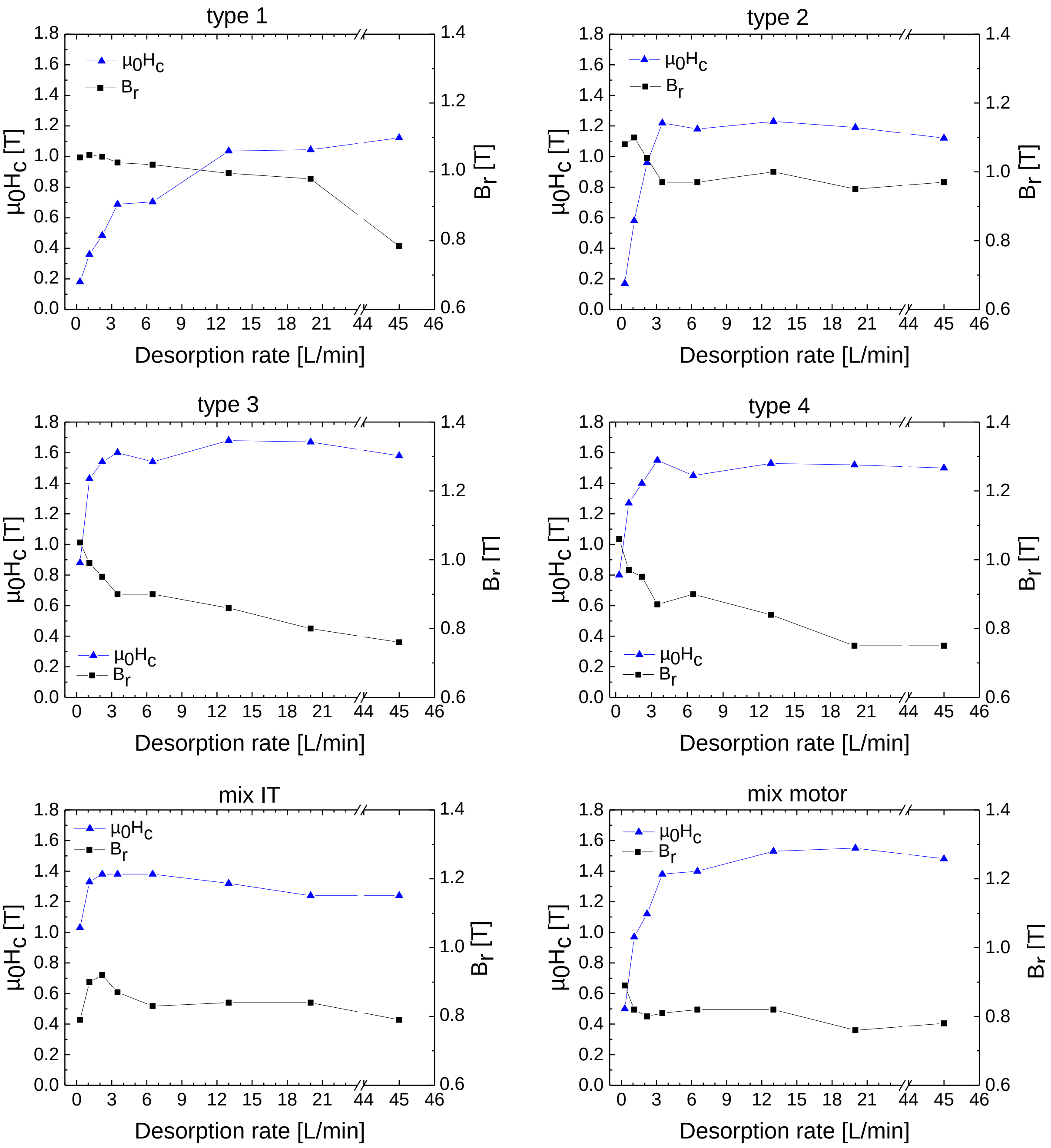

Figure 4.34: The coercivity and remanence plotted against the variation of the desorption rate for the 6 types of scrap magnets.

It is well-known that the HDDR process requires an optimization of the hydrogen evacuation rate during the recombination process because a too rapid evacuation would cause a large undercooling effect which is detrimental for the texture **[94]**. This observation comes in agreement with the results. For low desorption rates the coercivity of the powder is low, but by raising the rate of the hydrogen desorption the coercivity is improved. It is important to emphasize that for high desorption rates (>15 L/min) the obtained powder is isotropic, while for desorption rates smaller than 15 L/min the powder texture is improved. This behavior is illustrated in figure 4.35.

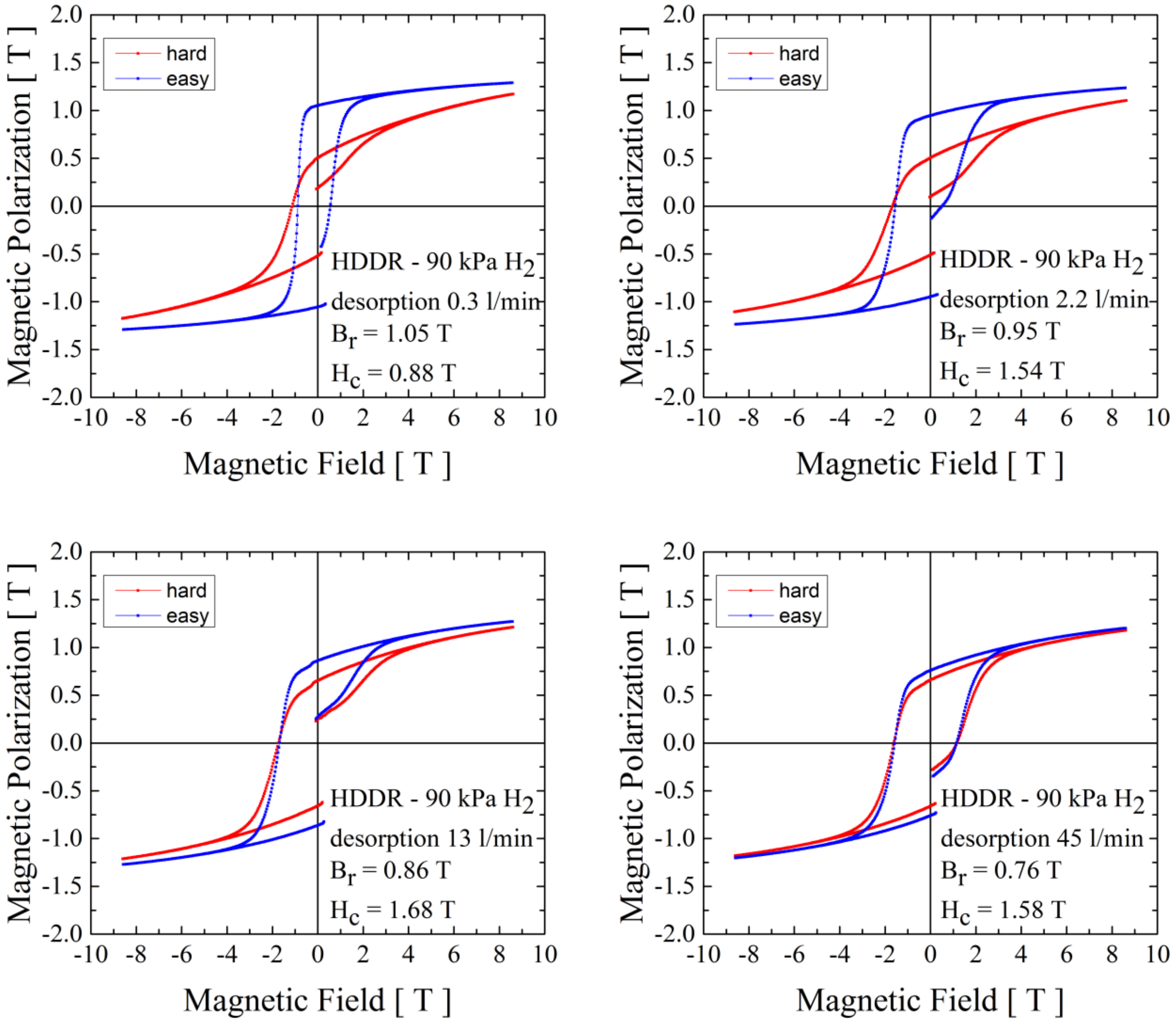

Figure 4.35: Hysteresis loops evolution with the increasing of the hydrogen pressure for the *type 3* magnets.

The HDDR process temperature was also varied while the hydrogen pressure was kept at 90 kPa and the desorption rate at 2.2 L/min. It is known that at temperature between 700 °C and 900 °C the reactions transformation rate during HDDR is at its maximum **[92]**. As a result, the following temperature were applied: 680/740 °C (on graph as 740 °C), 730/790 °C (on graphs as 790 °C), 780/840 °C (on graph as 840 °C), 830/890 °C (on graph as 890 °C). The evolution of the resulting magnetic properties is presented in figure 4.36.

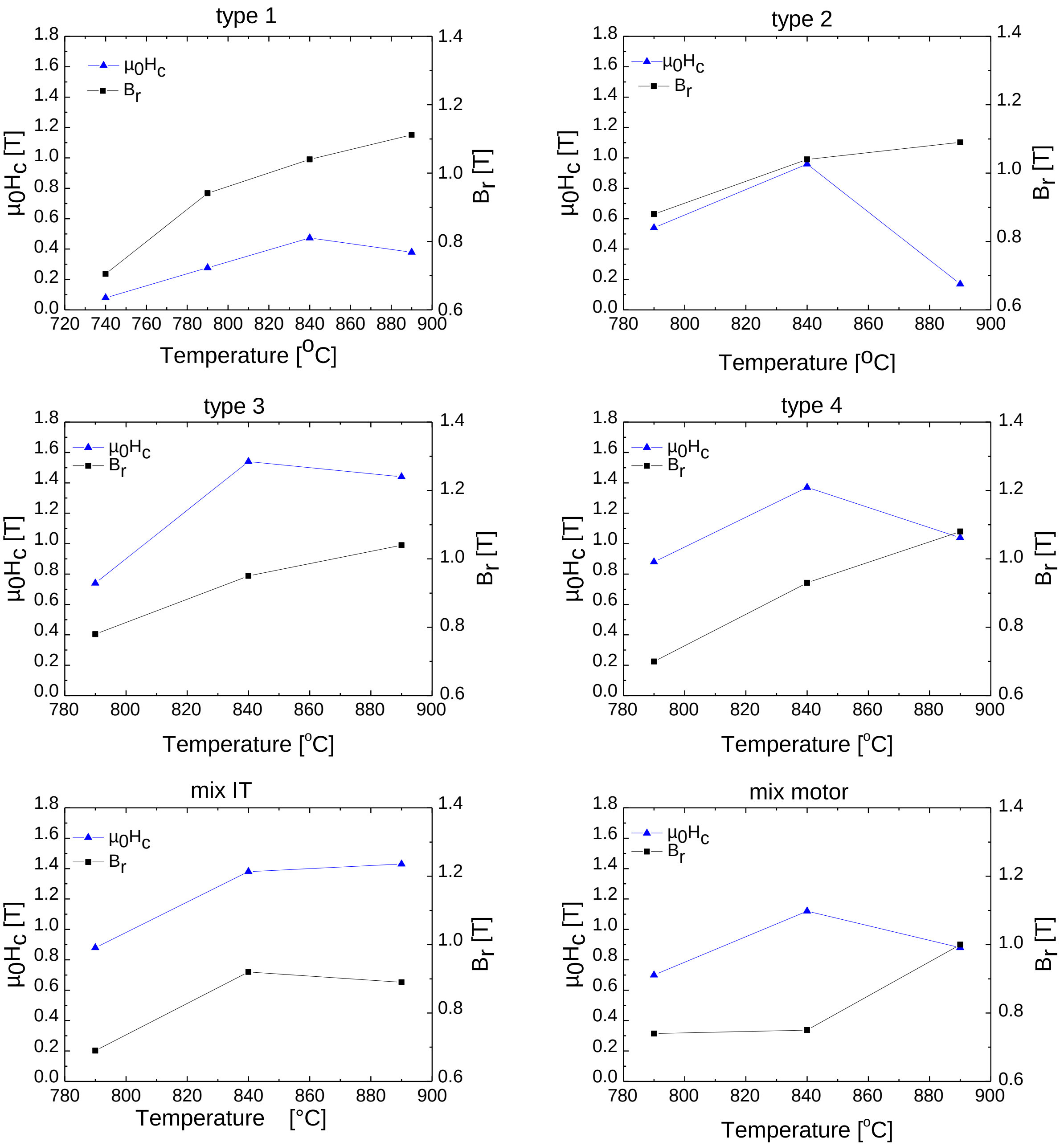

Figure 4.36: The evolution of the magnetic properties with the increase of the HDDR process temperature.

The experiments show that within the chosen temperature range, all powder samples are textured as a result of the adapted HDDR process. The decrease of the coercivity for the series prepared at 830/890 °C can be explained by grain growth at these high temperatures which is illustrated by SEM investigation performed on powders prepared at different temperature (figure 4.37).

By analyzing the SEM images, it can be observed that the samples prepared at a temperature of 730 °C for the first plateau and 790 °C for the second plateau, presents submicronic grains in the range 200 nm – 500 nm. For the samples prepared at this temperature was observed a bigger concentration of oxide particles on the surface of the powder, which may explain the lower magnetic properties. The number of oxide particles is decreasing with the increasing of the temperature or with the increasing in the grains size. For the powders prepared at the temperature of 780 °C for the first plateau and 840 °C for the second plateau, the grains are slightly bigger with grain sizes between 300 nm and 500 nm. In this case the grain size distribution is better: most of the grains having a size between 350 nm and 450 nm. For the powders prepared at the temperature of 830 °C for the first plateau and 890 °C for the second plateau, a visible increase in grain size can be observed. In this case the grains have a grain size between 300 nm and 1μm. For some particles, beside the submicronic grains, huge grains were observed as it is shown in figure 4.38. This is also the reason of the coercivity decrease.

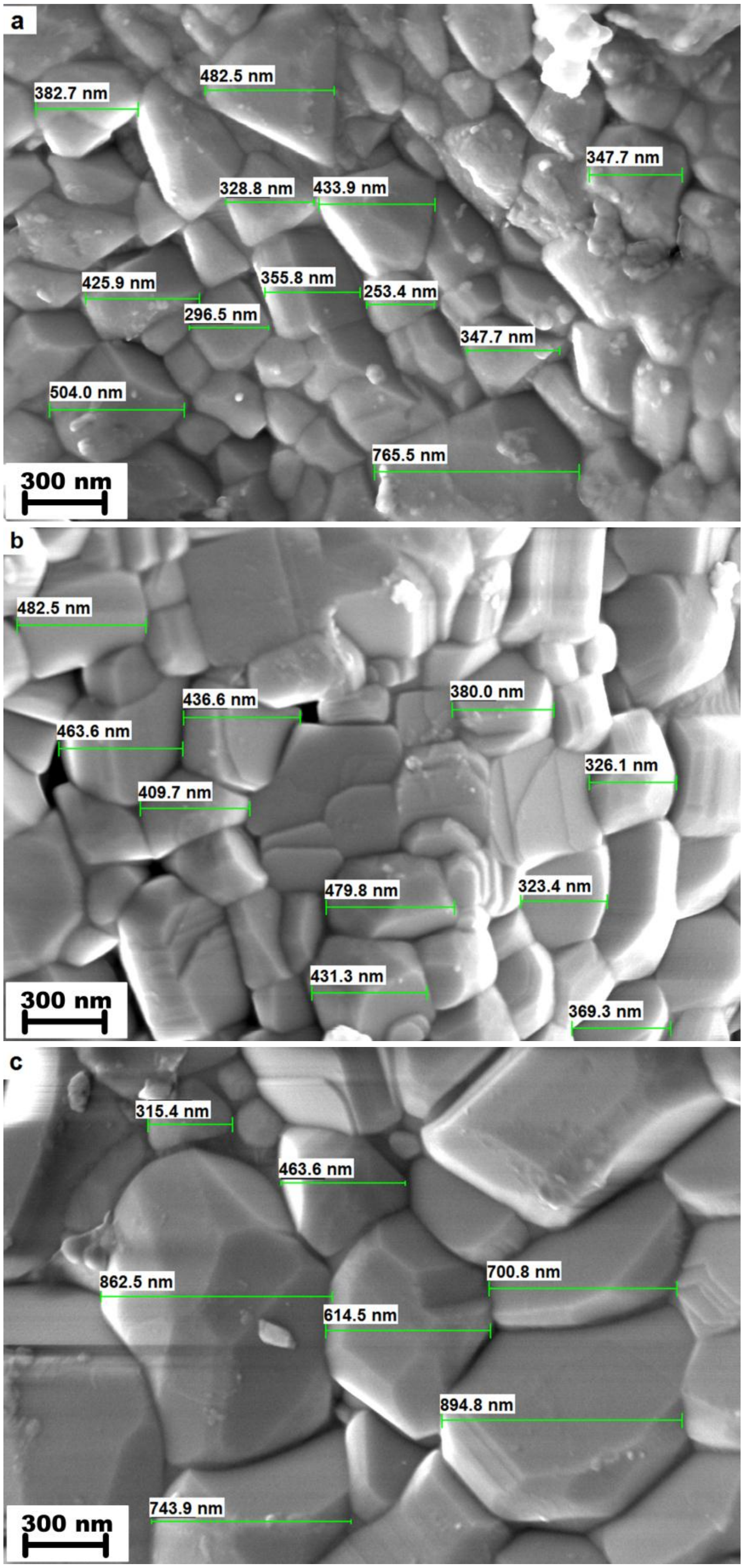

Figure 4.37: SEM images of the *mix IT* type of magnets which show the grains growth that occurs at different processing temperature: a) 730/790 °C, b) 780/840 °C, c) 830/890 °C.

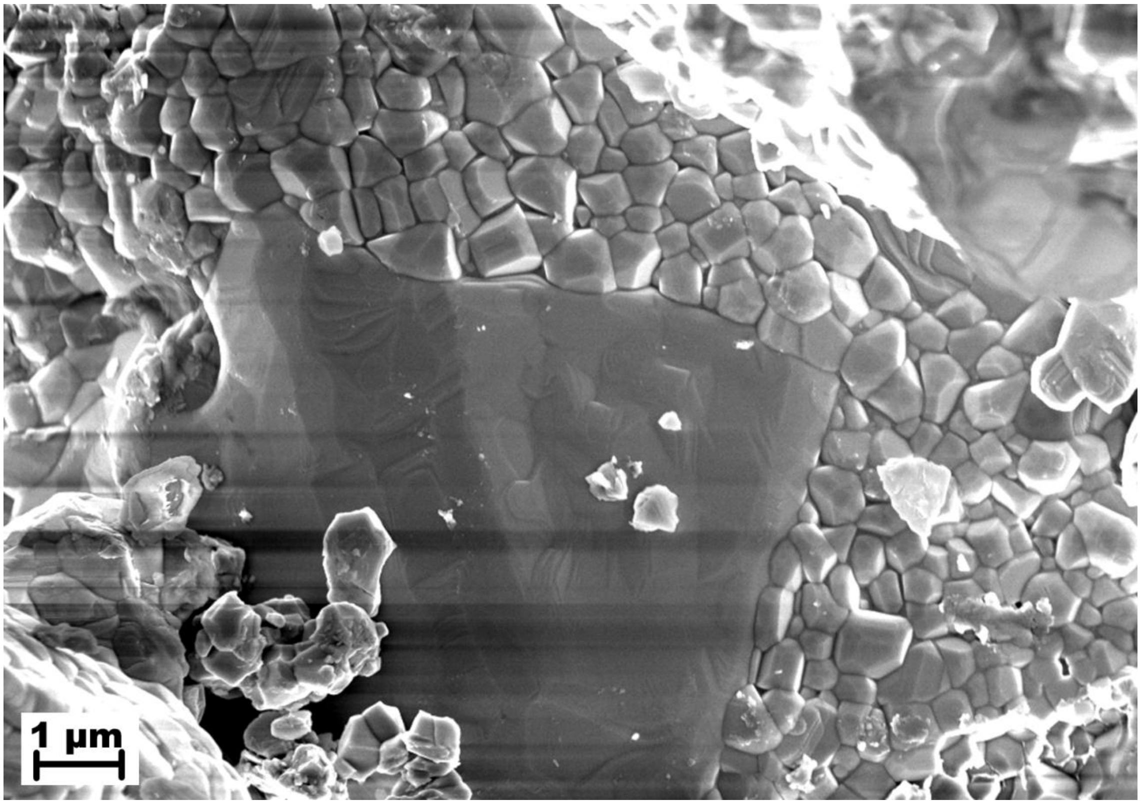

Figure 4.38: SEM images of the mix IT type of magnets which show the grains growth for the samples processed at the temperature of 830/890 °C.

4.5 Effect of Dy content on the HDDR processing parameters

To have a better understanding on how Dy content influence the disproportionation and recombination reactions, 4 types of powders with different Dy content were prepared. For this, 2 alloys were prepared by induction melting, $Nd_{15}Fe_{79}B_6$ and $Nd_{10.875}Dy_{4.125}Fe_{79}B_6$ respectively. After melting the two alloys were homogenized in vacuum for 48 hours at 1100 °C. To determine that the alloys are properly homogenized, SEM and XRD analyses were performed and the results are shown in figure 4.39.

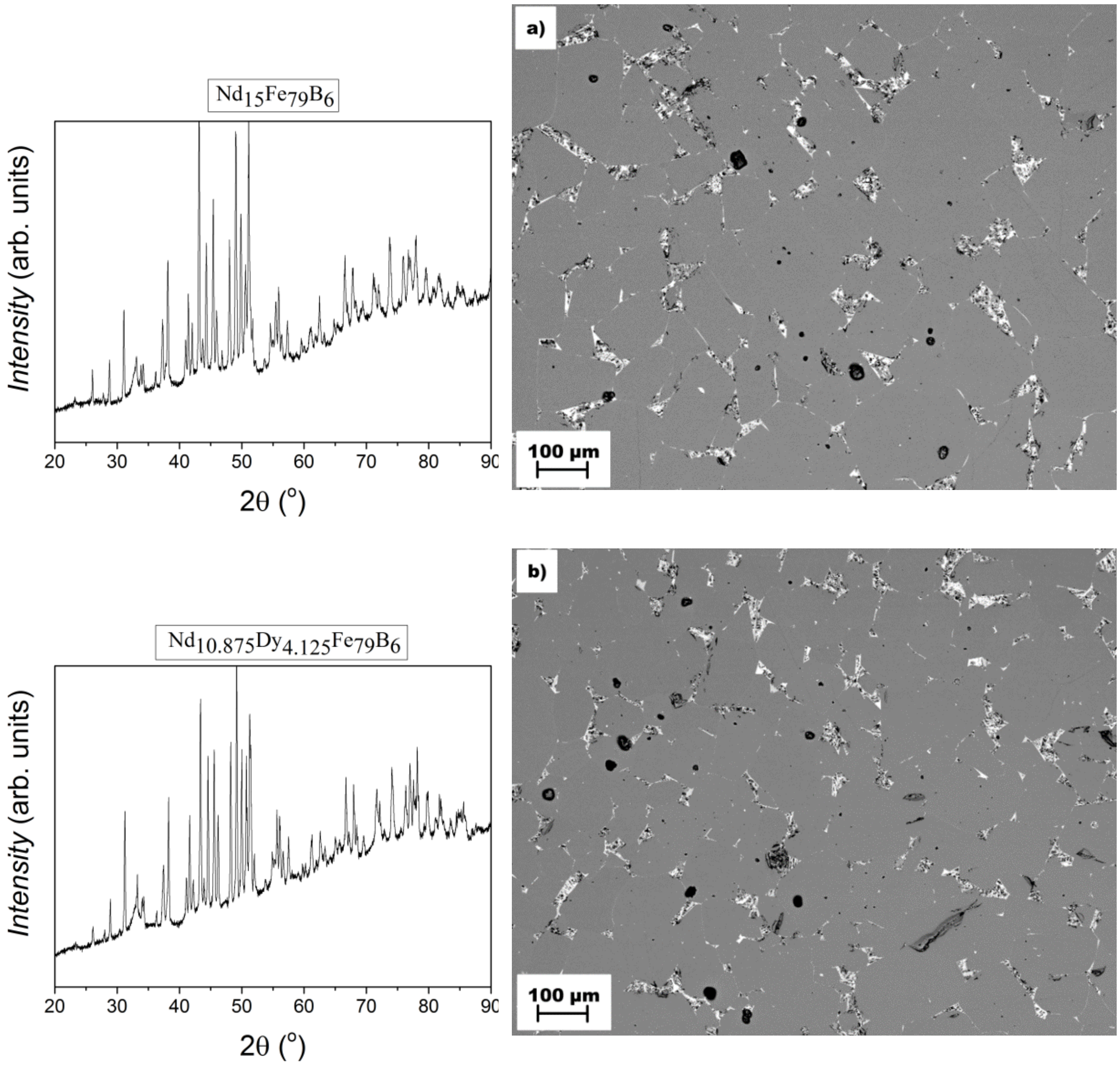

Figure 4.39: XRD analysis and SEM backscattered electrons images of: a) $Nd_{15}Fe_{79}B_6$ and b) $Nd_{10.875}Dy_{4.125}Fe_{79}B_6$ homogenized samples.

From the XRD and SEM analysis as it can be observed from the above images, the main crystallographic phases evidenced are: the matrix $Nd_2Fe_{14}B$ (gray contrast in the SEM image) phase and the surrounding intergranular rare earth rich phase Nd-Dy or Nd (white contrast in the

SEM image), and no other secondary phases. The homogenized alloys were decrepitated under 1 bar hydrogen pressure at room temperature. The resulted decrepitated powders were grinded in the Argon box with mortar and pestle. Then, the two powders were mixed between them, in order to create $Nd_{15}Fe_{79}B_6$ powder with different Dy content, according to the following stoichiometric calculation.

Starting materials: $Nd_{15}Fe_{79}B_6$ and $Nd_{10.875}Dy_{4.125}Fe_{79}B_6$

$$M = \frac{m}{n} \tag{3}$$

where M is the molar mass in kg/mol or g/mol, m is the mass of the chemical compound in grams, n amount of the chemical compound in mol.

For $Nd_{15}Fe_{79}B_6$: M ($Nd_{15}Fe_{79}B_6$) = 6640.245 g/mol

$Nd_{10.875}Dy_{4.125}Fe_{79}B_6$: M ($Nd_{10.875}Dy_{4.125}Fe_{79}B_6$) = 6715.559 g/mol

So if we want to obtain $Nd_{15}Fe_{79}B_6$ + 5 % Dy

$$Z = \frac{Dy}{Nd}\ \% \quad \text{in our chase will be 5\%} \tag{4}$$

This means that the formula is kept as $(Nd\text{-}Dy)_{15}Fe_{79}B_6$ and Dy content is the only element that varies, to simplified the calculation Fe and B can be neglected in the next calculation.

If we consider: $n_1 \cdot Nd_aFe_bB_c$

$n_2 \cdot Nd_dDy_eFe_fB_g$

From eq. (4) => $Z = \frac{n_2 \cdot e}{n_1 \cdot a + n_2 \cdot d}$

=> $n_2 \cdot e = Z \cdot (n_1 \cdot a + n_2 \cdot d)$

=> $n_2 \cdot (e - Z \cdot d) = Z \cdot n_1 \cdot a$

=> $n_2 = \frac{Z \cdot n_1 \cdot a}{e - Z \cdot d}$

For 10 g of $Nd_{15}Fe_{79}B_6$ $n_1 = \frac{m_1}{M_1} = \frac{10}{6640.245} = 150.597 \cdot 10^{-5}\, mol$

=> $n_2 = \frac{Z \cdot n_1 \cdot a}{e - Z \cdot d} = \frac{0.05 \cdot 150.597 \cdot 10^{-5} \cdot 15}{4.125 - 0.05 \cdot 10.875} = \frac{112.947 \cdot 10^{-5}}{3.58125} = 31.538 \cdot 10^{-5}\, mol$

=> $m_2 = M_2 \cdot n_2 = 6715.559 \cdot 31.538 \cdot 10^{-5} = 2.118\, g$

So 10 g of $Nd_{15}Fe_{79}B_6$ needs to be mixed with 2.118 g of $Nd_{10.875}Dy_{4.125}Fe_{79}B_6$ in order to obtain $Nd_{15}Fe_{79}B_6$ + 5%Dy.

Considering the presented stoichiometric calculations, the following mixture were obtained $Nd_{15}Fe_{79}B_6$ + 1%Dy; $Nd_{15}Fe_{79}B_6$ + 2%Dy; $Nd_{15}Fe_{79}B_6$ + 5%Dy. It was chosen this method of obtaining different alloys with different Dy content, because in this way the obtained mixture is closer to the situation found in the recycling process, where different magnets with different Dy content will be mixed together.

The obtained mixtures together with the starting $Nd_{15}Fe_{79}B_6$ alloy were used to study the influence of Dy content on the disproportionation and recombination reactions. For the 4 types of mixture with different Dy content the absorption and desorption reactions were studied using a differential thermal analyzer (DTA). The study was performed on one gram of powder, a hydrogen pressure of 1 bar at room temperature and a heating rate of 10 K/min. The results are shown in figure 4.40.

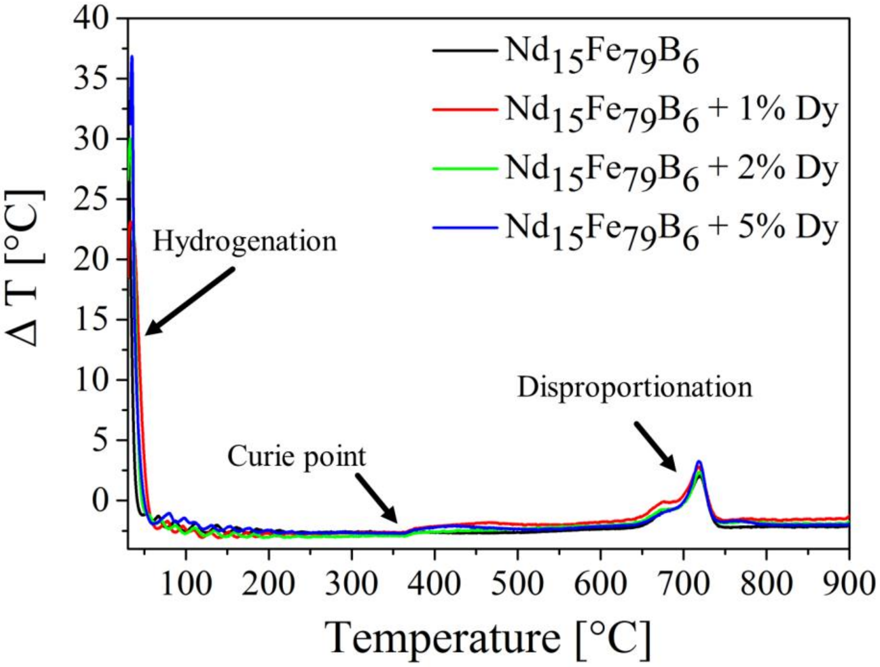

Figure 4.40: DTA absorption plot of $Nd_{15}Fe_{79}B_6$ and $Nd_{15}Fe_{79}B_6$ with different Dy content, heated in 1 bar hydrogen pressure at a rate of 10 K/min.

As it was expected and as it can be seen from the figure 4.41 the Curie temperature of the hydrogenated powders is not changing by the increasing of the Dy content. The Curie temperature of all hydrogenated mixtures is 364 °C. In figure 4.42 is presented a detailed view of the disproportionation reaction. The DTA results show that the disproportionation reaction is not influenced by the increasing of the Dy content. The disproportionation reactions start at 640 °C and the peak of the reaction is at 719 °C. For all the compositions the reaction finished at the temperature of 740 °C.

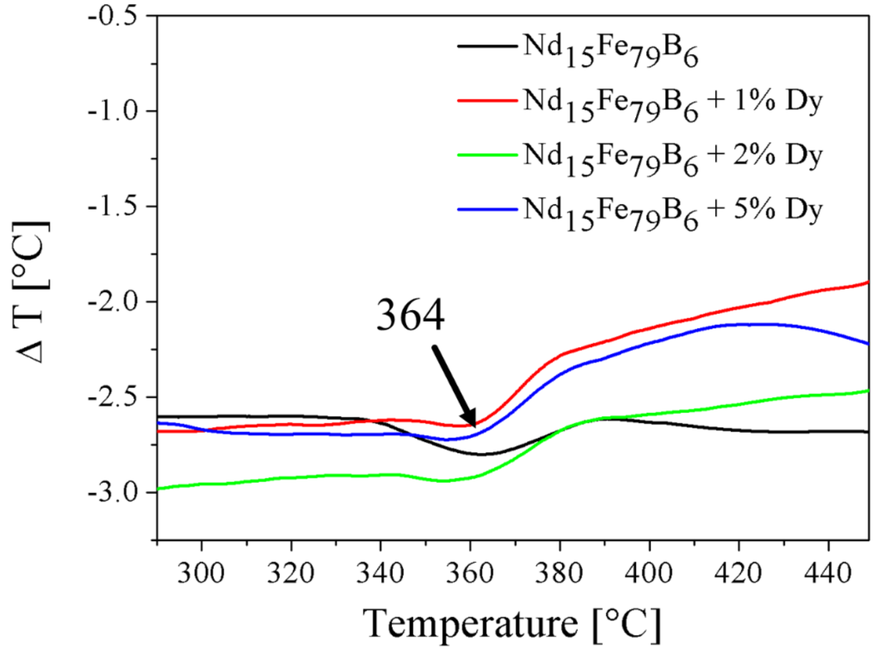

Figure 4.41: DTA absorption plot showing the Curie temperature of the hydrogenated of $Nd_{15}Fe_{79}B_6$ and $Nd_{15}Fe_{79}B_6$ with different Dy content.

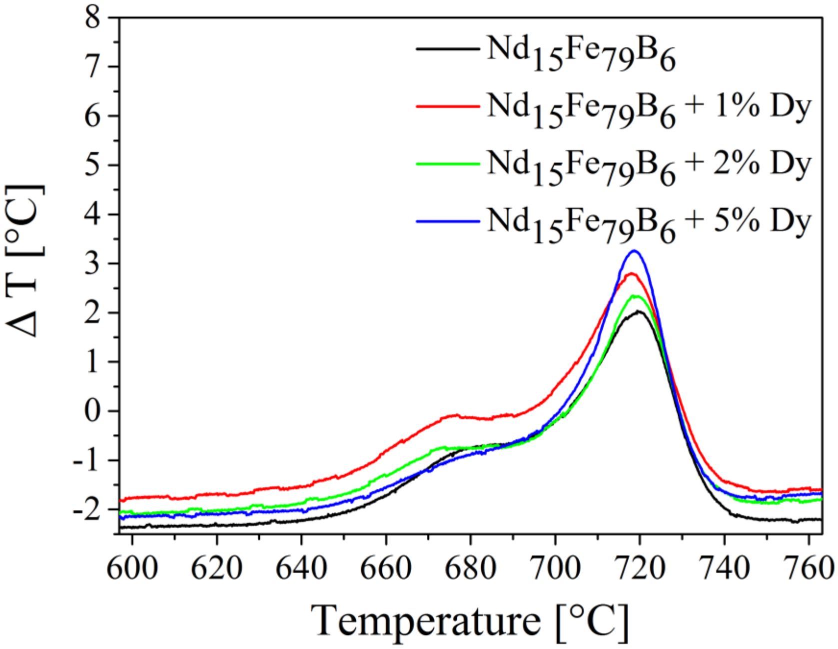

Figure 4.42: DTA plot showing the disproportionation reaction of $Nd_{15}Fe_{79}B_6$ and $Nd_{15}Fe_{79}B_6$ with different Dy content.

In order to investigate the recombination behavior of the mixtures with different Dy content, samples were disproportionated in a DTA in 1 bar hydrogen like it was presented in figure 4.40, then cooled to room temperature, evacuated and then heated under vacuum with a heating rate of 10 K/min. The results of the analysis are presented in figure 4.43.

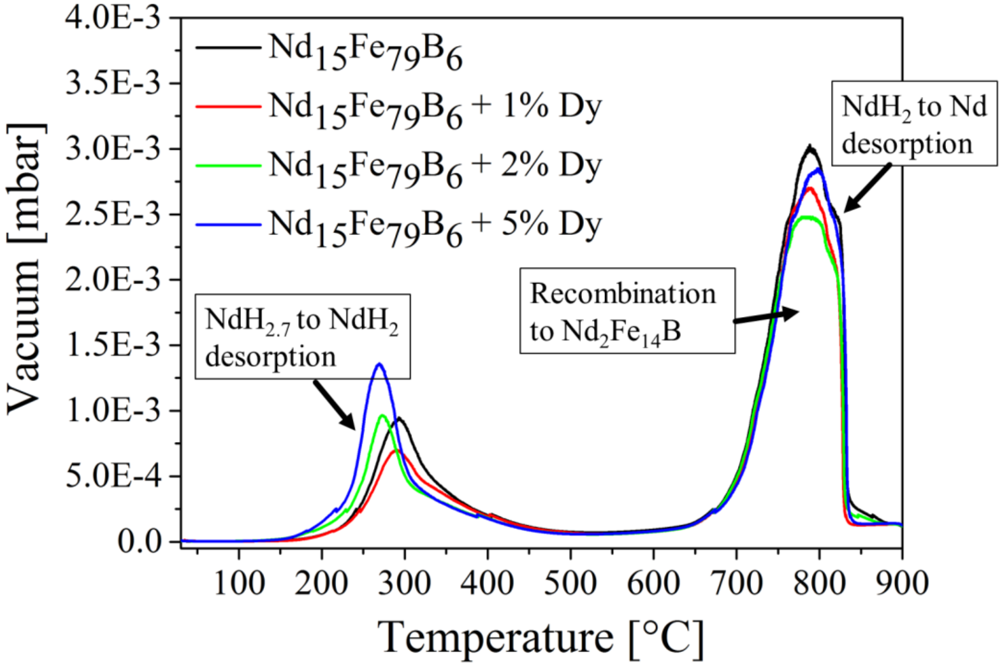

Figure 4.43: DTA desorption plot of the disproportionated powders heated under vacuum at 10 K/min.

Between 150 °C and 400 °C the $NdH_{\sim 2.7}$ from all disproportionated samples desorb and form Nd dihydride which corresponds with the literature **[39, 44, 88]**. But it can be observed that by increasing the Dy content, the desorption reaction peaks are shifted to lower temperature. So if for the $Nd_{15}Fe_{79}B_6$ the maximum peak of the reaction is reached at the temperature of 293 °C, by increasing the Dy content to 1 wt% the maximum reaction is achieved at the temperature of 290 °C. For 2 wt% and 5 wt% Dy the shift is more pronounced, the mixtures reaching the maximum of the reactions at the temperatures of 273 °C for 2 wt% Dy, and 269 °C for 5 wt % Dy. A detailed image of the hydrogen desorption from $NdH_{\sim 2.7}$ to Nd dihydride is presented in figure 4.44.

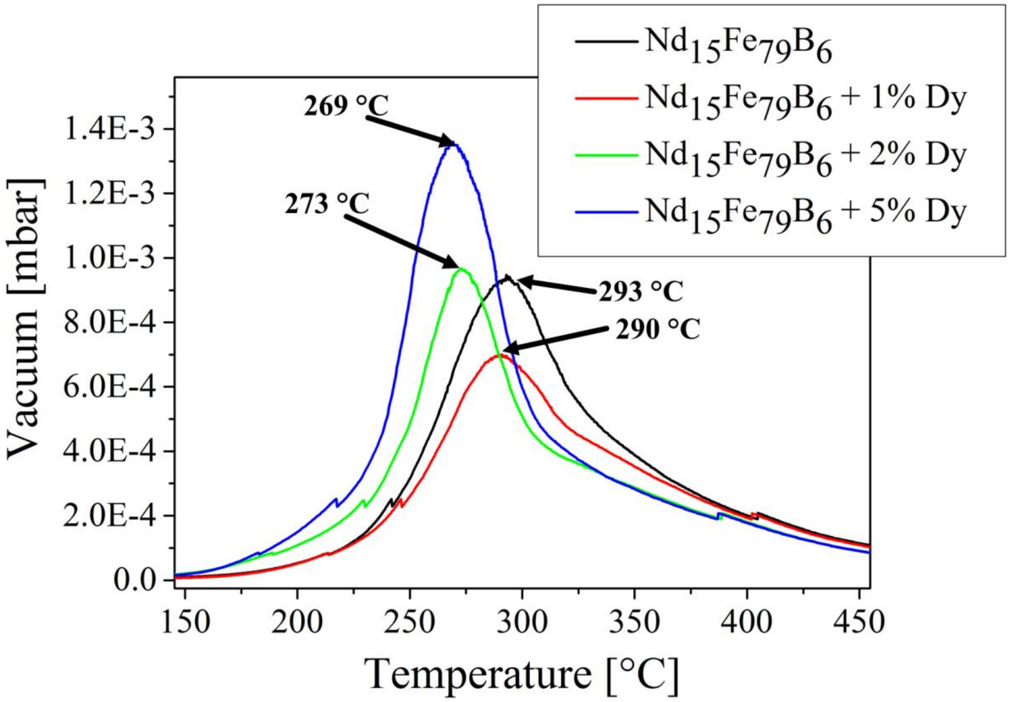

Figure 4.44: DTA hydrogen desorption from $NdH_{\sim 2.7}$ to Nd dihydride of disproportionated mixture, heated under vacuum at 10 K/min.

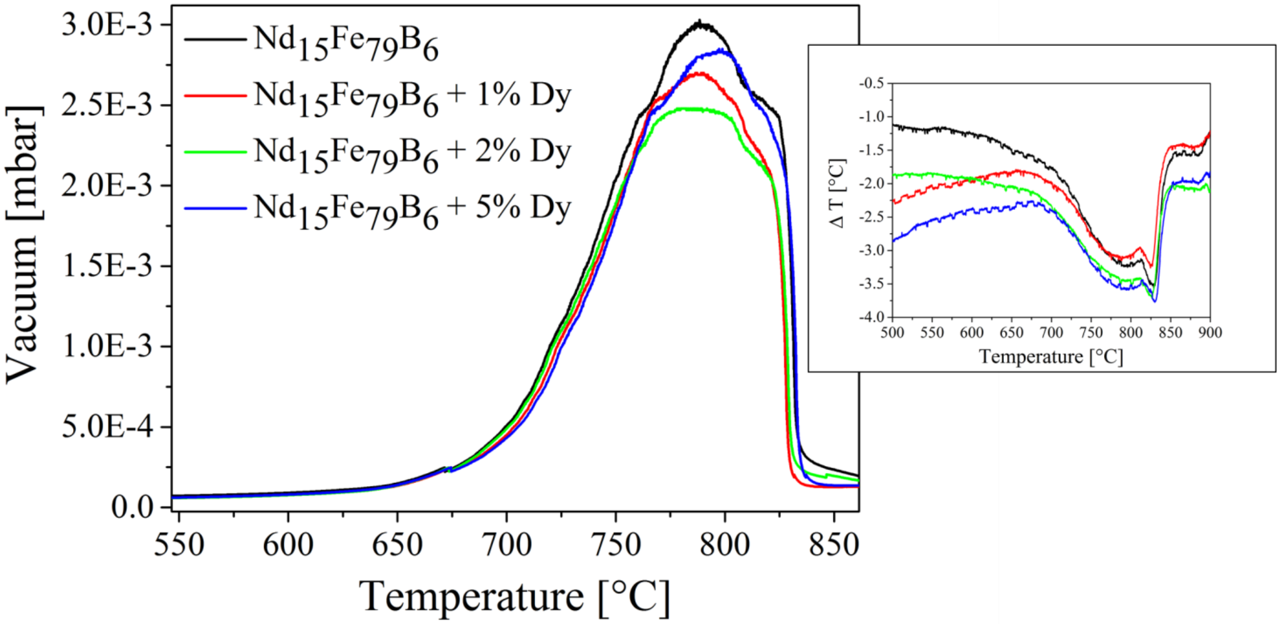

Figure 4.45: DTA desorption plot of disproportionated mixture corresponding to the recombination reaction and an insert of the differential temperature illustrating the exothermic nature of the recombination reaction of the same mixture.

The recombination reactions of the disproportionated powders take place at the temperature above 650 °C. As it can be observed from figure 4.45 where is presented the recombination reaction, the peak is broad and it is thought that this peak in composed to the Nd dihydride desorption to form Nd, as the remaining constituents combine and reform the $Nd_2Fe_{14}B$ phase. As it can be observed from the insert image at temperatures above 825 °C a second peak appears on the differential temperature diagram, which is corresponding with the right-hand shoulder from the vacuum diagram. This shoulder represents the desorption of the Nd dihydride and the formation of the Nd. Therefore, the first part of the peak is related with the recombination of the $Nd_2Fe_{14}B$ phase, which corresponds also with the reported work of others authors on similar compositions **[41]**. The maximum of the recombination peak is achieved at the temperature of approximately 788 °C.

Additional to the DTA results, XRD analysis were performed on disproportionated powders processed at different hydrogen pressures. From this analysis, it was determined the ideal hydrogen pressure needed for the HDDR process, in order to obtain fully disproportionated powders. As it was shown in the DTA analysis the disproportionation of the $Nd_2Fe_{14}B$ phase take place at temperature above 650 °C.

The XRD patterns are illustrated in figure 4.46. In the images the peaks unmarked from the XRD patterns are the reflections of the $Nd_2Fe_{14}B$ hydride phase. Like in the previous case by rising the hydrogen pressure the $(Nd_2Fe_{14}B)H_x$ phase will further transform in α-Fe, $NdH_{(2\pm x)}$ and Fe_2B, resulting in the decrease of the $(Nd_2Fe_{14}B)H_x$ phase reflections intensity. It was considered that the disproportionation reaction is complete, when on the XRD patterns there are only reflections from the phases α-Fe, $NdH_{(2\pm x)}$ and Fe_2B and no reflections from the $(Nd_2Fe_{14}B)H_x$ phase. The DTA results showed that for all 4 types of $Nd_{15}Fe_{79}B_6$ with different Dy content, the disproportionation reaction takes place in the same range of temperatures. From the XRD analysis it can be seen that for the same disproportionation temperature, but by increasing the hydrogen pressure form 10 kPa to 90 kPa the powder is transforming from non / partially disproportionated to fully disproportionated. So, if for the $Nd_{15}Fe_{79}B_6$ a hydrogen pressure of 20 kPa is enough to obtain fully disproportionated powder, by increasing the Dy content with 1 wt% it is required to increase also the hydrogen pressure to 30 kPa in order to obtain a fully disproportionate powder. This trend is maintained also for the samples with 2 wt % Dy and 5 wt% Dy. For the $Nd_{15}Fe_{79}B_6$ with 2 wt% Dy it is needed a hydrogen pressure of 40 kPa and a hydrogen pressure of 70 kPa for the $Nd_{15}Fe_{79}B_6$ with 5 wt% Dy.

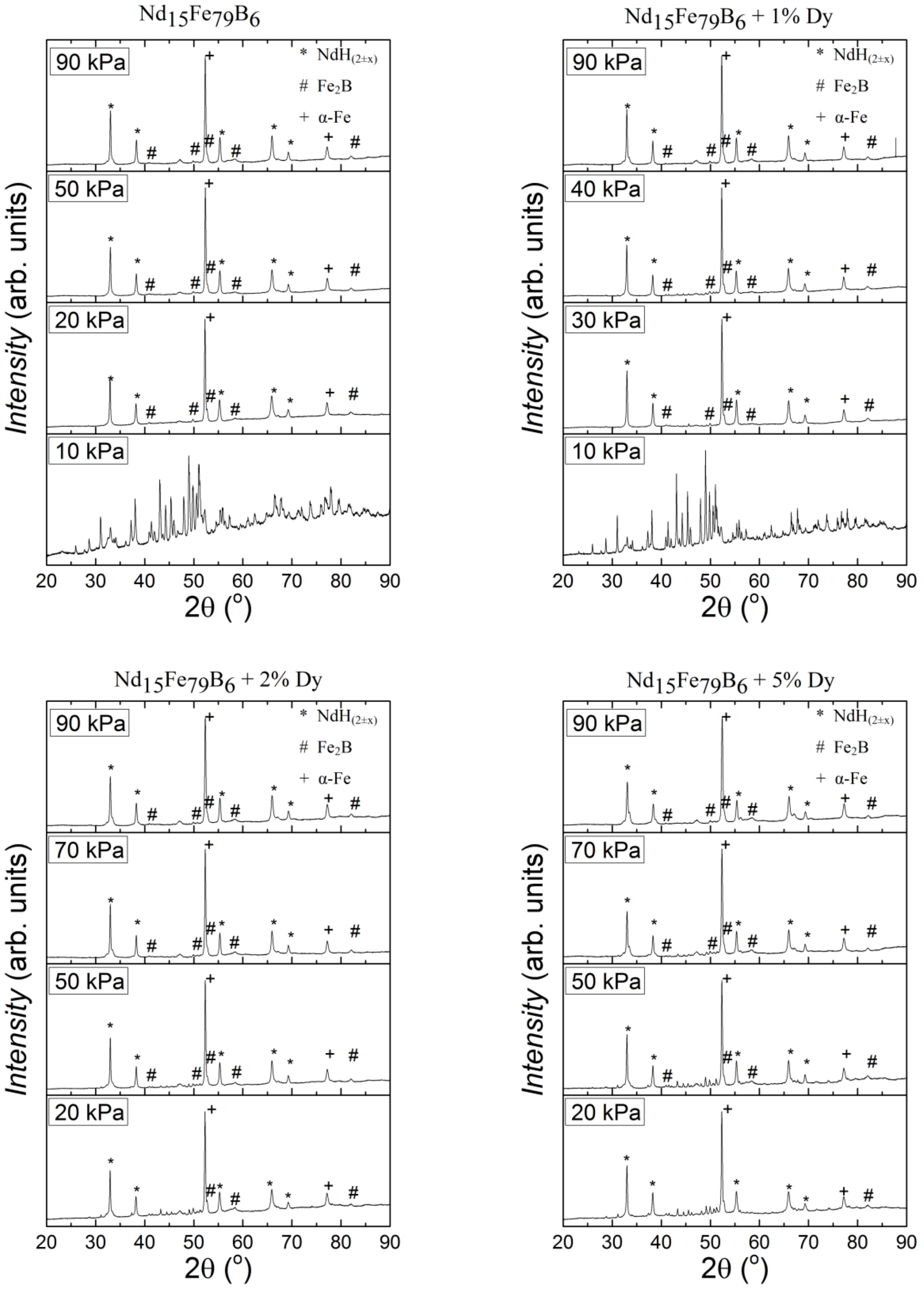

Figure 4.46: XRD patterns from the 4 types of HDDR (stopped before recombination) powders with different Dy content, showing the evolution with the hydrogen increase, from non/partially-disproportionated powders to fully disproportionated powders.

In the following section, for the 4 types of powders with different Dy content, are presented the magnetic properties variation with the increase in the hydrogen pressure. In this case the HDDR process was run entirely, at the temperature of 780 °C for the first plateau and 840 °C for the second plateau. The hydrogen desorption rate for this study was 2.2 L/min. The results are presented in figure 4.47.

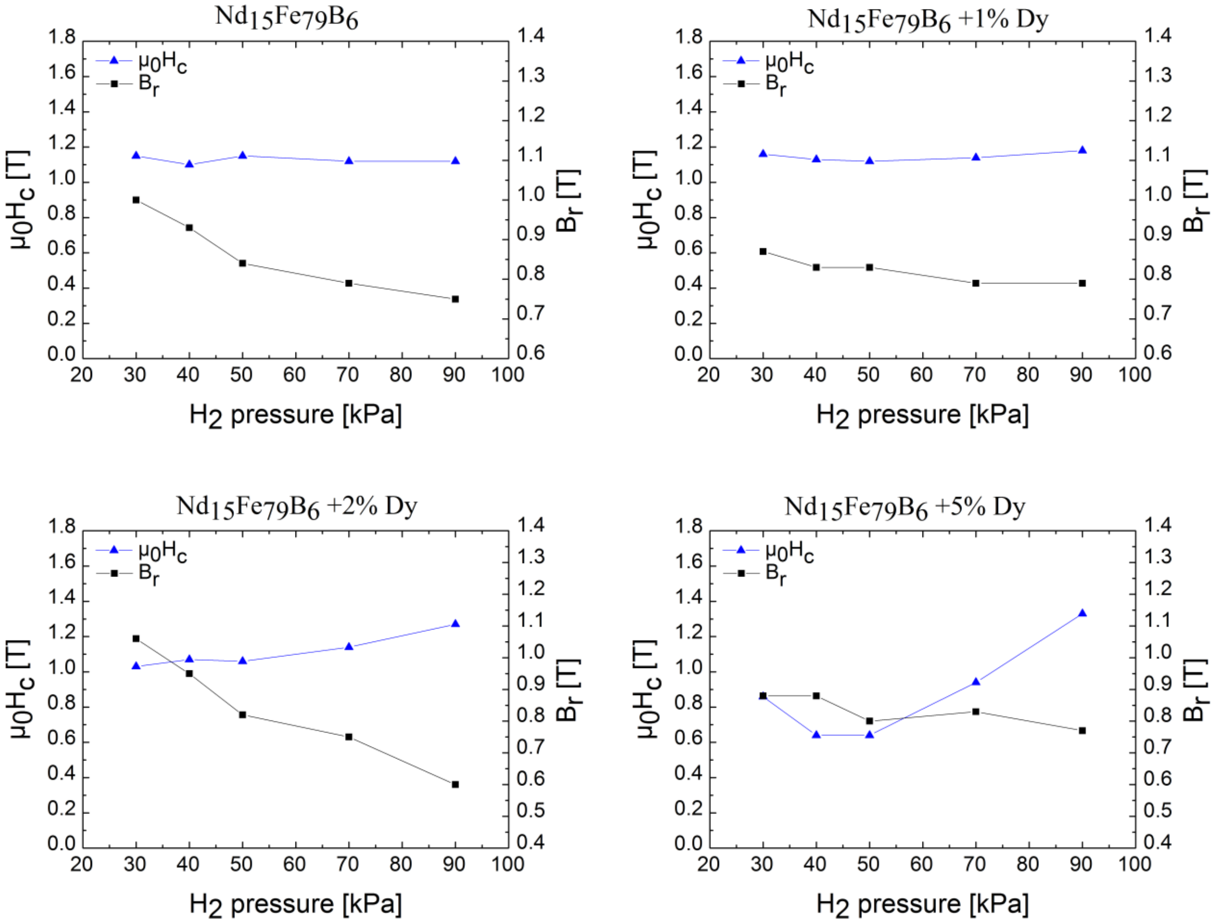

Figure 4.47: Coercivity μ_0H_c and remanence B_r of the powders after HDDR process at different hydrogen pressure, processed at a temperature of 780 °C/840 °C and a desorption rate of 2.2 L/min.

For the starting powder, $Nd_{15}Fe_{79}B_6$, and $Nd_{15}Fe_{79}B_6$ + 1wt% Dy the coercivity μ_0H_c remains constant (at values of ~1.1 T) with the increase of the hydrogen pressure. Regarding the remanence B_r of the samples, this is decreasing with the increase of the hydrogen. For the samples containing 2 wt% Dy and 5 wt% Dy by increasing the hydrogen pressure the coercivity is increasing up to a μ_0H_c of ~1.3 T. For these 2 cases the remanence is decreasing with the increase of the hydrogen pressure. To notice that if for low hydrogen pressure (30 kPa) the powders are highly anisotropic, by increasing the hydrogen pressure the anisotropy of the powder is loosed and for hydrogen pressure of 90 kPa the obtained powder is isotropic. This could explain also the decrease in remanence with the increase of the hydrogen pressure. This behavior is shown in figure 4.48.

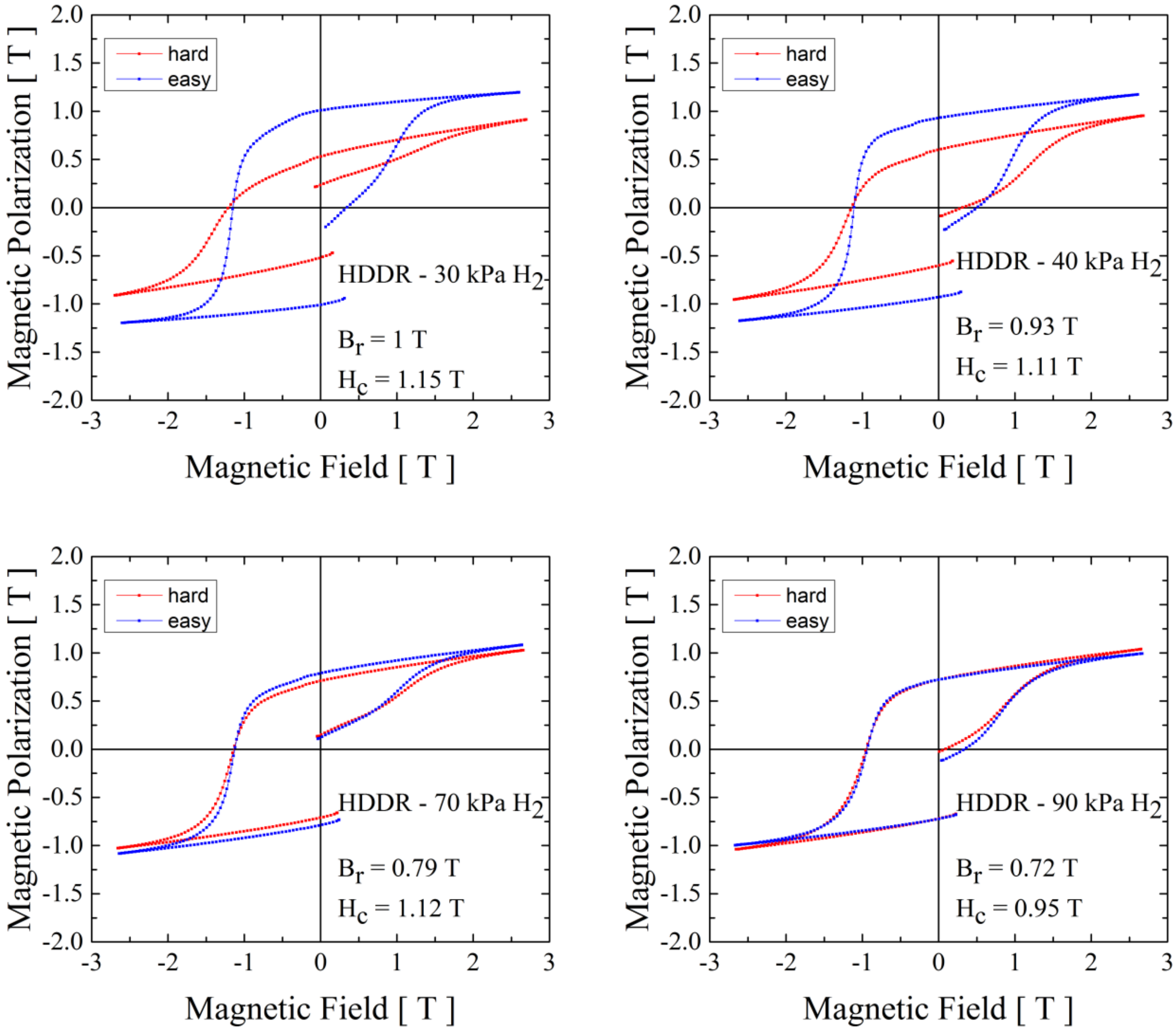

Figure 4.48: Texture evolution of the sample $Nd_{15}Fe_{79}B_6$ with the increase of the hydrogen pressure.

It was observed that by increasing the Dy content this affected also the shape of the hysteresis loop, by altering the rectangularity of the loop. This behavior is shown in figure 4.49. As a remark the squareness of the hysteresis loop can be controlled by adjusting the HDDR processing parameters. With the right adjusted parameters, e.g. hydrogen pressure and desorption rate, the rectangularity of the hysteresis loop can be recovered.

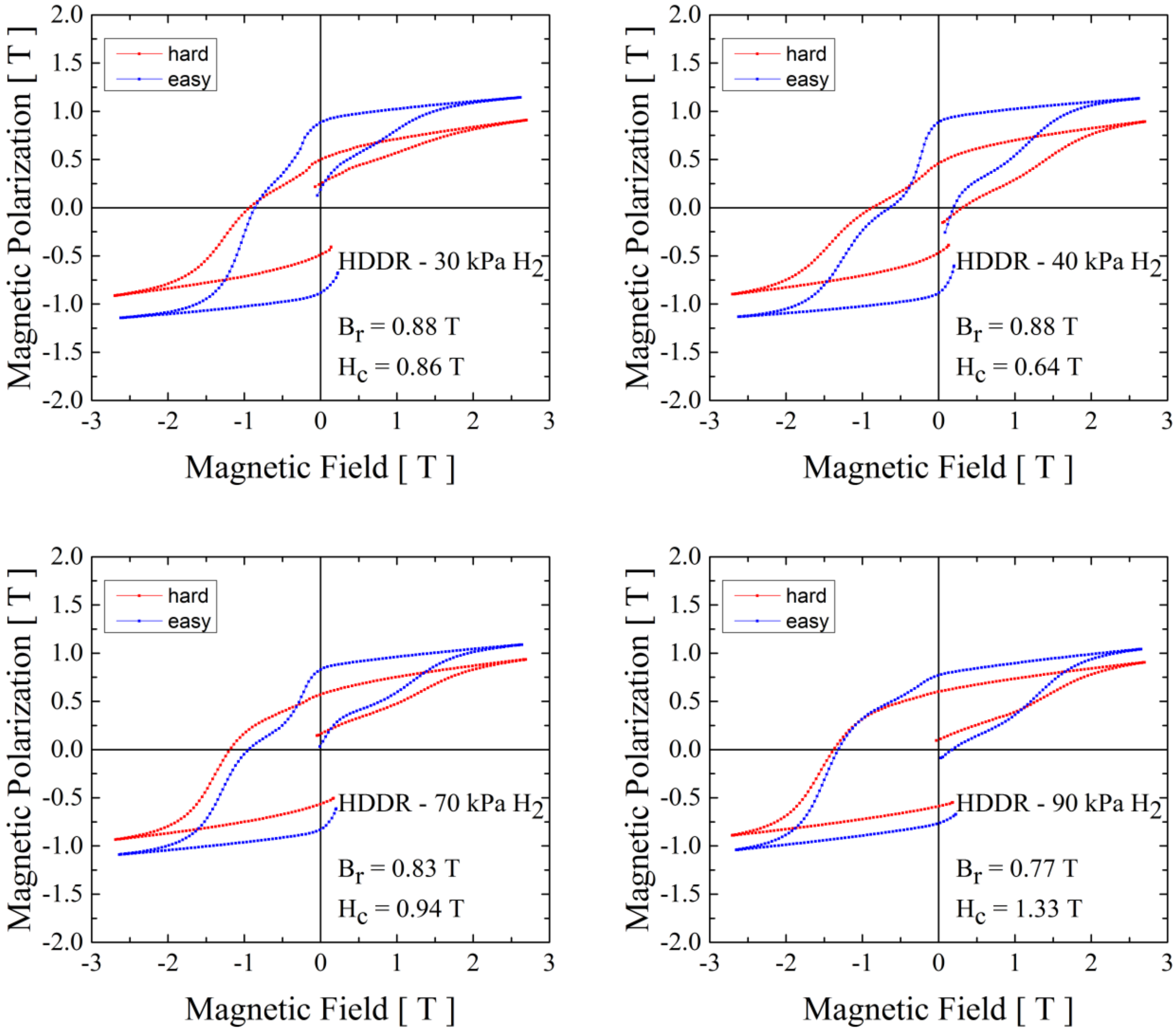

Figure 4.49: Different shapes of the hysteresis loops for $Nd_{15}Fe_{79}B_6$ + 5wt% Dy processed at different hydrogen pressures.

As in the previous presented case of the scrap magnets, the desorption rate for the $Nd_{15}Fe_{79}B_6$ powders with different Dy content was varied between 0.3 L/min and 45 L/min. The processing temperature for the study of the desorption rate was 780/840°C and the hydrogen pressure was set to 40 kPa. For the desorption rate of 0.3 L/min, the 90 minutes assigned was not enough to allow a complete desorption of the hydrogen from the sample chamber and when the turbo pump was connected the hydrogen pressure inside the sample chamber was higher than 1 kPa. The prepared samples were embedded and magnetically characterized. The dependence between the coercivity, remanence and hydrogen desorption rate (specific for this system) is presented in figure 4.50.

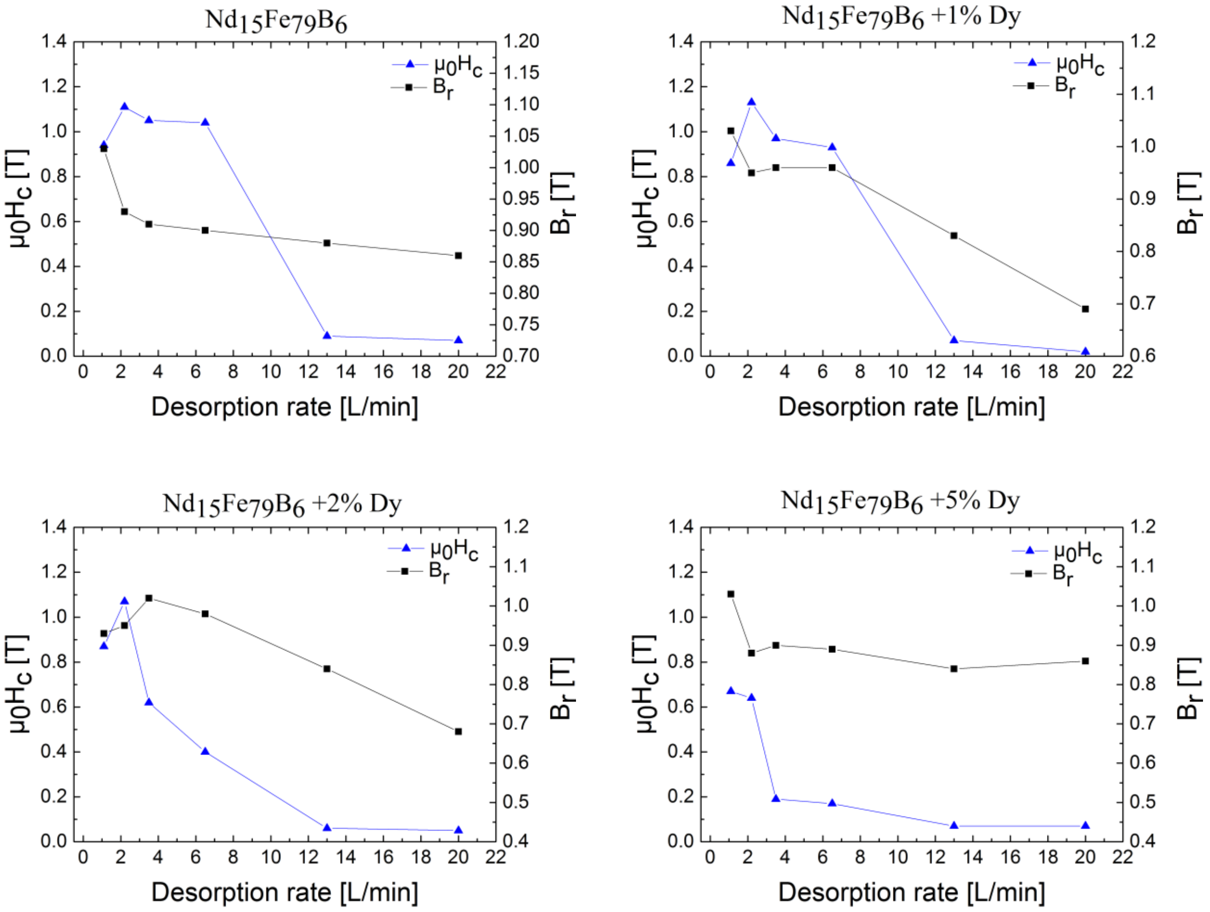

Figure 4.50: Coercivity and remanence of the $Nd_{15}Fe_{79}B_6$ with different Dy content processed at different hydrogen pressures.

For all 4 samples with different Dy content, the remanence of the samples after the HDDR process is decreasing with the increase of the desorption rate. The coercivity of the samples $Nd_{15}Fe_{79}B_6$ maintain an almost constant value up to a desorption rate of 7 L/min. For samples with 1 wt% Dy content, a small decrease of the coercivity is seen at the desorption rate of 6.5 L/ min, followed by a huge drop for the desorption rate of 13 L/min. The same decreasing trend is maintained also for the samples contained 2 wt% Dy, but here even more pronounced. The coercivity is decreasing dramatically for the sample prepared at a desorption rate of 3.5 L/min and this trend is continuing with the increase in the desorption rate. For the samples containing 5 wt% Dy, the decrease in coercivity can be observed starting with the lowest desorption rate used. It can be concluded that Dy is accelerating the desorption and recombination reactions and that the hydrogen desorption rate needs to be decreased with the increase of the Dy content. Another approach will be to maintain the desorption rate at a certain value and to reduce the time allocated to the desorption and recombination reactions, with the increase in the Dy content. By reducing the time of the desorption and recombination reactions, it can be also avoided an over processing of the powder and the grain growth.

During the adjustment routine of the processing temperature, for the 4 types of Nd-Fe-B powders with different Dy contents, the hydrogen pressure was kept at 90 kPa and the desorption rate of the hydrogen was 2.2 L/min. From the DTA results, it was determined that the disproportionation reaction, for the 4 types of powders, take place between 650 °C and 750 °C and the recombination reaction occurs at the temperatures 650 °C and 850 °C. For a proper study the following temperatures were applied: 730/790 °C (on graphs as 790 °C), 780/840 °C (on graph as 840 °C), 830/890 °C (on graph as 890 °C). The evolutions of the coercivity and remanence are presented in figure 4.51.

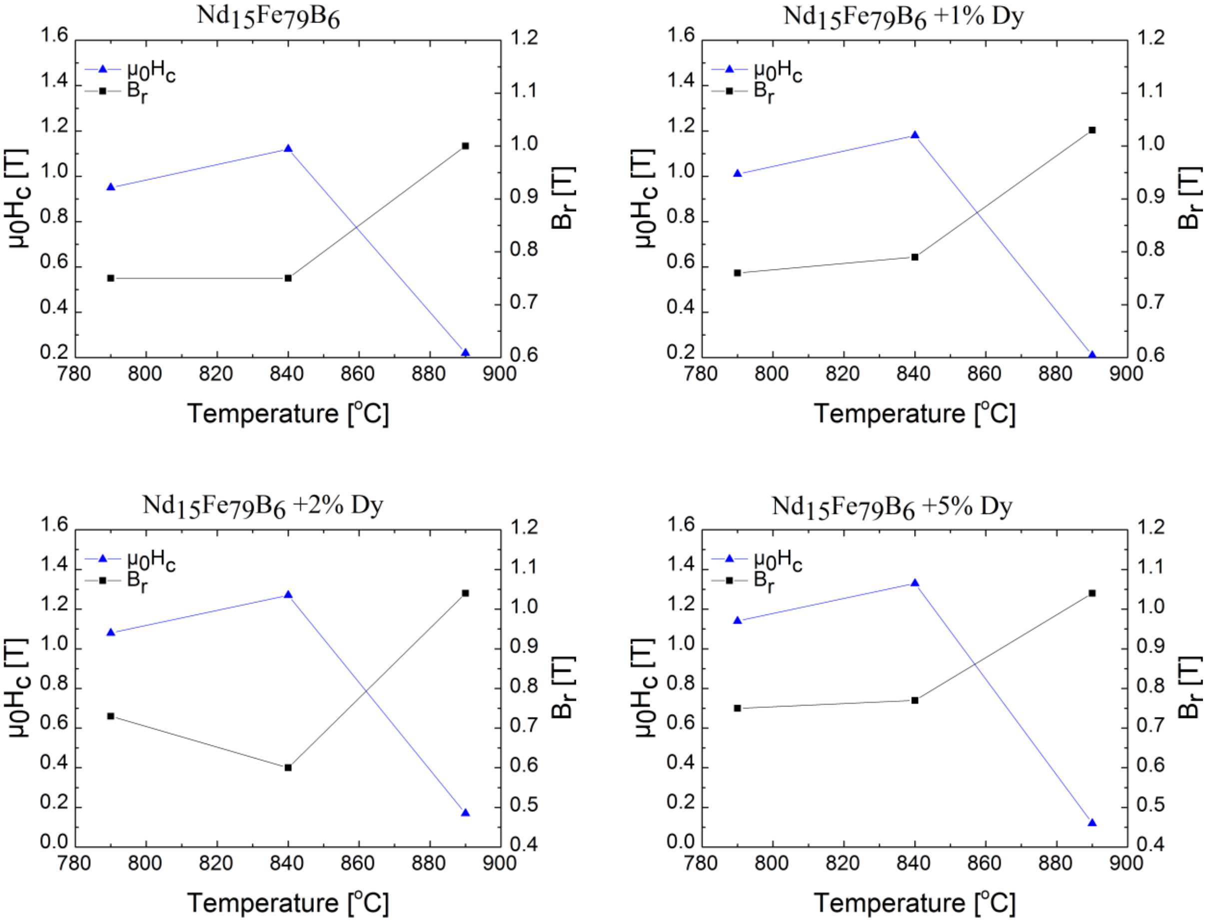

Figure 4.51: Coercivity μ_0H_c and remanence B_r of the 4 types of powders, after the HDDR process at different temperature, a hydrogen pressure of 90 kPa and a desorption rate of 2.2 L/min.

The results of the temperature study show that all the obtained samples are textured as a result of the HDDR processing parameters adaptation. The decrease in the coercivity for the series prepared at 830/890 °C can be explained by the grain growth at these high temperatures, as it was confirmed also by the SEM study on the previous presented scrap magnets.

4.6 Processing the recycled powders into magnets

After completion of the HDDR treatments, conventional consolidations procedure of the obtained powders includes technics like: resin bonding **[95, 96, 97]**, hot-pressing **[98, 99, 100, 101]**, and spark plasma sintering **[102, 103, 104]**. The following section will focus on the consolidation of the recycled powders. After adjusting the HDDR processing parameters to obtain highly anisotropic powder with good magnetic properties, the obtained powders were used to produce solid permanent magnets by resin bonding, spark plasma sintering and conventional sintering.

In the case of the bonded magnets the powder after the HDDR treatments was mixed with “R&G epoxy resin L” which has a cure time at 20 °C of 16-24 hours and 3 hours at 50 °C. The epoxy resin is composed of two parts, one part being the epoxy resin and the other the hardener, both in liquid form. The resin and the hardener were mixed in a 100 to 40 ratio resin to hardener. To the epoxy and hardener mixture was added ethanol (for the dilution of the resin) and was stirred continuously until a uniform dissolved solution is achieved. The Nd-Fe-B powder was then added in a ratio of 90 % Nd-Fe-B powder and 10 % resin. Then the resin and Nd-Fe-B solution was well mixed for the evaporation of the ethanol and in order to coat every particle with a thin layer of resin. After the mixing step, the powder was placed in a press form, a magnetic field of 1.6 T was applied for the alignment of the powder followed by pressing. After 30 minutes of pressing, the pressed sample is removed from the press form, and it is let 24 hours at room temperature to harden the resin.

For the conventional sintering and for spark plasma sintering, the powder obtained after the HDDR process was placed into a die, and then a magnetic field of 1.6 T was applied in order to align the powder. Afterwards the aligned and pressed samples were subjected to the sintering process.

4.6.1 Preparation and characterization of Nd-Fe-B bonded magnets

Isotropic bonded magnets were pressed under rectangular shapes of 10 mm x 10 mm x 5 mm (figure 4.52), using a uniaxial hydraulic press. In order to determine the optimum pressing force required for good magnetic properties, a series of bonded magnets pressed at different forces was prepared. For the following study was used type *mix motor* scrap powder. After pressing, the density of the obtained bonded magnets was determined using an Archimedes balance. The magnets were weighed in air and afterwards in water. The density was calculated according the following equation:

$$\rho = \frac{object\ mass\ weighed\ in\ air}{volume\ of\ the\ water\ \ displaced} \qquad (5)$$

As a last step the bonded magnets were pulse magnetized under a pulse field of 7 T, and the magnetic properties were measured using a pulsed field magnetometer.

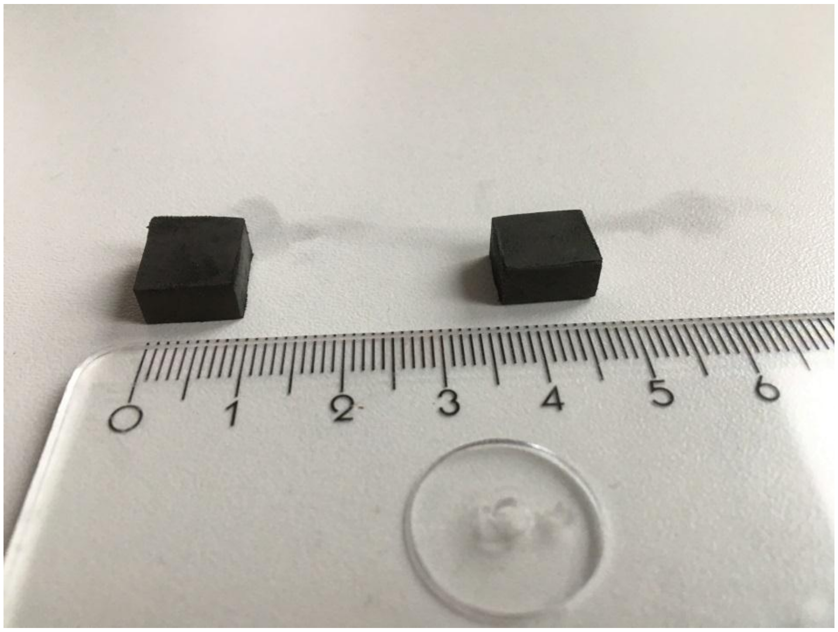

Figure 4.52: Image of two isotropic epoxy resin bonded magnets.

A series of magnets at different pressure, starting from 0.2 GPa till 1.2 GPa with a step of 0.2 GPa were prepared. The densities, coercivity μ_0H_c and remanence B_r are presented in figure 4.53. It can be observed that by increasing the pressing force the density of the bonded magnets increases. For pressing force of 1.0 - 1.2 GPa the density of the bonded magnets is ~6 g/cm^3 which corresponds with the density usually seen at the bonded magnets **[105, 106]**. The maximum density of a bonded magnet can be calculated as shown in the following:

$$\rho_{theoretical} = (\rho_{NdFeB} \cdot Vf_{NdFeB}) + (\rho_{Epoxy} \cdot Vf_{Epoxy}) \quad (6)$$

where: $\rho_{theoretical}$ = theoretical density; ρ_{NdFeB} = NdFeB density; ρ_{Epoxy} = epoxy density; Vf_{NdFeB} = volume fraction of Nd-Fe-B; Vf_{Epoxy} = volume fraction of epoxy.

Replacing the values in relation (6), it is obtained:

$$\rho_{theoretical} = (7.50 \cdot 0.90) g/cm^3 + (1.14 \cdot 0.10) g/cm^3 = 6.75 g/cm^3 + 0.114 g/cm^3 = 6.864\ g/cm^3$$

As it was expected the remanence of the bonded magnets is increasing with the increase of the compression pressure due to the increase in samples density. This correspond also with the work reported by Zhang et al. **[107]**, which showed that increasing the compaction pressure to 620 MPa, for epoxy resin bonded magnets processed from melt-spun powder, led to an increase in remanence due to the improvement of the magnets density. Regarding the coercivity of the bonded magnets, by increasing the compaction pressure the coercivity tends to decrease.

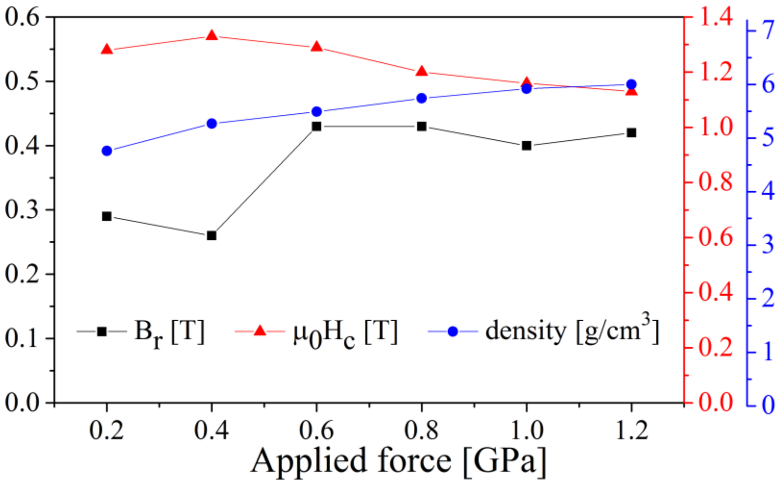

Figure 4.53: Image illustrating the variation of the remanence B_r, coercivity μ_0H_c, and density with the increase in the pressing force.

The production of the anisotropic bonded magnets was unsuccessful. In fact, all the produced “anisotropic” bonded magnets, in the end, proved to be isotropic. The reason for these unsuccessful tries, are assumed to be the viscosity of the mixture between the epoxy resin and the Nd-Fe-B powder. The viscosity of mixture epoxy resin and the hardener is quite high and is increasing even more when the powder is added. This viscosity is the cause of the particles are non-alignment when the magnetic field is applied. In this case the magnetic field applied for the alignment of the powder was about 1.6 T. A higher intensity of the magnetic field could overcome the viscosity of the powder and epoxy mixture. In his work Li et al. **[108]** used a 3 T magnetic field to align the mixture between epoxy and powder. The magnetic measurements of one of the samples measured on the direction of the alignment (easy) and perpendicular to the direction of alignment (hard) is presented in figure 4.54.

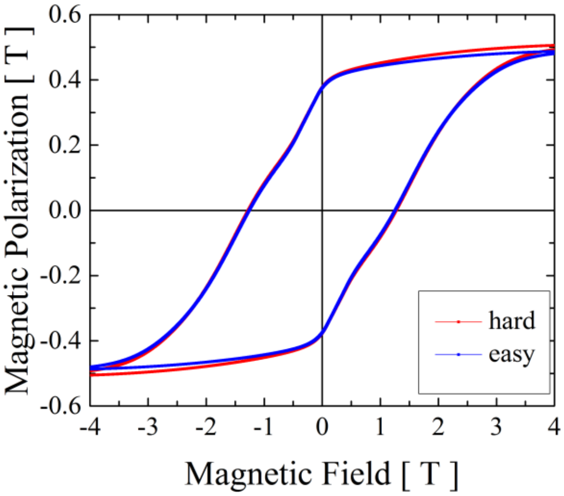

Figure 4.54: Hysteresis loops of a bonded sample (subjected to a magnetic field of ~1.6_T prior pressing) showing measurements on the direction of the alignment (blue hysteresis loop) and perpendicular to the direction of alignment (red hysteresis loop).

4.6.2 Processing and characterization of Nd-Fe-B SPS magnets

In order to determine the right sintering temperature for good magnetic properties, decrepitated powder of scrap magnets (*type 1*, *type 3, type 4* and *mix motor*) was subjected to a desorption process followed by sintering via SPS (spark plasma sintering). Hydrogen desorption of the decrepitated powder was realized at a temperature of 600 °C for one hour.

For the first step of the study, where it was searched the optimum sintering temperature, desorbed powder obtained after the hydrogen decrepitation of the scrap magnets was used. In this case, isotropic magnets were prepared. They are shown in figure 4.55. For all the magnets prepared by SPS 10 grams of powder were used. During the SPS process the sintering temperature was increased form 700 °C to 1000 °C, with at step size of 100 °C. The compression pressure used was 39 MPa. The compression pressure was limited by the graphite die. Higher pressures than 39 MPa, cause the breaking of the die. In the image can be seen how the height of the samples decreases with the increase in the sintering temperature.

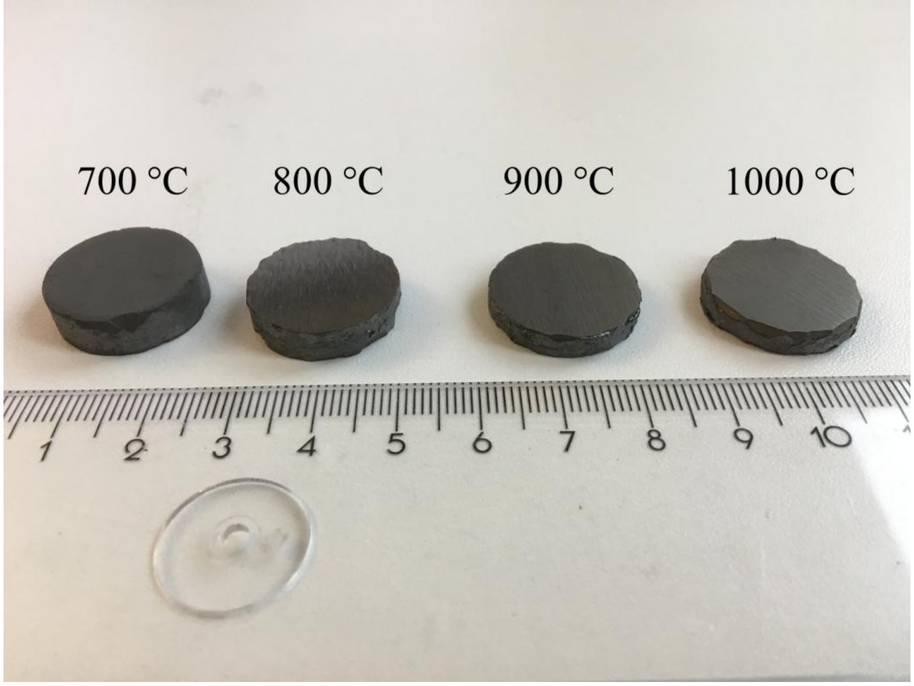

Figure 4.55: Image showing isotropic magnets consolidated by spark plasma sintering.

In literature the sintering temperature and the applied pressure used to consolidation Nd-Fe-B by SPS process are very diverse. Wang et al. **[109]** used a sintering temperature of 850 °C and a pressure of 60 MPa, Hu et al. **[110]** used 700 °C with 300 MPa, Žagar et al. **[111]** used a temperature of 700 °C, and the pressure of 50MPa. Suresh et al. **[112]** studied the consolidation of HDDR powder by SPS using an applied pressure of 80 MPa, for which the sintering temperature was varied between 550 °C, 575 °C and 600 °C. He reported densities of 7.06 g/cm^3, 7.24 g/cm^3 and 7.49 g/cm^3 respectively.

The magnetic properties and the density of the samples prepared in this study are presented in figure 4.56.

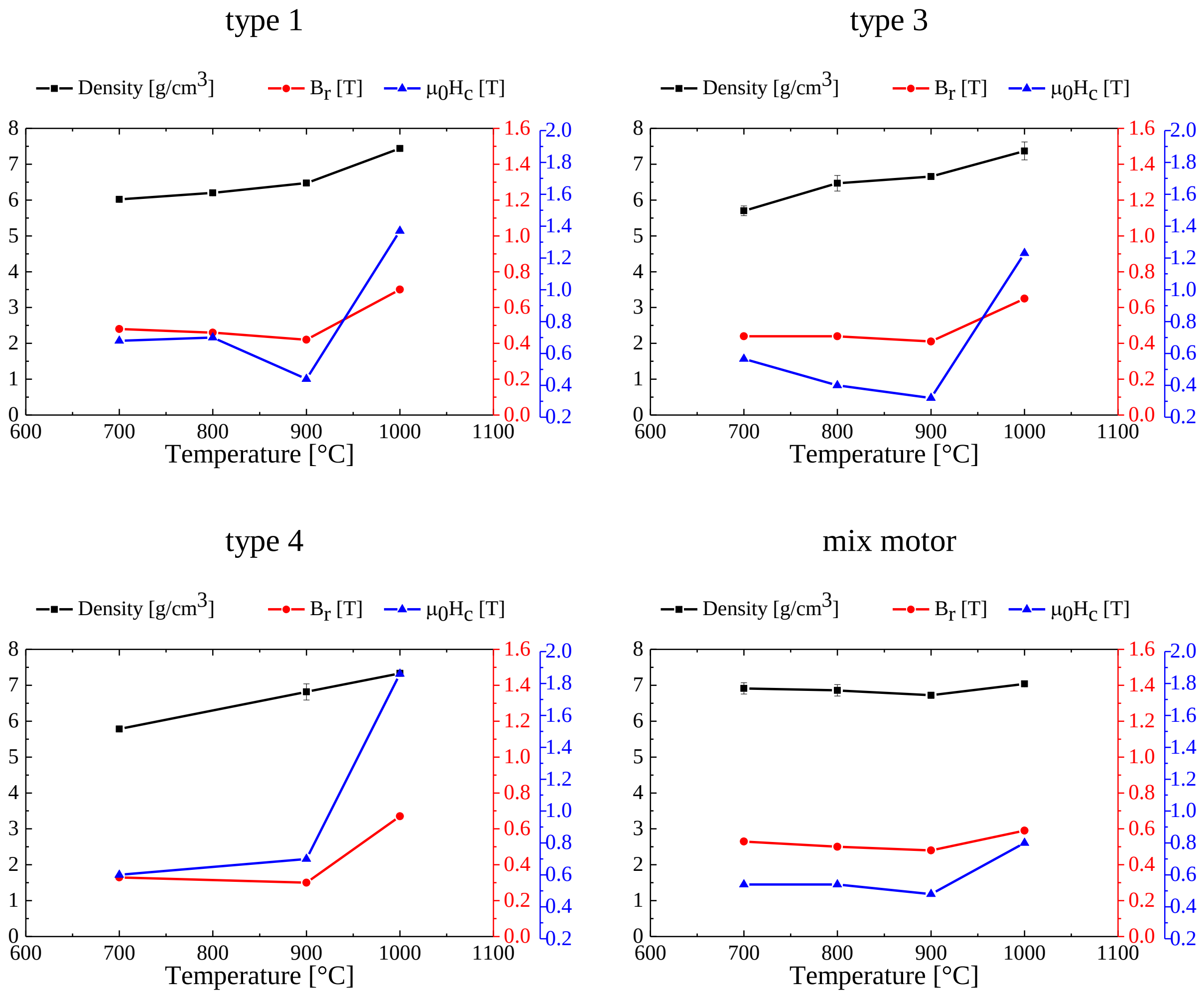

Figure 4.56: Variation of the density, remanence B_r and coercivity μ_0H_c with the increase in the sintering temperature of the SPS process, for the *type 1*, *type 3*, *type 4* and *mix motor*.

By increasing the sintering temperature, an improvement in the samples densities was achieved. For sintering temperature of 1000 °C were obtained densities of 7.05 to 7.55 g/cm^3. Improvement of the density of the samples will increase the remanence. The highest values of remanence were obtained for the samples prepared at 1000 °C. At this sintering temperature, a remanence between 0.6 to 0.7 T was achieved for the isotropic magnets, which corresponds with the values of remanence reported by others researchers **[113, 114]**. The coercivity of the magnets is increasing also with the increase of the sintering temperature. For the sintering temperature of 1000 °C the highest coercivities was achieved. Prior to the SPS process the powder was dispersed in Argon box with a mortar and pestle and then sieved to a particle size up to 40 µm. Adding an intermediate milling step, between the HD process and SPS process, through which the powder particle size is reduced, can improve further the coercivity. In figure 4.57 is presented two SEM images of the *type 3* samples sintered at the temperature of 700 °C (top image) and 1000 °C (bottom image).

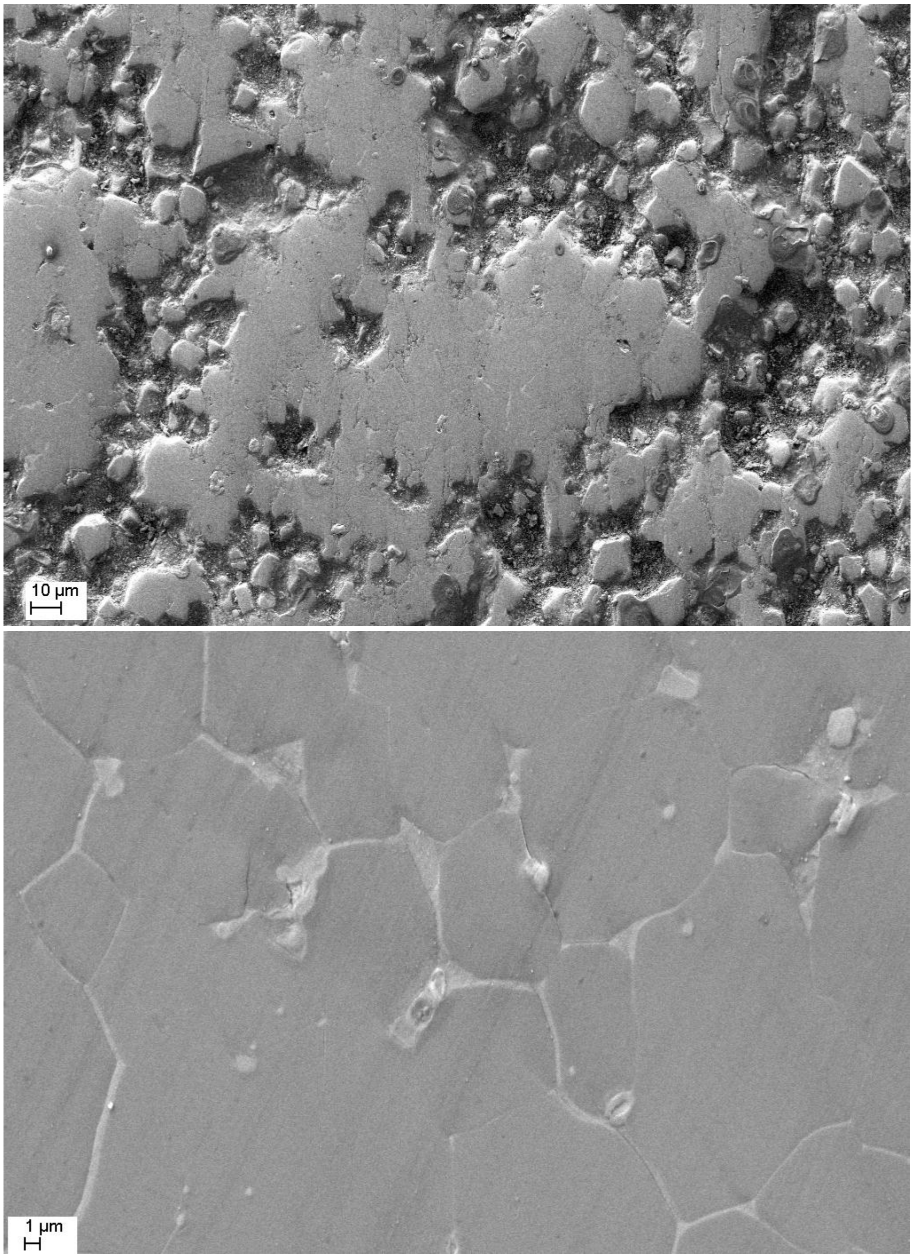

Figure 4.57: SEM images of the *type 3* magnets after spark plasma sintering at the temperature of 700 °C (top) and at 1000 °C (bottom).

The SEM images confirm the low density of the sample prepared at the sintering temperature of 700 °C, showing a very porous sample. This was seen even from the polishing process of the samples, by seeing powder particles that were detaching from the sample. The sample sintered at the temperature of 1000 °C presents a typical microstructure of a sintered magnet, consisting of $Nd_2Fe_{14}B$ grains surrounded by a rare earth rich grain boundary phase.

For the production of anisotropic magnets by SPS route, desorbed HD powder and HDDR powder was used, and prior to the sintering process the powder was aligned in a magnetic field of approximately 1.6 T. The HD/HDDR oriented powders were sintered at 1000 °C, and the magnetic properties are shown in figure 4.58.

type 1 *type 3*

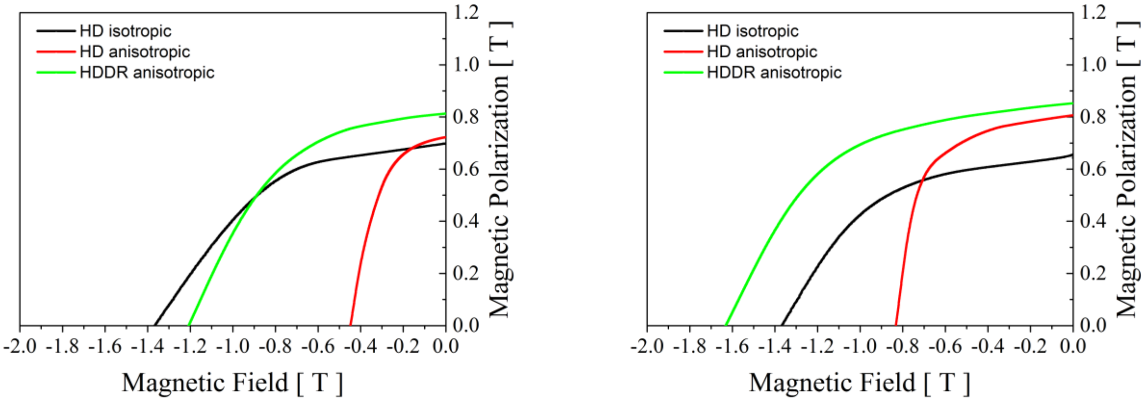

type 4 *mix motor*

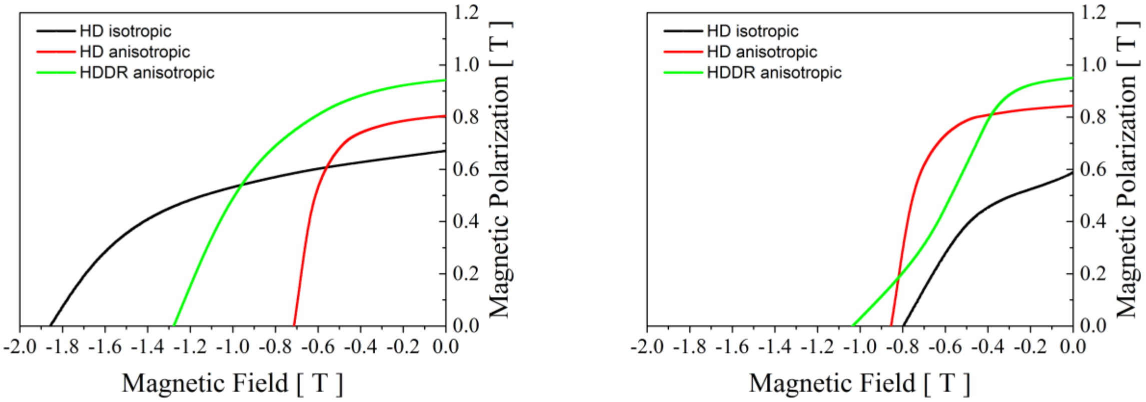

mix IT

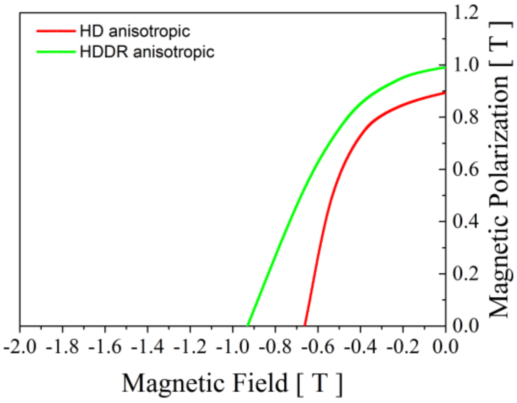

Figure 4.58: Demagnetization curves showing comparisons between the desorbed HD powder and HDDR powder, oriented and non-oriented before the SPS process. The samples were sintered at 1000 °C in vacuum, under a constant compacting pressure of 39 MPa.

For all the different types of scrap magnets the HDDR processed powders presents better remanence values. Comparing the HD + SPS samples with the HDDR + SPS, the HDDR treated samples prior to the SPS process presents better remanences and coercivities. In the case of *mix motor* HDDR anisotropic sample, the deformed demagnetization loop is due to wrong HDDR processing parameters. The squareness of the demagnetization loop can be recovered by increasing the hydrogen pressure during the HDDR process, from 70 kPa to 80 kPa. The degree of alignment for the powder was calculated according to the ratio J_r/J_S and is shown in table 4.14.

Table 4.14: The degree of alignment for the HD and HDDR processed scrap magnets, sintered at 1000 °C via SPS.

Type of scrap magnets	**Degree of alignment for the HDDR samples**	**Degree of alignment for the HD samples**
type 1	87 %	90 %
type 3	85 %	81 %
type 4	89 %	88 %
mix motor	90 %	89 %
mix IT	87 %	77 %

Because was used a sintering temperature of 1000 °C, this was not benefit for the microstructure developed during the HDDR process. In order to study the grain growth that occurs during the SPS process, samples of *type 3* processed with the adjusted HDDR parameters and then sintered at 1000 °C by SPS, were polished and analyzed by SEM. In figure 4.59 (top) is shown the grain size of one of the samples. If after the HDDR process the grains had a size between 200 nm and 500 nm, after the SPS process the grain size is between 300 nm and 1.5 µm. Isolated big grains around 10 - 20 µm appeared, like is shown in the figure 4.59 bottom image. Looking closer to these big grains, they have a core-shell aspect with Dy-rich core and depleted shell. Pr is not present in these structures, but it is segregated together with Nd in the intergranular phase, as is shown in the figure 4.60.

Takagi et al. **[115]** investigate the grain growth of HDDR processed Nd-Fe-B powder, during the SPS processes. The SPS process was done at temperature between 603 °C and 1031 °C and at different compressive pressures (from 38 to 600 MPa). In his work he concluded that the coercivity is decreased for the SPS prepared samples not due to the grain growth, but due to the loosing of the Nd-rich phase along the grain boundaries. However, by post-annealing the samples, Takagi et al. reported that he recovered the coercivity of all the samples. Other authors used hot-deformation process to increase the magnetic properties after the SPS process. The authors, spark plasma sintered the powders at temperature between 600 °C and 900 °C, under pressing force between 40 MPa and 300 MPa, and the obtained magnets were subjected to hot deformation processes using a pressure of ~ 300 MPa and temperatures between 750 °C and 900 °C. This sequence of processes increased the remanence of the magnets and the (BH)max values **[116, 117, 118, 119, 120, 121].**

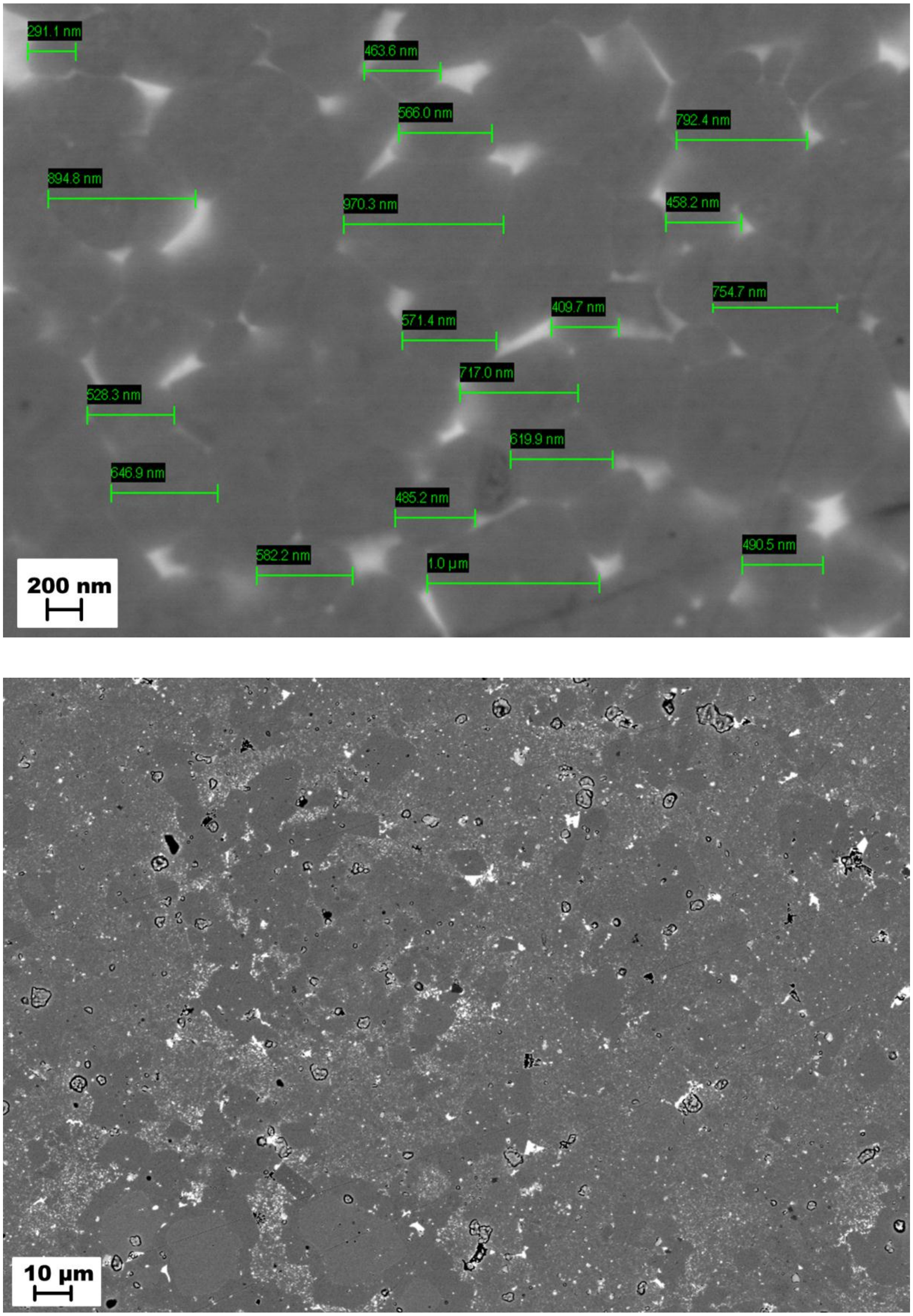

Figure 4.59: Backscattered electron SEM images of the sample *type 3* processed with the optimized HDDR parameters and sintered via SPS at 1000 °C in vacuum, under a constant compacting pressure of 39 MPa. Top images show a detailed image with the size of the grains developed during the HDDR process and the bottom images shows an overview of the same sample.

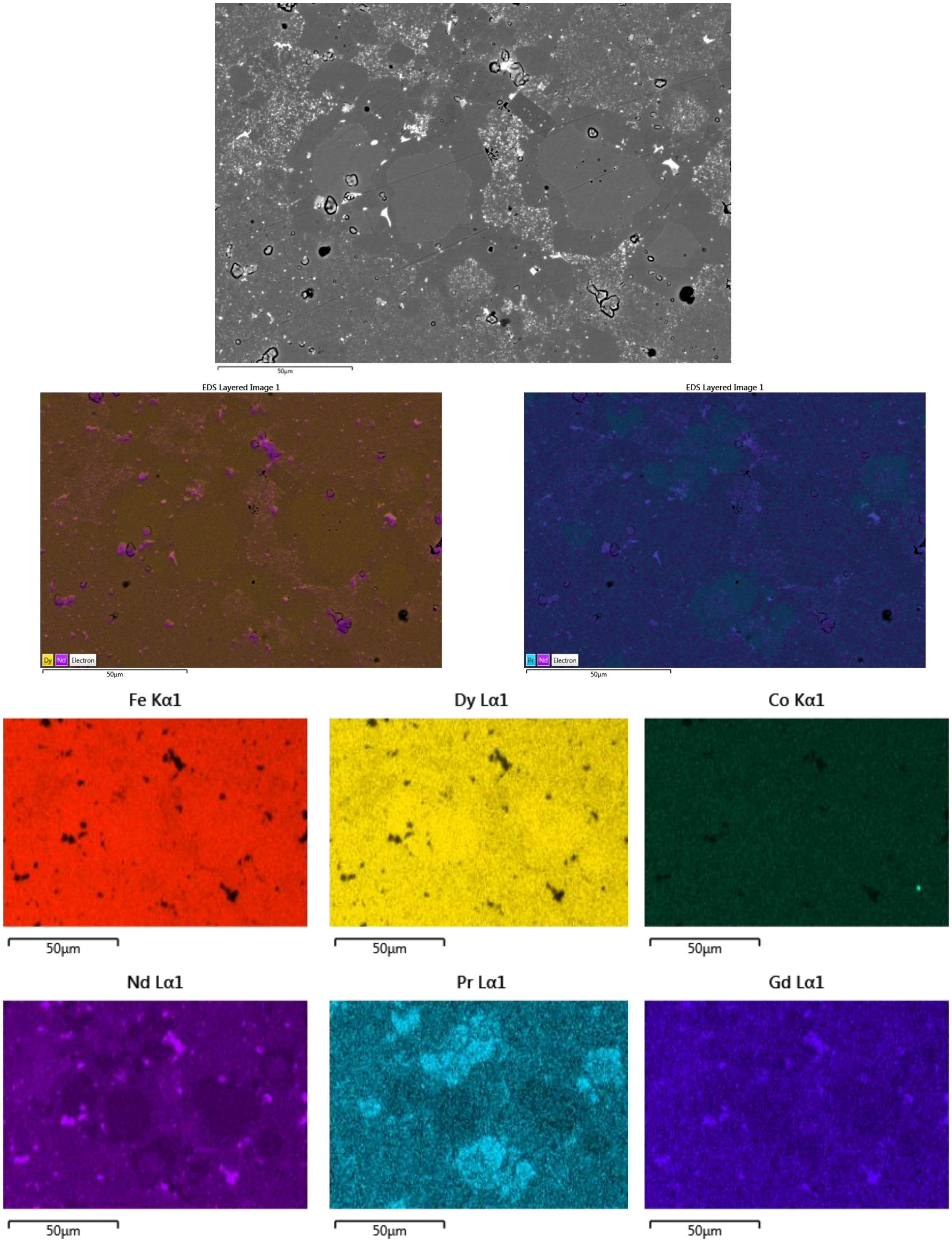

Figure 4.60: Backscattered electron SEM image of the recycled *type 3* scrap magnets after the SPS process and the individual element maps showing the isolated big grains by EDX (scale bar: 50 µm).

4.6.3 Processing and characterization of Nd-Fe-B conventional sintering magnets

Powder obtained after the hydrogen decrepitation of scrap magnets (*type 1*, *type 3*, *type 4* and *mix motor*) was used for the conventional sintering. After the HD process the powder was grinded in the Argon box, with a mortar and a pestle, and then was sieved to a particle size up to 40 µm. For each magnet, 1.5 grams from the resulted powder was placed into the die and a magnetic field was applied in order to align the powder. Afterwards a compression pressure of 260 MPa was applied. The obtained green compact was sintered under vacuum at different temperatures. The obtained magnets have a rectangular shape and have similar dimensions, approximately 10 mm x 5 mm x 5 mm. One series of magnets, sintered at different temperatures, from *type 4* scrap magnets is shown in figure 4.61.

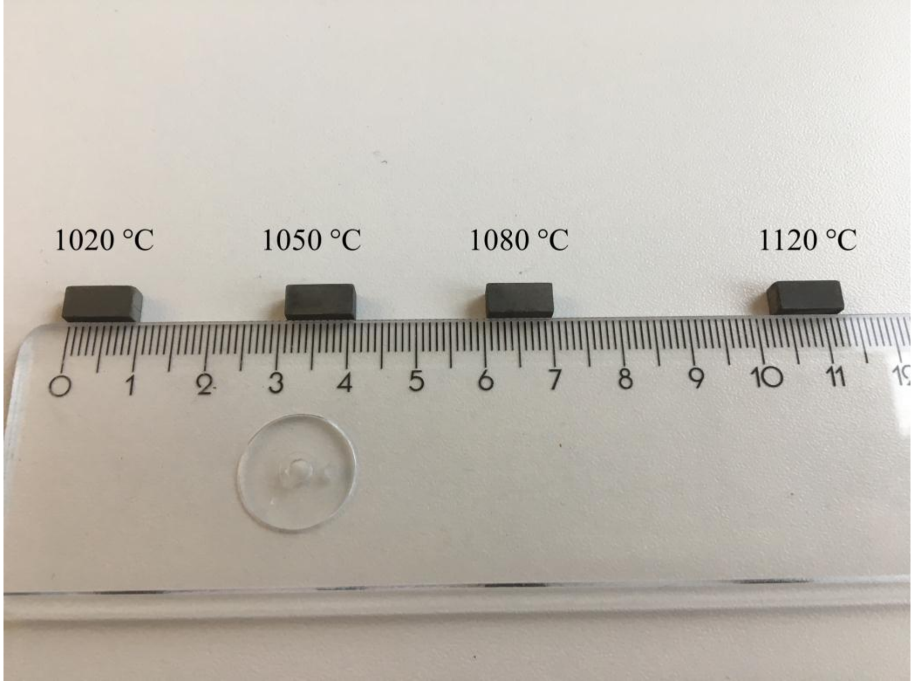

Figure 4.61: Image showing magnets of *type 4* powders, sintered at different temperature.

The magnetic properties and the densities of the obtained magnets after the sintering process are shown in figure 4.62.

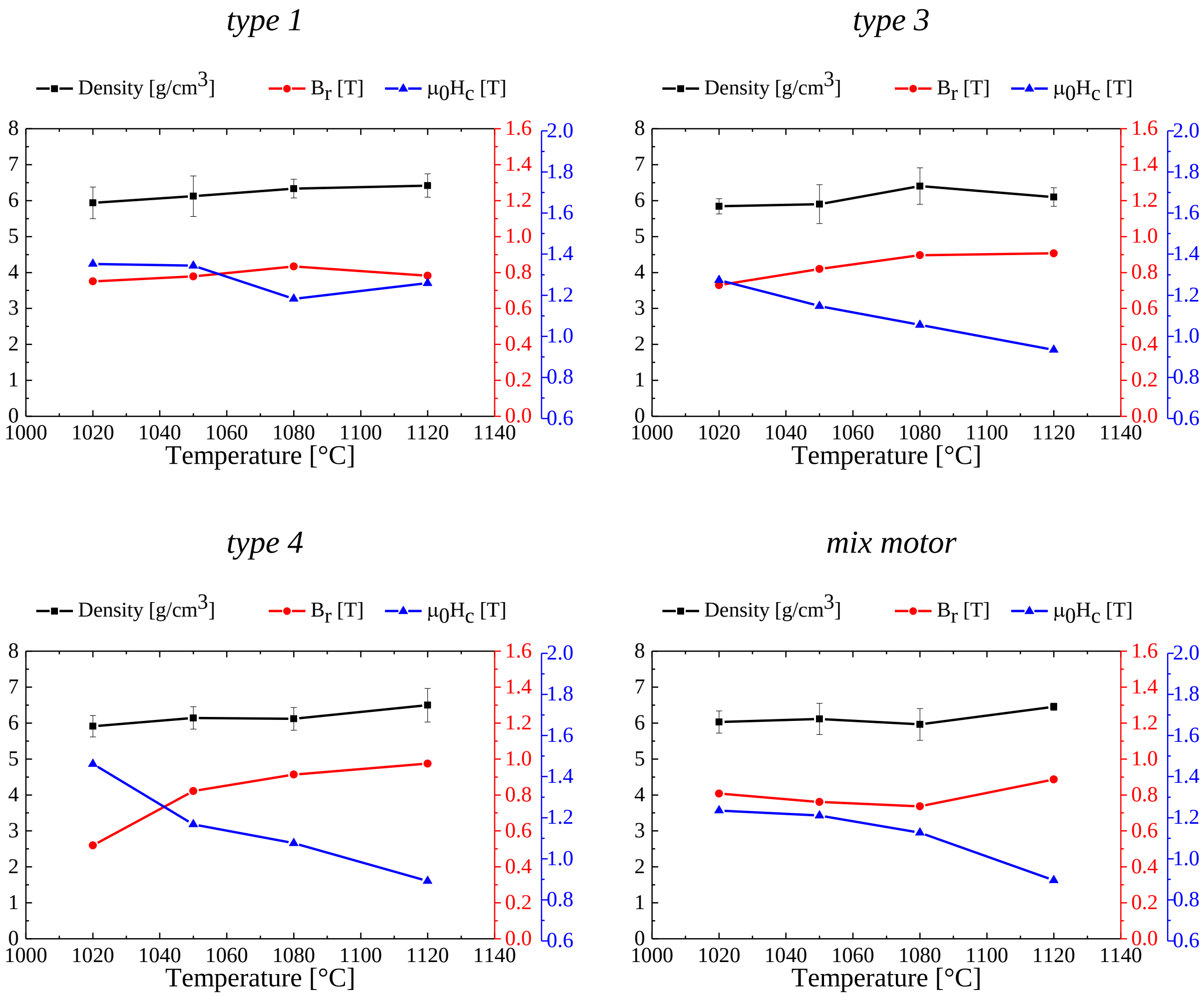

type 1

type 3

type 4

mix motor

Figure 4.62: Variation of the density, remanence B_r, and coercivity μ_0H_c with the increase in the sintering temperature, for the *type 1*, *type 3*, *type 4* and *mix motor*.

By increasing of the sintering temperature an improvement in the density of the samples was observed. The densities of these samples are between 6 and 6.5 g/cm^3. These values of the densities are low; usually an Nd-Fe-B sintered magnet has a density of 7.5 g/cm^3. The remanence of the magnets is improving with the increase of the sintering temperature, but the coercivity is decreasing. This variation in the magnetic properties with the increase in the sintering temperature can be better seen in the figure 4.63.

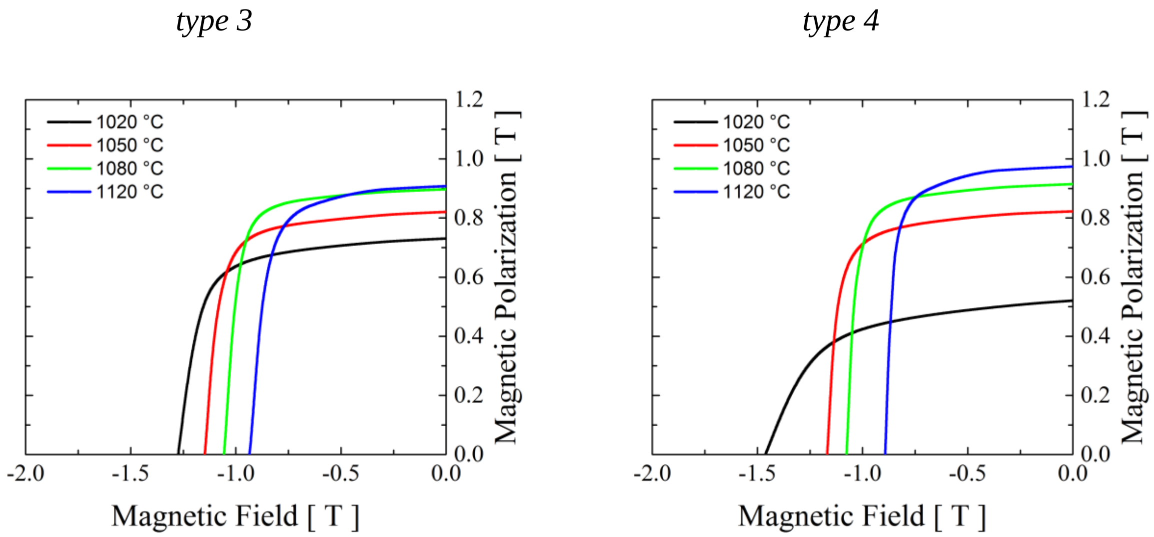

Figure 4.63: Demagnetization loops for the *type 3* and *type 4* samples, showing the variation in the remanence and coercivity with the increase of the sintering temperature.

After analyzing the densities and the magnetic properties of the samples it was determined that a sintering temperature of 1080 °C is a proper sintering temperature for these magnets. This temperature is in concordance also with the reported work of others researchers **[122, 123, 124, 125]**.

After sintering the samples at 1080 °C for one hour, to recover the coercivity, an annealing step of two hours at lower temperature was performed. The annealing temperatures performed were 550 °C, 600 °C, 650 °C and 700 °C. The magnetic properties and the densities of the obtained magnets after the sintering plus annealing processes are shown in figure 4.64. Adding an annealing step preceding the sintering process is improving slightly the magnetic properties and the density. For these 4 types of scrap magnets that were studied the density was improved by 10 - 12%. For the annealing temperature of 600 °C the density of the samples is 6.3 – 6.45 g/cm^3, which is still a low density for sintered magnets. Due to the low densities and magnetic properties, as a next step, the recycled powders were mixed with different rare earths alloys. This approach tends to refresh the intergranular phase rich in rare earths, and to regain the coercivity. As a refreshing powder, two eutectic low melting point alloys were considered, $Nd_{90}Al_{10}$ and $Pr_{75}(Cu_{0.25}Co_{0.75})_{25}$. The melting point of $Nd_{90}Al_{10}$ is 700 °C; $Pr_{75}(Cu_{0.25}Co_{0.75})_{25}$ is an alloy consisting of two phases with melting points at 468 °C and 560 °C. The two eutectic alloys were prepared by induction melting. Afterwards the alloys were subjected to hydrogen decrepitation. The eutectic powder was mixed with the powder from the *mix motor* type in a ratio of 90:10, scrap powder to eutectic powder. The mixture was sintered at 1080 °C for one hour, followed by an annealing treatment at 600 °C for two hours. The magnetic properties of these magnets are shown in figure 4.65.

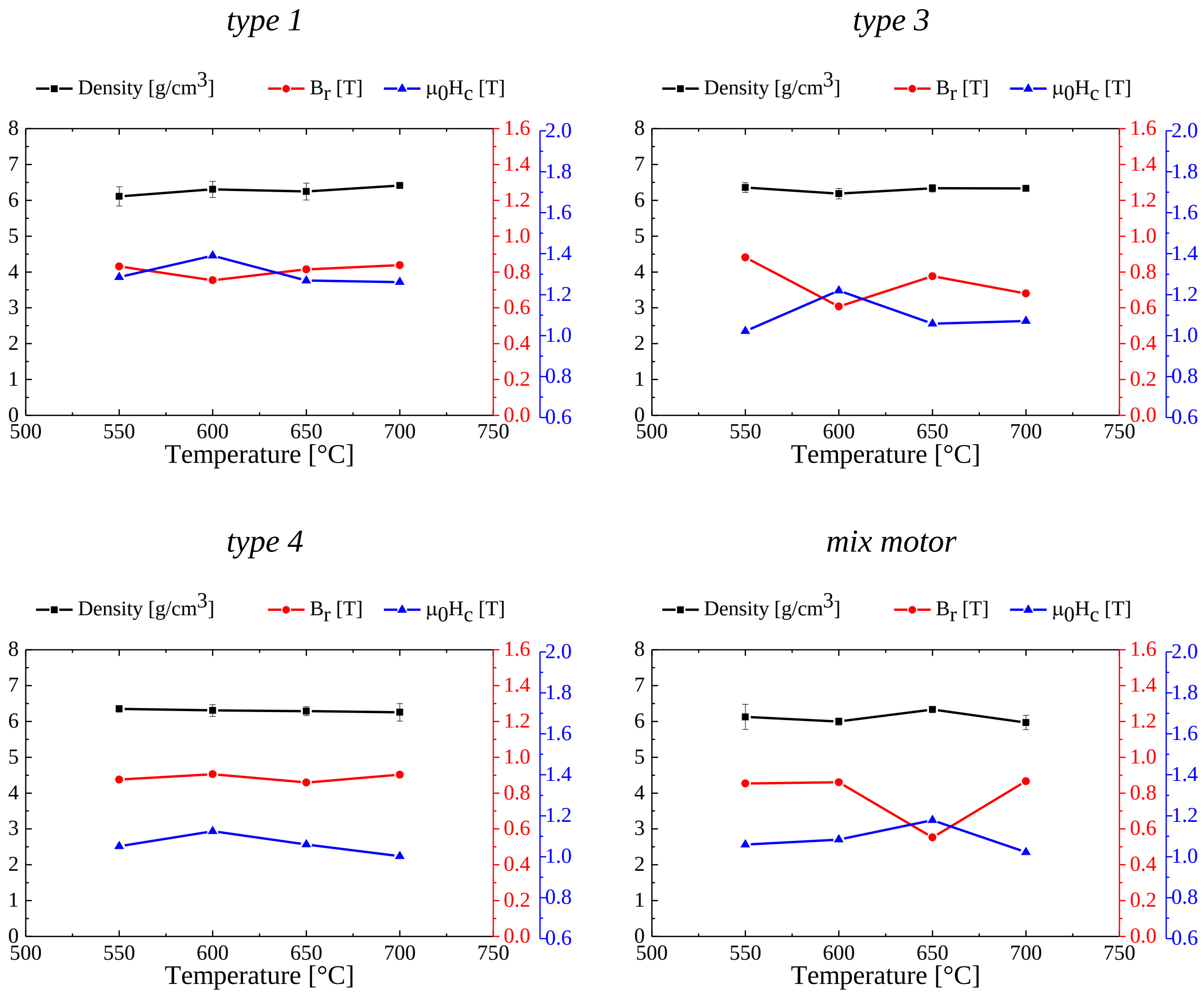

Figure 4.64: Variation in the density, remanence B_r, and coercivity μ_0H_c with the increase in the annealing temperature, for the *type 1*, *type 3*, *type 4* and *mix motor*, sintered prior the annealing step at the temperature of 1080 °C.

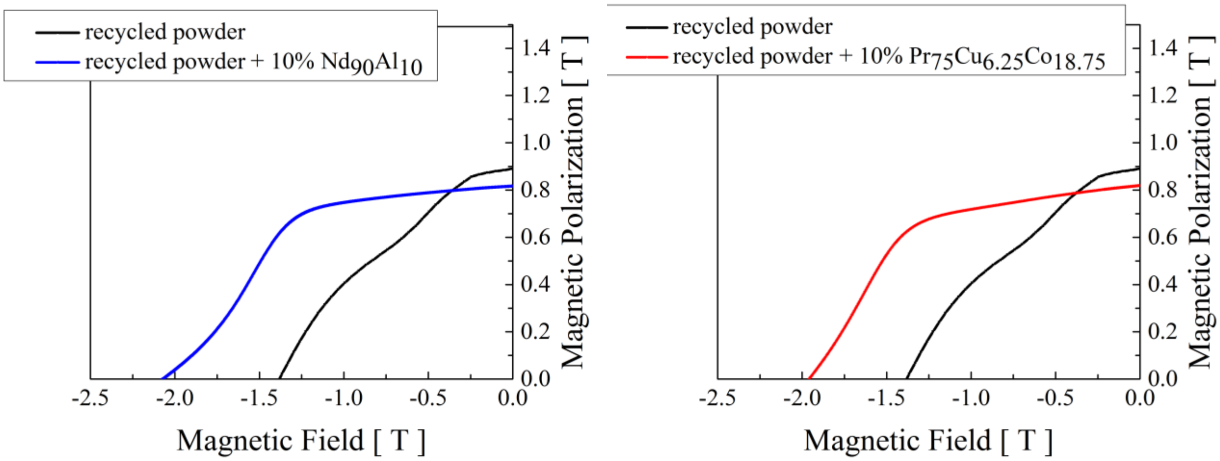

Figure 4.65: Demagnetization loops of the *mix motor* type (black), *mix motor* + 10 wt% $Nd_{90}Al_{10}$ (left), and *mix motor* + 10 wt% $Pr_{75}(Cu_{0.25}Co_{0.75})_{25}$ (right).

The demagnetization loops of the recycled magnets containing fresh additives, presents a squareness which is not suitable for a sintered magnet. As it can be seen from the SEM investigations the rare-earth phase is not well distributed along the grain boundary. In figure 4.66 is presented the recycled sintered magnet containing 10 wt% $Nd_{90}Al_{10}$ additions.

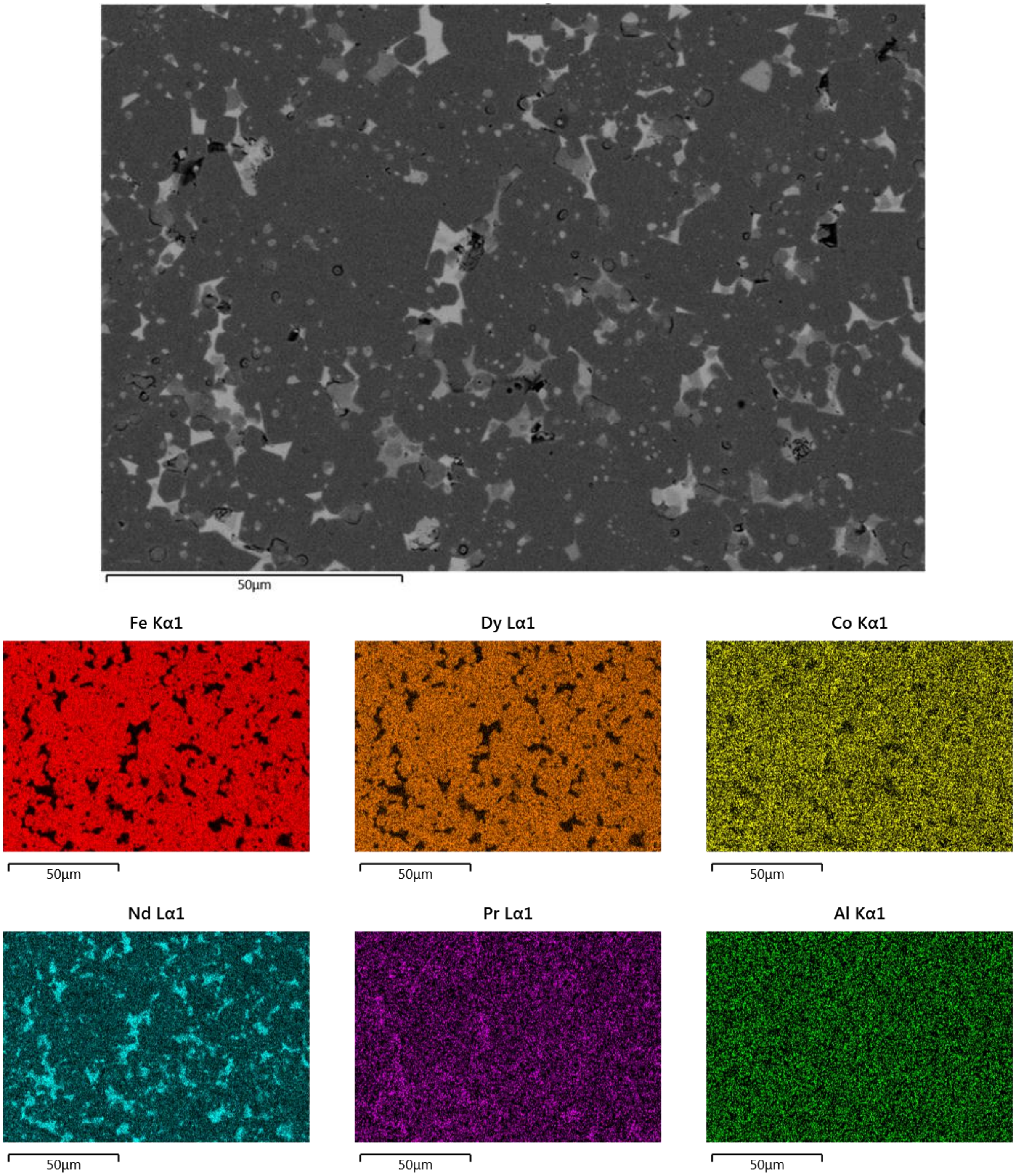

Figure 4.66: SEM backscattered electron image of the sintered mix motor + 10 wt% $Nd_{90}Al_{10}$ magnet and the individual element maps (scale bar: 50 µm).

As it can be observed the rare earth rich phase (in the electron image the brighter zones) is conglomerated in different part of the samples. Ideally will be that the rare earth rich phase (bright zone) to surround the $Nd_2Fe_{14}B$ (gray zone). These regions rich in rare earth are even more pronounced and developed for the sintered *mix motor* + 10 wt% $Pr_{75}(Cu_{0.25}Co_{0.75})_{25}$, as it can be observed from figure 4.67.

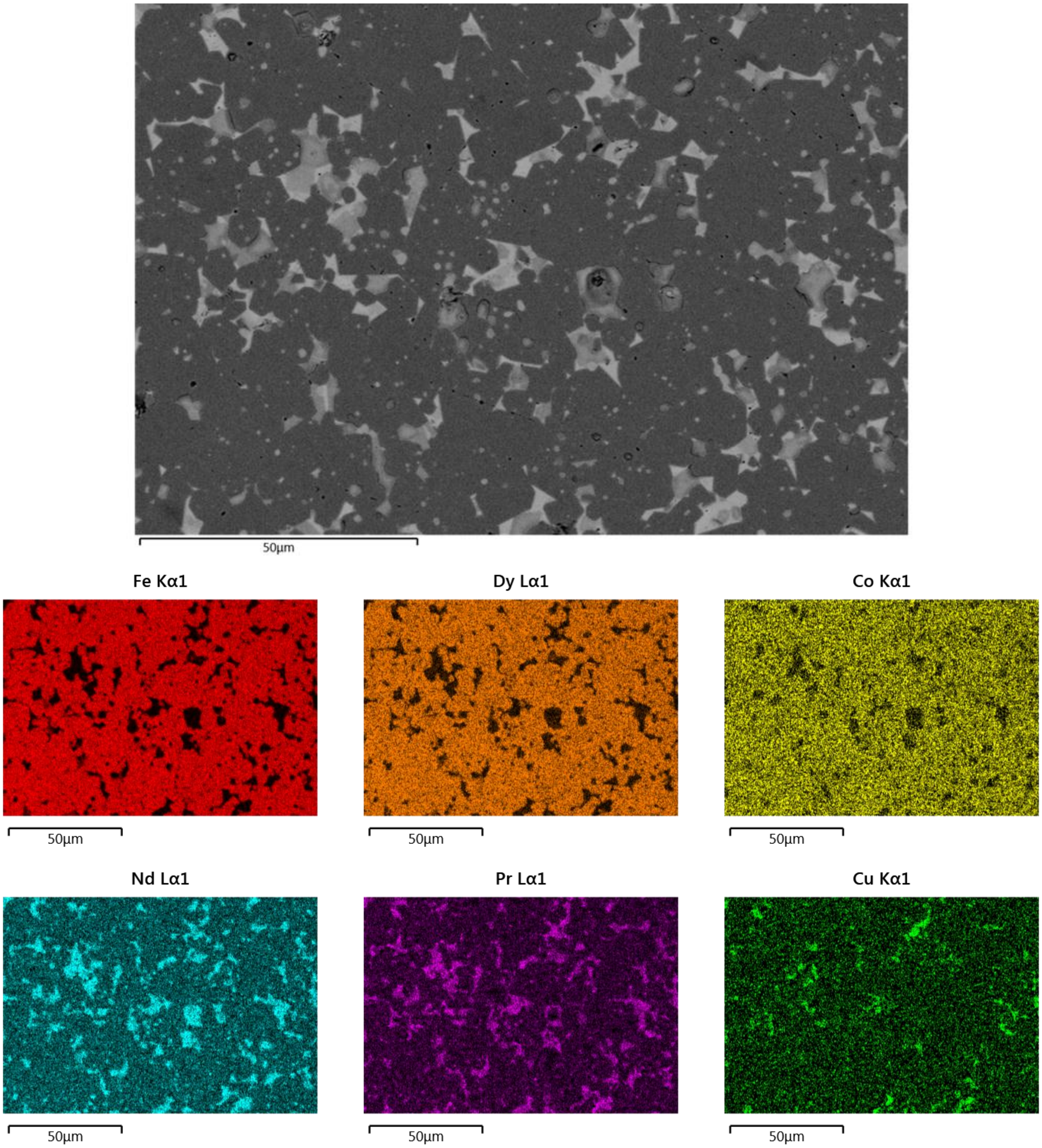

Figure 4.67: SEM backscattered electrons image of the sintered *mix motor* + 10 wt% $Pr_{75}(Cu_{0.25}Co_{0.75})_{25}$ magnet and the individual element maps (scale bar: 50 µm).

A two-step annealing approach for the *mix motor* type results in further improvement of the magnetic properties. In this case the *mix motor* powder; *mix motor* powder + 10 wt% $Nd_{90}Al_{10}$ and *mix motor* + 10 wt% $Pr_{75}Cu_{6.25}Co_{18.75}$ were sintered at 1080 °C for one hour, whereupon were subjected to a first annealing step at 850 °C for two hours, and then to a second annealing step at 600 °C for 4 hours. The magnetic properties of the obtained magnets are shown in figure 4.68. Compared with the sintering process with only one step annealing, an improvement in the coercivity is observed. The coercivity is increasing from 2 T to nearly 2.5 T, for the recycled mix motor type + $Nd_{90}Al_{10}$ and to nearly 2.2 T in the case of *mix motor* + $Pr_{75}Cu_{6.25}Co_{18.75}$.

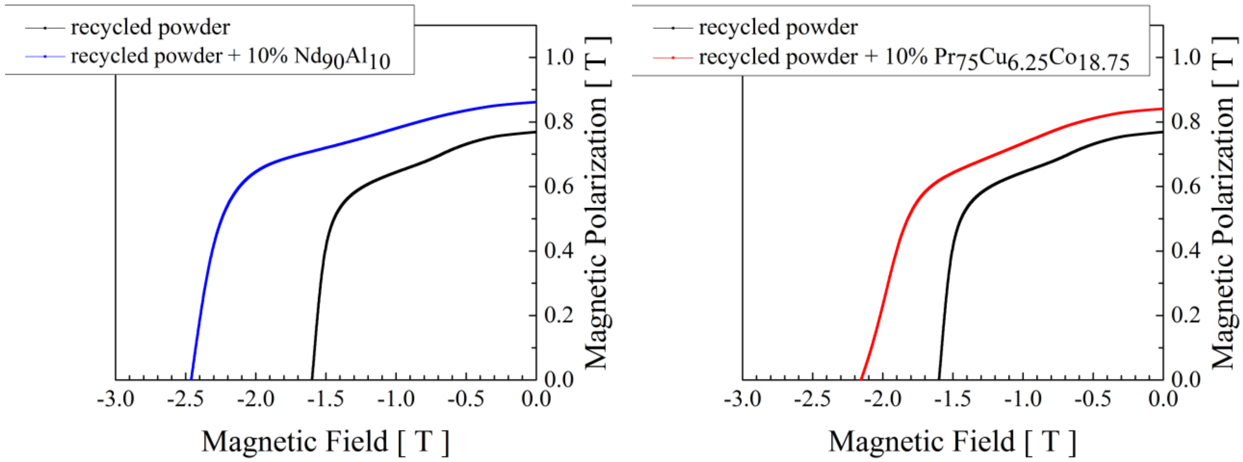

Figure 4.68: Demagnetization loops of the *mix motor* type (black), *mix motor* + 10 wt% $Nd_{90}Al_{10}$ (left), and *mix motor* + 10 wt% $Pr_{75}Cu_{6.25}Co_{18.75}$ (right) obtained by sintering and followed by a two-step annealing process.

The impurities play a crucial role on the magnetic properties of the final recycled magnets. Impurities like oxygen and carbon appears during the recycled process. In figure 4.69 is shown the oxygen and carbon content measured at different steps of the recycling process. The oxygen content is increasing after each step of the recycling process, resulting for the recycled magnets a concentration between 0.5 and 1.1 wt %. The carbon content is lower than the oxygen content and situated between 0.25 wt% and 0.4 wt %. The carbon content is increased after the sintering process. These values are falling in the value range reported by others authors researching on the recycling of Nd-Fe-B magnets **[124, 125]**. These values can be improved by having a better control on the recycling process.

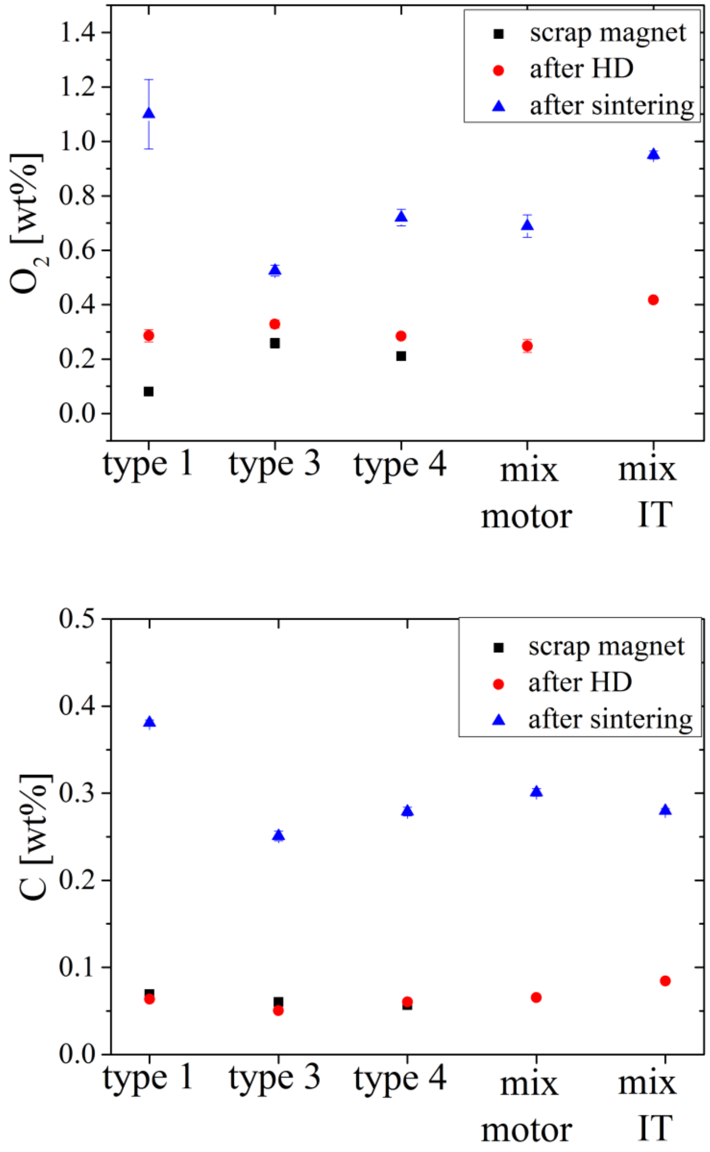

Figure 4.69: Oxygen (top image) and carbon (bottom image) evolution during different stages of the recycling process.

4.6.4 Comparison between the different recycled magnets obtained via the presented routes

In the following section a comparison between the magnetic properties of the scrap magnets and the magnetic properties of the recycled magnets obtained by different routes is presented. The demagnetization curves of the different magnets before and after the recycling process are shown in figure 4.71. Before the recycling process, the scrap magnets were measured magnetically in the as received stage. In figure 4.71 the as-received scrap magnets are represented by the red demagnetization curves. The blue demagnetization curves represent the recycled HDDR powder prepared with optimized parameters, which was embedded in paraffin wax. The green demagnetization loops represent the powder that was sintered by conventional sintering after the hydrogen decrepitation process. The magenta demagnetization loops represent the powder subjected to the optimized HDDR process and consolidated by spark plasma sintering.

type 1 *type 2*

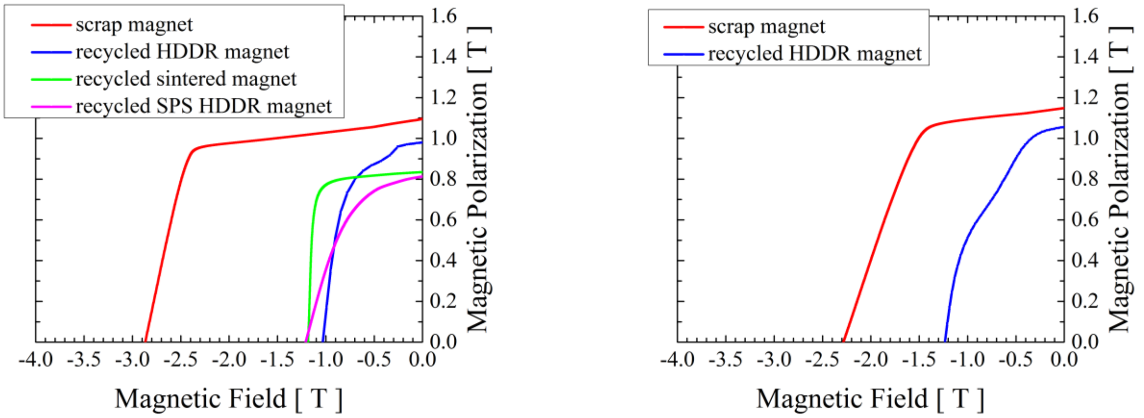

type 3 *type 4*

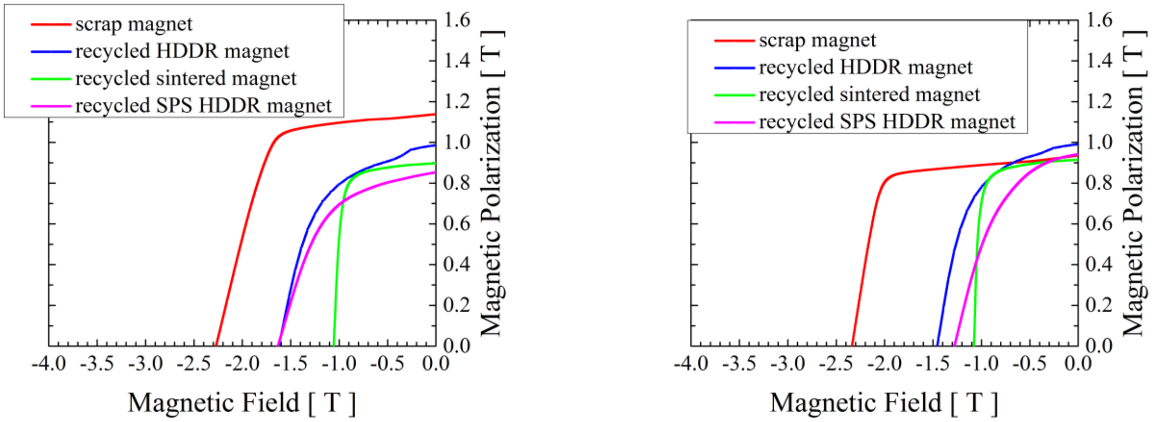

Figure 4.71: Demagnetization loops corresponding to different scrap magnets and to the recycled magnets consolidated by different routes.

For the *type 2* magnets is presented only the demagnetization loops of the scrap magnet and of the recycled magnet after the HDDR process, because the scrap magnets received were not enough to prepare also recycled magnets consolidated by SPS or by conventional sintering. For all the recycled magnets the prepared powder was aligned in magnetic field prior the consolidation step. For all 4 types of scrap magnets, the magnetic properties corresponding to the recycled magnets are smaller compared with the magnetic properties of scrap magnets. M. Zakotnik et al. **[76]** reported that by recycling Nd-Fe-B magnets a decrease in magnetic properties of the recycled magnets of 20 % was observed. In the case of the magnets from laptops and flat TV loudspeakers (*mix IT* type), which have a low content of Co and Dy compared to the magnets from electric motors, a better recovery of the magnetic properties was obtained. The magnetic properties of the recycled magnets corresponding to *mix IT* type were compared with three randomly selected loudspeaker magnets. After the magnetic measurement of the three randomly selected magnets, a small part of the powder obtained after the hydrogen decrepitation process, was treated with the optimized HDDR parameters corresponding to the *mix IT* type, and the other part was used to form the *mix IT* type. The comparison between the magnetic properties of the three types of magnets (scrap magnets – red demagnetization curve –, randomly selected magnets treated with the optimized HDDR parameters for *mix IT* – blue demagnetization curve – and the recycled *mix IT* – black demagnetization curve –) are shown in figure 4.72.

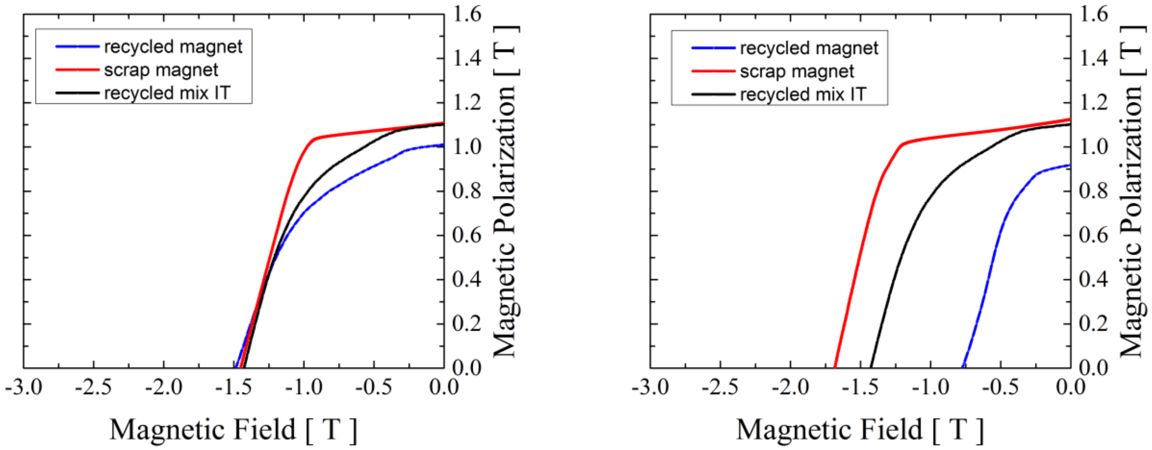

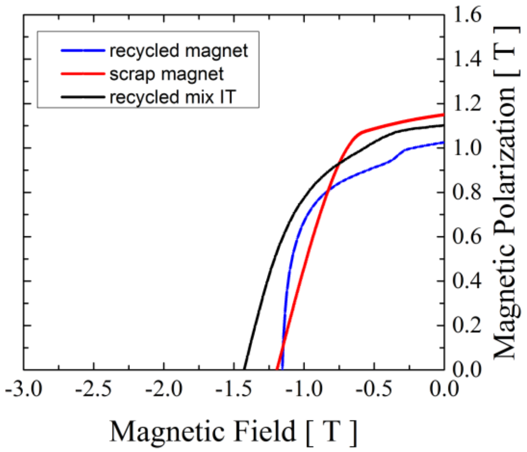

Figure 4.72: Demagnetization curves corresponding to the randomly selected scrap magnets from loudspeakers (red curve), the three randomly selected recycled scrap magnets with the optimized parameters for the *mix IT* type (blue curve), and the *mix IT* type processed with optimized HDDR parameters (black curve).

From figure 4.72 it can be observed that for the recycled magnets for which it was not used an optimized HDDR process (blue demagnetization curves), the magnetic properties are lower in comparison with the magnetic properties of the scrap magnets (red demagnetization curves). For the *mix IT* which was processed with optimized HDDR parameters it can be observed that magnetic properties are roughly the same like the magnetic properties of the scrap magnets. The difference in the coercivity can be explained by the difference in the chemical composition. The scrap magnets may contain more/less Dy than the *mix IT* type. So, it can be concluded that for the *mix IT* type, where it was achieved roughly 100 % recovery of the magnetic properties, the recycled process works better for these magnets with low Dy and Co additions.

5. Conclusions

The aim of this work was to systematically study the possibility of using a combination of low and high temperature hydrogen treatments - hydrogen decrepitation and dynamic hydrogenation disproportionation desorption recombination - for the production of highly anisotropic recycled magnets from different scrap sintered Nd-Fe-B magnets with various additives. Nd-Fe-B magnets from end-of-life products are currently in small proportion recycled on an industrial scale, despite the fact that they would represent a major source of highly concentrated, technologically and economically relevant rare earth metals. Scrap magnets could present a cost efficient, environmentally friendly alternative resource from the technosphere, if the materials are collected and separated systematically from waste streams and an economic reprocessing of the materials will take place.

Various WEEE streams and products known as possible sources containing permanent magnets were studied in order to identify those that contain Nd-Fe-B magnets. Nd-Fe-B magnets were found in loudspeakers and hard disk drives integrated in IT and communication devices, where the overall device dimensions have a role to play in the marketing of the product, why it needs a stronger magnet to cope with the smaller space. It was observed that all the loudspeakers in the laptops studied and most of the loudspeakers in the flat TV sets and PC screens contain Nd-Fe-B magnets, whereas normal external loudspeakers contain mainly ferrites. Since at the company Stena Technoworld, where the study was realized, the LCDs and laptops are being dismantled already in the recycling process; it would be an easy task to extract the speakers from these devices. LEDs and plasma TVs, which are not dismantled, would require extra labor if the magnets were to be extracted. Hard disk drives have been suggested by several projects or researchers to be the perfect candidate for Nd-Fe-B magnet recycling. It has also been suggested, that in order to recycle the Nd-Fe-B magnets, the magnet has to be removed before the shredding step, where a lot of it would be lost otherwise. If such a solution is implemented, where all the magnets are collected together, a rough estimation based on the flows at this recycling plant suggests that the amount of Nd-Fe-B could be almost doubled if loudspeakers magnets from laptops and flat screens are included. It should also be noted that although the overall amount of the Nd-Fe-B magnet is still relatively small for the recycling plant like Stena, a central processing plant (in EU or whole Europe) collecting the Nd-Fe-B magnets scrap from different WEEE recycling plants would still feasible for a REE recovery. A detailed feasibility study is needed to determine a minimum economic scale, based on the findings of the plant data from this study.

In the presented work, six different types of scrap sintered magnet batches were used to test a magnet-to-magnet recycling procedure. Four of the six types of scrap magnets are sintered magnets used in electric motors, and the last two types are mixture of sintered magnets from different electric motors and mixture of sintered magnets from loudspeakers from flat TV sets and laptops. All the starting scrap materials were well characterized in terms of composition, microstructure and magnetic properties. The hydrogen absorption / desorption behavior of the starting scrap material was investigated. It was confirmed that the magnet additives influence the disproportionation reaction. For the magnets with a higher Co and Ga content it was observed that the disproportionation reactions take place at higher temperatures in comparison with those of the *mixt IT* type, which has a lower temperature of 661 °C corresponding to the disproportionation reaction due to their low Co and Ga content. For the desorption and recombination processes, the DTA study shows that for the magnets with a higher Co and Ga content the recombination reaction starts earlier, at lower temperatures compared with the *mix IT* type which has a low Co and Ga content and for which the recombination reaction take place at a slightly higher temperature of 793 °C. In different DTA studies, which were performed at different hydrogen pressures (from 1.20 bars up to 75 bars) the type *1* magnets show that by increasing the hydrogen pressure, the disproportionation reaction has a peak at lower temperature. In this case, if for 1.2 bars hydrogen pressure the peak of the disproportionation reaction is at 737 °C, for 75 bars the peak of the disproportionation reaction is at 698 °C.

A detailed XRD study on HDDR disproportionated powders, corresponding to all six types of scrap magnets was done. The goal of the study was to determine the lowest hydrogen pressure from which the powders are fully disproportionated. For hydrogen pressures below 50 kPa, the powder is non-disproportionated or only partially disproportionated. Hydrogen pressures above this limit leads to fully disproportionate powders. The XRD study confirms the DTA results, which says that the $Nd_2Fe_{14}B$ scrap magnets with high content of Co and Ga require a higher temperature for completing the disproportionation reaction. From the XRD study resulted that for the processing temperature of 780 °C for the first plateau and 840 °C for the second plateau, the scrap magnets with higher Co and Ga content require a higher hydrogen pressure for the completion of the disproportionation reaction. It was determined that in order to obtain fully disproportionated powders, *type 1* requires a hydrogen pressure of 90 kPa; *type 2*, *type 3* and *type 4* needs 70 kPa*; mix motor* type 80 kPa, and *mix IT* type 50 kPa hydrogen pressure.

The coercivity and remanence variation with the increase of the hydrogen pressure, hydrogen desorption rate and HDDR processing temperature was studied. It was determined that the obtained HDDR power is anisotropic for hydrogen pressure of up to 20 kPa, above the hydrogen pressure point where the powder starts to be completely disproportionated. Above this limit of +20 kPa the obtained powder is isotropic. Regarding the desorption rate, the determined optimum parameters are characteristic to this system and to the specific weight of the batch that was used in the process. However, for low desorption rates was obtained low coercivities, but by rising the rate of the hydrogen desorption the coercivity is improved. For higher desorption rates (>15 L/min) results in isotropic powder, while for desorption rates smaller than 15 L/min the obtained powder was anisotropic. For all scrap magnets from electric motors containing high Co and Dy contents the optimal hydrogen desorption rate was determined to be 13 L/min. For the *mix IT* type magnet batch with lower Dy and Co contents the optimum desorption rate is 2.2 L/min. For the HDDR processing temperature it was determined that by increasing the temperature from 740 °C to 840 °C, the obtained powder presents better magnetic properties. But it was shown that a too high processing temperature results in grain growth, which has as a result low coercivities (obtained for the processing temperature of 890 °C).

Different compacting methods were applied to the HDDR powder processed with optimum processing parameters. For the resin bonded magnets coercivities of 1.2 T and remanences of 0.45 T were obtained in the chase of isotropic magnets, compacted at a pressure of 0.8 GPa. The production of anisotropic bonded magnets was unsuccessful due to inefficient alignment of the powder before pressing. For the recycled magnets consolidated by spark plasma sintering, a study made at different sintering temperature under a constant pressure of 39MPa, shows that densities of ~ 7.4 g/cm^3 are obtained at the sintering temperature of 1000 °C. At this temperature for all the types of recycled magnets were recorded the best coercivities and remanences. At this sintering temperature of 1000 °C, the submicronic grains developed during the HDDR process, grew up and reached dimensions between 300 nm and 1.5 μm and isolated big grains around 10 - 20 μm appeared. Conventional sintering was used for hydrogen decrepitated powder to obtained recycled magnets. In this case lower densities of 6.5 g/cm^3 were obtained, with a remanence of ~0.8 T and coercivities of 1.1 - 1.2 T. A post-sintering annealing step improves slightly the density and the magnetic properties of the powder. To regain the magnetic properties the recycled powders were mixed with different eutectic low melting point alloys like $Nd_{90}Al_{10}$ and $Pr_{75}(Cu_{0.25}Co_{0.75})_{25}$. This approach increased the coercivity with 35 % and drop the remanence by 10 %. A detailed SEM study shows that the new additions of fresh powders are not equally distributed in the entire recycled magnets, big "islands" of the fresh powders being discovered.

Surprisingly the oxygen and carbon content of the scrap magnets is low, between 0.1-0.3 wt% for oxygen and 0.05 - 0.1 wt % for the carbon content. After each step of the recycling process, an increase in the oxygen content, resulting in the recycled magnets an oxygen content between 0.5 and 1.1 wt % was recorded. The final carbon content in the recycled magnets is between 0.25 wt% and 0.4 wt %.

Comparing the starting scrap magnets with the recycled magnets recovery of ~90 % in remanence was achieved. For the coercivity of the recycled magnets lower recovery values were achieved. So, for the magnets with high content of Co and Dy, recovery in coercivity of 37 % for *type 1*; of 54 % for *type 2*; of 72 % for *type 3* and 62 % for *type 4*, were achieved. For the magnets from loudspeakers, *mix IT* type, which contains a low Dy and Co content, the recovery of the magnetic properties can be considered roughly 100 %.

Future work may result in improving the magnetic properties of the recycled magnets. A milling step prior the sintering process will reduce the particle size, which can improve the coercivity of the recycled magnets. Further adjustments on the spark plasma sintering process, like different pulse durations, different break time between the pulses or different number of pulses per burst, can further improve the magnetic properties of the recycled magnets. A more equal and better distribution of the fresh powder in the recycled magnets may improve further the magnetic properties. A continuous flux of the recycling process can reduce the oxygen content gained during the recycling process.

Acknowledgments

I thank Prof. Dr. Oliver Gutfleisch for supervising my Ph.D. and for giving me the opportunity to prepare my Ph.D. in his group.

Furthermore, I want to thank Prof. Dr. Yongxiang Yang, who kindly agreed to be co-referee of my Ph.D. thesis.

I thank to my colleagues from Fraunhofer IWKS, Dr. Roland Gauß and Konrad Güth for their support and discussions, to Iuliana Poenaru for her help and advices in the XRD and SEM analyses and to Anna-Lisa Bachmann, for the help with the ICP-OES measurements.

My thanks go also to Prof. Dr. Wilhelm Kappel from National Institute for Research and Development in Electrical Engineering Advance Research, for his support and that he allowed me to use the entire equipments of the institute, in realizing the SPS study. Also, my thanks go to Dr. Eros Patroi and Dr. Delia Patroi, for their support, advice and the many discussions that we had.

I am thankful to Björn Hall from Stena Metall for allowing us to realize the WEEE study at Stena Technoworld, and to my colleagues who contributed and helped in realizing the study, Dr. Allan Walton and Christian Jönsson from Unversity of Birmingham and to Prof. Dr. Yongxiang Yang and Prakash Venkatesan from Delft University of Technology.

I also want to thank my colleagues from TU Darmstadt, Dr. Léopold V.B. Diop for his help and very useful discussions during my Ph.D. and Dr. Iliya Radulov for his useful discussions and patience in teaching me the hidden parts of the PPMS.

Last but not least, I am grateful to Prof. Dr. Koen Binnemans, for the versatile and exciting hints given during the EREAN workshops.

The research leading to these results has received funding from the European Community’s Seventh Framework Programme ([FP7/2007-2013]) under grant agreement no. 607411 (MC-ITN EREAN: European Rare Earth Magnet Recycling Network). This publication reflects only the authors’ view, exempting the Community from any liability. Project website: http://www.erean.eu.

References

[1] J.M.D. Coey: *“Hard Magnetic Materials: A perspective”,* IEEE Transactions on magnetics 47, 12, 2011.

[2] J.F. Herbst: *“$R_2Fe_{14}B$ materials: intrinsic properties and technological aspects”*, Reviews of Modern Physics. 63, 819, 1991.

[3] J.J Croat, J.F. Herbs, R.W. Lee, F.E. Pinkerton: *“Pr-Fe and Nd-Fe-based materials: A new class of high-performance permanent magnets”* Journal of Applied Physics 55, 2078, 1984.

[4] M. Sagawa, S. Fujimura, N. Togawa, H. Yamamoto, Y. Matsuura: *“New material for permanent magnets on a base of Nd and Fe”*, Journal of Applied Physics 55, 2083, 1984.

[5] E. F. Kneller, R. Hawig: *“The Exchange-Spring Magnet A New Material Principle for Permanent Magnets”,* IEEE Transactions on Magnetics, 27, 1991.

[6] R. Skomski, J. M. D. Coey: *“Giant energy product in nanostructured two-phase magnets”* Physical Review B 48, 21, 1993.

[7] Y. Kaneko: *“Highest Performance of Nd–Fe–B Magnet Over 55 MGOe”*, IEEE Transactions on Magnetics 36, 5, 2000.

[8] W. Rodewald, B. Wall, M. Katter, K. Uestuener: *“Top Nd-Fe-B Magnets: >56 MGOe, Energy Density, 9.8 kOe Coercivity”*. IEEE Transactions on magnetics 38, 5, 2002.

[9] R. Schulz, M. Bucherta: *“Estimates of global REE recycling potentials from NdFeB magnet material”,* Resources, Conservation and Recycling 113, 12–27, 2016.

[10] H. Mikami, K. Ide, Y. Shimizu, M. Senoo, H. Seki: *“Historical Evolution of Motor Technology”*, Hitachi Review 60, 38–45, 2011

[11] B. Sprecher, R. Kleijn, G. J. Kramer*: “Recycling Potential of Neodymium: The Case of Computer Hard Disk Drives”,* Environmental Science and Technology 48, 9506−9513, 2014.

[12] V. Panchanathan, M. L. Spencer: *“Bonded Permanent Magnets – an overview”,* TMS (The Minerals, Metals & Materials Society), 2013.

[13] S. Sugimoto: *“Current status and recent topics of rare-earth permanent magnets”,* Journal of Physics. 44, 064001.

[14] US Department of the Interior, US Geological Survey report on: *“Mineral Commodity Summaries”,* 2011.

[15] J. Wübbeke: *“Rare earth elements in China: Policies and narratives of reinventing an industry”,* Resources Policy 38, 384–394, 2013.

[16] S. Massari, M. Ruberti: *“Rare earth elements as critical raw materials: Focus on international markets and future strategies”*, Resources Policy 38, 36–43, 2013.

[17] European Commission, report on: “*Critical raw materials for the EU”,* May 2014.

[18] A. Golev, M. Scott, P. D. Erskine,S. H. Ali, G. R. Ballantyne: *“Rare earths supply chains: Current status, constraints and opportunities”*, Resources Policy 41, 52–59, 2014.

[19] K. Binnemans, P. T. Jones: *“Rare Earths and the Balance Problem”,* Journal of Sustainable Metallurgy 1:29–38, 2015.

[20] K. Binnemans, P. T. Jones, B. Blanpain, T. V. Gerven, Y. Yang, A. Walton, M. Buchert: *“Recycling of rare earths: a critical review”*, Journal of Cleaner Production 51, 1-22, 2013.

[21] K.H.J. Buschow: *“Permanent Magnet Materials Based on 3d-rich Ternary Compounds”* from: *“Handbook of Magnetic Materials”*, Volume 4, edited by: E. P. Wohlfarth, K. H. J. Buschow, Elsevier, 1988.

[22] R. Skomski: *“Permanent Magnets: History, Current Research, and Outlook”,* from: “*Novel Functional Magnetic Materials”*, edited by A. Zhukov, Springer, 2016.

[23] R. Skomski, D. J. Sellmyer: *“Intrinsic and Extrinsic Properties of Advanced Magnetic Materials”*, from: “*Handbook of Advanced Magnetic Materials”, volume 1: Advanced Magnetic Materials: Nanostructural Effects*, edited by: Y. Liu, D. J. Sellmyer, D. Shindo, Tsinghua University Press, Springer, 2006.

[24] J.M. D. Coey: *“Magnetism and Magnetic Materials”,* Cambridge University Press, 2010.

[25] N. A. Spaldin: *“Magnetic Materials: Fundamentals and Applications”,* Cambridge University Press, 2011.

[26] R. Skomski: *“Simple Models of Magnetism”*, Oxford University Press, 2008.

[27] B.D. Cullity, C.D. Graham: *“Introduction to magnetic materials”,* second edition, IEEE Press, 2009.

[28] S. Liu: *“Recent Developments in High-Temperature Permanent Magnet Materials”,* from: *“Handbook of Advanced Magnetic Materials”, volume 1: Advanced Magnetic Materials: Nanostructural Effects,* edited by: Y. Liu, D. J. Sellmyer, D. Shindo, Tsinghua University Press, Springer, 2006.

[29] K. H. J. Buschow, F. R. de Boer: *"Physics of Magnetism and Magnetic Materials",* Kluwer Academic Publishers, 2004.

[30] H. Kronmüller: *"Micromagnetism and Magnetization Processes in Modern Magnetic Materials",* from: *"Science and Technology of Nanostructured Magnetic Materials",* edited by G.C. Hadjipanayis and G. A. Prinz, NATO ASI Series B: Physics vol. 259, 1991.

[31] E. Burzo: *"Permanent magnets based on R–Fe–B and R–Fe–C alloys* Reports on Progress in Physics 61, 1099–1266, 1998.

[32] K. H. J. Buschow: *"Magnetism and Processing of Permanent Magnet Materials"*, from: *"Handbook of Magnetic Materials"*, vol. 10, Elsevier Science, 1997.

[33] A. Rusu-Petroaia: *"Contribuţii la studiul proprietăţilor magneţilor permanenţi cu pământuri rare",* Ph.D. thesis, Universitatea Politehnică Bucureşti, 1999 – in Romanian.

[34] W. F. Brown Jr: *"Virtues and Weaknesses of the Domain Concept",* Reviews of Modern Physics 17, 1945.

[35] W. F. Brown Jr: *"Micromagnetics: Domain Walls*", Journal of Applied Physics 30, 4, 1959.

[36] H. Kronmüller, K.-D. Durst, M. Sagawa: *"Analysis of the magnetic hardening mechanism in RE-Fe-B permanent magnets",* Journal of Magnetism and Magnetic Materials 74, 1988.

[37] P. Dalmas De Réotier, D. Fruchart, P. Wolfers, P. Vulliet, A. Yaouanc, R. Fruchart, P. L'Héritier: *"Properties of hydride* $RE_2Fe_{14}B$ *compounds",* Journal de Physique Colloques 46, 1985.

[38] I. R. Harris, C. Noble, T. Bailev: *"The hydrogen decrepitation of an* $Nd_{15}Fe_{77}B_6$ *magnetic alloy"*, Journal of the Less-Common Metals 106, 1985.

[39] D. Book, I.R. Harris: *"Hydrogen absorption/desorption and HDDR studies on* $Nd_{16}Fe_{76}B_8$ *and* $Nd_{11.8}Fe_{82.3}B_{5.9}$*"*, Journal of Alloys and Compounds 221, 1995.

[40] V.A. Yartys, A.J. Williams, K.G. Knoch, P.J. McGuiness, I.R. Harris: *"Further studies of anisotropic hydrogen decrepitation in* $Nd_{16}Fe_{76}B_8$ *sintered magnets"*, Journal of Alloys and Compounds 239, 1996.

[41] B. Saje, J. Holc, S. Besenicar: *"The sequence of fracture processes in hydrogen-decrepitated* $Nd_{16-x}Dy_xFe_{76}B_8$ *alloy"*, Journal of Magnetism and Magnetic Materials 101, 1991.

[42] M. Verdier, J. Morros, D. Pere, I. R. Harris: *"Hydrogen Absorption Behaviours of Some Nd-Fe-B-Type Alloys"*, IEEE Transactions on Magnetics 30, 2, 1994.

[43] I. R. Harris, P. J. McGuiness, D. G. R. Jones, J. S. Abell: *"Nd-Fe-B permanent magnets: hydrogen absorption/desorption studies (HADS) on* $Nd_{l6}Fe_{76}B_8$ *and* $Nd_2Fe_{14}B$*"*, Physica Scripta, T19, 435-440, 1987.

[44] A. J. Williams, P. J. McGuiness, I. R. Harris: *"Mass spectrometer hydrogen desorption studies on some hydrided NdFeB- types alloys"*, Journal of Less Common Metals 171, 149 – 155, 1991.

[45] V.A. Yartys, O. Gutfleisch, V.V. Panasyuk, I.R. Harris: *"Desorption characteristics of rare earth (R) hydrides (R = Y, Ce, Pr, Nd, Sm, Gd and Tb) in relation to the HDDR behaviour of R–Fe-based-compounds"*, Journal of Alloys and Compounds, 253–254, 1997.

[46] K. Oesterreicher, H. Oesterreicher: *“Structure and Magnetic Properties of* $Nd_2Fe_{14}BH_{2.7}$*”,* Physica Status Solidi A 85, K61, 1984.

[47] G. Wiesinger, G. Hilscher, R. Grössinger: *“Effect of hydrogen absorption on the magnetic properties of* $Nd_{15}Fe_{77}B_8$*”*, Journal of the Less Common Metals 131, p409-417, 1987.

[48] P. L'Héritier, P. Chaudouet, R. Madar, A. Rouault, J. P. Sénateur, R. Fruchart: *"Une nouvelle série d'hydrures métalliques ferromagnétiques de type* $Nd_2Fe_{14}BH_x$ *(0<x<5)”,* C. R. Académie des Sciences Paris, t. 299, series 2, no. 13, p 849 – 852, 1984, in French.

[49] J. M. Cadogan, J. M. D. Coey: *“Hydrogen absorption and desorption in* $Nd_2Fe_{14}B$*”,* Applied Physics Letters 48, 442, 1986.

[50] O. Gutfleisch, M. Matzinger, J. Fidler, I. R. Harris: *“Characterisation of solid-HDDR processed* $Nd_{16}Fe_{76}B_8$ *alloys by means of electron microscopy”*, Journal of Magnetism and Magnetic Materials 147, p. 320-330, 1995.

[51] I. R. Harris, P. J. McGuiness: *“Hydrogen: Its Use in the Processing of NdFeB-type Magnets and in the Characterization of NdFeB-Type Alloys and Magnets”,* Proceedings of the eleventh international workshop on rare earth magnets and their applications, 1990.

[52] S. Sugimoto, H. Nakamura, K. Kato, D. Book, T. Kagotani, M. Okada, M. Homma: *“Effect of the disproportionation and recombination stages of the HDDR process on the inducement of anisotropy in Nd–Fe–B magnets”*, Journal of Alloys and Compounds, 293–295, p. 862–867, 1999.

[53] T. Takeshita, R. Nakayama: Proceedings the 12th Int. Workshop on Rare-Earth Magnets and Their Applications. Canberra, Australia, p. 670, 1992.

[54] S. Sugimoto, D. Book: *“HDDR Process for the Production of High Performance Rare-Earth Magnets”*, from: “*Handbook of Advanced Magnetic Materials”, volume 1: Advanced Magnetic Materials: Nanostructural Effects*, edited by: Y. Liu, D. J. Sellmyer, D. Shindo, Tsinghua University Press, Springer, 2006.

[55] T. W. Capehart, R. K. Mishra, F. E. Pinkerton: *“Determination of the zirconium site in zirconium-substituted* $Nd_2Fe_{14}B$*”,* Journal of Applied Physics, 73, p 6476, 1993.

[56] K. H. J. Buschow, P. C. P. Bouten, A. R. Miedema: *“Hydrides formed from intermetallic compounds of two transition metals: a special class of ternary alloys”*, Reports on Progress in Physics 45, 1982.

[57] K. H. J. Buschow: *“New developments in hard magnetic materials”*, Reports on Progress in Physics 54, 1991.

[58] C. Burkhardt, M. Steinhorst, I.R. Harris: *“Detailed SEM studies of the HDDR behaviour of direct-reduced* $Nd_{15}Fe_{77}B_8$ *and* $Nd_{15}Fe_{77-x}B_8Ga_x$ *powders”*, Journal of Alloys and Compounds 237, p. 113-120, 1996.

[59] K. H. J. Buschow: *“Trends in rare earth permanent magnets”*, IEEE Transactions on Magnetics 30, 2, 1994.

[60] H. Nakamura, S. Sugimoto, T. Tanaka, M. Okada, M. Homma: *“Effects of additives on hydrogenation, disproportionation, desorption and recombination phenomena in* $Nd_2Fe_{14}B$ *compounds”*, Journal of Alloys and Compounds 222, p. 136-140, 1995.

[61] A. Fujita, I. R. Harris: *“Magnetic Anisotropy in Arc-Cast Nd-Fe-B-Zr Alloys”* IEEE Transactions on Magnetics 29, 6, 1993.

[62] H. Nakamura, R. Suefuji, S. Sugimoto, M. Okada, M. Homma: *“Effects of HDDR treatment conditions on magnetic properties of Nd-Fe-B anisotropic powders”*, Journal of Applied Physics 76, p. 6828-6830, 1994.

[63] H. Nakamura, K. Kato, D. Book, S. Sugimoto, M. Okada, M. Homma: *“Enhancement of the anisotropy of Nd-Fe-B powders by varying the HDDR conditions”*, Journal of the Magnetics Society of Japan 23, p. 300-305, 1999.

[64] H. Nakamura, K. Kato, D. Book, S. Sugimoto, M. Okada, M. Homma: *“Enhancement of Coercivity in High Remanence HDDR Nd-Fe-B Powders”*, IEEE Transactions on Magnetics 35, 5, 1999.

[65] O. Gutfleisch, G. Drazic, C. Mishima, Y. Honkura: *“Texture Inducement During HDDR Processing of NdFeB”*, IEEE Transactions on Magnetics 38, 5, 2002.

[66] O. Gutfleisch, K. Khlopkov, A. Teresiak, K.-H. Müller, G. Drazic, C. Mishima, Y. Honkura: *“Memory of Texture During HDDR Processing of NdFeB”*, IEEE Transactions on Magnetics, 39, 5, 2003.

[67] M. Zakotnik, E.Devlin, I. R. Harris, A. J. Williams: *“Hydrogen decrepitation and recycling of NdFeB-type sintered magnets”*, Proceedings of 19th International Workshop on Rare Earth Permanent Magnets & Their Applications, p. 289-295, 2006.

[68] A. Walton, H. Yi, N. A. Rowson, J. D. Speight, V. S. J. Mann, R. S. Sheridan, A. Bradshaw, I. R. Harris, A. J. Williams: *“The use of hydrogen to separate and recycle neodymium-iron-boron-type magnets from electronic waste”*, Journal of Cleaner Production 104, p. 236-241, 2015.

[69] M. Zakotnik, A. J. Williams, I. R. Harris: *“Possible methods of recycling NdFeB-type sintered magnets using the HD/Degassing or HDDR Processes”*, Proceedings: 18th Workshop on High Performance Magnets & their Applications, 2004.

[70] E. A. Périgo, S. C. da Silva, R. V. Martin, H. Takiishi, F. J. G. Landgraf: *“Properties of hydrogenation-disproportionation-desorption-recombination NdFeB powders prepared from recycled sintered magnets”*, Journal of Applied Physics 111, 07A725, 2012.

[71] B. F. A. da Silva, S. R. Janasi, D. Rodrigues, H. Takiishi, M. F. de Campos: *“Hybrid bonded rare-earth magnets produced with strontium ferrite and recycled NdFeB powders”*, Proceedings 22 International Workshop on Rare Earth Permanent Magnets and their Applications, p322-325, 2012.

[72] O. Gutfleisch, K. Güth, T. G. Woodcock, L. Schultz: *“Recycling used Nd-Fe-B sintered magnets via a hydrogen-based route to produce anisotropic, resin bonded magnets”*, Advanced Energy Materials 3, p. 151–155, 2013.

[73] R. S. Sheridan, R. Sillitoe, M. Zakotnik, I. R. Harris, A. J. Williams: *“Anisotropic powder from sintered NdFeB magnets by the HDDR processing route”*, Journal of Magnetism and Magnetic Materials 324, p. 63–67, 2012.

[74] R. S. Sheridan, A. J. Williams, I. R. Harris, A. Walton: *“Improved HDDR processing route for production of anisotropic powder from sintered NdFeB type magnets”*, Journal of Magnetism and Magnetic Materials 350, p. 114–118, 2014.

[75] Directive 2012/19/EU of the European Parliament and of the Council, 2012.

[76] M. Zakotnik, I.R. Harris, A.J. Williams: *“Possible methods of recycling NdFeB-type sintered magnets using the HD/degassing process”*, Journal of Alloys and Compounds 450, p. 525–531, 2008.

[77] J. H. Rademaker, R. Kleijn, Y. Yang: *“Recycling as a strategy against rare earth element criticality a systemic evaluation of the potential yield of NdFeB magnet recycling”*, Environmental Science & Technology 47, p. 10129−10136, 2013.

[78] B. Sprecher, R. Kleijn, G. J. Kramer: *“Recycling potential of neodymium: the case of computer hard disk drives”*, Environmental Science and Technology 48, p. 9506−9513, 2014.

[79] K. Habib, K. Parajuly, Henrik Wenzel: *“Tracking the flow of resources in electronic waste - the case of end of- life computer hard disk drives”,* Environmental Science & Technology 49, p. 12441-12449, 2015.

[80] M. Uuberschaar, V.S. Rotter: *“Enabling the recycling of rare earth elements through product design and trend analysis of hard disk drives”*, Journal of Material Cycles and Waste Management 17, p 266-281, 2015.

[81] Ph. Tenaud, H. Lemaire, F. Vial: *“Recent improvements in NdFeB sintered magnets”*, Journal of Magnetism and Magnetic Materials 101, p. 328-332, 1991.

[82] K. Morimoto, N. Katayama, H. Akamine, M. Itakura: *“Coercivity enhancement of anisotropic Dy-free Nd–Fe–B powders by conventional HDDR process”*, Journal of Magnetism and Magnetic Materials 324, p. 3723–3726, 2012.

[83] F. M. Ahmed, A. Ataie, I.R. Harris: *“HDDR behaviour of Nb-containing Nd-Fe-B near-stoichiometric alloys”*, Journal of Alloys and Compounds 237, p. 93-100, 1996.

[84] M. Matsuuraa, A. Ashfaqa, M. Sakuraib, T. Tomidac, N. Sanoc, S. Hirosawa: *“Ga site occupancy in HDDR-treated Nd Fe B-based alloy by XAFS”*, Journal of Alloys and Compounds 293–295, p. 872–876, 1999.

[85] H. Sepehri-Amin, W.F. Li, T. Ohkubo, T. Nishiuchi, S. Hirosawa, K. Hono: *“Effect of Ga addition on the microstructure and magnetic properties of hydrogenation–disproportionation–desorption–recombination processed Nd–Fe–B powder”*, Acta Materialia 58, p. 1309–1316, 2010.

[86] S. Sugimoto, O. Gutfleisch, I.R. Harris, “*Resistivity measurements on HDDR phenomena in Nd-Fe-B alloys with Co, Ga, Zr additions*”, Journal of Alloys and Compounds 260, p. 284-291, 1997.

[87] B. Rupp, A. Resnik, D. Shaltiel, P. Rogl: *“Phase relations and hydrogen absorption of neodymium-iron-(boron) alloys”*, Journal of Materials Science 23, p. 2133-2141, 1988.

[88] A. J. Williams, P. J. McGuiness, 1. R. Harris: “*Mass spectrometer studies of hydrogen desorption from hydrided NdFeB*” IEEE Transactions on Magnetics 26, 5, p. 1945-1947, 1990.

[89] O. M. Ragg, G. Keegan, H. Nagel, I.R. Harris: *"The HD and HDDR processes in the production of Nd-Fe-B permanent magnets"*, International Journal of Hydrogen Energy 22, 2/3, p. 333-342, 1997.

[90] A. Handstein, M. Kubis, O. Gutfleisch, B. Gebel, K.-H. Müller: "*HDDR of Sm-Co alloys using high hydrogen pressures"*, Journal of Magnetism and Magnetic Materials 192, p. 73-76, 1999.

[91] O. Gutfleisch, M. Kubis, A. Handstein, K.-H. Müller, L. Schultz: "*Hydrogenation disproportionation desorption recombination in Sm-Co alloys by means of reactive milling", Applied Physics Letters* 73, p. 3001-3003, 1998.

[92] S. B. Rybalkaa, V.A. Goltsova, V.A. Didusa, D. Fruchart, "*Fundamentals of the HDDR treatment of $Nd_2Fe_{14}B$ type alloys",* Journal of Alloys and Compounds 356–357, p. 390–394, 2003.

[93] S. Rivoirard, J. Lyubina, E. Beaugnon, O. Gutfleisch: "*Magnetic field effect on the hydrogen desorption and recombination reaction in disproportionated Sm-Co-type alloys", Applied Physics Letters* 93, 172509 1-3, 2008.

[94] O. Gutfleisch, I. R. Harris, "*Fundamental and practical aspects of the hydrogenation, disproportionation, desorption and recombination process",* Journal of Physics D 29, p. 2255–2265, 1996.

[95] Y. Honkura, H. Mitarai, K. Maekawa, Y. Sugiura: *"Production method for anisotropic resin-bonded magnets"*, patent US 5886070 A, 1999.

[96] K. Bandyopadhyay, K. Tandon, A. Chakrabarti: *"Polymeric resin bonded magnets"*, patent US20040045635 A1, 2004.

[97] H. Mitarai, K. Noguchi, C. Mishima, H. Matsuoka, M. Yamazaki, Yuusuke Kawasugi: *"Development of compound for anisotropic bonded Nd magnets using d-HDDR magnet powder"*, IEEE Transactions on Magnetics 50, 11, 2014.

[98] P. J. McGuiness, X. J. Zhang, K. G. Knoch, X. J. Yin, M. J. Wyborn, I. R. Harris: *"HDDR hot-pressed magnets: magnetic properties and microstructure"*, Journal of Magnetism and Magnetic Materials 104-107, p. 1169-1170, 1992.

[99] O. M. Ragg, I. R. Harris, H. Nagel, P. Böhm: *"Hot Pressing Nd-Fe-B HDDR Powders"*, IEEE Transactions on Magnetics 32, 5, 1996.

[100] O. Gutfleisch, A. Kirchner, W. Grünberger, D. Hinz, H. Nagel, P. Thompson, J. N. Chapman, K. H. Müller, L. Schultz, I. R. Harris: *"Textured NdFeB HDDR magnets produced by die-upsetting and backward extrusion"*, Journal of Physics D 31, p. 807–811, 1998.

[101] N. Nozawa, H. Sepehri-Amin, T. Ohkubo, K. Hono, T. Nishiuchi, S. Hirosawa: *"Coercivity enhancement of HDDR-processed Nd–Fe–B permanent magnet with the rapid hot-press consolidation process"*, Journal of Magnetism and Magnetic Materials 323, p. 115–121, 2011.

[102] R. Gopalan, H. Sepehri-Amin, K. Suresh, T. Ohkubo, K. Hono, T. Nishiuchi, N. Nozawac, S. Hirosawac: *“Anisotropic Nd–Fe–B nanocrystalline magnets processed by spark plasma sintering and in situ hot pressing of hydrogenation–decomposition–desorption–recombination powder”*, Scripta Materialia 61, p. 978–981, 2009.

[103] K. Suresh, T. Ohkubo, Y. K. Takahashi, K. Oh-ishi, R. Gopalan, K. Hono, T. Nishiuchi, N. Nozawa, S. Hirosawa: *“Consolidation of hydrogenation–disproportionation–desorption–recombination processed Nd–Fe–B magnets by spark plasma sintering”*, Journal of Magnetism and Magnetic Materials 321, p. 3681–3686, 2009.

[104] X. Li, L. Li, K. Hu, Z. Chen, S. Qu, C. Yang: *“Microstructure and magnetic properties of anisotropic Nd−Fe−B magnets prepared by spark plasma sintering and hot deformation”*, Transactions of Nonferrous Metals Society of China 24, p. 3142−3151, 2014.

[105] R. K. Gray, W. Mich: *“Epoxy bonded rare earth-iron”*, patent 4558077, 1985.

[106] J. Herchenroeder, D. Miller, N. K. Sheth, M. C. Foo, K. Nagarathnam: *“High performance bonded neo magnets using high density compaction”*, Journal of Applied Physics 109, 07A743 2011.

[107] X. H. Zhang, W. H. Xiong, Y. F. Li, N. Song: *“Effect of process on the magnetic and mechanical properties of Nd–Fe–B bonded magnets “*, Materials and Design 30, p. 1386–1390, 2009.

[108] X. Li, M. Yue, M. Zakotnik, W. Liu, D. Zhang, T. Zuo: *“Regeneration of waste sintered Nd-Fe-B magnets to fabricate anisotropic bonded magnets”*, Journal of Rare Earths 33, 7, p. 736-739, 2015.

[109] G. P. Wang, W. Q. Liu, Y. L. Huang, S. C. Ma, Z. C. Zhong: *“Effects of sintering temperature on the mechanical properties of sintered NdFeB permanent magnets prepared by spark plasma sintering”*, Journal of Magnetism and Magnetic Materials 349, p. 1–4, 2014.

[110] Z. H. Hu, L. H. Chu, J. Li, Y. Liu: *“Effect of die-upset level on the mechanical properties and microstructure of Nd–Fe–B magnets prepared by spark plasma sintering”*, Journal of Magnetism and Magnetic Materials 324, p. 101–104, 2012.

[111] K. Žagar, A. Kocjan, S. Kobe: *“Magnetic and microstructural investigation of high-coercivity net-shape Nd–Fe–B-type magnets produced from spark-plasma-sintered melt-spun ribbons blended with DyF_3”*, Journal of Magnetism and Magnetic Materials 403, p. 90–96, 2016.

[112] K. Suresh, T. Ohkubo, Y. K. Takahashi, K. Oh-ishi, R. Gopalan, K. Hono, T. Nishiuchi, N.Nozawa, S. Hirosawa: *“Consolidation of hydrogenation–disproportionation–desorption–recombination processed Nd–Fe–B magnets by spark plasma sintering”*, Journal of Magnetism and Magnetic Materials 321, p. 3681–3686, 2009.

[113] T. Schrefl, J. Fidler, H. Kronmüller: *"Remanence and coercivity in isotropic nanocrystalline permanent magnets"*, Physical Review B 49, 9, p. 6100- 6110, 1994.

[114] E. Castlen, S. Grasso, M. Reece, R. Sheridan, A. Walton: *"Rapid sintering of anisotropic, nanograined Nd–Fe–B by flash-spark plasma sintering"*, Journal of Magnetism and Magnetic Materials 417, p. 279–283, 2016.

[115] K. Takagi, M. Akada, R. Soda, K. Ozaki: *"Preparation of Nd–Fe–B sintered magnets from HDDR-processed powder"*, Journal of Magnetism and Magnetic Materials 393, p. 461–466, 2015.

[116] M. Yue, M. Tian, J. X. Zhang, D. T. Zhang, P. L. Niu, F. Yang: *"Microstructure and magnetic properties of anisotropic Nd–Fe–B magnets produced by spark plasma sintering technique"*, Materials Science and Engineering B 131, p. 18–21, 2006.

[117] R. Gopalan, H. Sepehri-Amin, K. Suresh, T. Ohkubo, K. Hono, T. Nishiuchi, N. Nozawa, S. Hirosawa: *"Anisotropic Nd–Fe–B nanocrystalline magnets processed by spark plasma sintering and in situ hot pressing of hydrogenation–decomposition–desorption–recombination powder"*, Scripta Materialia 61, p. 978–981, 2009.

[118] Z. Hu, L. Chu, J. Li, Y. Liu: *"Enhanced magnetic properties in Nd-Fe-B magnets prepared by spark plasma sintering via die-upsetting process"*, Journal of Rare Earths 29, 7, p. 660, 2011.

[119] Z. H. Hun, J. Li, L. H. Chu, Y. Liu: *"Effect of hot deformation temperature on the magnetic and mechanical properties of Nd–Fe–B magnets prepared by spark plasma sintering"*, Journal of Magnetism and Magnetic Materials 323, p. 104–107, 2011.

[120] Y. H. Hou, Y. L. Wang, Y. L. Huang, Y. Wang, S. Li, S. C. Ma, Z. W. Liu, D. C. Zeng, L. Z. Zhao, Z. C. Zhong: *"Effects of Nd-rich phase on the improved properties and recoil loops for hot deformed Nd-Fe-B magnets"*, Acta Materialia 115, p. 385-391, 2016.

[121] Z. H. Hu, H. Dong, D. W. Ma, C. Luo: *"Enhanced magnetic and mechanical properties of die-upset Nd–Fe–B magnets prepared by spark plasma sintering via alloy powder blends"*, Journal of Magnetism and Magnetic Materials 401, p. 169–172, 2016.

[122] M. Zakotnik, I. R. Harris, A. J. Williams: *"Multiple recycling of NdFeB-type sintered magnets"*, Journal of Alloys and Compounds 469, p. 314–321, 2009.

[123] X. T. Li, M. Yue, W. Q. Liu, X. L. Li, X. F. Yi, X. L. Huang, D. T. Zhang, J. W. Chen: *"Large batch recycling of waste Nd-Fe-B magnets to manufacture sintered magnets with improved magnetic properties"*, Journal of Alloys and Compounds 649, p. 656-660, 2015.

[124] W. Liu, C. LI, M. Zakotnik, M. Yue, D. Zhang, X. Huang: *"Recycling of waste Nd-Fe-B sintered magnets by doping with dysprosium hydride nanoparticles"*, Journal of Rare Earths 33, 8, p. 846-849, 2015.

[125] M. Zakotnik, C. O. Tudor: *“Commercial-scale recycling of NdFeB-type magnets with grain boundary modification yields products with ‘designer properties’ that exceed those of starting materials”*, Waste Management 44, p. 48–54, 2015.

[126] C. Mishima, N. Hamada, H. Mitarai, and Y. Honkura: *“Development of a Co-Free NdFeB Anisotropic Bonded Magnet Produced from the d-HDDR Processed Powder”*, IEEE Transactions on Magnetics 37, p. 2467-2470, 2001.

Own publications and conference contributions

A. Lixandru, P. Venkatesan, C. Jönsson, I. Poenaru, B. Hall, Y. Yang, A. Walton, K. Güth, R. Gauß, O. Gutfleisch: "*Identification and recovery of rare-earth permanent magnets from waste electrical and electronic equipment"*, Waste Management 68, 482-489, 2017.

A. Lixandru, I. Poenaru, K. Güth, R. Gauß, O. Gutfleisch: *"A systematic study of HDDR processing conditions for the recycling of end-of-life Nd-Fe-B magnets"*, Journal of Alloys and Compounds 724, 51-61, 2017.

A. Lixandru, I. Poenaru, K. Güth, R. Gauß, O. Gutfleisch: *"Study of processing conditions for the recycling of end-of-life Nd-Fe-B magnets using HDDR"*, in Proc. 25th Int. Workshop on Rare Earth and Future Permanent Magnets and their Applications (REPM) 2016.

Curriculum vitae

PERSONAL INFORMATION

Lixandru Alexandru

📍 Street Ziduri intre Vii 19, Doamna Ghica Plaza, bl. A, ap. 225, Bucureşti, Sectorul 2, 023321, Romania

☎ +40213468297 (ext.127) 📱 +40 (751) 268 468

✉ alex.lixandru@icpe-ca.ro , lixandru.alexandru@gmail.com

lixandru.alexandru@live.com

Sex M | Date of birth 09/02/1988 | Nationality Romanian

WORK EXPERIENCE

July 2013 - present

Research Assistant

INCDIE ICPE-CA Bucharest, Splaiul Unirii 313, district 3 Bucharest, 030138, Romania

Department of Advance materials

- Magnetic measurements
- Low and high hydrogen treatments
- Production and recycling of the rare earth permanent magnets

Business or sector: Research & Development

January 2014 - December 2016

Research Assistant

Fraunhofer ISC, Brentanostraβe 2, Alzenau, 63755, Germany

Project Group Materials Recycling and Resource Strategies

- Magnetic measurements
- Low and high hydrogen treatments
- Recycling of Nd-Fe-B permanent magnets

Business or sector: Research & Development

EDUCATION AND TRAINING

Jun 2014 - present

PhD in Material Science

Level 8 EQF

Technische Universität Darmstadt

- Thesis: "Dynamic hydrogenation disproportionation desorption recombination of the extracted powders, from scrap rare earth magnets, to produce bonded magnets"

October 2011 – July 2013

Master in Electrical Engineering

Level 7 EQF

Universitatea Politehnica Bucureşti, Faculty of Electrical Engineering

Thesis: "Nanocomposite Nd-Fe-B"

October 2007 - July 2011

Bachelor in Electrical Engineering

Level 6 EQF

Universitatea Politehnica Bucureşti, Faculty of Electrical Engineering

- Thesis: “ Study of a recuperative braking for a diesel locomotive

PERSONAL SKILLS

Mother tongue

Romanian

Other languages

	UNDERSTANDING		SPEAKING		WRITING
	Listening	Reading	Spoken interaction	Spoken production	
English	C1	C1	C1	C1	B2
French	B1	B1	B1	B1	A2
German	A2	A2	A2	A2	A1

Levels: A1/A2: Basic user - B1/B2: Independent user - C1/C2 Proficient user
Common European Framework of Reference for Languages

Communication skills

- *“Leadership and communication skills”* training given by Chalmers University doctoral programme officers
- *“Project writing”* training given by TU Darmstadt doctoral programme officers

Organizational / managerial skills

- “*IP training and tech transfer*” training given by KU Leuven Tech transfer office in cooperation with IWT
- *“Good scientific conduct & lab safety”* training given by Umicore – Rhodia
- *“Project management”* training given by University of Birmingham doctoral programme officers and Tech transfer office TU Delft
- “*Time management and work/life balance*” training given by Helsinki University doctoral programme officers
- “*Career development*” training given by Helsinki University doctoral programme officers
- “*Business development and entrepreneurship”* training given by Tech transfer office TU Delft

Job-related skills

- “*Training in Casting and sintering route for producing sintered magnets”* given by Allan Walton, University of Birmingham
- *“Bonded magnets and applications”* given by Oliver Gutfleisch, Fraunhofer ISC
- “*Training on REE alloy production and qualification*” at Less Common Materials facilities
- “*Training on solvent extraction”* at Chalmers facilities
- “*Training on collection and preprocessing of WEEE*” at Stena Metall facilities
- *“Training on magnetism and challenges for permanent magnets in energy applications”* given by Oliver Gutfleisch
- *“Basics of LCA methodology”* given by Matthias Buchert
- “*Training on ion exchange chromatography*” at University of Helsinki facilities
- “*Training on electrodeposition from molten salts: application of molten salt chemistry in extraction and refining of rare-earth metals*” at University of. Cambridge/Nottingham, SINTEF, University of Tokyo, and TU Delft facilities

Digital competence

SELF-ASSESSMENT

Information processing	Communication	Content creation	Safety	Problem solving
Independent user	Independent user	Independent user	Independent user	Independent user

Levels: Basic user - Independent user - Proficient user
Digital competences - Self-assessment grid

Driving license

B

ADDITIONAL INFORMATION

Publications

Only first author publications:

A. Lixandru, I. Poenaru, K. Güth, R. Gauß, O. Gutfleisch: *„A systematic study of HDDR processing conditions for the recycling of end-of-life Nd-Fe-B magnets",* Journal of Alloys and Compounds Volume 724, November 2017, Pages 51-61

A. Lixandru, P. Venkatesan, C. Jönsson, I. Poenaru, B. Hall, Y. Yang, A. Walton, K. Güth, R. Gauß, O. Gutfleisch: *„Identification and recovery of rare-earth permanent magnets from waste electrical and electronic equipment",* Waste Management Volume 68, October 2017, Pages 482-489

A. Lixandru, I. Poenaru, K. Güth, R. Gauß, O. Gutfleisch: *"Study of processing conditions for the recycling of end-of-life Nd-Fe-B magnets using HDDR"*, in Proc. 25th Int. Workshop on Rare Earth and Future Permanent Magnets and their Applications (REPM) 2016.

Patents

E. Brouwer, O. Diehl, A. Dirks, K. Güth, H. Hibst, A. Lixandru, A. Buckow, R. Gauß, O. Gutfleisch: *„Verfahren zur Wiederverwendung von Permanentmagneten als isotropes Magnetpulver und als Verbundmagneten aus diesem Pulver*"2016

Conferences

- **EREAN Summer School** (08.2014)
  KU LEUVEN, Belgium
- **IEEE Magnetics Society Summer School** (06.2015)
  University of Minnesota, Minneapolis, USA.
  A. Lixandru et al.: "Recycling of rare earth permanent magnets" (poster session)
- **MMM | Intermag 2016** (01.2016)
  San Diego, California, USA
  A. Lixandru et al: *"Recycling of rare earth permanent magnets by hydrogen treatment"* (oral presentation session)
- **JEMS** (08.2016)
  Glasgow, UK
  A. Lixandru et al.: *"Energy-efficient recycling of rare earth permanent magnet scrap material by hydrogen treatment routes: from waste selection to magnet recycling"* (poster session, won Institute of Physics best poster award)
- **REPM** (09.2016)
  Darmstadt, Germany
  A. Lixandru et al. "Recycling of scrap rare earth permanent magnets by hydrogen decrepitation (HD) and hydrogenation disproportionation desorption recombination (HDDR) process" (poster session)

Honors and awards

Best poster award at JEMS 2016 conference for the poster entitled: "*Recycling of rare earth permanent magnet scrap material by hydrogen treatment routes: from waste selection to magnet recycling*"

Memberships

Marie Curie Alumni (2014)
European Rare Earth Magnet Recycling Network member (2014)